The Development of a Bioreactor for the Tissue Engineering of Anterior Cruciate Ligaments

Mitchell, Mark

Award date:
2009

Awarding institution:
University of Bath

The Development of a Bioreactor for the Tissue Engineering of Anterior Cruciate Ligaments

Mark Samuel Mitchell

A thesis submitted for the degree of Doctor of Philosophy

University of Bath

Department of Mechanical Engineering

May 2009

ABSTRACT

The anterior cruciate ligament (ACL) is a major ligament within the knee joint. Its role is to provide stability and maintain the physiological kinetics and kinematics of the joint. ACL injuries are common as a result of sporting and traffic accidents and current therapeutic options do not fully restore the joint kinetics and kinematics. As such, patients often suffer from increased joint laxity and joint pain following an ACL reconstruction and this can lead to secondary problems such as osteoarthritis. It is believed that improving the ACL graft could help restore the normal kinetics and kinematics of the knee joint and hence postpone or prevent the onset of primary and secondary problems.

Tissue engineering has the potential to provide functional tissue to repair or replace injured or diseased tissues in the patient. The ACL is a tissue which could benefit from such developments and thus improve the success of the reconstruction. However, the ACl is a complex structure made up of a highly orientated collagen hierarchy which experiences three dimensional loading *in vivo*. For an engineered tissue to be functional it is necessary for this orientated structure to be replicated.

The appropriate structure is achieved by replication of the *in vivo* ACL strain pattern which requires combined tensile and torsional loading. Current custom-made and commercially available bioreactors have not been able to fully replicate this motion with the necessary feedback and monitoring of mechanical parameters.

The aim of this project was to develop a novel bioreactor with physiological mechanical conditioning for the tissue engineering of an anterior cruciate ligament. A bioreactor capable of applying complex tensile and torsional loading to a developing ACL was designed, manufactured and validated.

The bioreactor which has been developed is a novel research tool which allows the effect of a number of parameters to be investigated in a 3-D loading environment. It can be used for the engineering of connective tissues such as ligaments and tendons and has the potential to be adapted for use with other musculoskeletal tissues such as bone. It could also be used for research to understand the processes involved in the growth and development of tissues.

ACKNOWLEDGEMENTS

Firstly, I would like to thank my supervisors, Prof. Tony Miles and Dr. Sabina Gheduzzi who provided excellent guidance throughout this project and kept me motivated and moving forward especially after I had "been thinking" and thought it was never going to work. Richard Weston is the best technician I've ever known. It seems there is nothing he can't manufacture or repair and his input was invaluable. Though I think I will be most grateful to him for introducing me to Radio 2 and in particular pop master, the many games of darts and pool and those afternoon chats which kept me going when I was particularly bored.

Many thanks to Dr. Mark Perry from the University of Bristol for his help during the biological study. His contribution and efforts were a major factor in the success of the project. Also, thanks to Vijay Rajput and Colin Brain for their help with the instrumentation and control software.

I was also given help and assistance through this project by Dr Richard Forsey from Chemical Engineering, Jon Hampshire of Baldor UK and Prof. Robert Brown from UCL.

Finally, many thanks to my friends and family for supporting me and keeping me entertained over the last few years.

CONTENTS

LIST OF FIGURES

LIST OF TABLES

GLOSSARY

Actin: a globular protein within the cell associated with cell structure, mobility and muscle contraction.

Allogeneic: derived from a different individual of the same species.

Anterior: towards the front or ventral surface of the body.

Apoptosis: genetically programmed cell death.

Autologous: derived from the same organism.

Centriole: a barrel-shaped microtubule structure involved in the process of cell division.

Centrosome: a region in the cytoplasm containing a pair of centrioles orientated perpendicular to each other.

Chondrocytes: mature cartilage cells.

Cilia: tail-like projections from the cell body with sensory or locomotion functions.

Coronal/frontal plane: a sectional plane that divides the body into an anterior portion and a posterior portion.

Cytoplasm: the material between the cell membrane and the nuclear membrane.

Cytoskeleton: a network of microtubules and microfilaments in the cytoplasm.

Cytosol: the fluid portion of the cytoplasm.

Cytotoxic: poisonous to cells.

Distal: movement away from the point of attachment or origin; for a limb, away from its attachment to the trunk.

Extension: a movement that increases the angle between two articulating bones.

Fibroblasts: connective tissue cells.

Flagella: tail-like projections from the cell body with locomotion functions.

Flexion: a movement that reduces the angle between two articulating bones.

Immunogenic: elicits an immune response.

Integrin: a glycoprotein which acts as a cell surface receptor and mediate attachment between the cell and the surrounding matrix.

Kinematics: the study of motion without regards to the forces which caused the motion.

Kinetics: the study of forces responsible for the motion of bodies.

Lateral: away from the midline of the body; pertaining to the side.

Ligand: a short amino acid sequence on the matrix which binds to an integrin molecule.

Medial: towards the midline of the body.

Microtubule: hollow tube composed of the protein tubulin with a diameter of approximately 25nm.

Morphogenesis: the development of a cell's structural shape or form.

Multipotent: capable of producing many daughter cell types.

Necrosis: death of cells from disease or injury.

Olgipotent: capable of producing a few daughter cell types.

Organelle: a structure within the cell which performs a particular function.

Phenotype: physical characteristics that are determined genetically.

Pluripotent: capable of producing most daughter cell types.

Posterior: towards the back or dorsal surface of the body.

Proximal: towards the attached base of an organ or structure.

Sagittal plane: a sectional plane that divides the body into left and right portions.

Somatic: pertaining to the body.

Totipotent: capable of producing all daughter cell types.

Transverse plane: a sectional plane that divides the body in a horizontal direction.

Tubulin: a globular protein with a molecular weight of approximately 55 kiloDaltons which forms microtubules within the cell.

Unipotent: capable of producing one daughter cell type.

Varus: bending or turning inwards towards the midline of the body.

Valgus: bending or turning outwards away from the midline of the body.

Xenogeneic: derived from an individual of a different species.

1 BACKGROUND

1.1 Anatomy of the knee

The knee is a diarthrodial (freely moving) joint linking two of the longest bones in the body. It acts to transmit load and participates in movement of the lower limb. Its main motion is a rotation in the sagittal plane, however, it displays a great deal more complexity than a simple hinge. The knee joint actually consists of two joints: the tibiofemoral joint (Figure 1-1) and the patellofemoral joint (Martini 2001; Simon *et al.* 2000).

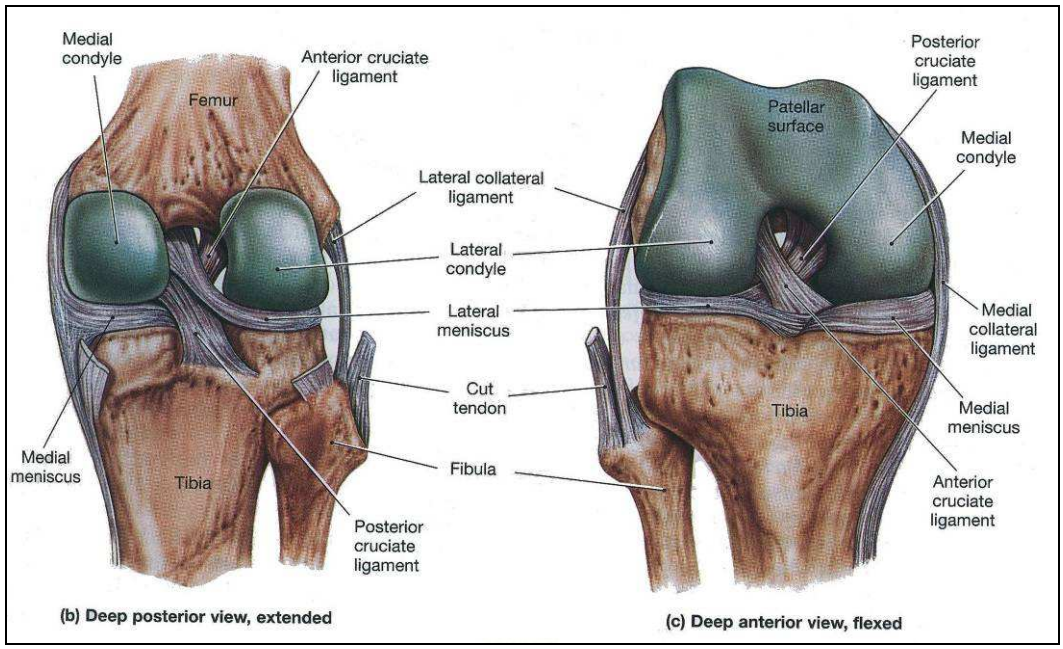

Figure 1-1 The anatomy of the knee (adapted with permission from Martini (2001))

In the tibiofemoral joint the femoral condyles articulate on the tibial plateau with both a rolling and sliding motion resulting in a constantly changing centre of rotation. The medial femoral condyle translates in the antero-posterior direction no more than ±1.5mm (a mainly sliding motion) whereas the lateral femoral condyle translates posteriorly around 15mm during flexion between 10° - 120° (both a rolling and sliding motion) (Freeman & Pinskerova 2005). This causes a tibial internal rotation of approximately 30° during flexion. There is very little varus/valgus motion during flexion unless one of the condyles lifts off the tibial plateau (Freeman & Pinskerova 2005). The meniscus acts to provide conformity between the differing radii of the femoral condyles and the tibial plateau and also provides a shock-absorbing function during impact.

The patellofemoral joint involves the patella articulating on the patellar surface of the distal end of the femur. The patella is embedded into the quadriceps tendon and as the tendon carries on distally past the patella it becomes the patellar tendon and attaches to the anteroproximal site on the tibia. The patellofemoral joint provides two main functions: firstly it aids knee extension by anteriorly displacing the quadriceps tendon thus increasing the lever arm of the tendon, and secondly it provides a wider distribution of the compressive stress being applied by the tendon to the femur (Martini 2001; Simon *et al.* 2000).

The knee joint is intrinsically an unstable joint with the stability being provided by the soft tissues as opposed to the bone shape. These soft tissues include ligaments and tendons. Ligaments connect bone to bone whereas tendons connect muscle to bone. There are four main ligaments which provide stability to the knee. The anterior cruciate ligament (ACL) arises from the anteriomedial part of the tibial plateau and extends to the posterolateral aspect of the intercondylar fossa of the femur (Woo *et al.* 2006). The ACL is the primary restraint to anterior tibial translation and also resists internal tibial rotation (Nordin & Frankel 2001; Woo *et al.* 2006). The posterior cruciate ligament (PCL) arises from the posterior lateral part of the tibial plateau and passes to the anteromedial aspect of the intercondylar fossa of the femur (Gray 2001; Woo *et al.* 2006). The PCL is the primary restraint to posterior tibial translation and also resists external tibial rotation (Nordin & Frankel 2001). The medial collateral ligament (MCL) originates from the medial epicondyle of the femur in a distal and anterior direction and inserts at the posteromedial tibial articular margin (Woo *et al.* 2006). The MCL is the primary restraint to valgus angulation (Nordin & Frankel 2001). The lateral collateral ligament (LCL) originates from the lateral epicondyle of the femur postero-distally and inserts at the top of the fibular head (Woo *et al.* 2006). The LCL is the primary restraint to varus angulation (Nordin & Frankel 2001).

There are minor ligaments anterior and posterior of the PCL (the anterior and posterior meniscofemoral ligament) which are found in some people (Woo *et al.* 2003).

Joint stability is augmented by superficial tendons and ligaments, including anterior support from the patellar tendon and posterior support from the popliteal ligament (Martini 2001).

In addition to the main flexion/extension movement in the sagittal plane generated during articulation of the knee, there is also a small internal/external rotation in the transverse

plane. As the knee is extended the tibia rotates externally as a consequence of the medial femoral condyle being larger than the lateral femoral condyle. At full extension this rotation tightens the ACL and jams the lateral meniscus between the femur and the tibia locking the knee in the extended position. This is known as the screw-home mechanism of the tibiofemoral joint and provides increased stability of the joint during full extension allowing a person to stand for prolonged periods without the use of muscles. Muscle contraction is then required to unlock the knee joint by rotation of the tibia or femur (Martini 2001).

1.2 The cruciate ligaments

The ACL and PCL are complex ligaments, each consisting of two distinct bundles. The ACL is heart-shaped in cross-section due to an indentation along the anterior surface (Clark & Sidles 1990). This separates the ACL into the anteromedial (AM) bundle which provides restraint primarily to antero-posterior translation, and the posterolateral (PL) bundle which provides restraint primarily to rotation (Woo *et al.* 2003). Dye and Cannon (1988) note the ACL as being oval in cross-section with a length of 31±3mm, a width of 10±2mm, a thickness of 5±1mm and a total volume of 2.3±0.4ml. Altman *et al.* (2002a) have recorded the human ACL as being in the order of 27mm long and 8mm in diameter, Goulet *et al.* (2000) noted the length as being approximately 32mm, whereas Smith *et al.* (1993) found from the literature an average ACL length of 31-38mm. The PCL consists of the anterolateral (AL) bundle, which is usually taut when the knee is passively flexed, and the posteromedial (PM) bundle, which is usually taut when the knee is passively extended (Harner *et al.* 2000; Woo *et al.* 2003). The AM, PL, AL and PM notation all refer to the position of the fascicles at the tibial insertion (Smith *et al.* 1993).

The ACL fascicles fan out as they approach the tibial insertion and consequently the tibial insertion site has a larger area than the femoral site. Ligament insertion into the bone can take two forms, either direct or indirect insertion. Direct insertion appears in the insertion sites of the ACL, within a distance of less than 1mm (Smith *et al.* 1993), and also in the femoral insertion of the MCL (Smith *et al.* 1993; Woo *et al.* 2006). The stages of direct insertion as noted by Woo *et al.* (2003) are ligament, fibrocartilage, mineralised fibrocartilage and bone.

Indirect insertion of the ligament into the bone, as appears in the tibial insertion of the MCL, involves superficial fibres which are attached to the periosteum while deeper

fibres attach directly to the bone at acute angles, the so called Sharpey's fibres (Smith *et al.* 1993; Woo *et al.* 2006; Woo *et al.* 2003).

1.2.1 Ligament structure

Ligaments are dense fibrous connective tissues which attach bone to bone. Their high tensile properties allow them to provide joint stability, guide joint articulation and prevent excessive motion. Water constitutes approximately two thirds of the wet weight of ligaments while collagen represents nearly three quarters of the dry mass (Frank *et al.* 1985). The remainder comprises matrix macromolecules such as elastin, proteoglycans and glycoproteins (Goh *et al.* 2003).

Lyons *et al.* (1991) observed that the cells in different ligaments can be quite dissimilar. They noted that ACL cells are oval shaped and more closely resemble chondrocytes, whereas the MCL contains long cells which are more similar to fibroblasts. Lyons *et al.* concluded that this difference may be due to the complex loading experienced by the ACL *in vivo* as discussed in Section 1.2.3.

In 1978 Kastelic *et al.* (1978) proposed a collagen organisational system for the structure of tendons, consisting of a number of hierarchies of fibrillar arrangements as shown in Figure 1-2.

Traditionally, it was believed that ligaments had a similar organisational structure. However, Danylchuk *et al.* (1978) proposed a different structure for the ACL (Figure 1-3). The smallest level is a collagen fibril with a diameter of approximately 150-250nm. These fibrils form a collagen fibre which then make up a sub-fascicle with a diameter of approximately 100-250µm. The sub-fascicle is surrounded by a loose connective tissue called endotenon and less than 20 sub-fascicles are arranged into a collagen fasciculus. The collagen fasciculus is again surrounded by loose connective tissue called epitenon and its diameter can vary from 250µm to several millimetres. Many fasciculi make up the ACL and it is surrounded by the thicker paratenon which is enveloped by a synovial sheath.

This structure was challenged by Clark and Sidles in 1990 (Clark & Sidles 1990). They observed collagen fibrils arranged into a round or oval fibre bundle with a diameter of approximately 20µm. The authors noted that these were similar to the sub-fascicle identified by Danylchuk *et al.*, however, the bundles were separated by a network of fine

fibrils and cells as opposed to loose connective tissue. These cells, in turn, were surrounded by a fibrous capsule and proteoglycans. Fibre bundles were arranged into a fascicle varying in diameter from 20µm to 400µm or greater. The fascicle was surrounded by a single or multiple thin sheets of tightly woven fibrils. A number of fascicles made up the ligament and it was observed that they did not cross or interweave. Fascicles were visible to the naked eye, and Clark and Sidles also observed at the site of ligament insertion the fascicles subdivided into smaller fascicles and the spaces between them grew and contained more membranous tissue.

The membranes observed by Clark and Sidles did not form concentric boundaries of fibre groups but instead divided the groups almost randomly as septae. Consequently, Clark and Sidles concluded there was no true epi- or endotenon in the ACL. They also hypothesised that the spaces between membranous layers may allow slippage between fascicles thus protecting neurovascular structures within these areas from shear damage.

All the organisational structures recognise that the ACL fibrils have a sinusoidal wave pattern known as a crimp. The ACL crimp has a wavelength of 45-60µm and amplitude of less than 5 µm (Khatod & Amiel 2003). The crimp is important for the mechanical properties of the ligament and will be discussed in the next section.

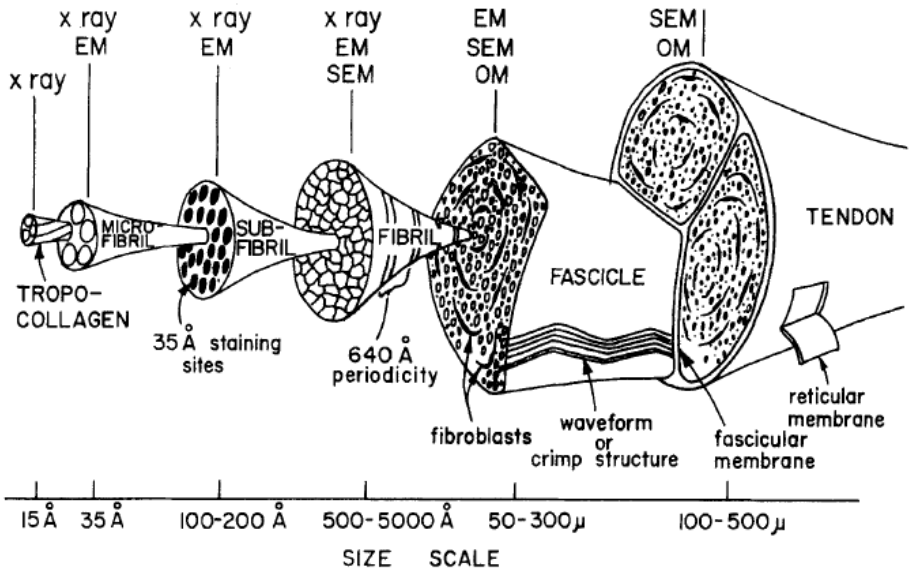

Figure 1-2 The hierarchical structure of a tendon proposed by Kastelic *et al.* (reproduced with permission from Kastelic *et al.* (1978))

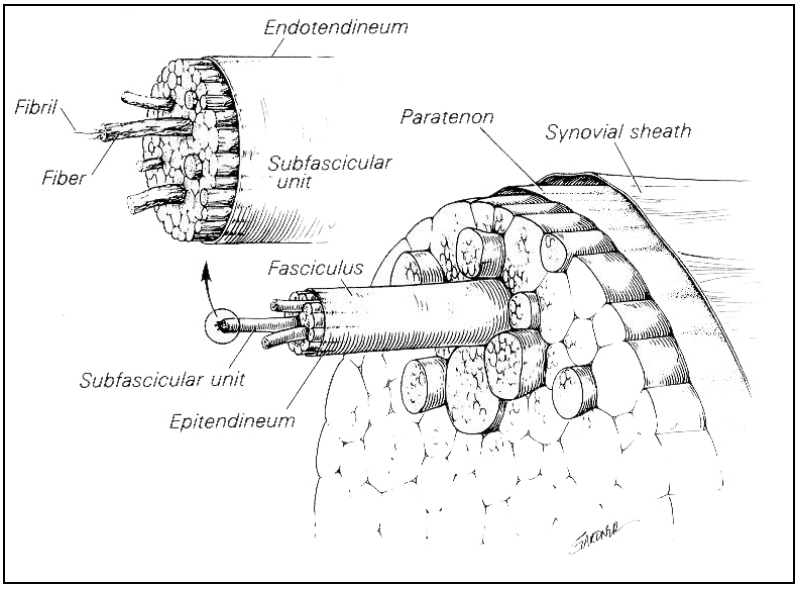

Figure 1-3 ACL structure proposed by Danylchuk *et al.* (reproduced with permission from Dye & Cannon (1988))

1.2.2 Mechanical properties of the ACL

A typical load-elongation curve for a ligament is shown in Figure 1-4. During the toe region at low levels of elongation the crimps in the fibre bundles of the ligament are straightened out and the ligament is characterised by low stiffness (Goh *et al.* 2003). The crimps act as a buffer to longitudinal elongation to prevent damage to the tissue and also function as a shock absorber (Khatod & Amiel 2003). The toe region leads onto a linear region where the fibres are parallel and the ligament possesses a constant stiffness. Further elongation causes microfailure of the fibres and eventually macroscopic failure of the ligament fibres (Goh *et al.* 2003).

Ligaments are viscoelastic in nature and therefore exhibit time dependent properties such as creep, stress relaxation and loading history dependence (Goh *et al.* 2003; Smith *et al.* 1993). Therefore, as a ligament is loaded and then unloaded it produces a hysteresis loop as energy is lost during the cycle. Repeated cyclic loading reduces the energy lost during each cycle, therefore, preconditioning during mechanical testing of these tissues can help to produce more uniform results (Smith *et al.* 1993). Preconditioning is discussed further in Section 1.9.3.

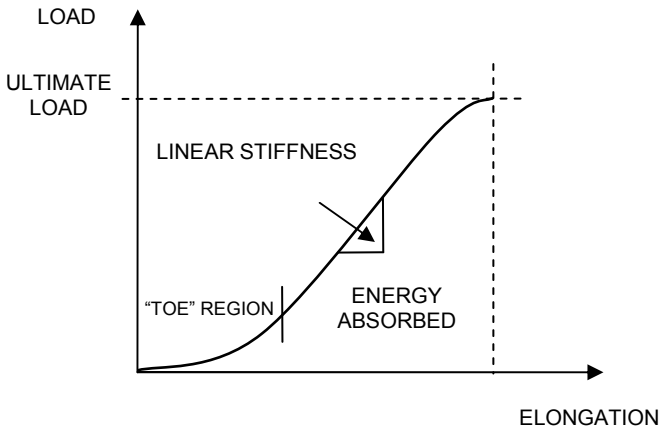

Figure 1-4 Typical load-elongation curve for a ligament (adapted from Smith *et al.* (1993))

Woo *et al.* (1991) determined the stiffness of the human ACL in its anatomical position for young people to be 242±28N/mm (22 to 35years) and measured an ultimate tensile strength of 2160±157N. Altman *et al.* (2002a) recorded a yield point in the order of 1200 N for the human ACL.

Woo *et al.* (2003) noted the overall elastic modulus of the ACL as being approximately 516MPa, however, they also noted that the ACL has non-uniform bundle properties. The AM bundle of the ACL as compared to the PL bundle has a larger elastic modulus, a larger tensile strength and a larger strain energy density (Woo *et al.* 2003). This difference was quantified by Woo *et al.* in 2006. They quote an elastic modulus of 283±114 MPa and 154±120 MPa for the AM and PM bundles of the human ACL respectively (Woo *et al.* 2006).

It is worth noting that this non-uniformity is also apparent in the PCL where the elastic modulus of the AL bundle (294±115MPa) is almost twice the modulus of the PM bundle (150±69MPa) (Woo *et al.* 2003).

These properties have been summarised in Table 1-1:

Table 1-1 Summary of human ACL properties

Length	~27-38mm
Diameter	~8mm
Width	10±2mm
Thickness	5±0.4mm
Stiffness	242±28 N/mm
Ultimate Tensile Strength	2160±157 N
Yield Point	~1200N
Overall Modulus	~516 MPa
AM Bundle Modulus	283±114 MPa
PL Bundle Modulus	154±120 MPa

1.2.3 ACL strain

The level of strain experienced by the human ACL is varied and depends on the angle of flexion, and which muscles and external forces are acting on the knee. Caution must be exercised when relying on strain measurements quoted in the literature as there can be a number of problems when trying to measure ACL strain. The ACL is composed of two bundles, therefore, obtaining a strain value for the whole ACL may not be representative as the AM bundle may be in tension while the PL bundle may be slack or vice versa. Simon *et al.* (2000) observed that in flexion the AM bundle is in tension, whereas, in extension the PL bundle is in tension. Work by Beynnon *et al.* (1992) showed that during the passive range of motion of the knee the AM bundle was unstrained until the knee was in extension, whereas, during the active range of motion the AM bundle is strained between 10° – 48° and unstrained between 48° – 110° (strain in the PL bundle was not measured in this study).

Additionally, the reference length for zero strain, against which the strain is calculated, can differ between various investigations. Some authors have used the zero strain reference length as that of the ligament when the knee is in the fully extended position (Renstrom *et al.* 1986) while others have used a zero strain reference length as the length at which the ligament fibres go through a slack-taut transition (Beynnon *et al.* 1992). This may result in difficulties when comparing strain measurements from different investigations as the measured values are relative to a zero strain value which may be different. Although affected by these issues, strain measurements do provide a useful guide to the working conditions experienced by the tissue *in vivo*.

Renstrom *et al.* (1986) carried out an investigation showing the effect of hamstring and quadriceps activity on ACL strain using a zero strain reference length defined as the ACL length when the knee is fully extended with no hamstring or quadriceps activity. Figure 1-5 illustrates how quadriceps and hamstring activity affect ACL strain during flexion. This is compared to the ACL strain during passive flexion of the knee. The addition of quadriceps muscle forces causes a significant increase in ACL strain during low angles of flexion (0° – 45°) whereas hamstring muscle forces do not increase the ACL strain.

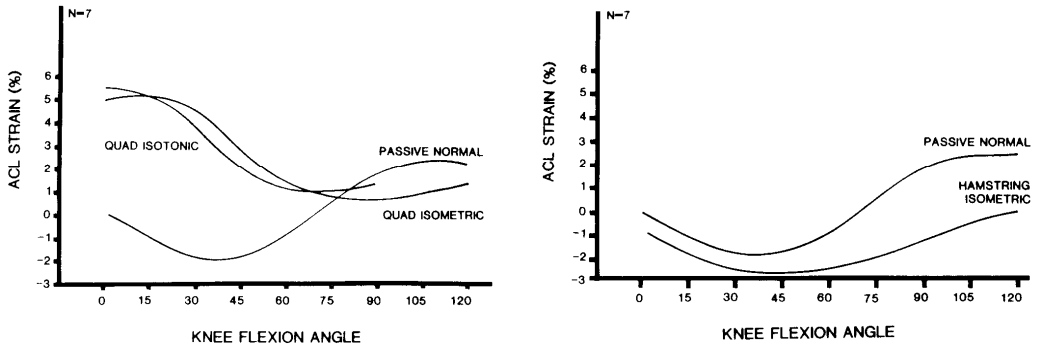

Figure 1-5 ACL strain during passive flexion compared to the ACL strain with muscle activity (reproduced with permission from Renstrom *et al.* (1986))

An (2003) collated a number of strain measurements from the literature for the ACL during a selection of activities and these are shown in Table 1-2 below:

Table 1-2 Summary of strain measurements from the literature (An 2003)

Strain (%)	*Activity*
4.4	Isometric Quadricep
2.8	Active flexion/extension without weight
3.8	Active flexion/extension with weight
3.6	Squatting without weight
4.0	Squatting with weight
4.7	Anterior shear load
1.2-2.1	Bicycling

In addition to longitudinal strain, the ACL also experiences torsional strain. Zavatsky and O'Connor (1994) refer to this as 'intra-ligamentary torsion'. This is caused by the inclination of the longitudinal axis of the ligament with respect to the axis of flexion, thus generating angular velocity vector components perpendicular and parallel to the axis of the ligament. These two components result in bending and twisting of the ligament fibres (Zavatsky & O'Connor 1994).

Simon *et al.* (2000) state that the ACL fibres rotate approx 90° on their longitudinal axis, however, they do not state at which angle of flexion this occurs. The rotation of the ACL due to knee articulation is shown in Figure 1-6. Zavatsky and O'Connor (1994) produced a three-dimensional computer model to predict how the ligaments were strained and changed shape during passive knee flexion. They used this model to predict, amongst other things, the intra-ligamentary torsion of the ACL and compared their results to some experimental data from a thesis by van Dijk (1983) (Figure 1-7). The angle of twist was defined as the relative rotation of the ends of the ligament about the longitudinal central axis. The zero twist reference point is that where all the fibres are parallel to the longitudinal axis. The angle of twist is positive for an external rotation of the tibial attachment area relative to the femoral attachment area (Zavatsky & O'Connor 1994). Zavatsky and O'Connor justified the differences between their numerical predictions and the experimental data of van Dijk for flexions greater than 20° because their model did not allow any internal tibial rotation.

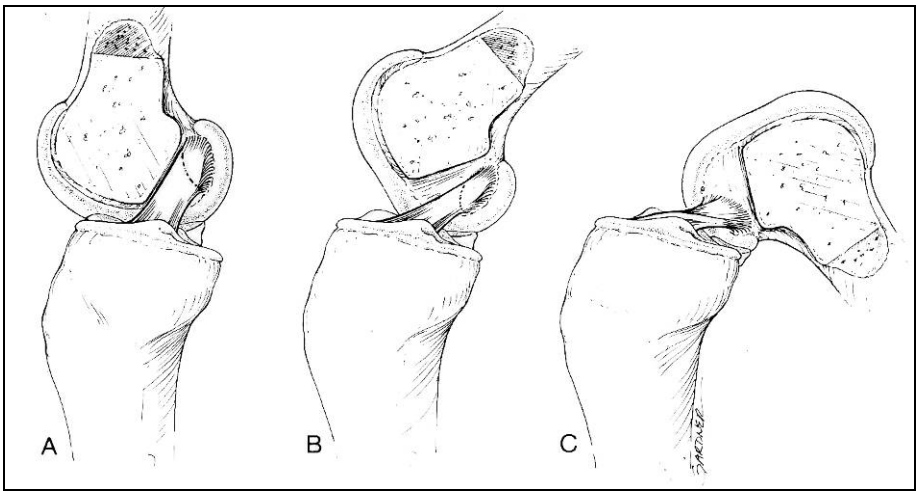

Figure 1-6 Diagram showing the rotation of the ACL during knee articulation (reproduced with permission from Dye & Cannon (1988))

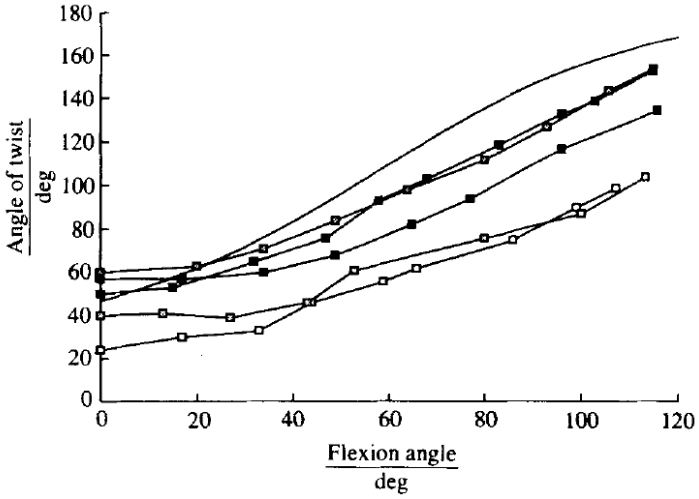

Figure 1-7 ACL angle of twist versus flexion angle. The numerical predictions of Zavatsky and O'Connor are shown as a solid line, the experimental results from van Dijk are shown as data points (reproduced with permission from Zavatsky & O'Connor (1994))

1.2.4 Mass transfer for the ACL

Cruciate ligaments are morphologically intra-articular, however, they are surrounded by a synovial layer making them extra-synovial structures (Butler *et al.* 2003; Woo *et al.* 2003). Woo *et al.* (2003) observe that nutrition for the ligament cells is provided by a uniform microvascular system originating from the insertion sites of the ligament. The blood supply for the ACL and PCL is provided by the middle genicular artery. Smith *et al.* (1993) report that the middle genicular artery vascularises the synovial membrane surrounding the ACL. Vessels extend into the ACL transversely and then branch into a network of longitudinal vessels running parallel to the collagen fibres within the ligament. Clark and Sidles (1990) found vessels to be exclusively within the interfascicular membranes of the ACL. The bone-ligament junction is not a major blood supply for the ACL. However, Butler *et al.* (2003) report that although there is bleeding in the knee after injury, the ACL relies on a nutrient supply from the synovium.

Skyhar *et al.* (1985) analysed the effect of continuous passive motion (CPM) on the uptake of nutrients by the ACL. Rabbit models were used and the animals were sacrificed to eliminate the effect of the ACL blood supply. A tracer was injected intraarticularly into both hind knees and the right knee underwent CPM for one hour while the left knee was immobilised as a control.

A greater uptake of the tracer was observed in the ACL of the immobilised knee than the knee that had undergone CPM. It was also noted that CPM facilitates transport of the

tracer out of the joint, as was measured in the quadricep tendon. From this, the authors concluded that the ACL used diffusion as a primary mechanism for nutrient transport. They went on to state that CPM does not increase nutrient uptake by the ACL in this avascular model. No explanation has been provided as to why there was a greater uptake of the tracer in the ACL of the immobilised knee.

In a later paper by this group (Danzig *et al.* 1987), a similar experiment investigating the effect of CPM on the nutrient uptake of the meniscus was performed. In explaining the findings of this investigation the authors mention that the increased transport of the tracer out of the joint during CPM may reduce the concentration of the tracer left within the synovial fluid compared with that of the immobilised knee. This may then result in a lower uptake of the tracer by the intraarticular structures. As such the conclusions made by Skyhar *et al.* (1985) may be flawed if this was not considered.

In a subsequent paper by the same group (Pedowitz *et al.* 1989) the knee intraarticular pressure (IAP) was measured during CPM. The IAP was found to vary with knee flexion/extension and subatmospheric pressures were attained at mid-flexion (40° – 50°). As the knee moved from full extension to 90° flexion and back to full extension again, a hysteresis effect was observed showing that energy dissipation can occur due to the viscoelasticity of the joint capsule and surrounding tissue. Pedowitz *et al.* hypothesised that the cyclic variation of the IAP leads to a pumping action which acts to move fluid and diffusible particles from the joint space into the intraarticular structures.

In an immobilised rabbit knee an increase in synovial fluid volume was observed which may be a way to replace the motion-induced pumping action (Pedowitz *et al.* 1989).

This suggests that both the vascular system and the synovium, possibly combined with the cyclic intraarticular pressure induced by knee articulation, are important for nutrient supply and mass transfer to the ACL.

1.3 Cytology

Biological tissue such as ligaments are made up of somatic (body) cells, extracellular matrix (ECM) and extracellular (or interstitial) fluid. The cell membrane provides a physical barrier between the interstitial fluid and the cell cytoplasm. This allows the cell to maintain a very different intracellular environment to the extracellular environment. The cell membrane also regulates the exchange of ions, nutrients and waste products

between the internal and external environments. The cell membrane is sensitive to changes in the extracellular fluid and has receptors which recognise specific molecules in the environment and may then trigger a response from the cell (Martini 2001).

The cell membrane consists of two layers of phospholipids with the hydrophobic lipid portions of the phospholipids orientated to the centre of the cell membrane. The cell membrane is 6-10nm thick and the hydrophobic nature of the lipid portion of the membrane prevents the penetration of water and solutes (Martini 2001).

Several types of proteins are involved in the cell membrane and these can either cross the membrane (integral proteins) or be bound to the inner or outer membrane surface (peripheral proteins). There are many more integral proteins than peripheral proteins. The membrane proteins can be specialised as, for example, anchoring proteins, recognition proteins, enzymes, receptors, carriers or channels (Martini 2001). Some of these proteins will be discussed later in further detail.

Attached to the membrane are carbohydrates, such as proteoglycans, glycoproteins and glycolipids, which extend from the external surface of the cell membrane forming the glycocalyx layer (Martini 2001). This is a viscous layer which acts to lubricate and protect the cell membrane. The membrane carbohydrates are sticky to aid anchorage and locomotion. The carbohydrates can act as receptors to specific extracellular compounds and are recognition molecules for the immune system.

The cytoplasm is the material found between the cell membrane and the nuclear envelope. It consists of the cytosol and organelles. The cytosol is the fluid portion containing dissolved nutrients, ions, waste products and dissolved or undissolved proteins. Organelles are structures within the cell that can perform specific functions such as controlling cell structure, maintenance and metabolism (Martini 2001). Organelles can be membranous or non-membranous depending on if they have a membrane to completely separate them from the cytosol.

An important organelle from the biomechanics perspective is the non-membranous cytoskeleton. This acts to give the cytoplasm strength and flexibility and is composed of microfilaments, intermediate filaments, microtubules and, in muscle cells, thick filaments (Martini 2001).

Microfilaments are protein strands with a diameter less than 6nm. They are typically composed of the protein actin and are usually found towards the cell periphery. They anchor integral proteins to the cytoskeleton, thus providing additional strength to the cell and securing the cell membrane to the cytoplasm (Martini 2001). Microfilaments can help to determine the consistency of the cytoplasm. A dense network of microfilaments gives the cytoplasm a gelatinous consistency, whereas dispersed microfilaments will give the cytoplasm a fluid consistency. Also, actin can interact with the protein myosin to give active motion of a cell portion or to change the shape of the whole cell (Martini 2001).

Intermediate filaments have a diameter between 7nm and 11nm. They provide additional strength and stability to the cell and stabilise the position of organelles within the cytoplasm. Intermediate filaments are attached to the cell membrane which acts to stabilise the position of the cell with respect to other cells. Intermediate filaments are insoluble and therefore are the most durable fibre in the cytoskeleton (Martini 2001).

Microtubules are hollow tubes composed of the protein tubulin and are the largest component of the cytoskeleton, having a diameter of approximately 25nm. They originate from the centrosome of the cell (the arrangement of centrioles composed of microtubule triplets which are responsible for chromosome movement during cell division and organisation of the cytoskeleton) and spread out towards the periphery. Microtubules anchor the position of major organelles and are the primary component of the cytoskeleton providing strength and rigidity to the cell (Martini 2001). A change in cell shape can be achieved by the disassembly of microtubules and this may possibly assist in cell movement. Also, proteins called 'molecular motors' can actively 'walk' organelles and other materials along the microtubules. Microtubules form the spindles during cell division to distribute chromosomes and form other organelles such as centrioles, cilia and flagella (Martini 2001).

1.4 Mechanobiology

Mechanobiology is the study of how mechanical stimuli regulate biological processes. Morphogenesis, the development of a cell's structural shape or form, is controlled by internal forces within the cell and external stimuli involving the cells and the extra-cellular matrix (ECM) (Cowin 2003).

A network of actin microfilaments can develop in the cytoskeleton of the cell. Actin is the most abundant cell protein and its polymerisation and depolymerisation ability is of great importance as this gives the actin cytoskeleton the capacity to change the cell morphology by the generation of contractile forces. This, in turn, is essential to many cell functions such as cell migration.

Integrins are glycoproteins which act as cell surface receptors and are a link between the ECM, the cell surface and the cytoskeleton. Ligands are short amino acid sequences on the ECM which bind to the integrin molecule (Simmons & Mooney 2003). Integrins are directly linked to the cytoskeleton filaments and the nucleus and they transfer mechanical stimuli directly into the cell. Due to this pathway, the interaction of integrins and ligands is responsible for a number of cellular actions including adhesion, migration, cell proliferation, secretion and morphological changes (Simmons & Mooney 2003). This linkage of the matrix to the integrin molecule and of the integrin molecule to the cytoskeleton not only means that the cell can detect mechanical stimuli from the matrix but it can also be used by the cell to exert force on the ECM (Banes *et al.* 2003).

The cell can detect or respond to mechanical stimuli by a number of other mechanisms in addition to the integrin molecules. These include ion channels, gap junctions and hemichannels. Ion channels allow ions to pass across the cell membrane and can be activated by strain, voltage or ligand attachment, whereas gap junctions and hemichannels allow molecules to pass between adjacent cells. Gap junctions and hemichannels can be activated by strain or voltage (Banes *et al.* 2003). It has been shown by Banes *et al.* (1999) that cells coordinate their response to mechanical stimuli by communicating through gap junctions. Banes *et al.* (1999) also showed that tendon cells respond to mechanical loading by releasing calcium through these channels thus, ultimately, affecting gene expression.

Simmons and Mooney (2003) noted that the ECM is a major factor in the response of cells to their microenvironment by cell adhesion, force balancing and the release of growth factors.

1.5 Clinical issues regarding the knee joint

1.5.1 Injuries to the ACL

There are in excess of 100,000 ACL injuries per year in North America and around 50% of these undergo ACL reconstruction (Frank & Jackson 1997; Hart *et al.* 2005). Furthermore, approximately 90% of knee ligament injuries involve the ACL or MCL (Woo *et al.* 2006). In the UK, injury to the anterior cruciate ligament is relatively common, often due to sporting activities, and treatment results in a substantial cost to the National Health Service (NHS). In England in 2007 – 2008 there were 6,584 recorded episodes of dislocation, sprain and strain of joints and ligaments of the knee which required 11,073 bed days (Department of Health 2009).

ACL injury causes an increase in joint laxity and joint pain. Major injuries to the ACL have practically no healing ability therefore surgical repair is often required (Woo *et al.* 1997). The results are initially very good following surgery with the knee showing an apparent full recovery, however, in the long term an increase in joint instability and pain has been recorded. Post-reconstruction approximately 20-25% of patients experience problems including instability which can lead to damage of other knee structures (Woo *et al.* 2006).

A number of factors compromise the healing of a partially injured ACL (Hart *et al.* 2005). There are insufficient appropriate cell types available for healing and these combine with components in the intra-articular environment that impair the healing process, e.g. hyaluronic acid which is known to affect the function of many cells (Hildebrand *et al.* 2005), modifiers of cell activity, etc. Additionally, the biomechanical environment is such that it is difficult to control movement at the injury site.

There are a number of reasons why healing of a completely torn ligament does not occur (Hart *et al.* 2005). If the ACL is torn from the femur, the ACL may 'heal' to the PCL by producing a scar. This doesn't help mechanical stability, however, the formation of a scar shows some healing potential within the intra-articular environment. If the ACL tear is mid-substance, the ends cannot find each other in space. Also the ACL preload leads to retraction of the ends increasing the distance between them. Over time post-injury, the ACL ends are resorbed either because of inflammation or lack of mechanical stimulation.

1.5.2 Current therapeutic options

The current therapeutic options for a torn ligament are the ligament healing alone or with augmentation, tissue reconstruction by autograft or allograft, or ligament replacement with a synthetic prosthesis.

However, all these options have problems associated with them. Surgical repair of a torn ACL can prove problematic for a number of reasons (Butler *et al.* 2003). There may be extensive damage throughout the whole of the ligament and the surgeons may experience problems trying to reconnect the correct bundles. Also, there is a limited blood supply to the healing tissue and healing of the ligament occurs in a harsh synovial environment.

Due to this, the patellar tendon repair has become the gold standard in the US. This consists of the removal of the middle third of the patellar tendon including patellar and tibial bone blocks. The bone-tendon-bone graft is then implanted into bone tunnels in the femur and tibia approximately where the ACL attachment sites are. However, hamstring tendon repair has become increasingly popular (Ageberg *et al.* 2009; Herrington *et al.* 2005). Two hamstring tendons (semitendinosis and gracilis) are harvested from the patient, doubled over, and fixed into bone tunnels using a combination of screws, endo loop buttons, cross pins, screw posts and staples (Konan & Haddad 2009).

However, even with these methods, revision surgery is becoming more frequent (Butler *et al.* 2003). Hart *et al.* (2005) report that the poor long-term performance of patellar tendon graft can be attributed to the graft tissue becoming more scar-like over time with the accompanying change in mechanical properties. The tissue can creep and become less functional. Also, poor tunnel position and inappropriate initial graft tension affect the graft performance. Meniscal and chondral injuries, which may have occurred at the same time as the ligament injury, or during the pre-operative stage when mechanical stability was compromised, can also impair the success of the reconstruction.

This autologous approach also presents problems associated with donor site morbidity with there being issues such as pain, tendonitis, a long recovery period and muscle atrophy (Altman *et al.* 2002a; Cooper, Jr. *et al.* 2006). Also, there may be insufficient patellar tendon tissue for a revision replacement (Cooper, Jr. *et al.* 2006).

Woo *et al.* (2006) add that the ACL acts to resist any anterior tibial load and also a rotational load during particular motions. Current replacement grafts replicate the resistance to anterior loads, however, they are poor at resisting rotational loads. It has been shown that the common single bundle reconstructive procedure places the graft too close to the central axis of the tibia and femur, reducing its resistance to rotation. However, a double bundle reconstruction replicating the AM and PL bundles of the ACL produces results closer to that of the intact knee than the single bundle graft.

This again highlights the importance of considering the two bundles when replacing the ACL or PCL.

Hart *et al.* (2005) mentioned the problem of the graft tissue becoming scar-like over time. Scar tissue differs from normal tissue in a number of ways which have been outlined by Hildebrand *et al.* (2005). It has a different chemical composition compared to normal tissue, for example, the ratio of collagen I to collagen III normally is 3:1 but in early scar tissue the ratio is approximately 1:1. In scar tissue, the matrix is not deposited in an orientated arrangement resulting in severely compromised mechanical properties. Additionally, early scar tissue exhibits increased cellularity and vascularisation compared to normal tissue. The increased vascularity of the healing tissue helps to provide the required nutrients to the increased number of cells. Avascular tissue, such as that of ligaments, does not have the same angiogenic response associated with other scar tissue and therefore healing is poor. However, it is worth noting that although scar tissue is not 'normal', it may still be functional for most activities (Hildebrand *et al.* 2005).

A further issue regarding current therapeutic options is the effect of immobilisation on the injured ligament and the surrounding soft tissue structures. In a rabbit model, following 9 weeks immobilisation of a leg, it took up to 1 year of remodelling to return the MCL bone complex to it original mechanical properties (Woo *et al.* 2006). Woo *et al.* (2006) reported that immobilisation causes negative changes such as subperiosteal bone resorption at the insertion site and microstructural changes to the ligament substance.

Rumian *et al.* (2006) stress-shielded an ovine patellar tendon and then restressed the tendon. They found that the elastic modulus deteriorated and did not recover very well upon restressing. However, the stiffness of the tissue returned to normality much quicker due to an increase in cross-sectional area.

1.5.3 Osteoarthritis

Osteoarthritis (OA) is the most common joint disease in the world and in 2001 was estimated to affect between 1,325,000 and 1,750,000 people in England and Wales (National Institute for Clinical Excellence (NICE) 2001). A report from the Office of National Statistics recorded the prevalence of arthritis and rheumatism in Great Britain in 2003 as 5.1% and 8.6% for the total population of males and females respectively. They also recorded a prevalence of 12.4% and 22.3% for males and females over the age of 65 years respectively (Office of National Statistics 2003). This compares to an estimate from the World Health Organisation of 10% of the world's population having significant clinical problems due to OA (World Health Organisation 2003). Medical care of arthritic patients is costing the National Health Service in the UK approximately £560m – £920m annually in direct costs (National Institute for Clinical Excellence (NICE) 2001).

Over the years OA has proved difficult to fully define. The disease can be categorised into two main forms: primary and secondary. Primary OA is the condition where no local factors are evident that predispose the afflicted person to the arthrosis. Secondary OA is the condition where the diseased state is produced by another systemic condition or previous injury (Moskowitz *et al.* 2006).

There are a number of pathologies which characterise OA. These include focal areas of loss of articular cartilage, hypertrophy of bone in the joint (osteophytes and subchondral bone sclerosis) and thickening of the joint capsule (World Health Organisation 2003). This can produce a number of symptoms for the patient including joint pain, stiffness, loss of function and disability (World Health Organisation 2003). The disease is thought by many to be an inevitable consequence of old age and general wear and tear of the joint.

A number of theories exist as to which tissue changes result in the progression of the arthrosis. The view held by this author and many others is that changes in the soft tissues of the joint, i.e. the ligaments and synovium, affect the structure of the cartilage or bone which leads to the development of OA.

A study by von Porat *et al.* (2004) observed a high prevalence of OA in male athletes 14 years after the repair of an ACL tear. A number of other studies have shown a link between ACL trauma and the development of OA (Cushner *et al.* 2003; Johnston *et al.*

2003; Wohl *et al.* 2001). It is therefore believed that strengthening the ACL post trauma by repair or replacement would impede or arrest the onset of OA.

1.6 Tissue engineering

The need for human tissue has increased over recent years due to advances in surgery, the increasing population and a demand for higher quality of life whilst the availability of these tissues has decreased mainly because of risks of contagious diseases. Currently, in the US more than 120,000 patients per year undergo tendon or ligament repair (Goulet *et al.* 2000). Tissue engineering could potentially help to meet this demand and in the last decade approximately $3.5 billion has been invested worldwide in research and development in the area of tissue engineering (Yarlagadda *et al.* 2005).

It is believed that tissue engineering can provide functional tissue grown *in vitro* which can further develop due to the physical and biochemical conditions *in vivo*. Ideally, the engineered tissue would have the same mechanical properties as the natural tissue and there would be no problems associated with degradation or immunogenic response if the tissue was grown from the patient's own cells. Engineered tissue could also provide scientific models for the study of repair mechanisms and the influence of environmental and cellular factors *in vitro*.

Successful tissue engineering requires cellular components to differentiate into appropriate lineages, a scaffold to provide structural support to the developing cells and a bioreactor to maintain appropriate biochemical, physical and mechanical conditions.

Stem cells or progenitor cells have been used to produce endothelial progenitor cells which can differentiate into the endothelial cells which line the inside of blood vessels. These endothelial progenitor cells can then be seeded onto vascular grafts for implantation. This improves the life of the graft and producing endothelial progenitor cells from stem cells is much more desirable than surgically removing vessels to harvest endothelial cells (Sales *et al.* 2005).

There has been significant success experienced with the engineering of human skin substitutes and it is hoped that this can be repeated with engineered ligaments. However, there continue to be a number of challenges facing ACL tissue engineering which need to be addressed (Goh *et al.* 2003; Hart *et al.* 2005). Appropriate density and differentiation of suitable cells needs to be achieved whilst a suitable scaffold material and design needs

to be developed. The optimal biomechanical and biochemical environment has yet to be determined and currently the majority of engineered ligaments do not achieve the required strength *in vivo*. At present the rate of tissue regeneration is too slow and parameters for engraftment need to be improved as, with current techniques, problems arise due to the abnormal interface between host bone and the new tissue. Finally, biological diversity of patients creates a broad requirement specification for the engineered tissue.

A population of cells for seeding on a tissue engineering scaffold could be grown from differentiated ligament cells. However, a potential disadvantage of using differentiated cells rather than mesenchymal stem cells (MSCs) is that as the population is expanded from a small sample there is a greater risk of altering the cells. Telomeres, the short lengths of DNA on the ends of the chromosomes in differentiated cells, shorten each time the cell divides. After so many divisions they are short enough to impair cell proliferation and function (Hart *et al.* 2005).

Cooper *et al.* (2006) seeded a PLLA braided scaffold with fibroblasts from the ACL, MCL, patellar tendon (PT) and Achilles tendon. Cell proliferation and matrix deposition was observed, however, the matrix was not orientated as no mechanical loading was applied. The tendon fibroblasts had faster proliferation whereas ACL fibroblasts were better at matrix production (Cooper, Jr. *et al.* 2006). Therefore, the authors concluded that ACL cells would be most suitable for further study due to their matrix production abilities.

Hart *et al.* (2005) state that mechanical loading acts as a control for matrix synthesis and remodelling. They also report that *in vitro* loading of engineered tissue would probably lead to increased synthesis and expression of matrix and suppression of molecules which would degrade the matrix or scaffold. The biomechanical environment relates to changes in stress, strain, fluid pressure, fluid flow and cellular deformation behaviour (Yarlagadda *et al.* 2005). Altman *et al.* (2001) report that the regulation of mesenchymal progenitor cells can be controlled by load, electromagnetic fields and ultrasound.

In 2001, Altman *et al.* (2001) produced ligament-like cells from mesenchymal progenitor cells by the application of mechanical stress. As the serum could support any cell type and was not ligament specific, it appears the mechanical loading was responsible for the differentiation of the bone marrow stromal cells (BMSCs) into the ligament-like cells.

Also, it has been shown by Maskarinec and Tirrell (2005) that mechanically directed migration can occur where cells move to stiffer parts of a matrix.

Different growth factors negate or amplify the effect of the mechanical strain applied to the developing tissue (Stegemann *et al.* 2005). Therefore, combined stimulation by biochemical and mechanical factors is essential to understand how the signalling pathways are linked and interdependent (Stegemann *et al.* 2005).

The natural ACL is loaded to only a portion of its ultimate strength, therefore, Hart *et al.* (2005) believe that engineered tissue does not need the same mechanical properties as the natural ACL at the time of implantation. In addition, changes to the remaining tissue in the joint post-injury may result in the requirements from the replacement tissue being different from that of the natural ACL (Hart *et al.* 2005).

Hart *et al.* (2005) reported that in order to assess the success of the replacement tissue a number of factors need to be evaluated. These include restoration of joint kinematics, increasing strength of implanted tissue with time, and whether the tissue assumes the histological and biochemical phenotype of the ACL with time (regenerative response) or if it becomes scar-like tissue (injury and healing response).

The development of scar-like tissue is not necessarily a bad outcome as it eliminates the need to harvest patellar/hamstring tendon and thus eliminates secondary site morbidity.

1.7 Cells for tissue engineering

Depending on the approach to regeneration of the damaged tissue, cells may be required *ex vivo* to populate the replacement tissue. If this is the case, there are a number of cell sources available to the tissue engineer. These are summarised in Table 1-3, along with the immunogenic and manufacture or supply implications of each cell source.

It should be noted that allogeneic tissue-engineered skin is currently produced, however, this does not illicit an immunogenic response because the fibroblasts and keratinocytes do not express major antigens (Nerem 2000). As has been suggested in Table 1-3, it may be possible to engineer immune acceptability for allogeneic cells, thus preventing the need for immuno-suppression therapy (Nerem 2000).

Table 1-3 Cell source (Nerem 2000)

Type	*Source*	*Immunogenicity*	*Manufacture/Supply*
Autologous	Patient's own cells	Immune acceptable	Does not lend itself to off-the-shelf availability
Allogeneic	Cells from another human source	May require engineering immune acceptance	Lends itself to off-the-shelf availability
Xenogeneic	Cells from a different species	May require engineering immune acceptance and the potential for animal virus transmission is a concern	Lends itself to off-the-shelf availability

The cell source selected for an engineered tissue has a major effect on the manufacturing process used. There are two possible approaches: a patient-specific tissue or a mass produced off-the-shelf tissue. An approach to produce patient-specific tissue would require the use of autologous cells. This negates any difficulties arising from noncompatibility with the patient's immune system (Hardin-Young *et al.* 2000). To obtain the required number of cells in the tissue either cell expansion or cell recruitment need to occur (Hardin-Young *et al.* 2000). For cell expansion a sample of healthy tissue is harvested as a biopsy. The cells contained in the biopsy are grown in culture and then reimplanted into the patient. Cell recruitment requires the migration of cells *in vivo* to the tissue and this may be achieved by the manipulation of the environment with, for example, growth factors.

Cell expansion is a relatively time consuming process (Hardin-Young *et al.* 2000). This places a critical limitation on the suitability of the technique, particularly in emergency applications. Also, there may be insufficient healthy tissue available to biopsy which again limits the suitability of the technique. Finally, there are serious cost implications for the manufacture of patient-specific tissue which may limit the feasibility of using the technique clinically (Hardin-Young *et al.* 2000).

A mass produced off-the-shelf tissue can be manufactured with the use of allogeneic cells thus alleviating the problems associated with limited supply of healthy tissue and therefore of suitable cells. The allogeneic cells can be screened and banked to produce a supply of safe and functional cells for tissue engineering (Hardin-Young *et al.* 2000). This reduces the variability associated with patient-specific manufacture and allows a more reproducible and consistent production method and final product. Reduced variability allows for a more cost effective manufacture of the tissue making it available when the patient needs it (Hardin-Young *et al.* 2000). There may be immunogenic issues

with the use of allogeneic cells. This may require the use of immunosuppressive drugs following implantation or for the cells to be engineered to prevent them eliciting an immunogenic response, as has been previously mentioned.

There are also a number of different types of cells from the selected cell source which can be used for tissue engineering. Figure 1-8 summarises the most common cell types currently utilised in research programmes and how these cells are related to each other.

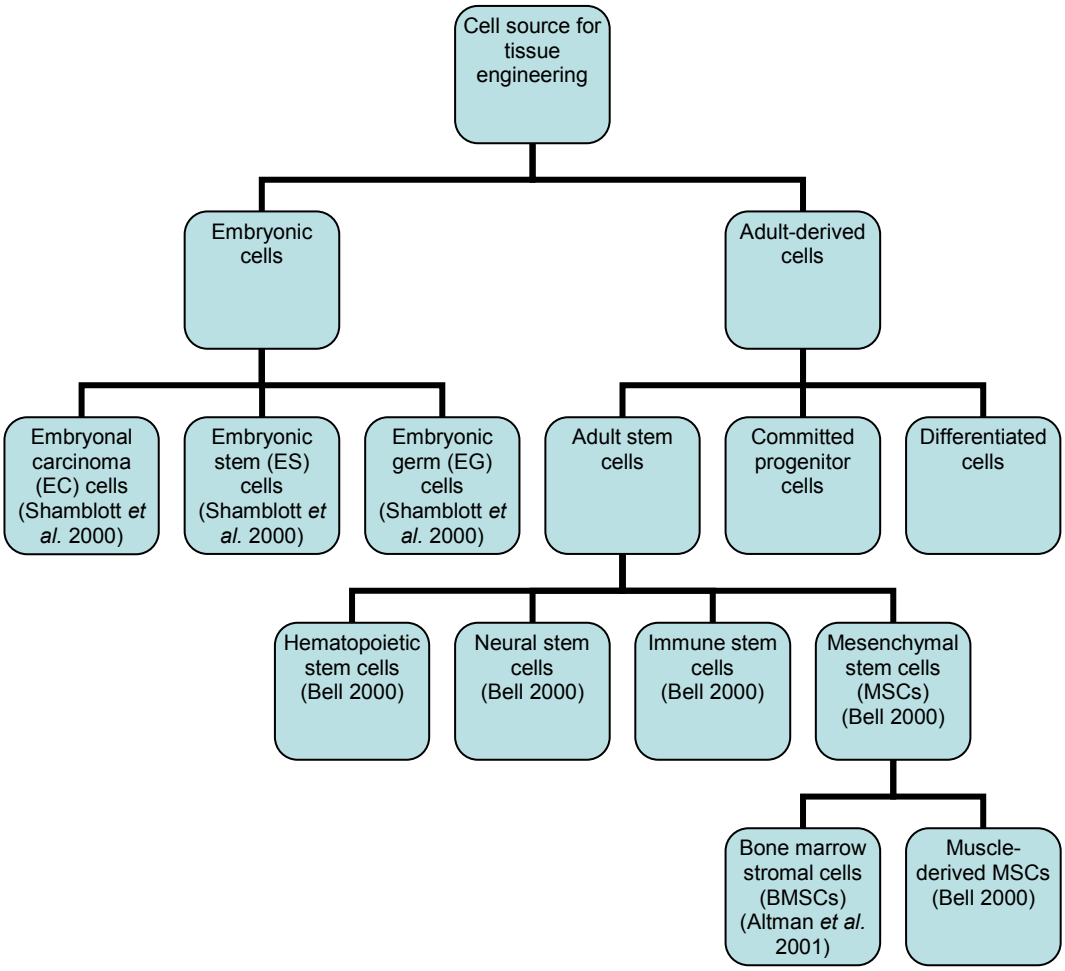

Figure 1-8 Cell types currently being investigated for use in tissue engineering

Stem cells are relatively unspecialised cells whose only function is to produce daughter cells (Martini 2001) which can then differentiate to create all the different cells in the body. They are thought to have unlimited replication potential and, therefore, are self-renewing (Enderle *et al.* 2000). Stem cell potency is the breadth of function which can be adopted by their differentiated daughter cells (Shamblott *et al.* 2000). The following terms are used to describe a continuum of possibilities for the number of different daughter cell types (Shamblott *et al.* 2000):

- Unipotent – one daughter cell type
- Oligopotent – a few daughter cell types
- Multipotent – many daughter cell types
- Pluripotent – most daughter cell types
- Totipotent – all daughter cell types

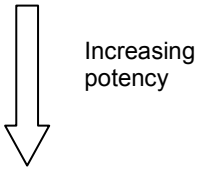

Martini (2001) states that a stem cell divides (by mitosis) producing two daughter cells. One daughter cell differentiates and specialises and the other remains an undifferentiated stem cell. However, Enderle *et al.* (2000) reports that there are a number of stem cell proliferation models. The clonal succession concept hypothesises that there is a reservoir of dormant stem cells. When required, a stem cell is activated and undergoes proliferation and differentiation. Eventually the cell 'burns out' and a new stem cell is activated to replace it. Alternatively, there is a theory of deterministic self maintenance and self-renewal whereby a stem cell divides and one daughter cell undergoes differentiation while the other remains a stem cell. Finally, the stochastic model hypothesises that division of a stem cell can produce either zero, one or two stem cells as daughter cells.

The cells used for tissue engineering can be either embryonic or adult derived. Embryonic cells have high potency and therefore are thought to have a lot of promise to deliver successful tissue engineering, however, there are many ethical concerns relating to their use. Embryonic cells can be extracted from embryos developed during IVF treatment which have not been implanted and which have been donated by the parents (Bell 2000). Also, embryonic stem cells can be recovered from human foetal tissue (Bell 2000). Only a few pluripotent cells have been identified including embryonal carcinoma cells, embryonic stem cells and embryonic germ cells (Shamblott *et al.* 2000).

Adult-derived cells include adult stem cells. As can be seen from Figure 1-8, there are a number of different adult stem cells including mesenchymal stem cells (MSCs) which are of particular interest in the orthopaedic field. This is because MSCs are multipotent (Shamblott *et al.* 2000) and can differentiate into cells which make up tissues such as bone, cartilage, muscle, bone marrow, tendons and ligaments (Figure 1-9). Bone marrow stromal stem cells are a type of mesenchymal stem cell (Reddi 2000) and therefore the bone marrow is often used as a source for MSCs. However, even in bone marrow, these cells are particularly rare and the MSC concentration in young adults is approximately

200 cells per ml of whole bone marrow (Bruder & Caplan 2000). Figure 1-9 shows the differentiation process of MSCs. The pathway which the MSC follows during differentiation is determined by the biochemical and mechanical conditions experienced by the cells. This will be discussed in greater detail in the next Section.

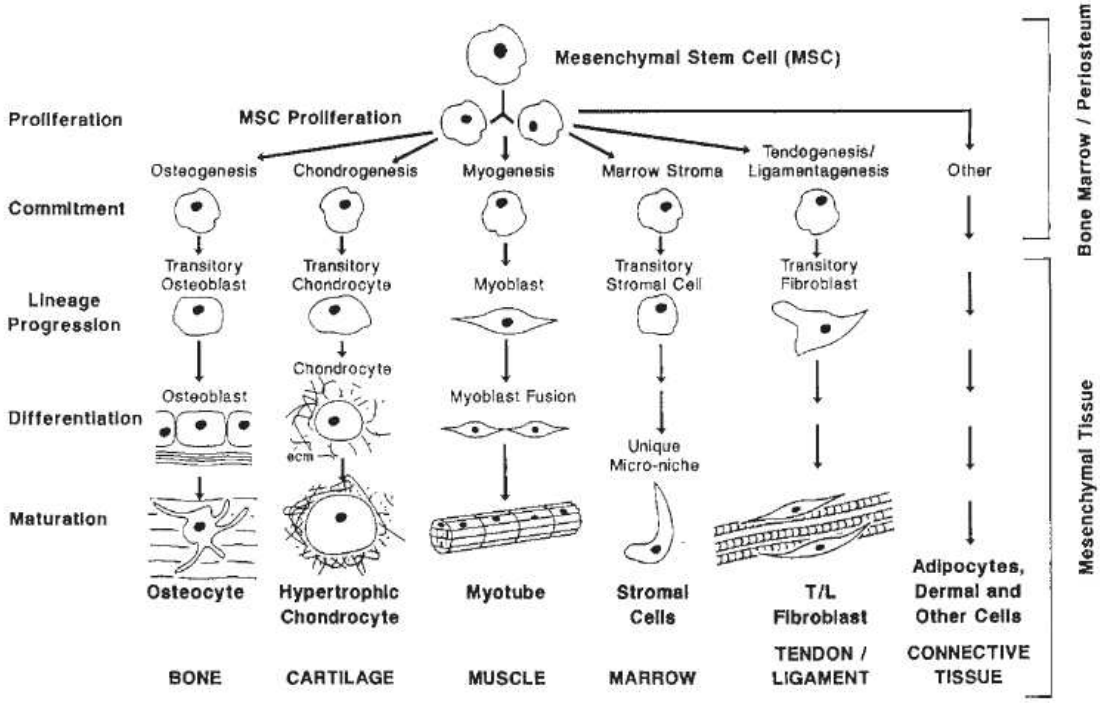

Figure 1-9 The mesengenic process (reproduced with permission from Caplan (2005))

1.8 Scaffolds

Porous scaffolds are used to provide structural support to the developing cells. They need to be made from a biocompatible material to avoid physiological reactions such as cytotoxicity, inflammation or an immune response.

Cells are initially seeded onto the scaffold, however, this can be a difficult process leading to non-uniform distribution of the cells (Curran & Black 2005). The cells eventually colonise the centre of the scaffold by migration and tissue ingrowth and receive nutrients via diffusion (Botchwey *et al.* 2003). It is thought by some that a high density of cells on the exterior of the scaffold depletes the nutrients supply before it diffuses to the interior cells (Botchwey *et al.* 2003). Diffusive limitations can also inhibit the release of metabolic waste and cytotoxic degradation products from the scaffold and this, combined with the inadequate oxygen and nutrient supply to the interior, can result in a core of necrotic cells (Botchwey *et al.* 2003; Curran & Black 2005). Attempts have been made to alter scaffold geometries to improve their diffusive properties and some successes have been achieved, however, diffusive limitations of 3D scaffolds still remain

a problem (Botchwey *et al.* 2003). A way to overcome these limitations in the design of scaffolds for ligament tissue engineering would be to construct a longer and thinner scaffold and then, when the tissue has developed, fold it over one or two times. This is similar to the approach currently used for ACL repair using a hamstring tendon graft. The thinner scaffold will reduce the distance over which diffusion occurs, thus improving the nutrient supply and waste removal for the internal cells. However, this may not be sufficient to resolve the current limitations associated with graft fixation.

An alternative method of cultivation of cells involves the use of biodegradable microcarriers. These encourage the cells to proliferate and aggregate with the correct environmental conditions (Chen *et al.* 2006). Cells which have developed on microcarriers may not have adequate mechanical support, however, these can be seeded onto a macroscopic scaffold or hydrogel to facilitate functional tissue development (Chen *et al.* 2006). This method is thought to improve the distribution of the cells and reduce the development of the core of necrotic cells. Microcarriers are also being developed to deliver chemicals such as growth factors to stimulate cell proliferation deep within the tissue with an appropriate time release (Zhu *et al.* 2008).

Altman *et al.* (2002a) seeded cells onto a silk fibre wire-rope design (this is discussed further in Section 1.8.4). With the seeding methodology used, cells appeared to form a 'wall' around the surface of the bundles preventing infiltration of the cells into the fibres in the bundle core. They identified a need to study different seeding methodologies including perfusion and bird-caging (separation of the bundle fibres caused by applying a compressive load) of the matrix during seeding.

Scaffolds can be natural or synthetic, and temporary or permanent (Yarlagadda *et al.* 2005). Young patients have a high tissue growth rate and as such a temporary scaffold is usually most suitable (Yarlagadda *et al.* 2005). This is because degradable polymer scaffolds require a high proliferation rate to replace 'defects' left by the degrading polymer with new cellular and matrix material (Hart *et al.* 2005; Stegemann *et al.* 2005). Defects greatly affect the mechanical properties of the scaffold and as such may compromise function (Hart *et al.* 2005).

However, older patients have a relatively low tissue growth rate and therefore, permanent scaffolds or temporary scaffolds with a very low degradation rate may be most suitable (Yarlagadda *et al.* 2005). Permanent titanium scaffolds have been used for a number of applications such as oral and maxillofacial surgery, however, these are associated with

problems including stress shielding, poor wear, and modulus mismatch (Yarlagadda *et al.* 2005).

Degradable scaffolds should be designed to degrade at a rate suitable to the rate of tissue development to ensure there is sufficient mechanical support for the developing tissue (S. Curran, *pers.comm.,* 19th April 2005). This is illustrated in Figure 1-10 below. As the mass and strength of the scaffold material reduces due to degradation, it is essential that the mass and strength of the developing tissue increases. This ensures that the whole structure has an overall strength which is sufficient to perform the required function.

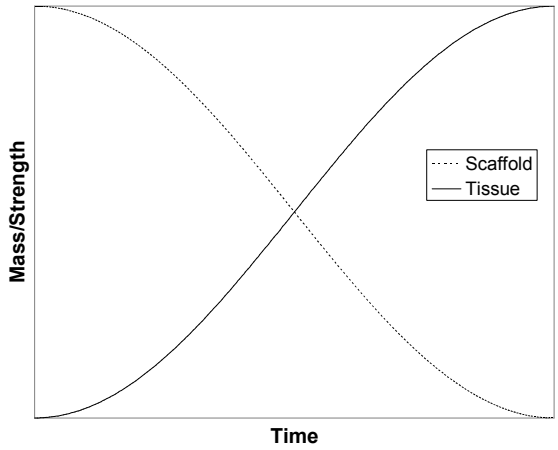

Figure 1-10 Rate of scaffold degradation compared to tissue development

There are a number of different types of degradable scaffolds including degradable polymers, naturally derived protein matrices and decellularised native tissue (Stegemann *et al.* 2005). These scaffold types will be discussed in more detail in the next sections.

1.8.1 Degradable polymers

There is a wide range of synthetic degradable polymers which could be used as a matrix material for tissue engineering. These include:

- Poly Lactic Acid (PLA) (Woo *et al.* 2003; Yarlagadda *et al.* 2005)
- Poly Glycolic Acid (PGA) (Woo *et al.* 2003; Yarlagadda *et al.* 2005)
- Poly-L Lactic Acid (PLLA) (Yarlagadda *et al.* 2005)
- Poly Lactic Glycolic Acid (PLGA) (Woo *et al.* 2003)
- Polyhydroxylbutyrate (PHB) (Yarlagadda *et al.* 2005)
- Polycaprolactene (PCL) (Yarlagadda *et al.* 2005)
- Elastin-Like Polymer (ELP) (Maskarinec & Tirrell 2005)
- Hydrogels (Yarlagadda *et al.* 2005)

Polyesters and copolyesters of naturally occurring hydroxy-acids such as glycolic and lactic acid have been extensively used as biomaterials over the years, including as degradable sutures (Hubbell 1995). These polymers are hydrophilic and degradation is a consequence of the ester bonds being hydrolytically unstable (Hubbell 1995). The polymers are biocompatible because their degradation products are simply glycolic and lactic acid which are also produced in the body. However, some inflammation may arise because as the polymer breaks up it is taken up by macrophages (Hubbell 1995).

The chemical, mechanical and degradation properties of a co-polymer can be controlled by altering the ratio of the constituent polymers. The degradation time for PLA and PGA *in vivo* is typically between six months and one year (Hubbell 1995). However, by forming a co-polymer of PLGA the life of the material *in vivo* is reduced to a few months (Hubbell 1995), while it retains the tough amorphous structure of PLA. Lu *et al.* (2005) carried out a scaffold optimisation study for ligament tissue engineering using PLLA, PGA and PLGA braided scaffolds.

Another option as a possible scaffold material is liquid Elastin-Like Polymer (ELP) (Maskarinec & Tirrell 2005). This would be particularly useful for cartilage repair. The polymer is liquid at room temperature and can hold chondrocytes in suspension, however, when the liquid is injected into the repair site, its temperature rises to physiological temperature at which point the ELP mixture aggregates to a stiff gel with cells entrapped within the matrix (Maskarinec & Tirrell 2005). The required mechanical properties can be achieved by defined cross-linking reactions (Maskarinec & Tirrell 2005).

Also, Yarlagadda *et al.* (2005) note that hydrogels have been used as a matrix material. Hydrogels are hydrophilic polymer chains which cause the matrix to absorb water and the cross linking can be controlled to provide the required structural strength. The matrix has a high permeability to oxygen, nutrients and other waste soluble metabolites providing favourable conditions for mass transfer.

Some of the advantages of using synthetic polymers as scaffold material are that the surface of the polymers can be modified to allow peptides to be attached to the chains (Hubbell 1995). This can be used to encourage or discourage cell attachment. Also, the processing method can allow parameters such as degradation rate, pore structure, pore size, pore distribution and geometry to be controlled (Hubbell 1995). Therefore, a consistent material, suited to the requirements of the application, is produced.

1.8.2 Naturally derived protein matrices

One of the most obvious materials to use as a scaffold for ACL tissue engineering is type I collagen, the main component of the natural ECM of ligaments (Hart *et al.* 2005). Collagen I is commercially available, cells can be incorporated into ligament-like structures by regulating the pH of the collagen solution (Hart *et al.* 2005), and the collagen contains cell adhesion sequences that elicit specific cellular interactions (Yarlagadda *et al.* 2005). Collagen I can be formed to allow mechanical loading, however, it is amorphous when it is poured, i.e. it doesn't have organised linear fibres. Recent developments in generating spun collagen fibres may be able to address this issue (Hart *et al.* 2005). Altman *et al.* (2001) used a collagen gel scaffold for the differentiation of BMSCs into ligament-like cells.

Alginate is another possible naturally derived matrix material. It is a polysaccharide isolated from seaweed and is used as an injectable cell delivery vehicle. However, it does not possess a biological recognition domain like that of collagen (Yarlagadda *et al.* 2005). Alginate discourages protein absorption and cell adhesion, hence it acts like a blank slate. Protein cell receptors can be added to alginate to control cell adhesion, proliferation etc. The addition of appropriate ligands can encourage the desired response while discouraging undesirable ones (Simmons & Mooney 2003).

And finally, silk produced from silkworms is used as a matrix material for ligament tissue engineering because it has unique mechanical properties, its biocompatibility is comparable to that of PLA or collagen (provided the glue-like protein, sericin, has been removed), and growth and adhesion factors can be added to side chains to elicit desirable cellular responses (Altman *et al.* 2002a; Yarlagadda *et al.* 2005). Also, it maintains its mechanical integrity in tissue culture and has a slow degradation rate (Altman *et al.* 2002a).

1.8.3 Decellularised native tissue

Yarlagadda *et al.* (2005) note that acellular tissue matrices are used for the regeneration of genitourinary tissues while Woo *et al.* (2003) note the use of small intestine submucosa (SIS), a porcine collagen matrix, as a scaffold material. Limited research has been conducted using decellularised native tissue for the engineering of ligaments, however, there has been much more research into applications in the vascular system which can also undergo complex loading patterns *in vivo*. In a review of heart valve

tissue engineering, Neuenschwander and Hoerstrup (2004) identify that there are significant possibilities for tissue engineering a heart valve using decellularised allogenic or xenogenic heart valves. Biological heart valves currently in clinical use are either acellular porcine valves that have been fixed with glutaraldehyde such as the Toronto SPV valve (St Jude Medical Inc., St Paul, MN, USA) or acellular bovine pericardial valves, again fixed with glutaraldehyde such as the Carpentier-Edwards Perimount heart valve (Edwards Lifesciences, Irvine, CA, USA). Allogenic or xenogenic matrices can either be seeded with autologous cells or implanted acellular with an aim for cell recruitment *in vivo*.

1.8.4 Scaffold design and manufacture

A range of scaffold materials is required to allow for the control of scaffold degradation and mechanical integrity, cellular interaction with the scaffold, and cellular function (Yarlagadda *et al.* 2005). Surface coatings can be added to improve cell adhesion and the biocompatibility of the material (Yarlagadda *et al.* 2005), while the release of growth factors from the matrix can be controlled by mechanical stimuli (Simmons & Mooney 2003). Composite scaffolds are also an option available to the tissue engineer and may be necessary for loaded tissues such as ligaments (Yarlagadda *et al.* 2005).

The molecules which make up the structure of the biodegradable scaffold can be engineered in particular configurations to optimise the matrix organisation and mechanical properties (Hart *et al.* 2005). It has been shown that a micro-grooved substrate seeded with fibroblasts causes them to organise and produce ECM similar to that produced *in vivo* (Woo *et al.* 2003). Also, if fibres are incorporated into the scaffold design, they provide a large surface area to volume ratio for cell attachment and a path for rapid diffusion of nutrients (Yarlagadda *et al.* 2005).

Scaffold stiffness determines the ability of the matrix to resist cell-based tractional forces. The tractional forces from the cytoskeleton of cells can cause the contraction of a compliant substrate. If the cells are seeded on a compliant substrate then they contract and become rounded. However, if the cells are seeded on a stiff substrate then this leads to a strengthening of the integrin-cytoskeleton linkages, stiffening of the cytoskeleton and the cells are able to spread. Hence, the stiffness of the substrate is a major contributing factor determining the cell shape which in turn plays a major role in cell behaviour and characteristics, for example, growth and differentiation (Simmons & Mooney 2003).

The PLLA braided scaffold used by Cooper *et al.* (2006) for the tissue engineering of an ACL replacement was a square braid with an intraarticular zone of 2.7mm x 23mm x 2.7mm. It was designed with a porosity of 59±12%, a surface area of 70±9cm^2 and a pore diameter of 212±22μm (mean ± standard deviation).

In 2002, Altman *et al.* (2002a) developed a silk fibre wire-rope design as an ACL scaffold. This design had a hierarchical structure with five levels making up the ACL matrix. Two of the levels incorporated a twist – the strand and the cord, and a schematic of the hierarchy is shown in Figure 1-11.

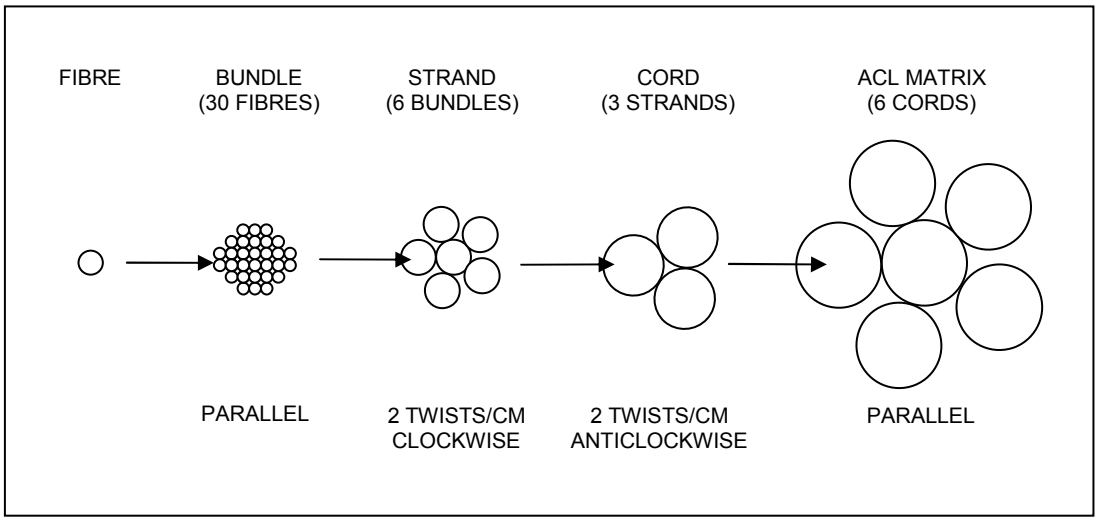

Figure 1-11 Schematic of an ACL 6-cord matrix hierarchy (adapted from Altman *et al.* (2002a))

Altman *et al.* showed their silk fibre wire-rope design to have similar mechanical properties to that of the ACL (Table 1-4) whilst having a smaller diameter. The authors felt this was advantageous as the smaller diameter allowed room for host tissue ingrowth and reduced mass transfer limitations (Altman *et al.* 2002a).

Table 1-4 Mechanical properties of the 6-cord silk matrix compared to that of the human ACL (adapted from Altman *et al.* (2002a))

	Ultimate Tensile Strength (N)	*Stiffness (N/mm)*	*Yield Pt (N)*	*Elongation (%)*
6-cord silk matrix	2337±72	354±26	1262±36	38.6±2.4
Human ACL	2160±157	242±28	~1200	~33

The manufacture of the matrices requires precise control of the porosity and internal pore architecture (Yarlagadda *et al.* 2005). There are a number of techniques available for matrix manufacture including moulding, extrusion, solvent processing, fused deposition modelling (FDM), selective laser sintering (SLS), stereolithography (STL) and direct 3D printing (3DP) (Hubbell 1995; Yarlagadda *et al.* 2005).

1.9 Bioreactors

Recently, there has been a considerable amount of research in the field of tissue engineering aimed at investigating the effect of mechanical stress on cellular differentiation. As such a number of different bioreactors have been developed. Bioreactors are essential to provide a controlled environment to direct cell responses toward a specific tissue type (Altman *et al.* 2002b). Ideally the bioreactor should maintain an appropriate environment (temperature, humidity) and biochemical conditions (pH, pO_2, nutrients, growth factors) to support cell proliferation and differentiation. It also should provide sufficient metabolite transport for the developing tissue in addition to structural support and mechanical conditioning (Altman *et al.* 2002b).

A thorough review of custom-made and commercially available bioreactors was carried out and is presented in Appendix A.

1.9.1 Metabolite transport

Martin and Vermette (2005) identify two distinct flow types during metabolite transport to cultured cells. The culture medium can flow to the external surface of groups of tightly clustered cells (cell lumps) by bulk convection and then the metabolites penetrate the cell lumps by diffusive flow. However, the distance over which diffusion can occur is limited. Martin and Vermette (2005) note that in an hepatocyte culture (liver tissue), cells must be within 150-200μm to be supplied by diffusion alone. In an osteoblast

culture the possible diffusive distance is approximately 240μm (Martin & Vermette 2005).

Martin and Vermette (2005) also state that blood can carry 45 times the amount of O_2 than can be dissolved in culture medium, hence, for large sized tissues, an oxygen-carrying fluid may be required. In addition to oxygen-carrying fluid, tissue irrigation and small cell lumps may be necessary to provide sufficient nutrient and waste transport, especially for large sized tissues. The mass transfer can be modulated by controlling the fluid velocity and cell lump size (Martin & Vermette 2005).

Altman *et al.* (2001) recognise that the differentiation of BMSCs observed in their investigation may have been influenced by the different fluid transport characteristics due to the mechanical loading which was applied. That is, the mechanical forces may have induced fluid flow into the sample which would have altered the mass transport characteristics compared to the controls.

Currently, 2D reactors can produce flat sheets of tissue including skin, liver sheets and cardiovascular patches (Martin & Vermette 2005). However, due to the small thickness of the tissue the mass transport requirements are limited as the tissue can easily be provided with nutrients from the surfaces via diffusion (Martin & Vermette 2005).

Dynamic culture methods are often used to provide a well mixed environment and to supply culture medium flow within and around cells developing on 3D scaffolds or microcarriers (Botchwey *et al.* 2003). Dynamic culture bioreactors include spinner flasks, rotating, annular, perfusion and airlift bioreactors. The most effective dynamic culture method has not as yet been agreed.

The first generation of reactors with a dynamic culture were agitated Petri dishes and spinner flasks (Martin & Vermette 2005). In spinner flasks the stirred culture medium moves past the fixed scaffold. The impeller produces unstable, poorly defined flow fields which can lead to the development of both laminar and turbulent flow regions. This can cause shear damage particularly at the impeller tips (Curran & Black 2005). Also, it has been shown that spinner flasks can lead to a decrease in interior cell density in the scaffold (Botchwey *et al.* 2003).

Rotating and annular bioreactors support the scaffold or microcarriers in continuous free fall within the culture medium. Rotating bioreactors produce a more uniform

distribution of cell growth within a scaffold (Botchwey *et al.* 2003) and annular bioreactors provide a low shear stress environment for tissue development usually using microcarriers (Curran & Black 2005).

Perfusion bioreactors involve the culture medium being directly perfused through the developing tissue by a uniform pressure. This produces a uniform distribution of cell growth through the developing tissue (Botchwey *et al.* 2003). Bancroft *et al.* (2003) developed a perfusion bioreactor for bone tissue engineering. The perfusion flow is top-to-bottom to ensure no air bubbles get trapped beneath the scaffold which would disrupt the flow. The scaffold is held in a cassette which can easily be changed to accommodate different scaffold sizes. Also, the scaffold can be made in the cassette to ensure a tight fit, thus preventing non-perfusion flow around the outside of the scaffold. The bioreactor produced by Altman *et al.* (2002b) for ACL tissue engineering utilised perfusion flow through the scaffold and annular flow linearly along the exterior length of the developing tissue.

Airlift bioreactors have also been developed, where agitation of the culture medium is achieved by the buoyancy of air bubbles passing up through the culture. However, it has been shown that as the bubbles collapse a region of high shear stress occurs and this can reduce the viability of the cells (Curran & Black 2005).

Hollow fibre membrane bioreactors employ a network of embedded hollow fibre membranes within the scaffold (Ye *et al.* 2006). These hollow fibre membranes are semi-permeable and the culture medium is pumped through the fibres with the cells seeded externally on the fibres. The pore size of the membrane can control the permeation of molecules in the medium. Oxygen, nutrients, waste products and possibly growth factors can diffuse across the membrane, however, cells are too large to permeate (Ye *et al.* 2006). The network of hollow fibres is similar to a vascular network and provides a more uniform distribution of diffused molecules. It also prevents the cells experiencing large shear stresses due to the fluid flow. Ye *et al.* (2006) have used a hollow fibre membrane bioreactor for the tissue engineering of bone.

A final consideration is that, depending on the method of production of the engineered tissue, it may be necessary to mass produce the particular tissue. This presents a very different problem from a metabolite transport perspective as it is unlikely to be possible to simply scale up a bioreactor used to develop a single piece of tissue. Martin and

Vermette (2005) discuss these issues in great detail and note that mass culture bioreactors do exist for the growth of plant hairy roots and solid-state fermentation.

1.9.2 Mechanisms for application of strain

A number of bioreactors have been developed which provide either uniaxial loading, loading from pulsatile flow or more complex three dimensional loading. The majority of bioreactors developed have applied simple uniaxial cyclic traction to developing tissues (Garvin *et al.* 2003; Goh *et al.* 2003; Goulet *et al.* 2000; Toyoda *et al.* 1998) or to cell-seeded constructs for studying mechanobiology (Peperzak *et al.* 2004). This traction is achieved either by some form of linear actuation directly attached to the seeded scaffold (Goh *et al.* 2003; Goulet *et al.* 2000; Peperzak *et al.* 2004) or by deflecting a rubber membrane with the cells seeded on it via a vacuum force (Garvin *et al.* 2003; Toyoda *et al.* 1998). Banes *et al.* (1999) developed a 7 station uniaxial loading device. The motion was actuated by a cam-driven lever system and a displacement range was achieved by a variable fulcrum position. Hannafin *et al.* (1995) developed a tensile loading device using a d.c. motor-driven linear-screw actuator.

A 3D bioreactor has been developed to apply a pulsatile flow to direct smooth muscle cell alignment in order to grow tissue engineered cardiovascular patches (Sodian *et al.* 2001). Frank *et al.* (2000) developed a bioreactor to apply 3D shear and compression loading to stimulate the growth of cartilage or bone explants.

Altman *et al.* (2002b) have developed a 12 station bioreactor for ligament tissue engineering which can apply multi-dimensional strain to developing tissue i.e. tensile and torsional strain, in an effort to better replicate the loading experienced by a ligament *in vivo*. Lead screws driven by a stepper motor applied the tensile strain and a stepper motor via a gearing system applied the torsional strain. A tensile resolution of less than 0.1μm and torsional resolution of less than 0.1° was achieved.

A summary of the above mentioned studies and their method of loading is shown in Table 1-5.

Table 1-5 Summary of studies mechanically loading biological tissue

Authors	*Study*	*Mechanical loading*	*Loading method*
Altman *et al.* (2002b)	Tissue engineering of an ACL	Tensile and torsional	Tensile: lead screws driven by stepper motor Torsional: stepper motor and gear system
Banes *et al.* (1999)	Response of tendon cells to mechanical loading	Tensile	Cam-driven lever system
Frank *et al.* (2000)	Mechanical stimulation of cartilage/bone cells	Compression and shear	Compression: axial linear stepper motor Shear: stepper motor with gear reduction
Garvin *et al.* (2003)	Tissue engineering of tendons	Tensile	Deflection of a rubber membrane via a vacuum force (Flexcell International, Hillsborough, NC)
Goh *et al.* (2003)	Tissue engineering of tendons/ligaments	Tensile	–
Goulet *et al.* (2000)	Tissue engineering of tendons/ligaments	Tensile	–
Hannafin *et al.* (1995)	Effect of mechanical loading and stress deprivation on tendon properties	Tensile	DC motor-driven linear screw actuator
Peperzak *et al.* (2004)	Study of fibroblast mechanobiology	Tensile	Linear actuator
Sodian *et al.* (2001)	Tissue engineering of cardiovascular patches	Pulsatile	Pneumatic pressure from a respirator pump transmitted through a diaphragm to the culture medium
Toyoda *et al.* (1998)	Study of effect of loading on ACL cells	Tensile	Deflection of a rubber membrane via a vacuum force (Flexcell Corp, McKeesport, PA)

1.9.3 Loading regimes

A number of different strains have been used to stimulate the differentiation of ligamentous cells. Goulet *et al.* (2000) noted that a strain of 6% is the limit beyond which damage must be expected for a natural ligament and used an arbitrary strain of 2.5% which was increased to 5%, whereas Altman *et al.* in 2001 (Altman *et al.* 2001)

used a longitudinal strain of 10% combined with a rotational displacement of 90° (4.5° per mm of length). Altman *et al.* then modified this in 2002 (Altman *et al.* 2002b) to a longitudinal strain of 6.7% combined with a rotational displacement of 90° (3° per mm of length). Raif and Seedhom (2005) showed that there is a strain threshold of 1% below which cell proliferation was not significantly different than specimens with no strain. Loading frequency ranged from 0.0167Hz (one cycle per minute) (Altman *et al.* 2002b) to 1Hz (Goulet *et al.* 2000).

The motion control system used by Altman *et al.* (2002b) allowed the forward and return torsional and longitudinal displacement rates, the maximum amplitude of torsional and longitudinal displacements and the number of repetitions of the loading regime to be controlled. It also allowed rest periods at the home or extreme points to be included.

The stimulation period imposed in a number of studies working with musculoskeletal tissues ranged from one hour of stimulation per day to continuous stimulation for 21 days (Altman *et al.* 2002b; Banes *et al.* 1999; Frank *et al.* 2000; Garvin *et al.* 2003; Hannafin *et al.* 1995; Toyoda *et al.* 1998). However, Rubin and Lanyon (1984) observed that only four loading cycles per day at a physiological strain level of rooster ulnas were sufficient to prevent bone resorption associated with inactivity. Also, no bone changes were observed when the number of cycles was increased from 36 to 1800. This indicates a low number of physiological cycles is required to stimulate bone tissue. As bones are connected to ligaments within the musculoskeletal system it is likely that ligaments would respond to a similar number of loading cycles.

The procedure used to initiate the loading regime is also of great importance. Butler *et al.* (2003) noted that it may be appropriate to ramp up the mechanical stimuli so as to gradually condition the cells as opposed to shocking them. Also, during tensile loading of tendons, Banes *et al.* (1999) cyclically loaded the tendons for 5 minutes to allow the initial creep and load relaxation to reach steady-state and then the clamps were adjusted to remove any slack from the tissue.

1.9.4 Heating, circulation and gas exchange

Heating options have included wrapping the reactor vessel in a water jacket (Chen *et al.* 2004) to maintain a constant 37°C or using a Plexiglas chamber inside a tight-fitting brass casing which was placed on a 37°C heater (Bursac *et al.* 1999). The brass casing distributed the heat evenly to the chamber. Altman *et al.* (2002b) maintained a culture

medium temperature of 37 ± 0.2°C by using four 60W silicone heating strips for each reactor vessel and temperature feedback from thermocouples. Alternatively, Hannafin *et al.* (1995) maintained a temperature of 37°C by placing the testing unit in an incubator.

Altman *et al.* used a multi-channel peristaltic pump to circulate the culture medium at a flow rate of 2.5ml/min for all 12 reactor vessels. Bancroft *et al.* (2003) also used a multi-channel peristaltic pump as this would ensure equal flow is provided to all flow chambers. If a single channel peristaltic pump was used and the flow was branched off it then it would be difficult to accurately control the flow of medium to each chamber. Also, if a recirculating common reservoir is used then cross-contamination can occur between all the reactor vessels.

Bancroft *et al.* (2003) used platinum-cured silicone tubing to provide flow from their pump. This type of tubing was used because it minimised the amount of chemicals leached from the tubing, it limited the amount of protein binding to the inside of the tubing and it was gas permeable to allow for gas exchange of O_2 and CO_2.

The testing unit used by Hannafin *et al.* (1995) was kept in an incubator with a controlled atmosphere of 10% CO_2 whereas Garvin *et al.* (2003) maintained an atmosphere in an incubator of 5% CO_2. The bioreactor utilised by Bancroft *et al.* (2003) incorporates a reservoir for the culture medium. The fluid returning into the reservoir is dropped into the medium below as this allows for enhanced gas exchange and a visual verification of flow.

1.9.5 Scaffold anchorage

Compression of soft tissues can alter their biomechanical properties and therefore the method used to secure the scaffold is very important. In the past a number of attempts to clamp soft tissue have been made including methods such as special loops, fine-cogged steel-clamps, and sheets of metal covered with layers of textile and paper (Wieloch *et al.* 2004). All these methods had problems with the tissue slipping out of the fixation. Riemersa and Schamhardt (1982) developed the 'cryo-jaw'. Essentially this is a snap freezing of the soft tissue ends using liquid nitrogen that were fixed in metal clamps with indentation features. The cryo-jaw uses the interdigitation of the frozen tissue with the indentations of the clamp as the interface for force transfer, therefore the required compression is reduced. This is good for transferring high loads and has been used in a number of applications which mainly test the soft tissue to failure (Donahue *et al.* 2002; Pearsall *et al.* 2003; Sharkey *et al.* 1995; Wieloch *et al.* 2004).

Svendsen and Thompson (1984) developed a clamp made from two mating tapers. The soft tissue is drawn between the two tapers and complete angular squashing of the fibres resulted in no slipping and no cutting of the fibres. Again this was used to test tendons to failure. Weiss *et al.* (2002) used a customised clamp tightened with screws to apply a shear load to a medial collateral ligament and Banes *et al.* (1999) clamped their tendons with a 'serpentine' jaw which forced the tissue through a curve created by a clamped bar. Altman *et al.* (2002b) attached the collagen matrices to the anchors by either embedding the ends in epoxy adhesive (3M DP-100) or by suturing the ends using a 'whip-stitch'. The matrices' ends were then secured to the anchor-shafts via set-screws. However, previously in 2001 Altman *et al.* (2001) used coral and cancellous bone anchors to mimic ligament-bone attachment *in vivo* and to support tissue ingrowth *in vitro*.

2 AIMS AND OBJECTIVES

The biological or synthetic graft materials used in current ACL repairs do not have the same mechanical properties as the native ACL and therefore do not adequately restore the physiological kinematics and kinetics of the knee joint. This can lead to problems of increased joint laxity and pain for the patient in addition to increasing their risk of developing osteoarthritis. Tissue engineering has the potential to grow a graft with improved mechanical properties, however suitable mechanical conditioning is required. A bioreactor did not exist to apply complex mechanical loading to a tissue engineered ligament and monitor the response of the tissue.

The aim of this project was to develop a novel bioreactor with physiological mechanical conditioning for the tissue engineering of anterior cruciate ligaments.

This aim was achieved by meeting the following objectives:

1) To develop a requirement specification for the bioreactor based on current understanding of biology, physiology and ACL kinetics and kinematics.
2) To develop a prototype bioreactor incorporating cyclic tensile loading.
3) To incorporate torsional loading into the bioreactor design.
4) To develop a sealed biological chamber to contain the tissue and prevent contamination or infection.
5) To develop an appropriate tissue clamping technique.
6) To develop a media flow system for the tissue.
7) To develop a control system to apply the required mechanical loading and record the load and displacement parameters.
8) To fully characterise and validate the bioreactor.
9) To biologically validate the bioreactor.

3 DEVELOPMENT OF BIOREACTOR PROTOTYPE

3.1 Requirement specification

A requirement specification for the bioreactor was developed from the information provided from previous research as outlined in the literature review section of this report (Section 1). The requirement specification is summarised in Table 3-1 below and was based on the work of a number of authors (Altman *et al.* 2002b; Banes *et al.* 1999; Cooper *et al.* 2005; Hannafin *et al.* 1995; Raif & Seedhom 2005; Woo *et al.* 1991; Zavatsky & O'Connor 1994).

Table 3-1 Requirement specification for bioreactor

Mechanical loading - Cyclic Tension	
Load range	0N – 400N (Woo *et al.* 1991) Expected max operating load: 100 – 150N
Displacement range	Max: 0 – 5mm (50mm @ 10%) Min: 0 – 0.2mm (20mm@ 1% (Raif & Seedhom 2005))
Frequency	Max: 5Hz Operational: 1Hz Min: 0.0167Hz (Altman *et al.* 2002b)
Control	Load or positional control
Sensors	Must be able to monitor the load and displacement applied to the tissue in real-time.
Mechanical loading – Cyclic Torsion	
Torque	0 – 1Nm
Rotation range	Max: 0° – 150° (Zavatsky & O'Connor 1994) Min: 0° – 10°
Frequency	Max: 5Hz Operational: 1Hz Min: 0.0167Hz
Control	Torque or positional control
Sensors	Must be able to monitor the torque applied to the tissue in real-time.

Table 3-1 cont. Requirement specification for bioreactor

Control program	
Zero load and torque cells	Must be able to zero the reading from the load and torque cells
Preload	Must be able to apply a preload to the tissue
Operating mode	Must be capable of operating in position or load control with closed loop feedback
Loading waveform	Sine, square, triangular and custom wave forms.
Required user defined loading parameters	Frequency Amplitude Pauses at the start and end of the stroke Ramp-up and ramp-down cycles Loading duration
Data capture	Must be able to capture and save positional and load data from the bioreactor.
Required user defined capture parameters	Number of cycles to capture Time interval between capture sessions
Other requirements	Must provide a suitable user interface. Must include appropriate safety features to protect the operator and the equipment.
Biological Chamber	
Chamber volume	15 – 25 ml
Chamber dimensions	Must accommodate a maximum sample size of 30mm long.
Tissue fixation	Tissue must be able to be clamped within the chamber. Must withstand 100N of tensile loading.
Other design requirements	Chamber should be sealed to prevent contamination. Must be easy to assemble. The chamber should be able to be removed from the bioreactor. The sides of the chamber should be clear to permit optical analysis. The design must allow for the changing of medium and cleaning of components.
Media Flow	
Flow type	Flow into the chamber
Flow rate	> 45ml per day Preferably continuous flow: 0.05ml/min – 5ml/min (Altman *et al.* (2002b): 0.21ml/min)
Other flow requirements	Must be capable of supplying up to eight chambers with media.

Table 3-1 cont. Requirement specification for bioreactor

Cytotoxicity / Contamination	
Materials	All materials must be biocompatible. Materials should be able to be sterilised, preferably by autoclave, without significantly altering their properties e.g. Stainless steel, polycarbonate, PTFE.
Other requirements	
Experimental Duration	Max: 3 months Intermittent loading e.g. 8hrs active/day; 2hrs active/day; 10 mins active/day.
Physical requirements	Bioreactor must be able to fit within a standard incubator (600mm high).

In order to replicate the physiological loading of the native ACL, a combination of tensile and torsional loading was required. It was necessary to provide cyclic tensile loading with a maximum load of 400N. This load was estimated from data by Woo *et al.* (1991) as the approximate load provided by a human ACL at 4mm elongation. This was 10.5% strain based on the longest ACL length (Table 1-1). It was expected that a lower strain would require a maximum load of 100 – 150N.

The maximum required displacement range was 0 – 5mm based on a 50mm sample with a 10% strain. The minimum displacement range was 0 – 0.2mm based on 1% strain of a 20mm sample. 1% was the lower strain threshold shown to have an effect on cell proliferation by Raif and Seedhom (2005). The frequency ranged from 0.0167Hz (1 cycle per minute used by Altman *et al.* (2002b)) to 5Hz. An operational frequency of 1Hz was expected as this is typical walking frequency.

The cyclic tensile loading was required to operate in closed loop load or positional control. Appropriate sensors were required to monitor the load applied to the tissue for real-time diagnostics of the loading and post-experiment analysis.

There was no data in the literature regarding the torsional stiffness of an ACL under tensile load, therefore, a maximum torque of 1Nm was specified. The maximum rotational range was based on the work by Zavatsky and O'Connor (1994) shown in Figure 1-7. The frequency range was the same as that of the tensile loading. Closed loop torque or positional control was required, as was torque monitoring.

A program was required to control the bioreactor. It was necessary for the control program to include features to zero the outputs from the load and torque cells and apply

an initial preload to the developing tissue. The bioreactor had to be able to operate in position or load control with closed loop feedback from the encoders or load and torque cells respectively. The loading cycle to be imposed on the developing tissue was to have a sinusoidal waveform. It was also desirable to have the capacity to impose other waveforms such as square, triangular or custom waves. To ensure a versatile loading profile, user-defined loading parameters were required to stipulate the frequency and amplitude of the wave, to hold the tissue at the start and end of the stroke for a period of time and allow the amplitude to be ramped up and ramped down (see Section 1.9.3). Also the duration of the loading session should be able to be defined.

Additionally, the control program was required to capture and save the positional and load data from the bioreactor. The user needed to be able to define the number of cycles to be captured in each capture session and the time interval between each capture session. Finally, the program had to provide a suitable user interface to control the bioreactor and include appropriate safety features to protect the operator and equipment.

A biological chamber was required to house the developing tissue in a sealed aseptic environment. The chamber must also provide the tissue with an appropriate flow of media to replenish nutrients and remove any waste produced. The chamber was required to accommodate a maximum sample length of 30mm and have a volume of 15-25ml. This volume was comparable to the single sample ligament chamber produced by Tissue Growth Technologies (LigaGen L30-1X, Tissue Growth Technologies, Minnetonka, MN, USA) with a volume of 23ml. The biological chamber produced by Bose (Bose Corporation, ElectroForce Systems Group, Minnesota, USA) has a volume of 265ml, however, a smaller chamber was selected to reduce the volume of media required during biological experiments thus reducing the cost of consumables.

The chamber had to be easy to assemble whilst preventing contamination. Ideally it would provide a method for cell seeding with the scaffold already mounted in the chamber to prevent damaging or removing the cells whilst loading the scaffold into the chamber. The chamber had to be able to be removed from the bioreactor and the sides should be optically clear to permit analysis to be performed. The design had to allow for the changing of medium in aseptic conditions and the thorough cleaning of all the components.

It was necessary for media to flow through the chamber to provide fresh nutrients to the tissue and remove any waste products. The flow had to be in excess of 45ml per day to

sustain the tissue. Continuous flow was the preferred flow pattern as it reduced the peak fluid velocity thus reducing the fluid shear on the surface of the tissue. A flow rate of 0.05 – 5ml/min was required for a continuous flow solution. The flow system had to be capable of supplying up to eight chambers with the required medium as that was the maximum number of chambers which could fit within a standard incubator.

The chamber and flow system had to completely seal the tissue and media to prevent contamination. All materials used had to be biocompatible. Materials also had to be able to be sterilised, preferably by autoclave, without significantly altering their properties.

Experiments could run for a duration ranging from one week to 3 months. Loading of the tissue would be intermittent such that the tissue was loaded for a fixed period every day. Finally the bioreactor was required to fit within a standard incubator to regulate temperature and CO_2, therefore, the bioreactor could be a maximum height of 600mm.

A number of additional requirements were identified which would increase the versatility of the bioreactor (Table 3-2). These were not necessary for a bioreactor to tissue engineer an ACL, however, they would allow the device to stimulate other tissue types. Operating the bioreactor in compression in addition to tension would allow the tissue engineering of bone constructs. Meyer *et al.* (2006) applied 0.2 – 2% compressive strain to osteoblast-embedded collagen gel samples of 5mm thickness. This provides a minimum compressive displacement range of 0 – 0.01mm. Also, perfusion flow through the centre of the tissue has been used for bone and ligament tissue engineering and could be a useful feature to include. Finally, cyclic pressurisation of the media surrounding a developing ACL could be used to simulate the pressurisation *in vivo* of the knee joint cavity. This may increase mass flow into the core of the tissue and provide some mechanical stimulation as discussed in Section 1.2.4.

Table 3-2 Additional requirements for the bioreactor

Mechanical loading - Compression	
Additional requirements for alternative tissues	Bone: 0.2 – 2% compressive strain. Therefore, minimum displacement range: 0 – 0.01mm (5mm @ 0.2% (Meyer *et al.* 2006))
Media Flow	
Type	Perfusion
Flow details	Ligament: constant perfusion & annular flow at 0.05ml/min – 1ml/min (Altman *et al.* (2002b): 0.21ml/min) Bone: constant perfusion of 0.025 – 4ml/min (Janssen *et al.* 2006; Vance *et al.* 2005); cyclic perfusion of 0 – 40ml/min @ 1Hz (Vance *et al.* 2005).
Pressurisation	
Pressure range	Should be capable of maintaining hydrostatic and cyclic pressures. Expected pressure range: -20mmHg – +50mmHg (Pedowitz *et al.* 1989)
Frequency	Max: 5Hz Operational: 1Hz Min: 0.0167Hz

3.2 Mechanical loading concept designs

Four concept designs for the mechanical loading system of the bioreactor have been developed and are shown in Figure 3-1 and Figure 3-2. Concept 1 utilises a single motor rotating a leadscrew with a large pitch. Rotation of the leadscrew would cause both linear and rotational motion thus applying the combined tension and torsion to the developing tissue. Concept 2 employs both a motor and linear actuator. The motor is in-line with the upper chamber shaft and provides rotation directly to the shaft. The linear actuator applies tension to the tissue by moving the upper chamber shaft, motor and mounting bracket. Concept 3 employs two hollow shaft motors, in-line with the upper chamber shaft, to provide the tension and torsion. One motor is fitted with a leadscrew to provide linear motion. The other motor is fitted with a spline to transmit torsion whilst permitting linear motion. Rotation of the leadscrew motor with no rotation of the spline motor will cause linear motion. Synchronous rotation of the two motors will cause pure torsion to be transmitted to the tissue with no linear motion. The amount of tension and torsion applied can be adjusted by altering the rotation of the two motors. Concept 4 employs a fixed motor applying rotation to the upper chamber shaft and a linear actuator applying linear motion to the lower chamber shaft.

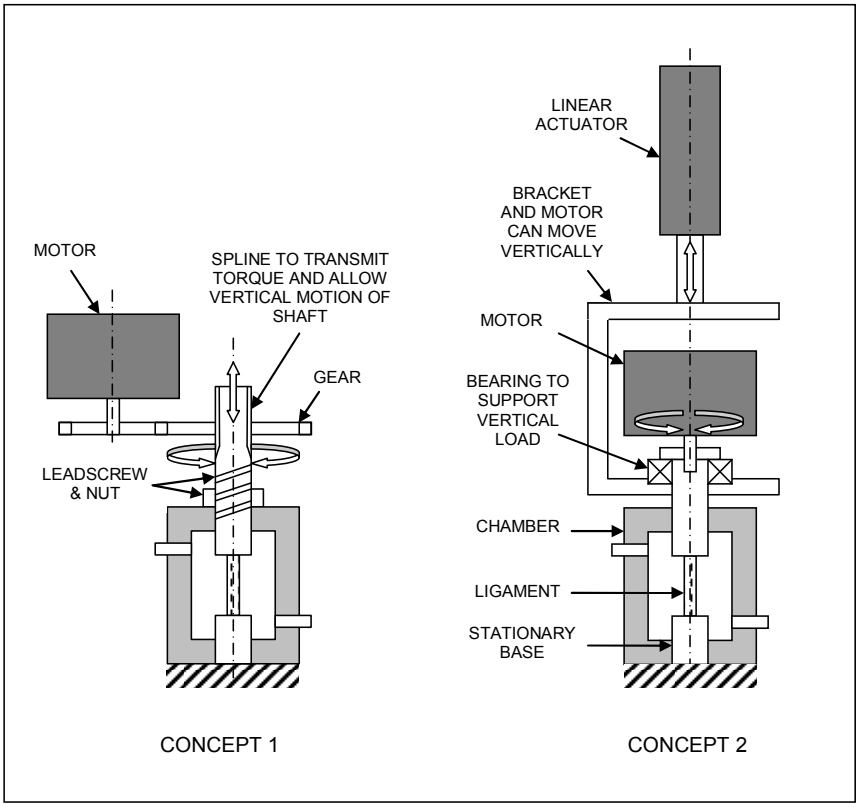

Figure 3-1 Mechanical loading concept 1 & 2

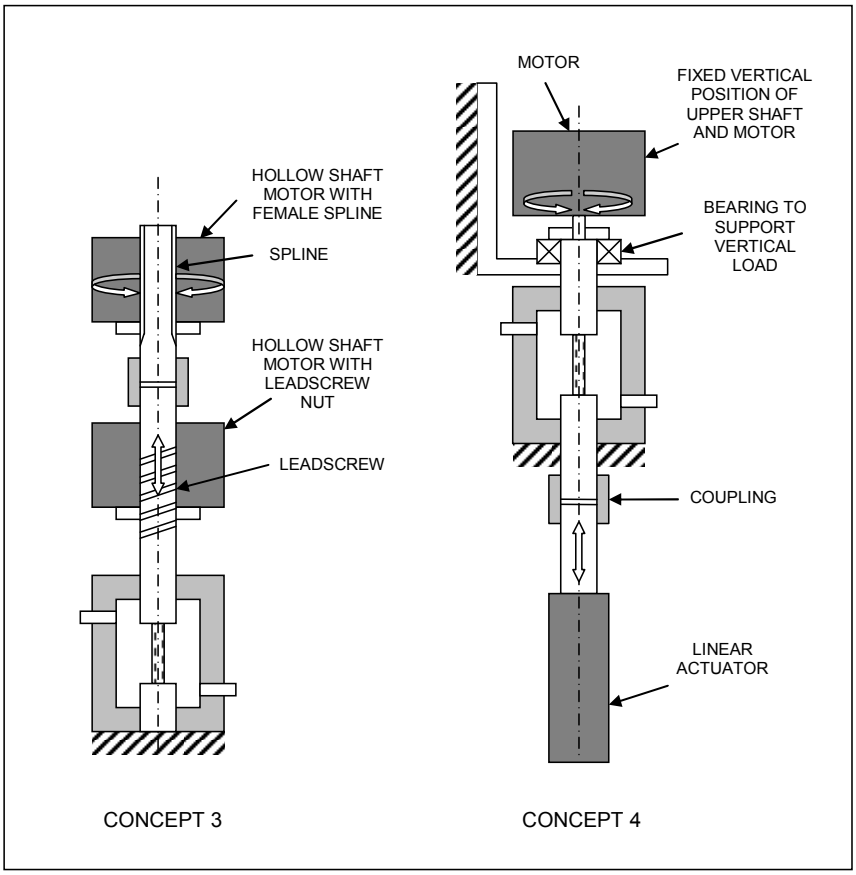

Figure 3-2 Mechanical loading concept 3 & 4

Concept 1 has a fixed ratio of rotational to linear displacement which is defined by the pitch of the leadscrew, for example, a leadscrew with an 8mm pitch would produce a displacement ratio of 45°/mm. Concepts 2 – 4 have a variable displacement ratio controlled by the independent motors and actuators. Another major difference is that concepts 1 – 3 provide both actuations through a single shaft whereas in option 4 the actuation is split between the two shafts, i.e. one shaft provides the rotation and the other shaft provides the linear motion.

The four concept designs were evaluated against a number of design criteria and this evaluation process is shown in Table 3-3. Concept 1 was dismissed due to it having a fixed ratio of rotational to linear displacement. It was considered that the versatility provided by having independent control of the displacements was of great importance and formed a major part of the requirement specification. It was felt that concept 2 may have problems due to the inertia of the motor assembly which provides the rotational motion. As this whole assembly moves with the linear motion, such a design may have poor dynamic response particularly at the higher velocities associated with larger strokes and higher frequencies of operation.

For these reasons options 3 and 4 were considered the most suitable concepts and should be taken forward to a more detailed design stage. This was due in no small part to the variable ratio of tensile to torsional strain offered by these options. As the optimum ratio of tensile to torsional strain has not yet been quantified, independent control of the two strains allows for optimisation of the mechanical loading regime to produce more functional tissue constructs.

It was recognised however that developing a bioreactor with independent control of tensile and torsional strains would increase the complexity of the design, both in terms of the mechanical components and the control system, and this in turn would have an impact on the cost of the device.

Table 3-3 Evaluation of concept designs

Design criteria	*Criteria weighting*	*Concept 1*	*Concept 2*	*Concept 3*	*Concept 4*
Simplicity of design	1	7	6	5	6
Simplicity of control system	1	6	3	3	3
Loading versatility	2	1	10	10	10
Cost effectiveness	1.5	8	6	4	6
Potential for problems (1=high, 10=low)	1.5	8	2	6	7
Weighted Total		**39**	**41**	**43**	**48.5**

3.3 Mechanical loading design development

As mentioned in the previous section, concepts 3 and 4 were taken on to a more detailed design phase to assess their suitability.

Concept 3 utilised hollow shaft motors. Sourcing of housed hollow shaft motors of an appropriate size for this application proved to be quite difficult. However, Harmonic Drive AG (Limburg, Germany) produced a range of housed hollow shaft servomotors of a suitable size utilising their compact harmonic drive gear box (FHA-C mini hollow shaft actuators). These motors were then combined with a high helix lead screw (Abssac Ltd., Evesham, UK) and a spline shaft and nut (THK UK, Milton Keynes, UK). The combination of these components, mounted with the appropriate bearings and supports would produce a system that could meet the mechanical loading requirements outlined in the requirement specification. The design was modelled using 3D CAD software (Solid Edge, UGS Corp, Plano, Texas, USA) and is shown in Figure 3-3 A & B. The two motors are positioned above the bioreactor chamber with a common shaft passing through them into the chamber. The lower shaft is held stationary and attached to load and torque sensors which will be discussed in greater detail in Section 3.4.

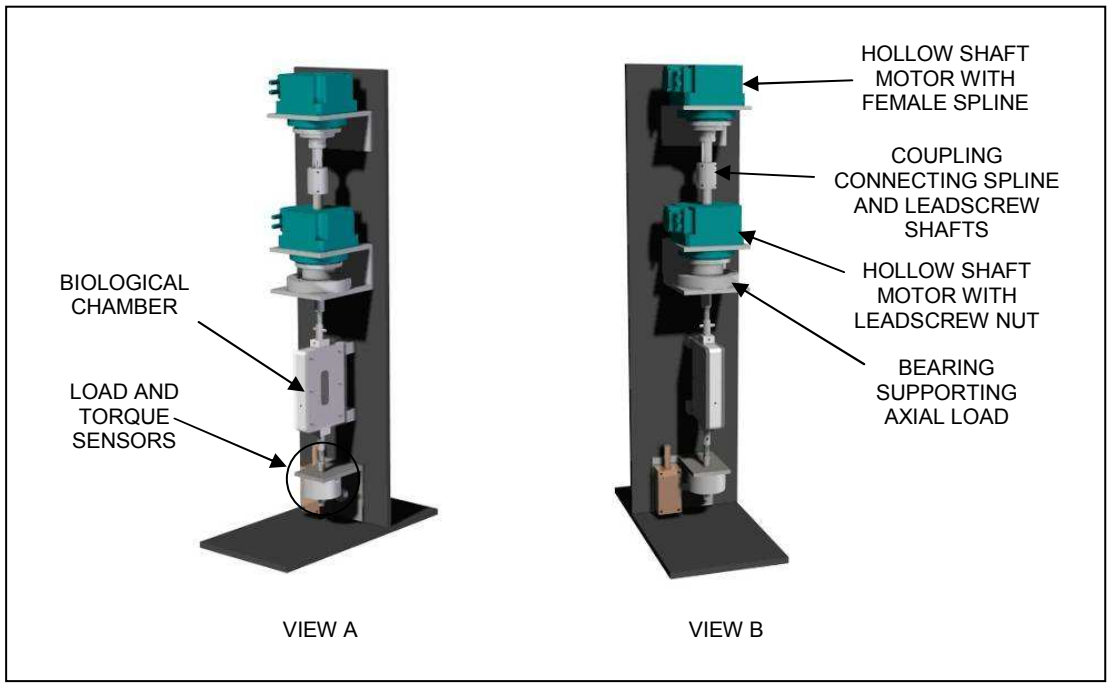

Figure 3-3 CAD model generated for concept 3

There were a number of possible methods for the linear actuation to be used in concept 4. The power source could be electric, pneumatic or hydraulic, however, it was felt that electrical actuation would be the most appropriate as an electrical supply is available in most laboratories, whereas a compressed air source is not always available. A hydraulic

pump would be large, loud and expensive, and leaking hydraulic fluid would be messy and have contamination issues.

Again there are a number of options for electrical linear actuation: a direct drive linear motor, a linear actuator (motor and ballscrew built-in) or a ballscrew and linear slide unit driven by a separate motor. Initial investigation into the possible use of a direct drive linear motor found that, although it may have good dynamics, it would be quite difficult to assemble and will also require additional components such as linear slides to maintain its alignment. In addition it was found to be prohibitively expensive and for these reasons it was deemed to be unsuitable for this application.

The linear actuator or the ballscrew and linear slide unit would be capable of meeting the loading requirements detailed in the requirement specification. However, another element from the requirement specification details geometric constraints. The bioreactor needs to be portable and able to fit within an incubator. Linear actuators tend to be longer components with the motor in-line with the internal ballscrew. With a separate motor and ballscrew unit, the motor can be placed alongside the ballscrew and slide unit with drive being transmitted through a timing belt. This will significantly reduce the height of the bioreactor which is the dominant dimension. Also, buying the motor and ballscrew unit separately reduces the cost of the linear actuation system. It was felt that a separate motor and ballscrew and linear slide unit was the best linear actuation method for concept 4, the CAD model of which is shown in Figure 3-4 A & B. In this design the upper chamber shaft provides the rotation and the linear actuation is provided through the lower chamber shaft. Again load and torque sensors are shown on the lower shaft and this will be discussed in Section 3.4.

The two concepts were evaluated and it was felt that there were advantages to decoupling the linear and rotational actuation as in concept 4. Two separate systems would be easier to build and it would mean that any unforeseen issues which may arise with one of the systems would not affect the other and would therefore be easier to identify and overcome. Also, the hollow shaft motors utilised in concept 3 were significantly more expensive than the mechanical loading components selected for concept 4. For these reasons, concept 4 was selected as the most suitable concept to develop into a prototype.

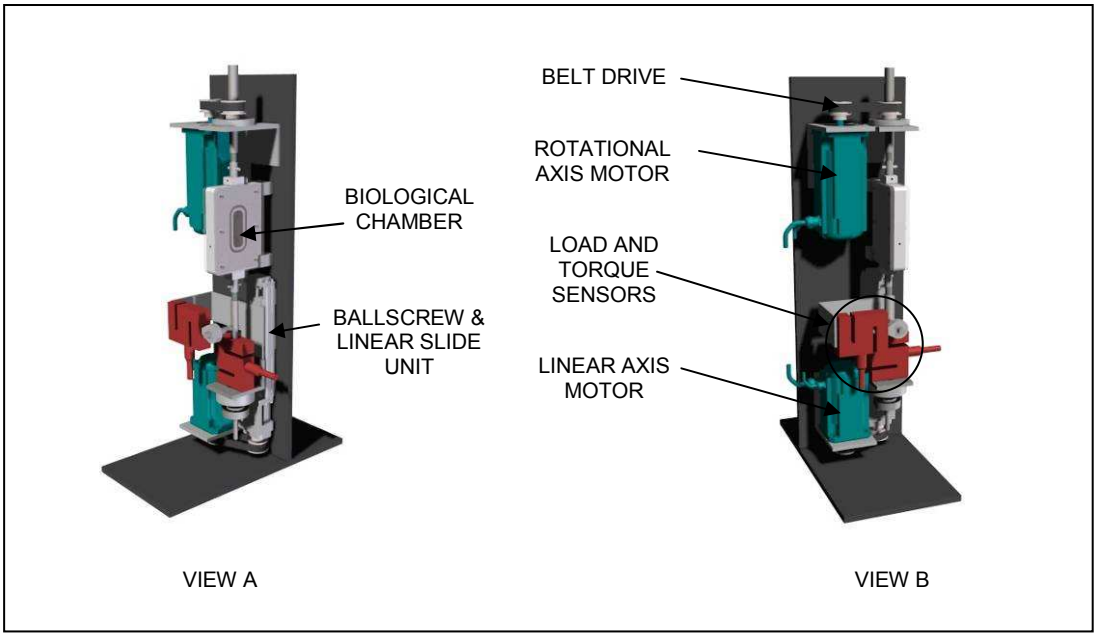

Figure 3-4 CAD model generated for concept 4

3.4 Mechanical parameter sensing

Whichever mechanical loading concept was selected, it was required to use servomotors with encoder feedback. Assuming that all the structures along the mechanical loading path are significantly stiffer than the construct being loaded, the encoder will provide accurate feedback for both the linear and rotational displacement imposed on the construct. This can be used to provide displacement feedback for the control loop and thus allow the bioreactor to operate in displacement control. Also, the encoders will provide real-time displacement data for monitoring and analysis.

It is also necessary for the bioreactor to incorporate load and torque sensing for a number of reasons. Firstly, it provides load and torque feedback to the control loop, thus allowing the bioreactor to be operated in load and torque control in addition to displacement control (further details of this can be found in the control program section of this report). Secondly, load and torque sensing will allow real-time monitoring of these parameters and the combination of this data with the displacement data will allow monitoring of the stiffness of the construct as it develops.

A number of methods were available for sensing the load and torques imposed on the construct. The load could be measured using a commercially available load cell such as an S-beam or washer load cell. Alternatively, a load cell could be built in-house, for example, using strain gauges mounted on a thin aluminium shaft. The torque could be

measured using a commercially available reaction torque cell or a torque cell could be built in-house using a strain-gauged shaft. Another option would be to use a commercially available load cell (e.g. S-beam type) positioned at 90° to the torsion axis to react the torque through a lever at a known distance. There are also commercially available combined load and torque cells.

A number of issues had to be considered when selecting which load/torque cell to use. These included cost and which design of load/torque cell could best be incorporated into the bioreactor. However, the main functional issue was whether the design should isolate the sensors so that the load cell only experiences pure tension and the torque cell only experiences pure torsion. For design reasons, it was felt that totally isolating both sensors would be unnecessary if sensors could be found whose function would not be significantly impaired by experiencing the other load or torque. In-house manufacturing limitations could result in significant 'cross-talk' of the combined loads experienced by a load or torque cell, therefore this option was rejected.

A commercially available combined load and torque cell was considered the preferred option. However, because the scale of the maximum load and torque are significantly different (400N compared to 1Nm) it was not possible to source a suitable component. It would be necessary to order a bespoke component to be designed and manufactured which would be financially prohibitive. Therefore, separate load and torque cells were sourced.

There were two main options for the commercially available load cell: an S-beam type or a washer type. The washer type load cell was more compact than the S-beam type load cell, however, it was significantly more expensive. It could be incorporated into the design with a bearing to measure tensile load whilst preventing the transmission of torsion through the washer load cell. However, it would be more difficult to use the sensor to measure compression in such a configuration. It was felt that the torsional effect on an S-beam load cell would not be significant and the ability to operate the cell in tension and compression was an advantage. Therefore an S-beam type load cell was selected for the final design.

High quality torque cells are very expensive compared to the cost of a load cell. For this reason, the possibility of using a load cell to measure torque was explored. Figure 3-5 shows a possible arrangement to achieve this. A torque is imposed onto the vertical shaft via the developing tissue. This torque is reacted by an S-beam load cell in

tension/compression which is positioned at 90° to the torsion axis and is connected to the main shaft via a lever arm. A rod eye is used to connect the load cell to the lever arm to allow some misalignment. This is the torque sensing method shown in Figure 3-4. However, it was felt that, although this method was sound in theory, due to manufacturing limitations, such as misalignments not allowed for by the rod eye connection, there could be considerable problems during the manufacture and commissioning phases. Commercial torque cells are available as either a reaction torque cell or rotating torque cell. A reaction torque cell is designed to remain static whereas a rotating torque cell has a shaft passing through it which is able to rotate. However, a rotating torque cell was significantly more expensive than a reaction torque cell. For these reasons, a commercially available reaction torque cell was selected for the final design.

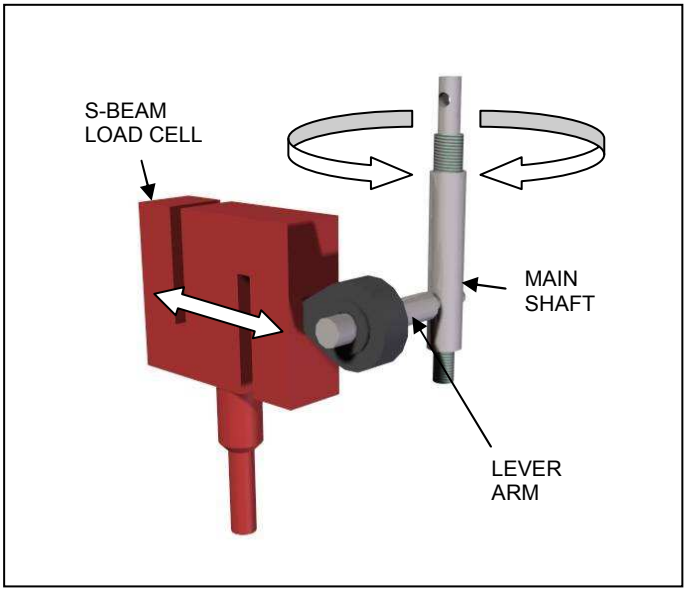

Figure 3-5 Possible method of using a load cell to measure torque

3.5 Biological chamber

A biological chamber was required to contain the construct. The chamber was to be filled with culture medium which could be circulated continuously through the chamber from a reservoir. The volume of the chamber which was selected was a balance between two factors. A larger volume would provide a buffer for the necessary nutrients, biochemicals and for waste molecules to be diffused into. A smaller volume would reduce the cost of the biochemicals required for the culture medium.

The prototype chamber (Figure 3-6) was manufactured from medical grade ultra high molecular weight polyethylene (UHMWPE) (Stryker Orthopaedics, Herouville Saint-Clair, France) which has been used extensively in orthopaedic implants and is known to have very good biocompatibility properties. An optically clear polycarbonate window was fitted to either side of the chamber to allow real-time observation of the developing scaffold. Medical grade polycarbonate was not used, however, this could easily be changed if it was deemed necessary. Also, it may be desirable to change the windows to glass to allow analysis of the scaffold by methods such as optical microscopy, and again this could easily be done in the future. The windows were sealed with a standard nitrile rubber o-ring seal (50-130, James Walker & Co Ltd., Crewe, UK) fitted within a groove in the chamber. The windows were secured in place with M4 stainless steel knurled nuts (DIN466-M4-NI, Elesa UK Ltd., Metheringham, UK) which screwed on to four lengths of stainless steel threaded bar screwed through the chamber.

Two stainless steel shafts passed into the chamber to support the scaffold and provide the mechanical loading. The chamber shafts had a recess in the end of them with a grub screw to allow for fixation of the sample. One shaft would provide rotational motion whilst the other provides linear motion. Therefore, these shafts need to be sealed to permit this motion while still preventing the leaking of culture medium and the ingress of contaminants. Initially, a viton rubber 'quad-ring' (QRAR4111A-V7002, Trelleborg Sealing Solutions, Solihull, UK) was selected. This was fitted into a 10mm hole with a 14.6mm counterbore drilled to fit the outside diameter of the quad-ring. The seal was then backed up with a stainless steel insert which was fixed to the outside of the chamber. This assembly resulted in a 10mm reamed bore, providing a sliding fit for the 10mm shaft with a groove of the appropriate dimensions for the quad-ring.

When constructed, it was found that the compression which was required to energise the elastomer quad-ring, combined with the coefficient of friction between the elastomer and polished stainless steel shaft, resulted in a significantly higher seal friction than expected. This friction was measured to be in the order of 15 – 20N and would have a major detrimental effect on the accuracy of the load and torque readings from the associated sensors. Therefore, the quad-ring was replaced by a 'Variseal' of the same size (RVA100100, Trelleborg Sealing Solutions, Solihull, UK). This is a PTFE seal with an integrated stainless steel spring to energise the seal. The PTFE seal has a much lower coefficient of friction associated with it and therefore was better suited to this application. The friction within the PTFE seal was evaluated and is discussed in Section 9.

Inlet and outlet ports were included in the design of the chamber to allow continuous flow of the culture medium. One hole was drilled in each side of the chamber, one towards the bottom of the chamber cavity and one towards the top of the chamber cavity. The holes were threaded with a 1/4-28 UNF which is a standard thread size for many fluid system components. This allowed a barbed adapter to be screwed into the chamber and a tube could be fitted to the barb.

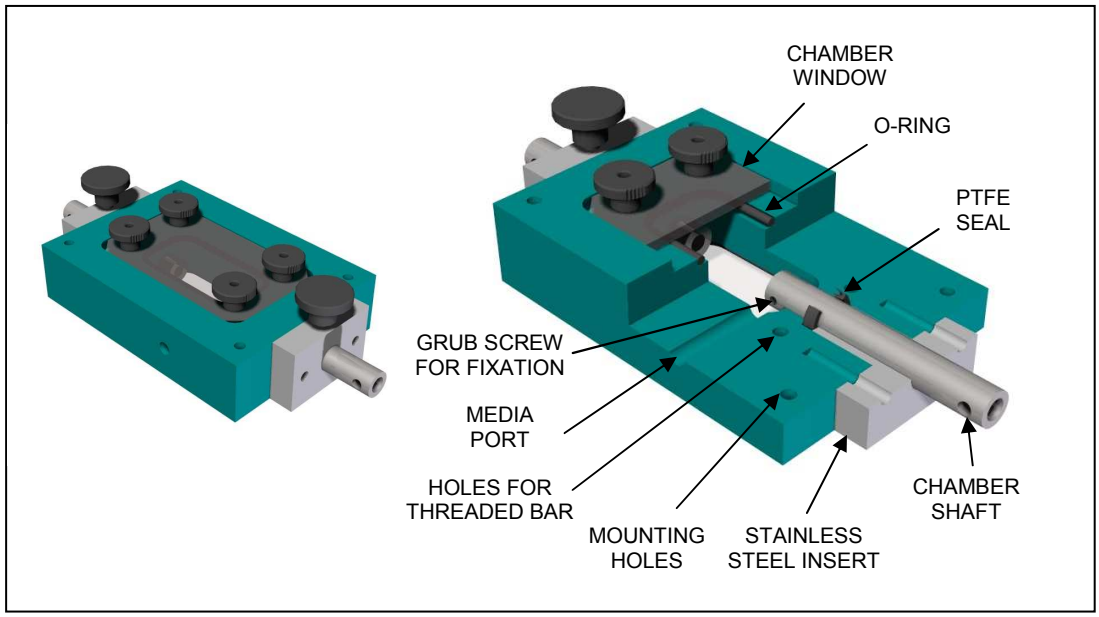

Figure 3-6 Design of the bioreactor chamber with a cut-out view to show the internal components

3.6 Tissue fixation

A suitable method of tissue fixation had to be developed to allow the loads and displacements generated by the bioreactor to be effectively transmitted to the developing tissue. The most appropriate fixation method is dependant on what loads are to be transmitted to the tissue and what the initial scaffold or tissue properties are. The fixation was required to be compatible with the grub screw recess in the end of each chamber shaft.

The literature review identified a number of methods of fixation previously used (Section 1.9.5). Cryoclamps have previously been used to clamp tendon (Riemersa & Schamhardt 1982), however, this would not be appropriate in this application as the ligaments had to be held long term in an incubator at 37°C. Also, there would be insufficient space for the cryoclamps inside the chambers. Altman *et al.* (2002b) set the ends of silk fibre scaffolds in epoxy. This method is suitable for an acellular scaffold but

would cause the tendons to dry out due to the 15 minutes curing time and the heat generated during curing could cause thermal damage to the tissue. The final option identified from the literature was physical clamping of the tissue. This could have been used to secure the ligaments, however, clamping would also affect the physical properties of the ligament close to the clamped end. Therefore, other options were considered.

A number of fixation options were investigated in a preliminary study using defrosted porcine flexor tendons. Initially a cyanoacrylate tissue adhesive (3M™ Vetbond™ Tissue Adhesive, Dechra Veterinary Products, Shrewsbury, UK) was used to secure the tendons. The concept was to glue the cut ends of the tendon to a cylindrical insert (Figure 3-7) which could be loaded into the chamber shafts and secured using the grub screw. A number of materials for the insert were evaluated, including stainless steel, PTFE, nylon and polycarbonate, to determine which would provide the best surface for the tendon to adhere to. Tendon samples were glued to the materials to be investigated. They were allowed to dry for approximately 3 minutes and a manual pull test was performed. The tendons adhered to the polycarbonate much better than the other materials and this material was selected for further testing to evaluate the effectiveness of the fixation method.

Porcine flexor tendons were cut into 25mm long samples and these were attached at each end to 5mm diameter x 10mm polycarbonate inserts (Figure 3-7). The inserts were cut from a 5mm diameter rod and the ends were filed smooth. To ensure a clean surface the ends of the inserts were wiped with methylated spirits and allowed to dry fully. The ends of the tendon were dried to provide a better surface for adhesion. A small drop of tissue adhesive was then placed on the end of the insert and, using tweezers, the end of the tendon was pressed to the insert and held for approximately 10 seconds. The tendon was then returned to water to keep it hydrated.

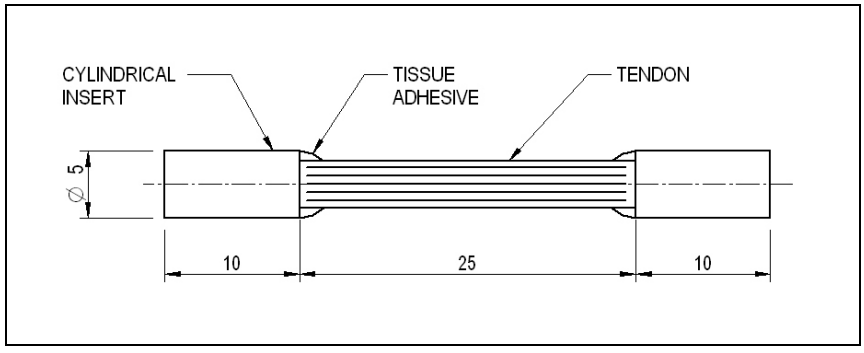

Figure 3-7 Tendon fixation with tissue adhesive and cylindrical inserts

The samples were loaded into a 5kN materials testing machine (Model 3365, Instron, High Wycombe, UK) and the polycarbonate inserts were held in the testing machine grips with serrated V-shaped grip faces installed. The samples were then loaded at a strain rate of 5mm/min until failure of the fixation at one end. The load versus extension results for this experiment are shown in Figure 3-8. The plots of each specimen have been offset along the x-axis for clarity and the maximum load of each loading specimen was identified with a black triangle. The samples were reinserted into the materials testing machine and the end of the tendon which had failed was clamped in a grip with flat serrated grip faces while the end with the remaining insert was held in the V-shaped grips as previously. The samples were loaded at the same rate as before until the glued fixation failed. These results are shown in Figure 3-9 and the specimen numbers five through eight refer to the second loading of samples one through four respectively. The maximum loads achieved by the fixation are summarised in Table 3-4. The maximum loads ranged from approximately 14.5N to 45.5N. This was well below the 100N of tensile load required for the biological experiments, therefore, this method needed to be improved if it was to be suitable.

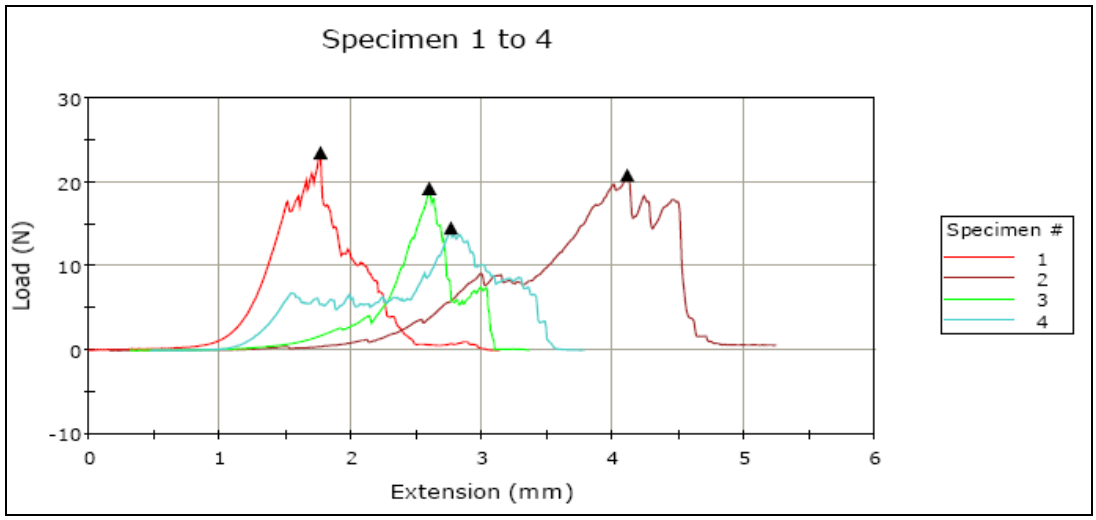

Figure 3-8 Load-extension plot of four tendon samples attached to polycarbonate inserts

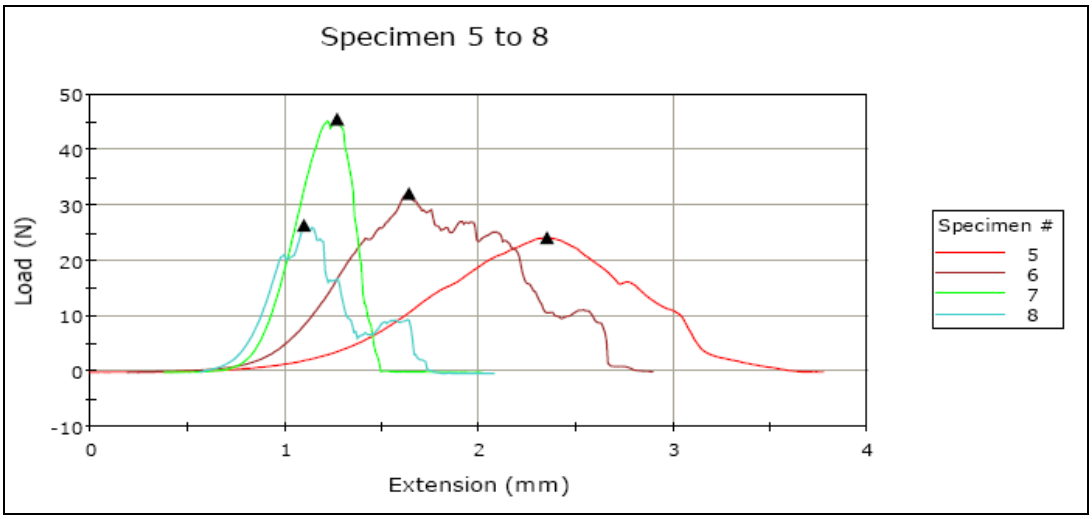

Figure 3-9 Load-extension plot of four tendon samples. One tendon end attached to polycarbonate inserts and the other end held in the tensile testing machine jaws.

Table 3-4 Maximum tensile loads of each end of the four tendon samples

Specimen	*Maximum Tensile Load (N)*
1	23.48
2	20.81
3	19.26
4	14.51
5	24.17
6	32.12
7	45.51
8	26.42

The range of maximum loads suggested that there may be some variability in the fixation technique. A second experiment was carried out which tried to ensure an improved and consistent fixation technique. Again, four samples were prepared. In order to achieve a better contact between tendon and insert and eliminate all the air at the interface, the ends of the polycarbonate inserts were polished using 1000 grit waterproof sandpaper. Also, a very clean cut was achieved on the ends of the tendons using a scalpel. A drop of glue was applied to the end of the insert. The tendon was held against the insert with tweezers for approximately 10 seconds to ensure sufficient compression was achieved at the interface and all the air was expelled. The insert on the other end was applied in the same way and the adhesive was allowed to dry for a further 20 – 30 seconds before the sample was placed in water to keep the tendon hydrated.

The four samples were loaded in a materials testing machine as described for the previous experiment. One of the samples failed at both ends, therefore, only three specimens were loaded to test the stronger ends. The loading results of the four samples

are shown in Figure 3-10 and the results from the second loading to test the stronger ends are shown in Figure 3-11. Table 3-5 shows a summary of the maximum tensile loads achieved by the fixation at each end of the tendon samples. The maximum loads ranged from approximately 16.5N to 59.5N. There is no significant difference between the results for the two techniques. The results using the improved technique were also very inconsistent and significantly lower than the required 100N.

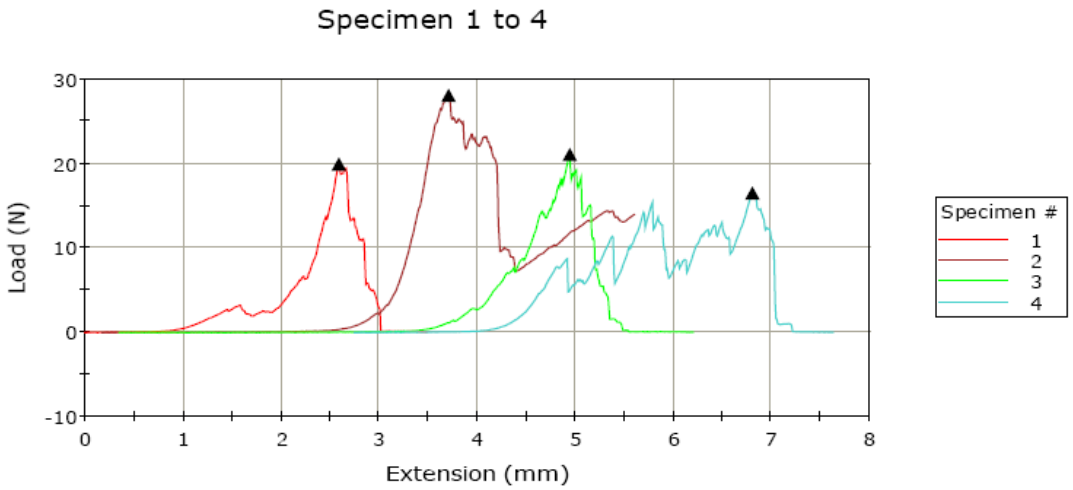

Figure 3-10 Load-extension plot of four tendon samples attached to polycarbonate inserts with improved fixation technique

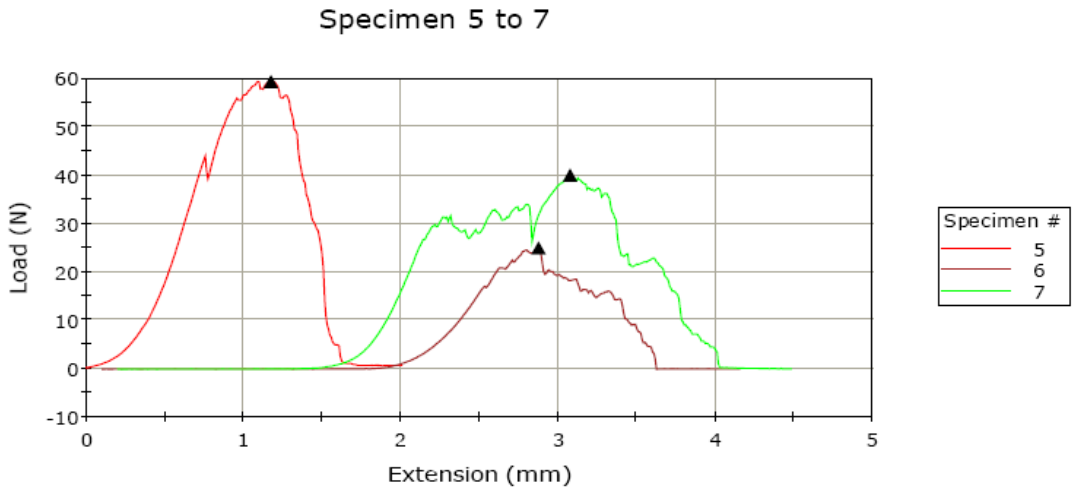

Figure 3-11 Load-extension plot of three tendon samples prepared with improved fixation technique. One tendon end attached to polycarbonate inserts and the other end held in the tensile testing machine jaws.

Table 3-5 Maximum tensile loads of each end of the four tendon samples prepared with improved fixation technique

Specimen	*Maximum Tensile Load (N)*
1	19.91
2	28.03
3	21.06
4	16.49
5	59.39
6	25.00
7	40.04

A new method for securing the tendons in the rig was developed. A polycarbonate circular insert was cut in half longitudinally to provide two semi-circular inserts. The cut faces were polished using 1000 grit waterproof sandpaper and cleaned with methylated spirits. A porcine flexor tendon specimen was cut to 45mm in length and the ends were patted dry with a paper towel. A drop of tissue adhesive was applied to the cut face of the insert and it was glued to the side of the tendon at one end (Figure 3-12). The insert and tendon were held together using tweezers for approximately 10 seconds. The same process was performed on the other end of the tendon and the tendon was left for 20 – 30 seconds and then placed in water to keep the tendon hydrated. This sample was able to be inserted into the recess in the chamber shafts and the grub screw could lock down on the polycarbonate. Initially, it was thought that this option would provide a larger surface area of adhesion and the adhesive might perform better in shear.

Two cylindrical steel holders were manufactured with the same bores and grub screw holes as the chamber shafts. The holders were clamped in the materials testing machine grips and the tendon samples were inserted into the bores in the ends of the holders and secured in place using the grub screws. The tendons were loaded at 5mm/min as in the previous experiments. The results of these four samples are shown in Figure 3-13. The loading profile of Specimen 4 suggests that it may have slipped during loading possibly due to one of the grub screws not being tightened sufficiently. After the first loading session, the tendons were reinserted into the materials testing machine with the intact end held in the holder with the semi-circular insert and the previously failed end held in the machine grips. These results are shown in Figure 3-14. The maximum tensile loads of each sample end are summarised in Table 3-6. The maximum tensile loads ranged from 84.6 – 218.0N. Although this is quite a wide range, the loads are significantly higher ($p<0.05$) than those which were found when the tendon ends were adhered to a cylindrical insert. The third sample in this experiment (specimen results 3 and 7) had to have one of its inserts removed as it was too large to fit in the shaft bore. A smaller

insert was put in its position, however, it was not glued in place. This sample had some of the largest maximum loads (122N and 143N) which suggested that fixation was due to compression of the tendon between the bore wall and the insert and not due to the adhesive. The adhesive was difficult to use as it would often stick the tweezers to the insert and tendon and would also squeeze out of the contact interface and form a film over some of the tendon. This may prevent nutrients and waste passing through the tissue. Therefore, it was felt that fixation by compression alone would be the best option for the biological experiment. The design of the insert was modified to improve the manufacturing process. Flat polycarbonate inserts of approximately 10mm x 3mm x 2mm were developed which provided the same compression.

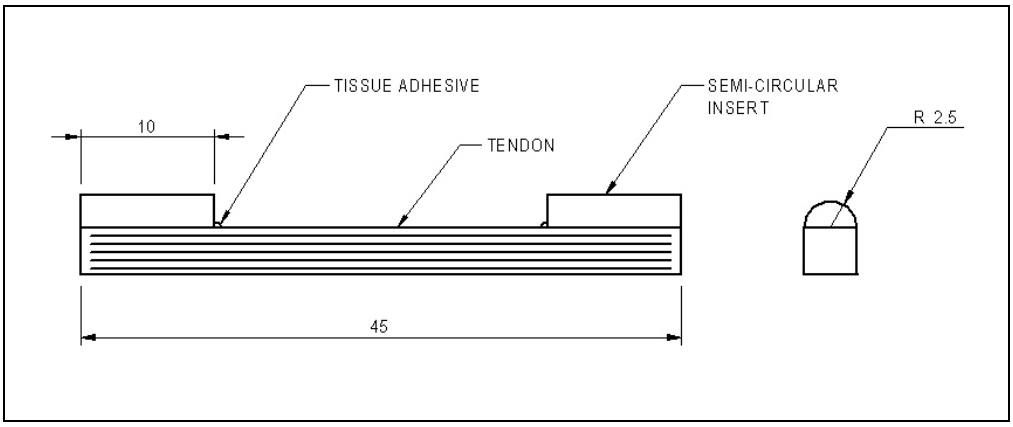

Figure 3-12 Tendon fixation with tissue adhesive and semi-circular inserts

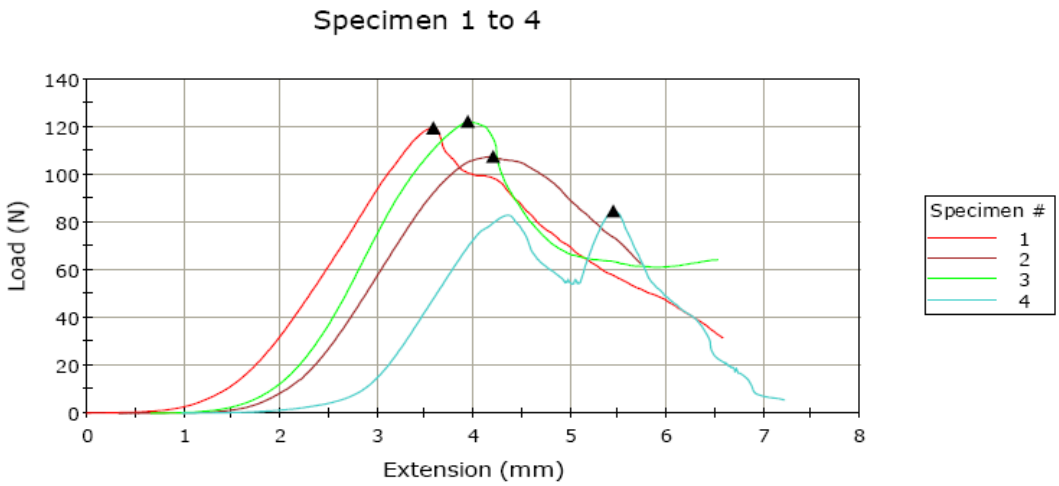

Figure 3-13 Load-extension plot of four tendon samples with semi-circular inserts

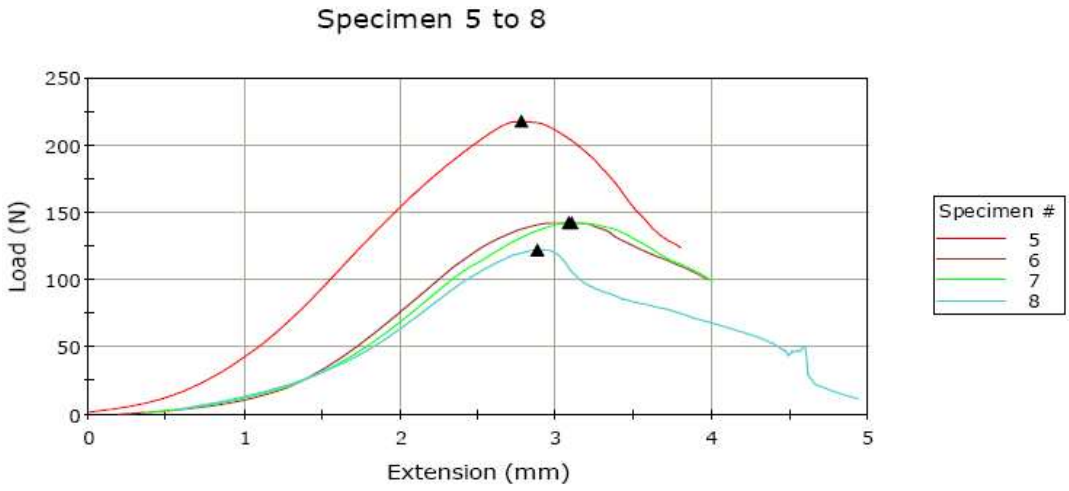

Figure 3-14 Load-extension plot of four tendon samples with semi-circular insert at one end

Table 3-6 Maximum tensile loads of each end of the four tendon samples with semi-circular insert

Specimen	*Maximum Tensile Load (N)*
1	119.47
2	107.47
3	122.17
4	84.61
5	217.98
6	142.86
7	142.96
8	122.54

3.7 Medium flow system

For successful tissue engineering, the developing tissue must be provided with sufficient nutrients and biochemical components, such as growth factors, and also be able to expel any waste materials which are produced. This can be achieved by ensuring flow of medium through the chamber. There are two possible flow regimes available: (1) a recirculating flow where medium is pumped from a reservoir, through the chamber and back into the reservoir; or (2) a non-recirculating flow system where medium flows from a supply reservoir, through the chamber, and is collected in a waste reservoir.

Both methods have their advantages and disadvantages. The recirculating system allows any biochemical components which are produced by the developing tissue itself to be recirculated in the medium and, if there are no leaks in the system, there will be no risk of the reservoir becoming empty. However, with time, the concentration of nutrients in the medium will decrease and the concentration of waste products will increase.

Conversely, the non-recirculating system does not allow any biochemical components produced by the developing tissue to be recirculated in the medium and, if the flow rate is not accurately controlled, there is a risk the supply reservoir could become empty. However, the non-recirculating system will ensure a constant concentration of nutrients and growth factors are supplied to the tissue and prevent any build-up of waste materials.

The ideal method to drive the flow in a recirculating system would be with an appropriate peristaltic pump, whereas the non-recirculating system could be driven by either a peristaltic pump or syringe pump which can be better suited to very small flow rates.

The pumping system was required to supply eight chambers, therefore an eight channel syringe pump or peristaltic pump with a quick release mechanism for the tubing would be the ideal pumping method. However, no such pump was available within the department and it was too expensive to justify purchase of the equipment. Therefore, it was necessary to develop a more cost effective method to drive the flow through the system. The objective of any flow system would be to provide equal flow to all chambers at the flow rate detailed in the requirement specification, i.e. 0.05 – 5ml/min.

The simplest option which required very little equipment was to have a non-recirculating gravity-fed flow system as shown in Figure 3-15. This system required a supply reservoir positioned higher than the waste reservoir to provide a pressure head to drive the medium through the chamber. Two chambers were supplied from a single reservoir to reduce space requirements and equipment costs. The supply tube was split using a "Y" connector to feed both chambers. The outlet tubing was fitted with a 3-way valve to allow a syringe to be connected to the system. The syringe was used to draw the medium from the supply reservoir into the chamber and initiate the flow through the system. The outlet tubing from the two chambers were combined with a "Y" connector and an adjustable tube clamp was fitted to the single outlet tube before it entered the waste reservoir. The tube clamp could be adjusted to alter the pressure loss through the tube, thereby controlling the flow in the chambers. The tube clamp was located on the single combined outlet from the chambers to try to ensure an equal flow for each of the chambers so long as the pressure losses through each chamber system was the same.

An initial prototype of the system was set-up to demonstrate proof of principle. It was shown that the syringe could be used to fill the system and initiate flow and the tube clamp was capable of adjusting the flow rate. For this reason a larger study was

performed to ensure the system would work over a long term whilst being maintained in an incubator in an environment of 37°C and 5% CO_2. Eight chambers were set-up in pairs and they were mounted on a custom-made stand to hold each pair. Platinum-cured silicone tubing (1.6mm inside diameter, 3.2mm outside diameter, Cole-Parmer Instruments Co. Ltd, London) was used throughout the system as it was gas permeable and therefore would allow the CO_2 to regulate the pH of the media. The reservoirs were fitted with 4-port screw caps (Fisher Scientific, Loughborough, UK) to seal the system and prevent bacterial ingress into the reservoir. Also, an air filter was fitted to the reservoir caps to allow gas exchange and pressure compensation as the medium volume changed, whilst again preventing bacterial ingress.

As before, the chambers could be filled and flow initiated by the syringes. However, due to the low flow rate required (0.05ml/min), it proved very difficult to adjust the tube clamp to accurately control the flow, i.e. a very small adjustment of the clamp screw would result in a large change of the flow rate. Although the flow could be initiated successfully, when the system was left overnight air bubbles would form in the tubing and stop the flow. This was caused by a combination of the gas permeable silicone tubing and the low flow rate which meant that there was more time for air bubbles to develop and there was insufficient flow to drive the air bubbles through the system. This proved to be a fundamental problem with this system and therefore this flow option was rejected.

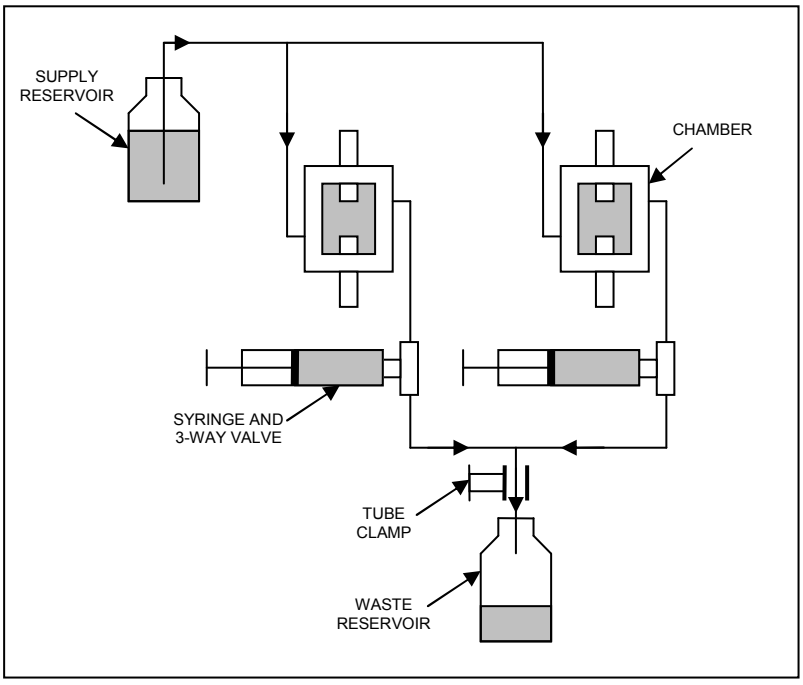

Figure 3-15 Schematic of gravity-fed non-recirculating flow system

Two peristaltic pumps were located and it was necessary to evaluate whether they were suitable to supply the chambers. The pumps were single-channel pumps (MHRE200, Watson-Marlow Ltd., Falmouth, UK) with 3-roller pump heads. Although the pumps were designed for a single tube, the tubing beds were quite wide and therefore it was though feasible to attempt to run the pumps with two tubes in each bed. A schematic of the set-up is shown in Figure 3-16. It was a very similar set-up to the gravity-fed system, with the tubing from the supply reservoir passing through the peristaltic pump. As there were only two peristaltic pumps, each pump had to supply up to four chambers and this is the set-up shown in Figure 3-16. Also, the speed of the pump could be used to control the flow rate, hence, there was no requirement for the tube clamp. The outlet tubing from each chamber could be inserted into the waste reservoir individually to allow the flow through each chamber to be monitored.

The tubing used throughout the system has a wall thickness of 0.8mm and this was too thin to operate successfully within the peristaltic pump. Therefore a small section of MasterFlex L/S14 tubing (1.6mm I.D., Cole-Parmer Instruments Co. Ltd, London) which had a larger wall thickness and was designed for use in peristaltic pumps was used. If the tubing was unconstrained, the pump head would draw more tubing into the tubing bed, which could damage the tubing or cause the pump to jam. Therefore, the tubing was clamped on either side of the tubing bed using circular cable clamps which were lined with rubber to provide a tight grip and prevent slipping (Figure 3-17).

The gap between the pump head rollers and the tubing bed can be adjusted to suit the tubing being used by altering the height of the bed. If the gap is too large then the pumping would be very inefficient as back flow of the medium would occur. If the gap was too small then an excessively large torque would be required to compress the tubing and the pump would stall. The tubing bed was manually adjusted to the height which prevented pump stall but ensured efficient pumping for the two tubes.

The eight chambers and two pumps were set-up as described and run for a number of days to evaluate the effectiveness of the system. Either the pumps or the syringes could be used to fill the chambers and the pumps were able to pump medium to all the chambers. To achieve the flow rates required the pump speed had to be significantly reduced to such a level that the pump motor would occasionally stall as it did not have sufficient power to compress the tubing. For this reason, the pumps were run at a higher speed and therefore a higher flow rate. The pumps were connected to an electrical socket timer which turned the pumps on and off to produce 10 flow cycles in a day and,

therefore, maintain the daily flow at the required level and prevent the supply reservoir from being emptied.

During this long-term test the pump was able to produce flow through both supply tubes. However, each supply line was split after the pump to feed the two chambers in each pair. As a consequence, should an air block develop in either the inlet or outlet lines for one of the chambers, all the flow would be directed through the other chamber. This was visible by monitoring the output flow from each chamber in the waste reservoir. As air blocks could be a regular occurrence, the flow system was not suitable in this configuration.

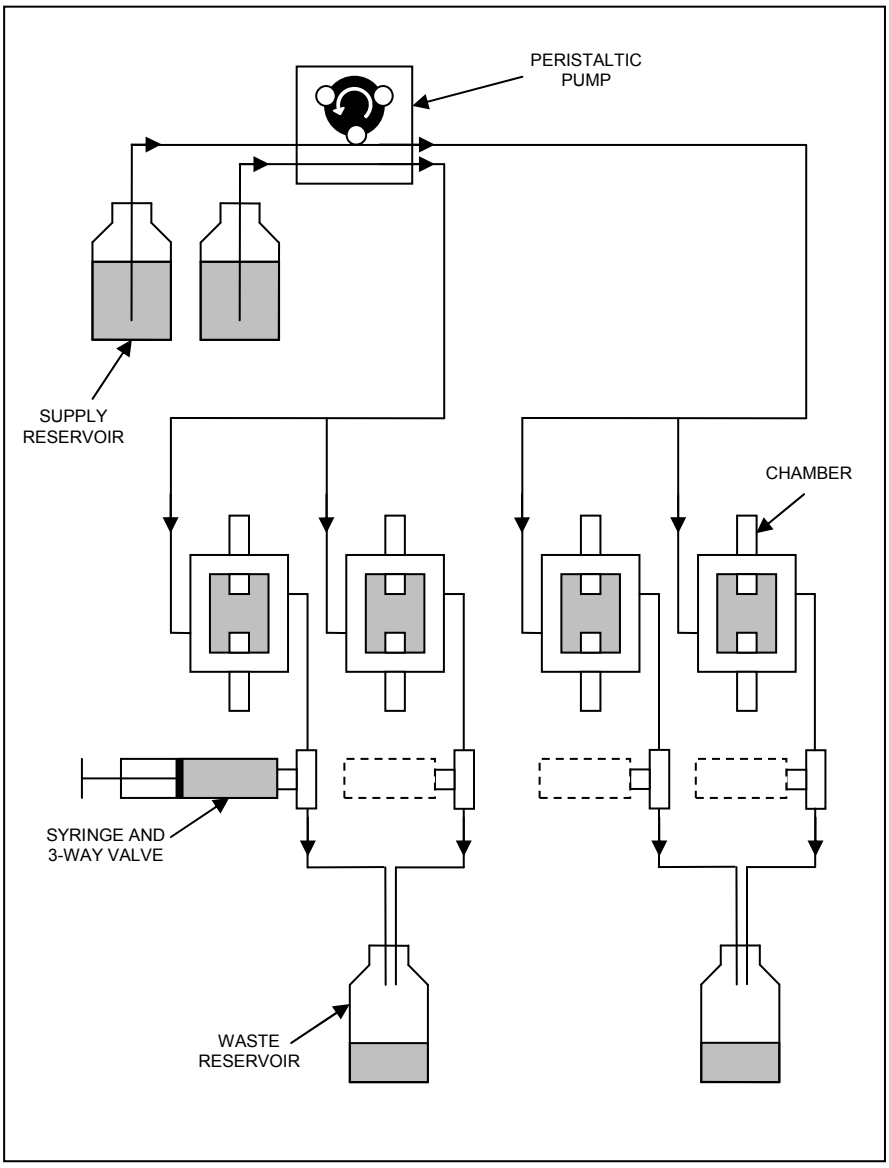

Figure 3-16 Schematic of two-channel pump driven non-recirculating flow system

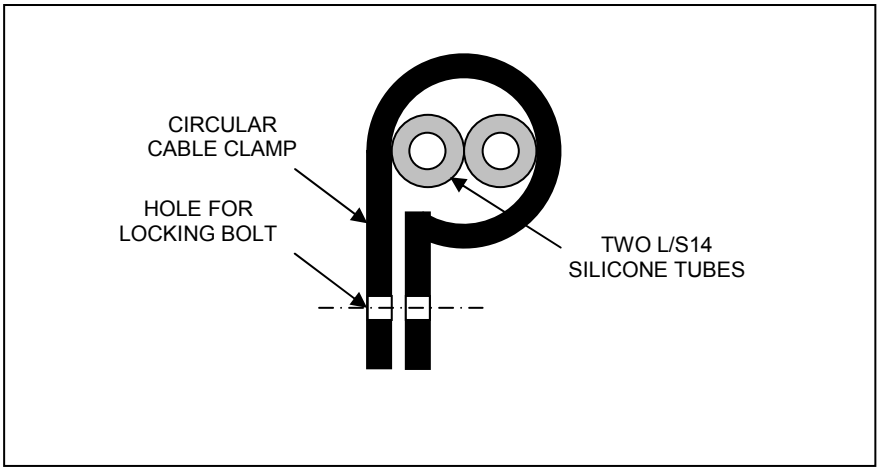

Figure 3-17 Circular cable clamp for clamping two peristaltic pump tubes

In order to ensure all the chambers were supplied with medium flow it was necessary to pump medium to them individually. Each pump had to be modified to allow pumping of four channels. This introduced a number of problems as the pumps were only designed for a single channel. The tubing bed was sufficiently wide to accommodate four L/S14 tubes side-by-side however there was little clearance on either side. It was necessary to effectively clamp the tubes to ensure they did not get drawn into the pump head as the outside tubes could slip off the side of the bed, in addition to the other problems of damage to the tubing and jamming the pump mentioned previously. Initially, a round cable clamp was used as with the two channel option. This fitted onto the pump and was able to hold the four tubes securely. However, this method of clamping was unsuitable because the position of the tubes could cause the pump to stall. The tubes were held in a circular configuration (Figure 3-18), but they had to lie flat on the tubing bed. The transition from a circular to flat configuration occurred too close to the pump head which meant that as the rollers first made contact with the tubes some of the tubes were still resting on top of others. This increased thickness caused the pump to stall. A new clamping method had to be found.

It was necessary to clamp the tubes in a flat configuration to prevent the problem described above. The first method investigated was securing the four tubes to the tubing bed using a cable tie (Figure 3-19). This had two main problems: firstly, the outer tubes were clamped much more than the two inner tubes such that to secure the inner tubes and prevent motion, the outer tubes were almost fully occluded. Secondly, the cable tie was able to slide towards the pump head. This clamping method was developed with the addition of a cable tie pad (Figure 3-20) which was able to evenly distribute the compressive load to all the tubes. To prevent the cable tie sliding towards the pump

head, it was fed through the screw hole in the tubing bed which had previously been used to secure the circular cable clamp. These modifications proved quite successful, however, it was difficult to tighten the cable tie sufficiently, the cable tie had to be cut to remove the tubing and it required some time and dexterity to clamp the tubing.

The tube clamps which were used to control the flow in the gravity-fed system were wide enough to accept four L/S14 tubes, were tightened and released with a simple thumb screw and had a hinged side to allow the tubes to be easily remove from the clamp. They were an ideal method of clamping the tubes in the peristaltic pump and the clamps were secured to the tubing bed using Araldite® Adhesive (Huntsman Advanced Materials, Basel, Switzerland) (Figure 3-21).

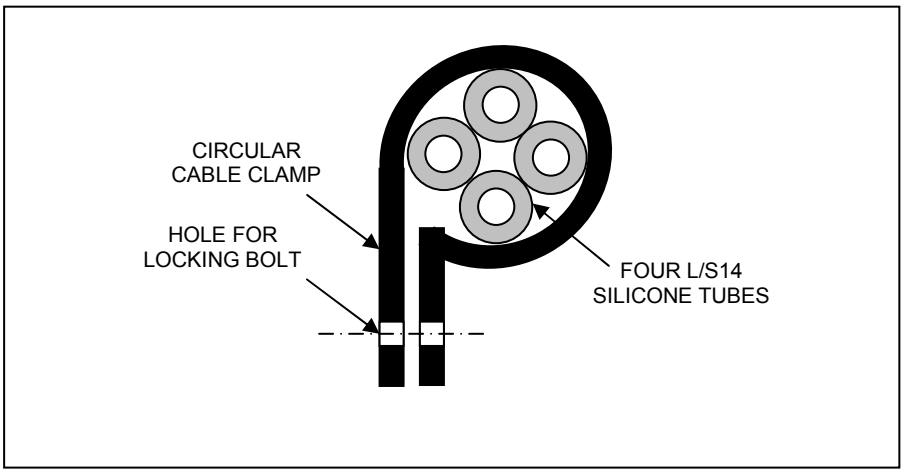

Figure 3-18 Circular cable clamp for clamping four peristaltic pump tubes

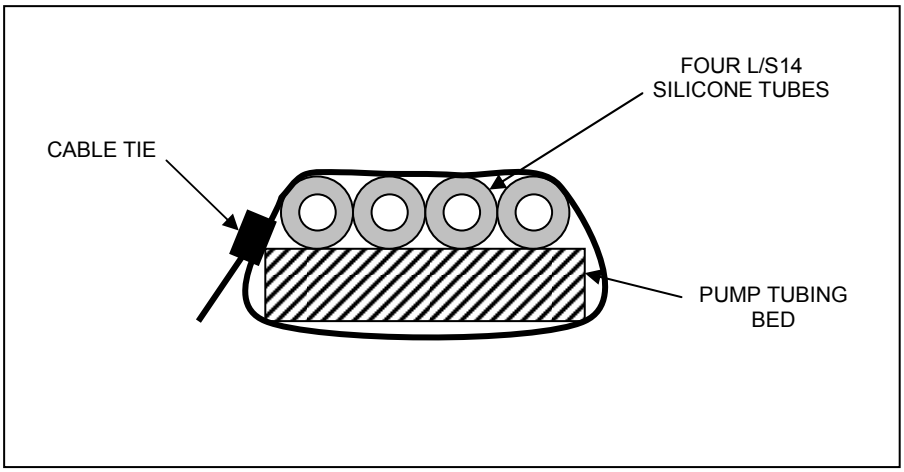

Figure 3-19 Clamping of four peristaltic pump tubes with cable tie

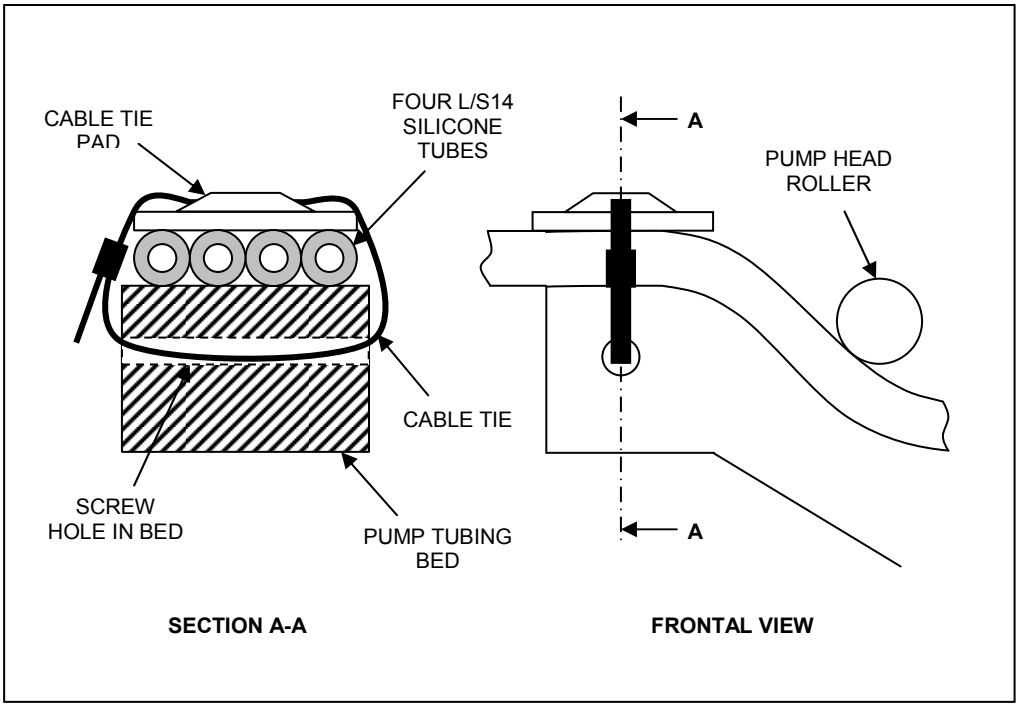

Figure 3-20 Clamping of four peristaltic pump tubes with cable tie pad

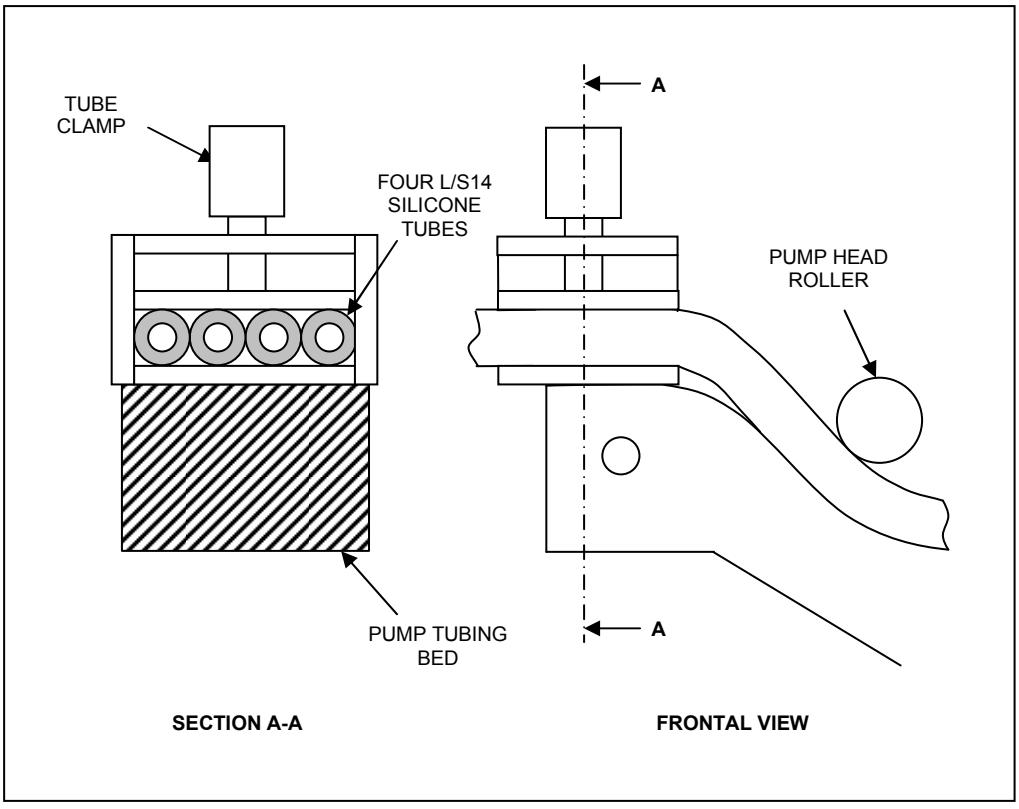

Figure 3-21 Clamping of four peristaltic pump tubes with tube clamp

With the pumps modified to accept four channels, the non-recirculating flow system was set-up as shown in Figure 3-22. Again, the system was run for a few days to allow any problems to be observed. Each pump was able to drive any air bubbles which had

developed through the system. Unfortunately, the pump did not supply equal flow to all the chambers. This was another problem caused by the pump being intended for use as a single channel pump. The tubing bed is approximately 30mm wide and is not perfectly parallel to the rollers. In the single channel configuration this would not be a problem as the tubing bed height could be adjusted to suit the tubing being used. However, with multiple tubes this caused a variation in the gap between the rollers and the tubing bed and hence a variation in the level of occlusion imposed on each tube. As the supply reservoir was positioned above the waste reservoir, providing a positive pressure head, a lower level of occlusion allowed a greater flow rate to occur. When the pump was switched off media was able to leak through the pump and when left overnight this could empty one of the supply reservoirs.

The roller spindles of the pump heads were adjusted to ensure they were as parallel as possible with the tubing bed, however, it was not possible to achieve perfect parallelism and media still leaked through the pump if it stopped at certain positions. It was concluded that it was not possible to ensure equal media flow to all the chambers with the equipment available. Therefore, a new objective for the flow system was developed which was to ensure a minimum flow rate could be maintained to all the chambers. This would ensure that all tissue was provided sufficient nutrients and a build up of waste products was prevented. However, this was not the ideal solution as it introduced an uncontrolled variable into the system.

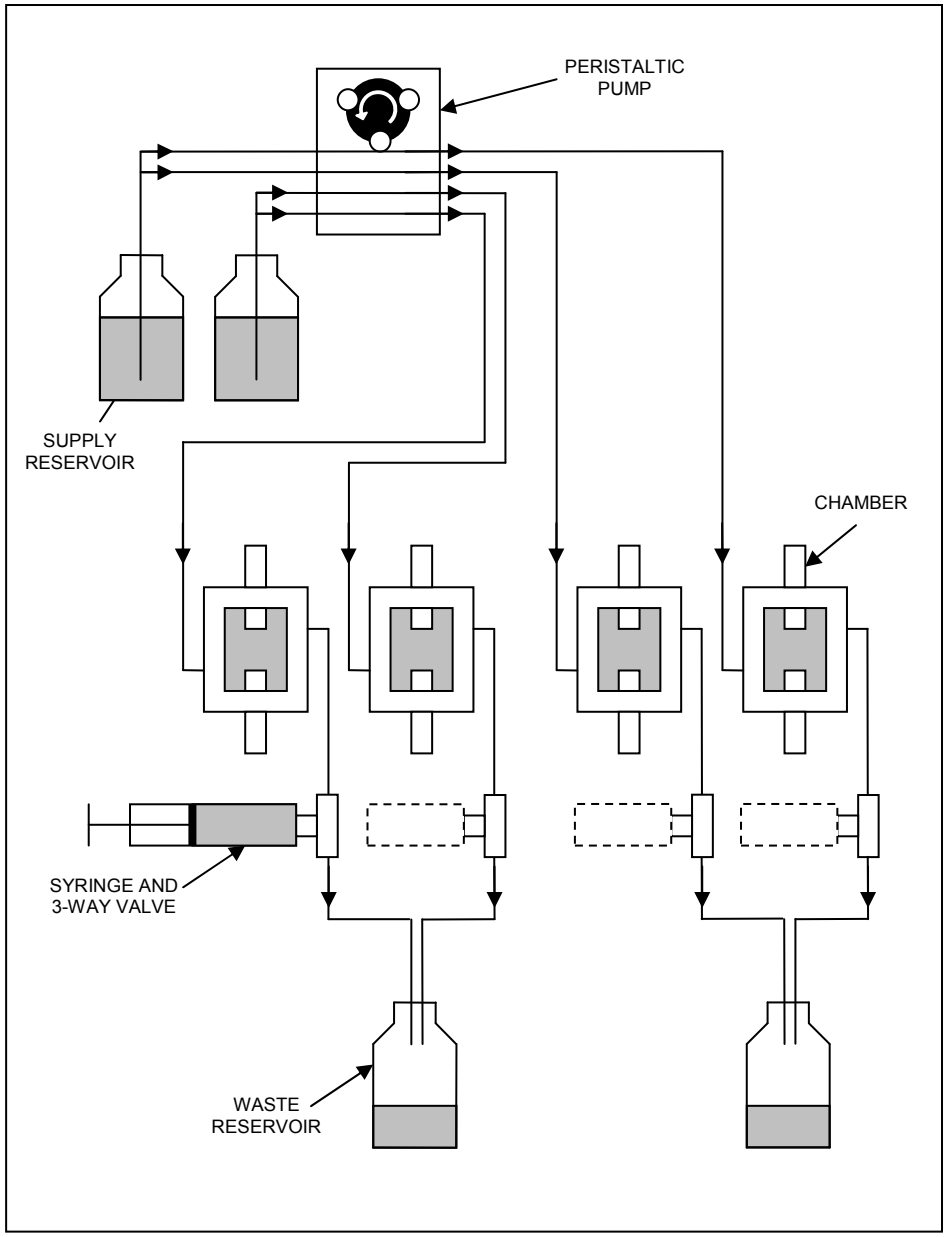

Figure 3-22 Schematic of four-channel pump driven non-recirculating flow system

The system shown in Figure 3-22 did not meet the new objective as it was possible that one of the supply reservoirs would become empty and therefore a minimum flow rate could not be maintained. For this reason, the system shown in Figure 3-22 was modified to form a recirculating system which is shown in Figure 3-23. In this new system, the outlets from the chambers were fed back into the single reservoir for each chamber pair. The outlet tubes were positioned in the reservoir just above the media level and this ensured that there was no significant head difference between the source and outlet. The speed of the pump was increased to ensure the tube with the lowest occlusion provided sufficient flow to its chamber. There was a greater flow through the other chambers but

this did not cause a problem as there was a common reservoir so the media level would never reduce regardless of flow rate (assuming no leaks occurred).

The inlet port to the chamber was positioned at the bottom of the chamber and the outlet port was at the top of the chamber. Also, the reservoir was positioned vertically such that the media level in the reservoir was just above the media level in the chamber. This ensured that media would not be able to drain from the chamber into the reservoir.

Although not perfect, the recirculation flow system shown in Figure 3-23 was the best system possible with the available equipment and was the option selected.

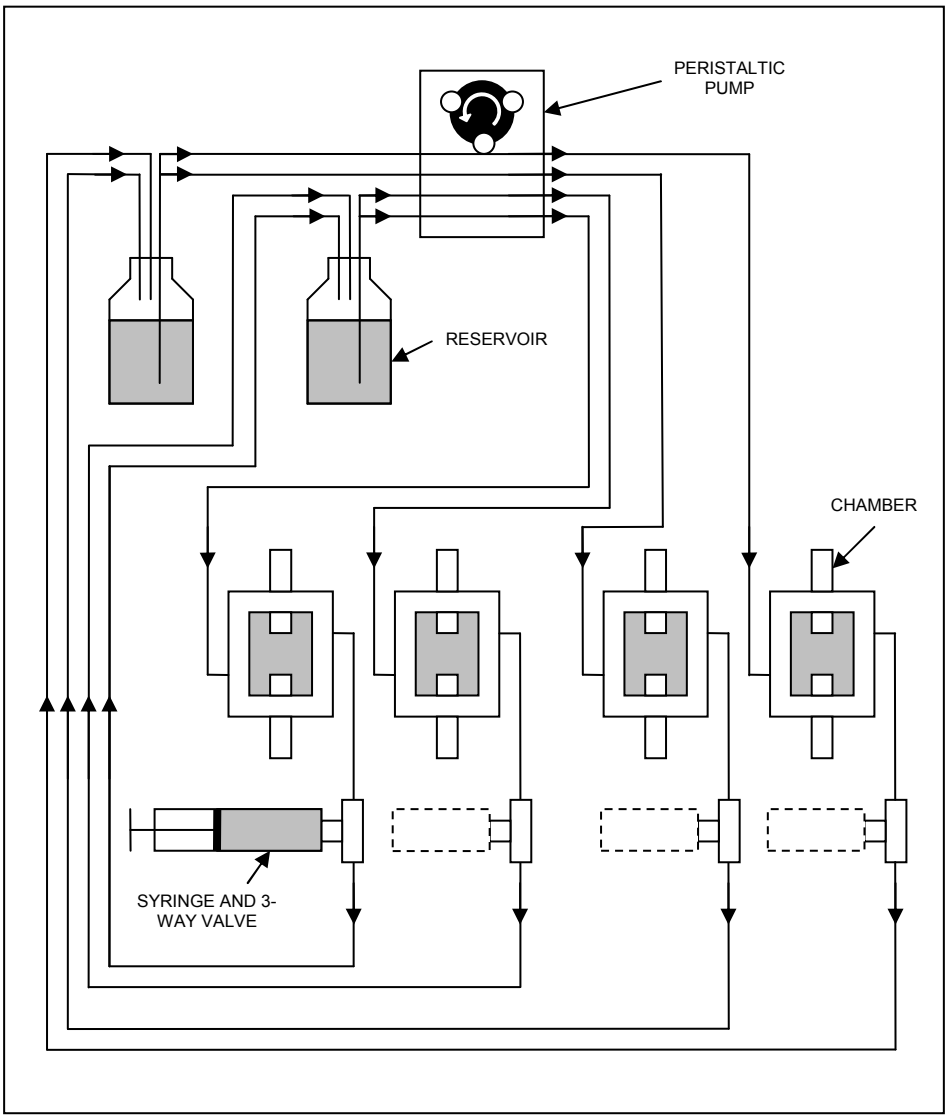

Figure 3-23 Schematic of four-channel pump driven recirculating flow system

3.8 Final bioreactor design

A detailed bioreactor design was developed to meet the requirement specification (Section 3.1) based on Concept 4 which was described in Sections 3.2 and 3.3. The design was drawn using 3D CAD software (Solid Edge, UGS Corp, Plano, Texas, USA) and is shown in Figure 3-24. A general assembly of the bioreactor is shown in Appendix B.

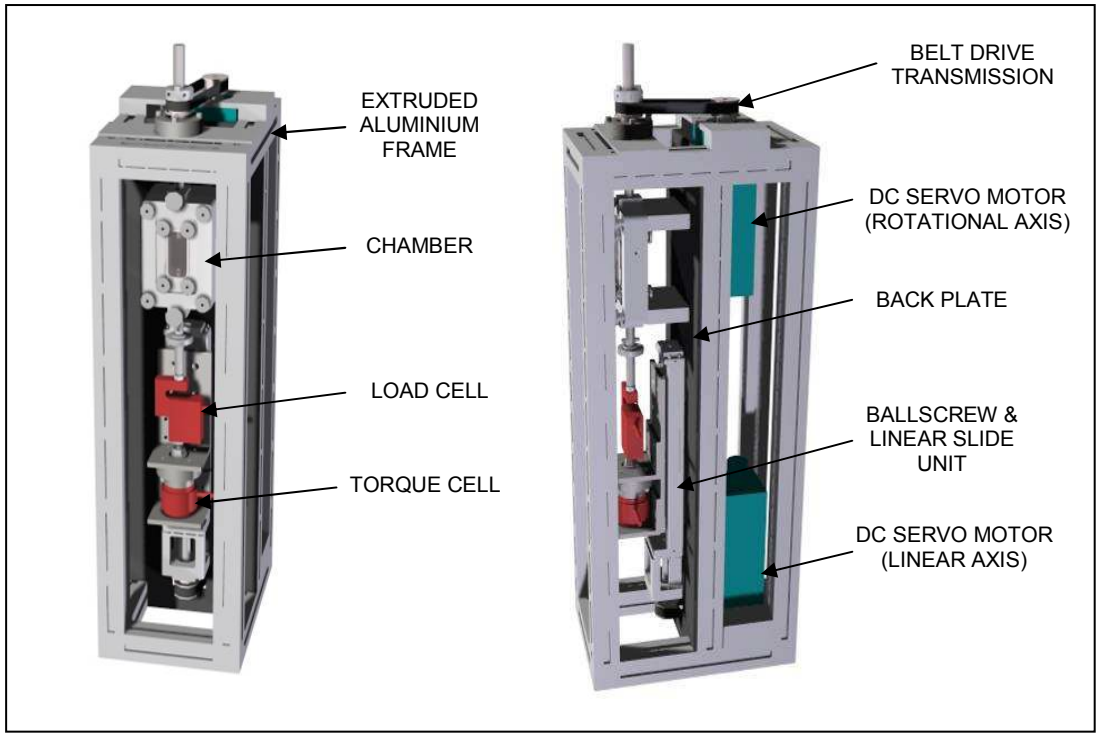

Figure 3-24 A front and side view of the final bioreactor design

3.8.1 Mechanical loading

The linear actuation was provided by a ballscrew and linear slide unit driven by a separate motor. Figure 3-25 shows the mechanical loading components mounted on the back plate and an expanded view of the linear actuation components and sensors. The motors mounted behind the back plate have not been shown. The linear load was transmitted through the linear slide to the bearing mounting bracket. It then passed through the bearing and torque cell shaft to the load cell. The load cell was directly connected to the lower chamber shaft via a pin joint (Figure 3-26) thereby transmitting the linear load to the developing tissue in the biological chamber.

A motor was selected to drive the ballscrew and linear slide unit and provide the linear load required in the specification (Table 3-1). The maximum motor torque required was

calculated based on a 5 mm stroke, a load of 400N, a frequency of 5Hz, a ballscrew pitch of 2mm, a screw efficiency of 0.9, a timing belt efficiency of 0.85 and a moving mass of 1.7kg. A torque of 0.143Nm was calculated to apply the load to the sample and 0.164Nm was calculated to accelerate the moving mass. The continuous torque of the motor was required to hold the sample at its maximum load and the peak torque was required to meet the load and acceleration torques (0.361Nm). A brushless d.c. servo motor was selected with a continuous torque of 0.45Nm and a peak torque of 1.8Nm (BSM50N-133, Baldor UK Limited, Bristol, UK). This provided a safety factor of 3.2 for the continuous torque of the motor.

The load was cantilevered from the front of the linear slide therefore a slide with two carriages was selected to react the moment created by the cantilever. The distance between the carriages was maximised to reduce moment loading whilst ensuring the slide had sufficient travel. The travel in the slide had to allow for a range of sample lengths in the chamber and permit the load cell shaft to be removed from the lower chamber shaft when disconnecting the pin joint and removing the chamber from the bioreactor (Figure 3-26). A travel of 38mm was sufficient and an appropriate ballscrew and slide was selected to meet the travel and load requirements (KR2602B+200L, THK UK, Milton Keynes, UK).

The load was transmitted through the bearing mounting bracket to a double row angular contact ball bearing (3200ATN9, SKF (U.K.) Limited, Luton, UK). The outer race was located on a recess machined in the mounting bracket and secured in place with the bearing retaining ring. The torque cell shaft was seated on the inner race of the bearing and located on the shoulder of the torque cell shaft. The shaft was secured on the other side of the inner race with a nut and washer. This arrangement allowed both tension and compression to be applied to the sample.

A 500N S-Beam load cell (SM-500N, Interface Force Measurements Ltd., Crowthorne, UK) was selected to measure the tensile/compressive load transmitted to the sample. It was mounted onto the torque cell shaft with an M6 thread and secured in place using a locking nut. A similar arrangement fixed the load cell shaft to the upper part of the load cell (Figure 3-26).

The load cell shaft could be coupled with the lower chamber shaft via a pinned connection (Figure 3-26). The end of the load cell shaft inserted into the recess drilled in the chamber shaft. A pin passed through a transverse hole in both the shafts and the

connection was secured by hand with a locking nut. This allowed tension and torsion to be transmitted through the coupling of the two shafts. The chamber shaft had a 5mm diameter recess drilled in the other end with a grub screw for fixation of the sample.

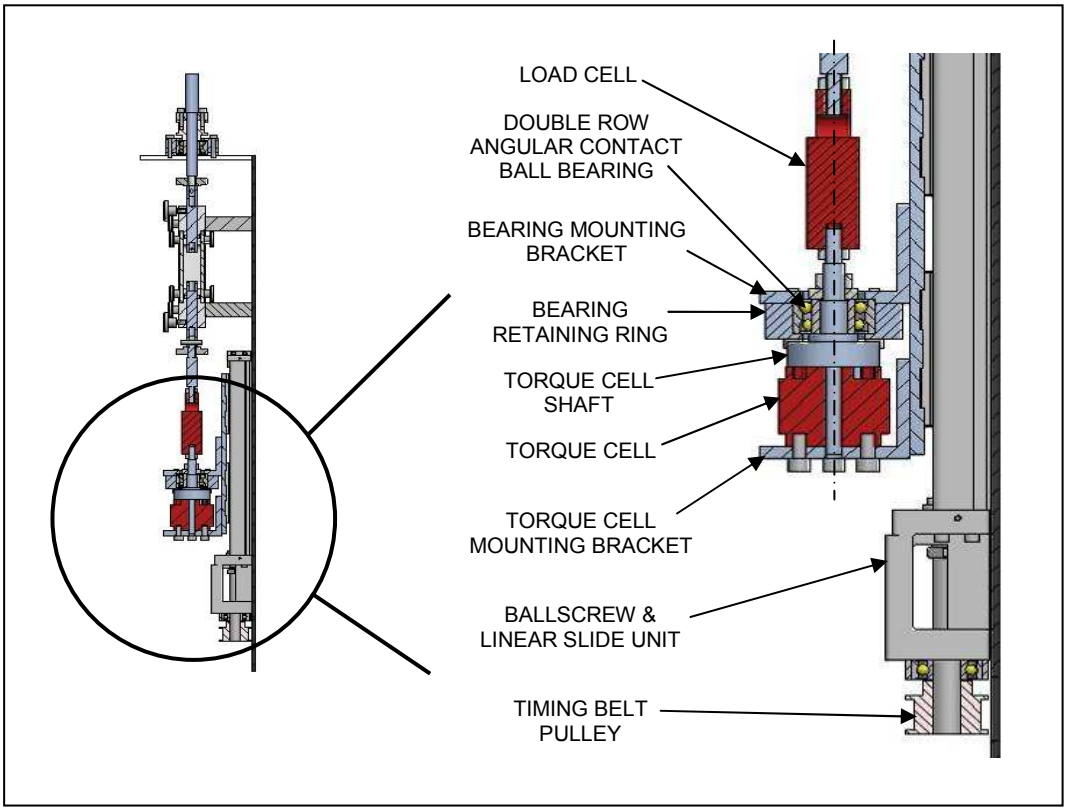

Figure 3-25 Linear actuation and sensor mounting

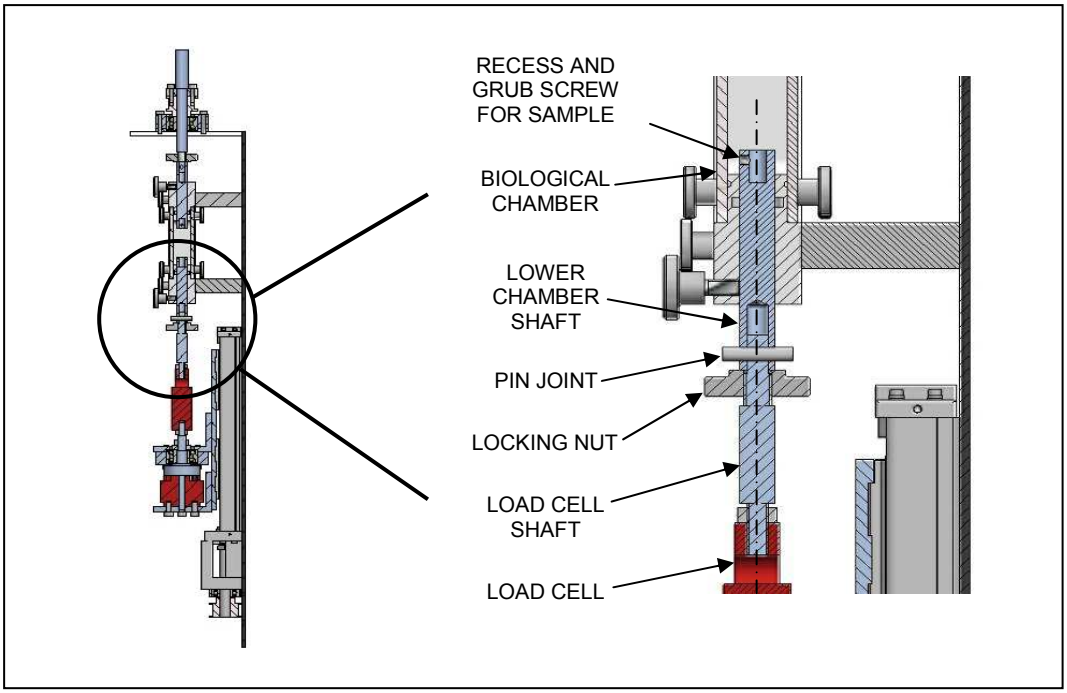

Figure 3-26 Chamber shaft coupling

Torsional loading was applied via the rotational shaft at the top of the bioreactor (Figure 3-27). A motor was selected to apply the torsion required in the specification (Table 3-1). The maximum motor torque required was calculated based on a 150° rotation, a torque of 1Nm, a frequency of 5Hz, a timing belt efficiency of 0.85 and a moment of inertia from the moving components of $1.5x10^{-5}$ kgm^2. There was no gearing between the timing belt pulleys therefore a continuous torque of 1Nm was required to hold the sample when loaded. A peak torque of 1.15Nm was calculated to apply the torque to the sample and accelerate the moving components. A brushless d.c. servo motor was selected with a continuous torque of 0.9Nm and a peak torque of 3.65Nm (BSM50N-233, Baldor UK Limited, Bristol, UK). This motor was slightly undersized for the calculated continuous torque. However, the requirement of 1Nm in the specification has a large safety factor built in as it was expected that the maximum torque required would be significantly lower than this value. Also, the peak torque has a safety factor of 3.2 meaning that if the sample was only required to be held for a short period of time at the maximum torque then the motor would be able to achieve this. Therefore, it was not necessary to select a more powerful motor.

The torque was transmitted through a timing belt to the pulley shown in Figure 3-27. A split shaft clamp was bolted to the pulley and when tightened it would clamp securely onto the rotational shaft enabling torque to be transmitted from the pulley to the rotational shaft. The shaft passed through a double row angular contact ball bearing which was located in the bearing mounting plate and the outer race was secured with a retaining ring. The bearing permitted rotation and resisted any moment induced by the tension in the belt drive. The shoulder of the rotational shaft located on the upper surface of the shaft clamp and the pulley rested on the inner race of the bearing. With this arrangement the bearing reacted the tensile load imposed on the sample thus preventing the upper chamber shaft moving vertically.

The upper chamber shaft was coupled to the rotational shaft via a pinned connection to transmit both tension and torsion. To remove the chamber the pin joint would be disconnected. The shaft clamp could then be released and the rotational shaft lifted vertically to decouple the rotational shaft from the chamber shaft. However, a large amount of linear friction was present between the rotational shaft and the pulley and bearing because tension in the timing belt was transmitted from the pulley to the bearing via the rotational shaft. This made it very difficult to lift the rotational shaft and release the chamber. Therefore, the design was modified to include a pulley and bearing sleeve (Figure 3-28). This allowed the belt tension to be transmitted from the pulley to the

bearing via the sleeve, leaving the rotational shaft unloaded when the pin joint was disconnected. Consequently, the rotational shaft was able to be lifted freely to allow the chamber to be removed.

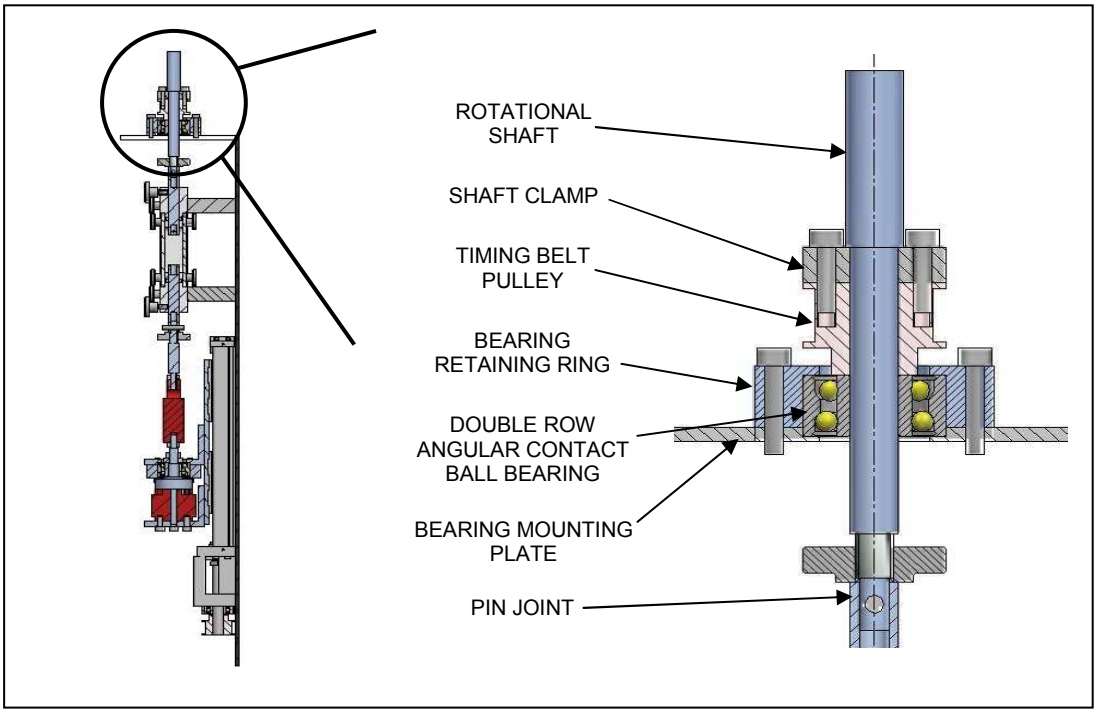

Figure 3-27 Rotational actuation assembly

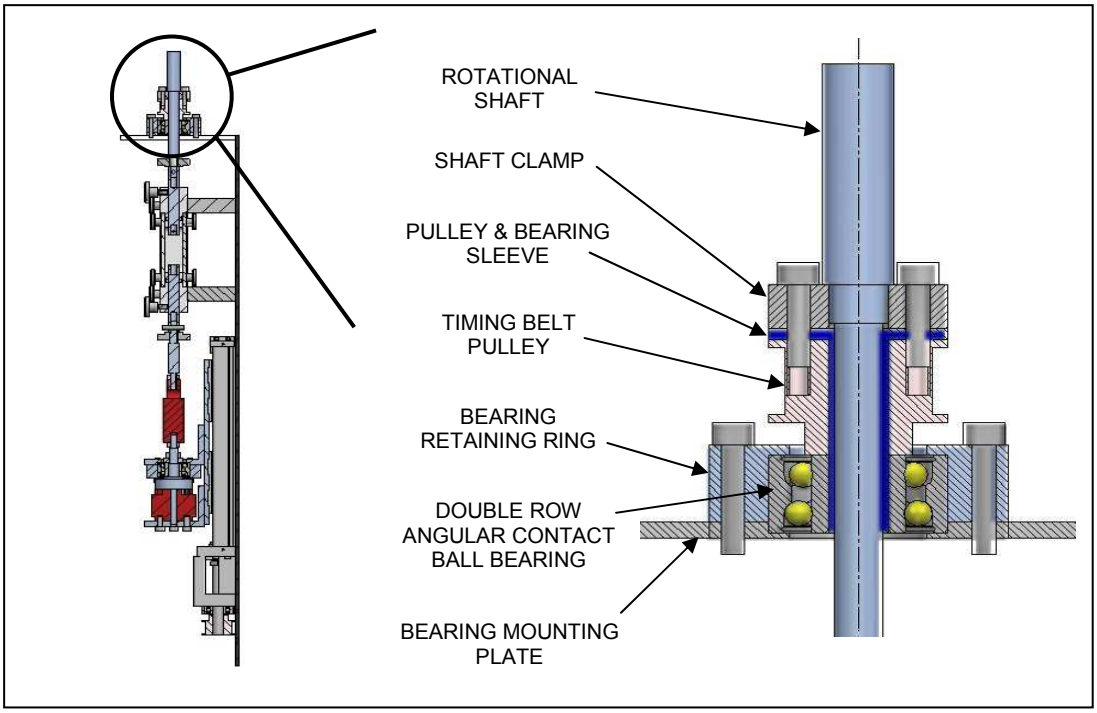

Figure 3-28 Rotational actuation assembly with pulley and bearing sleeve

3.8.2 Mechanical parameter sensing

The tension and torsion imposed on the sample was measured using commercial load and torque cells. A 500N S-Beam load cell (SM-500N, Interface Force Measurements Ltd., Crowthorne, UK) was used to measure the tensile or compressive load transmitted to the sample. It was mounted in-line with the lower chamber shaft as described in Section 3.8.1. A 2Nm reaction torque cell (MRT-2.0Nm, Interface Force Measurements Ltd., Crowthorne, UK) was selected to measure the torque transmitted to the sample.

One face of the torque cell was bolted to the torque cell shaft and the other was fixed to the torque cell mounting bracket (Figure 3-25). As torque is applied through the upper chamber shaft, it is transmitted from the lower chamber shaft through to the torque cell shaft and reacted by the torque cell. The mounting arrangement allowed the torque applied to the sample to be measured by the torque cell and protected the torque cell from experiencing axial load. The torque was transmitted through the load cell, however, it was felt that this simplified the design in addition to minimising the cost without significantly compromising the effectiveness of the load cell. The effect of this is evaluated in Section 6.3.2. Threadlocking compound (Loctite®, Henkel Ltd, Hemel Hempstead, UK) was applied to the threaded connections of the load cell to prevent rotation due to applied torque.

3.8.3 Biological chamber

Nine biological chambers were constructed as described in Section 3.5 and shown in Figure 3-6. The material used for the chambers was polycarbonate as opposed to medical grade ultra high molecular weight polyethylene (UHMWPE) as this was also biocompatible but could be sterilised by autoclave. It also had the advantage of being easier to machine and therefore better tolerances could be achieved. Each chamber had two stainless steel chamber shafts which were sealed with PTFE variseals (RVA100100, Trelleborg Sealing Solutions, Solihull, UK). The shaft seals were held in place by removable stainless steel inserts. Polycarbonate windows were manufactured and sealed with nitrile rubber o-rings. The windows were secured with stainless steel knurled nuts screwing on to stainless steel threaded bar which passed through both sides of the chamber. Inlet and outlet ports were included to allow the flow of media through the chamber. All materials used could be sterilised by autoclave.

3.8.4 Other design details

The method for tissue fixation and media flow system used were as described in Sections 3.6 and 3.7. The bioreactor framework was developed to mount the necessary components and is shown in Figure 3-24. Extruded aluminium section was used for the main frame to allow components to be easily mounted and moved if necessary and additional fixtures could be added at a later time to, for example, mount a camera or measuring equipment. A leak trap was added to the load cell shaft (Figure 3-29) to protect the load and torque cells should any fluid leak from the chamber when in the bioreactor.

The bioreactor was manufactured and is shown in Figure 3-30.

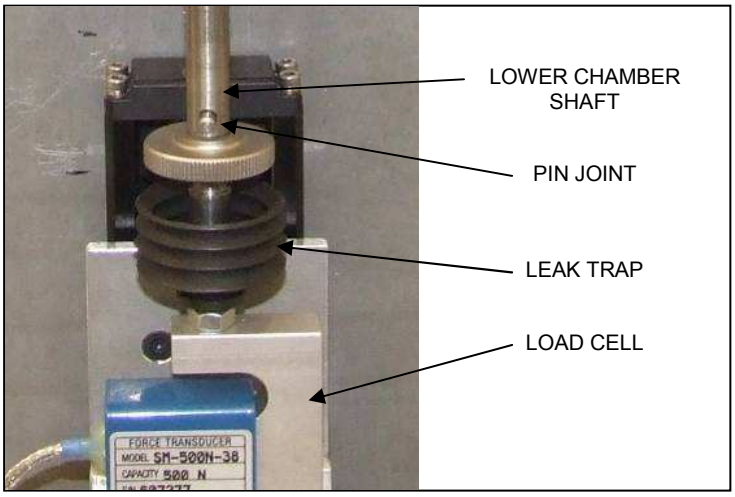

Figure 3-29 Leak trap

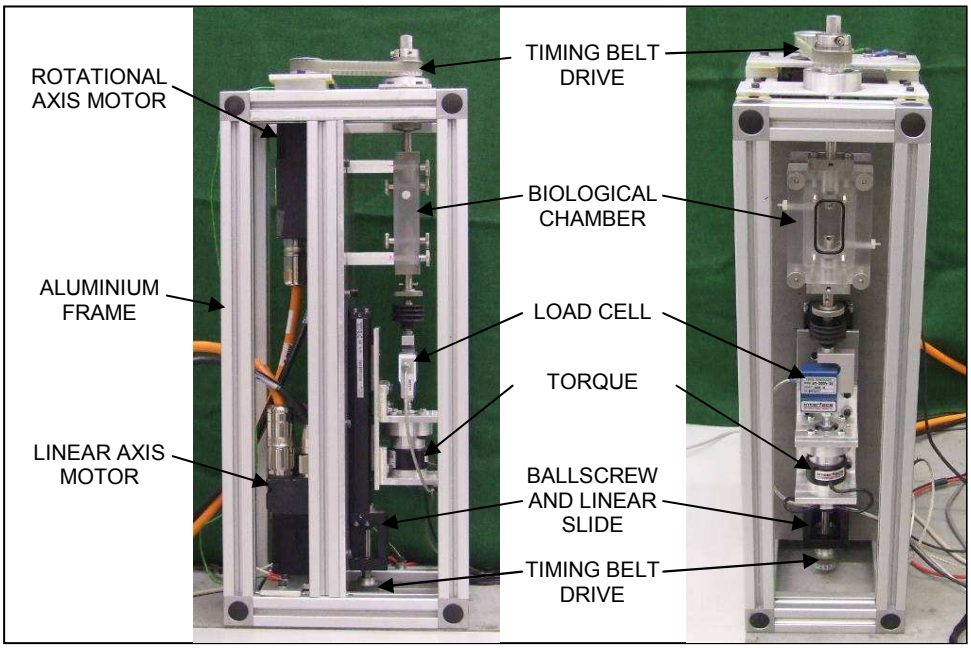

Figure 3-30 Final bioreactor

3.9 Conclusions

A requirement specification was developed for the bioreactor design based on current understanding of biology, physiology and ACL kinetics and kinematics. A prototype bioreactor was designed and manufactured to incorporate cyclic tensile and torsional loading. A sealed biological chamber was developed to contain the tissue and appropriate tissue clamping and medium flow systems were devised.

Through this, Objectives 1 – 6 were achieved.

4 CHALLENGES FROM ELECTRICAL SYSTEM

4.1 Introduction

An electrical system was designed which powered the motors for the linear and rotational axes and detected the load and torque reading from the relevant sensors. A personal computer was included in the system to act as a user interface for the bioreactor motion control system. It also acquired and stored appropriate data from the bioreactor.

4.2 Electrical system

The electrical system for the bioreactor (Figure 4-1) incorporated two brushless servo motors to provide actuation for the linear and rotational axes.

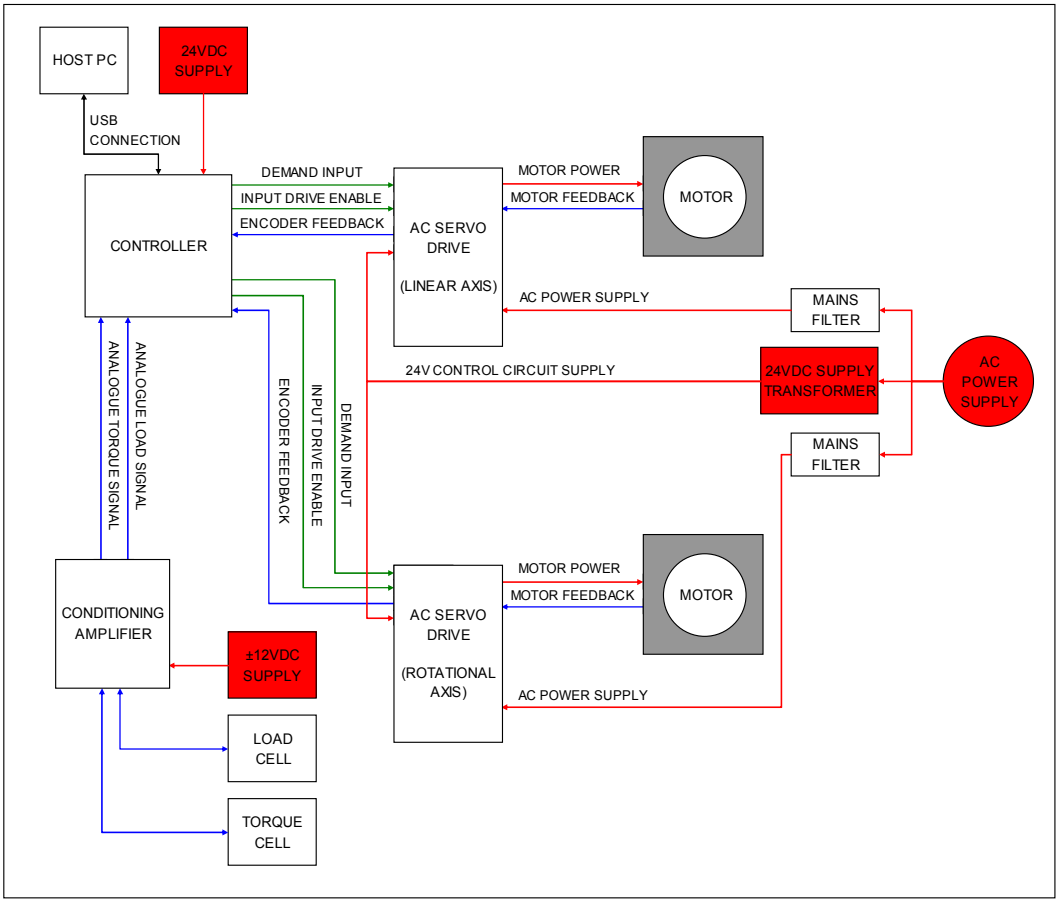

Figure 4-1 Bioreactor electrical wiring schematic

The controller (NextMove ESB, Baldor UK Limited, Bristol, UK) has a built-in servo loop which compares the current position of each motor with the demanded motor position. The error between these two positions is used to produce a torque demand for the motors. For each motor, the controller sends this torque demand to its associated

digital AC servo drive (MicroFlex, Baldor UK Limited, Bristol, UK) which amplifies the demand input up to the voltage supplied to the motor. The motor feeds back its encoder position to the servo drive which in turn passes it to the controller to utilise as positional feedback in the servo loop. Further details of the control loop can be found in Section 5.2. The controller also passes an enable signal to each of the servo drives. The servo drives have an AC power supply to amplify the input demand and the mains supply is filtered to reduce the transmission of mains noise to the servo drives. The control circuits of the servo drives have a 24V d.c. power supply. A separate 24V supply powers the controller and the host PC communicates with the controller via a USB connection.

A conditioning amplifier, manufactured in-house, supplies the load and torque cells with an excitation voltage. The transducers return a signal in millivolts which is amplified to a range of ±10V; this amplified signal is passed to the analogue inputs of the controller. The conditioning amplifier has a ±12V d.c. supply to amplify the signal.

4.3 Electrical noise

Electrical noise is an unwanted electrical signal which distorts or interferes with a desired signal (Park *et al.* 2003). Noise can occur as internal noise where the distorting signal originates from within the system itself or external noise where the noise is generated by an external source within the area. External noise can originate from sources such as mains powered equipment or cables, producing electromagnetic interference (EMI), switching of nearby a.c. or d.c. circuits, also producing EMI, or radio systems producing radio frequency interference. Sources of internal noise can include: thermoelectric potentials caused by temperature differences across components; shot noise, which can be caused by fluctuations within transistors, integrated circuits and other semiconductor devices; and imperfections in the electrical design (Morris 2001b; Park *et al.* 2003).

For an electrical noise problem to exist there must be a source of electrical noise, a mechanism coupling the noise to the affected circuit and a circuit carrying the sensitive signal (Park *et al.* 2003). Noise coupling can occur between signal wires in a measuring circuit and mains cables or equipment as inductive (magnetic) coupling, or capacitive (electrostatic) coupling. Noise resulting from inductive coupling is proportional to the magnitude and frequency of the noise current, to the area enclosed by the signal wires and to the inverse of the distance between the noise source and the signal wires. Noise induced by capacitive coupling is proportional to the magnitude and frequency of the

noise voltage, to the length of the signal wires and to the inverse of the distance between the noise source and the signal wires.

A number of standard techniques exist to reduce the noise coupling from these two mechanisms. Noise reduction can be achieved by increasing the distance between the signal wires and the noise source, reducing the magnitude and frequency of the noise source if possible, and twisting and shielding the signal wires. A minimum separation distance of 0.3m is essential and 1m is preferred (Morris 2001b) to minimise noise induced by both inductance and capacitance. Twisting of the signal wires alternates the induced noise between each twist loop causing the induced noise to cancel itself out. It also reduces the area between the wires of each loop thus reducing noise induced by inductive coupling. Shielding the signal wires in a low impedance braid and grounding the shield at one point reduces capacitive coupling because noise induced in the shield would flow preferentially along the low impedance shield rather than transfer to the signal wires. Also, a magnetic shield which is not grounded can be included to reduce inductive coupling.

Multiple earths can introduce noise into the measuring signal circuit. Ideally, the measuring signal circuit should be isolated from earth, however, it is often the case that leakage to earth from the sensor end and the measuring equipment end of the circuit can occur. This is not a problem if both earths have the same potential. However, if a piece of equipment carrying a large current is connected to the same earth as one of those in the measuring circuit then the potential between the earth planes can vary which results in a noise voltage in the measuring signal circuit.

This can be avoided by keeping earthing circuits separate. Separate earthing circuits should be used for: power earth – used in case a fault occurs in equipment power circuits; safety earth – connecting all metal parts in case any metal becomes electrified by power circuits; analogue earth – to provide a common reference or ground for all analogue signal circuits; and logic earth – to provide a common reference for all logical circuits.

Turning motors and other electrical equipment (both a.c. and d.c.) on and off can create spikes in the supply voltage which can in turn cause fluctuations in the voltage of measuring circuits connected to the same supply. Therefore, separate power supplies should be used for power circuits, logic circuits and analogue signal circuits.

A large source of electrical noise was present in the bioreactor in the form of the two MicroFlex servo drives which powered the motors. Within these drives were a vast array of transistors and other semiconductor devices which produced a significant amount of noise. They were also mains powered meaning they produced EMI. This was apparent when the drives were enabled and a large increase in the level of noise from the drives was visible on an oscilloscope. The electrical system of the bioreactor was designed with the noise reducing features detailed above to limit the transmission of this noise from the drives into the analogue signal circuits of the load and torque cells. Analogue signal cables and power cables were kept as far apart as possible to reduce noise coupling. Twisted signal wires were used throughout to ensure any induced noise cancelled itself out. The analogue signal cables of the load and torque cells were shielded and this shield was grounded at one end. The motor power cables were also shielded and metal power connection plugs were used to ensure the shield was earthed appropriately. A ferrite sleeve was attached to each of the 24V control circuit supplies close to the drives to act as magnetic shields and reduce inductive coupling between the drives and the control circuits. Separate power supplies were used for the conditioning amplifier, the controller, the servo drives' control circuits and the a.c. power supply to the servo drives. Separate earthing circuits were maintained for the analogue signal circuits and the power circuits.

Despite these measures, noise was still induced in the measuring circuits of the load and torque cells. Therefore, signal processing had to be carried out to improve the quality of the analogue signals. Signal filtering removes certain band widths from the measured signal (Morris 2001b) and the controller had a built-in digital low-pass filter which removed the band of frequencies above a set threshold frequency. The digital filter took a time constant as an argument to set the threshold frequency.

The time constant for the digital filter was varied to filter out sufficient noise while still maintaining an accurate signal. A time constant of 3ms was selected to give the optimum filtering. This produced a signal with a noise range of approximately ±0.05V (0.5%) for the load cell and ±0.025V (0.25%) for the torque cell which was acceptable for this application. This noise level can be seen in a 30 second sample of the load and torque signal with the bioreactor static shown in Figure 4-2. However, when a longer sample is taken a significant interference on the signal is apparent as shown in Figure 4-3. Here the data was sampled for 170 seconds and a repetitive distortion of both the

load and torque signal is apparent with a range of approximately ±0.25V (2.5%) on the load cell and ±0.21V (2.1%) on the torque cell.

Further analysis of the noise interference from the two drives was carried out using an oscilloscope to read the true unfiltered noise signals. This showed that there were two individual noise signals, one being produced by each of the servo drives. Furthermore, there was a very small difference in the frequency of the two noise signals. This caused the peaks of the two waves to gradually move towards each other and when they were sufficiently close constructive superposition of the waves occurred, a phenomenon known as "beating" (Pain 2005). This resulted in a large increase in the amplitude of the noise interference occurring approximately every 75 seconds. The digital filter was not able to filter out this beating. In order to reduce the beating effect, analogue low-pass filters were installed, with a threshold frequency of 100Hz, to filter out more of the induced noise. This reduction is shown in Figure 4-4 where the noise on the signal due to the beating effect has a range of approximately ±0.016V (0.16%) on the load cell signal and ±0.033V (0.33%) on the torque cell signal. This was satisfactory for this application.

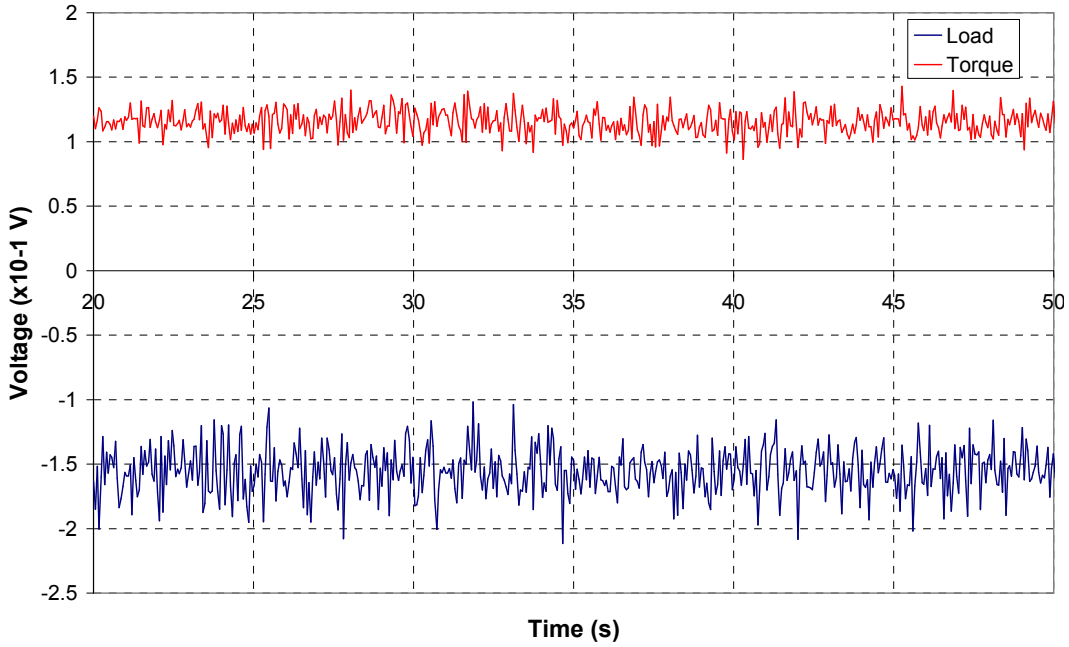

Figure 4-2 A 30 second sample of the filtered load and torque signal

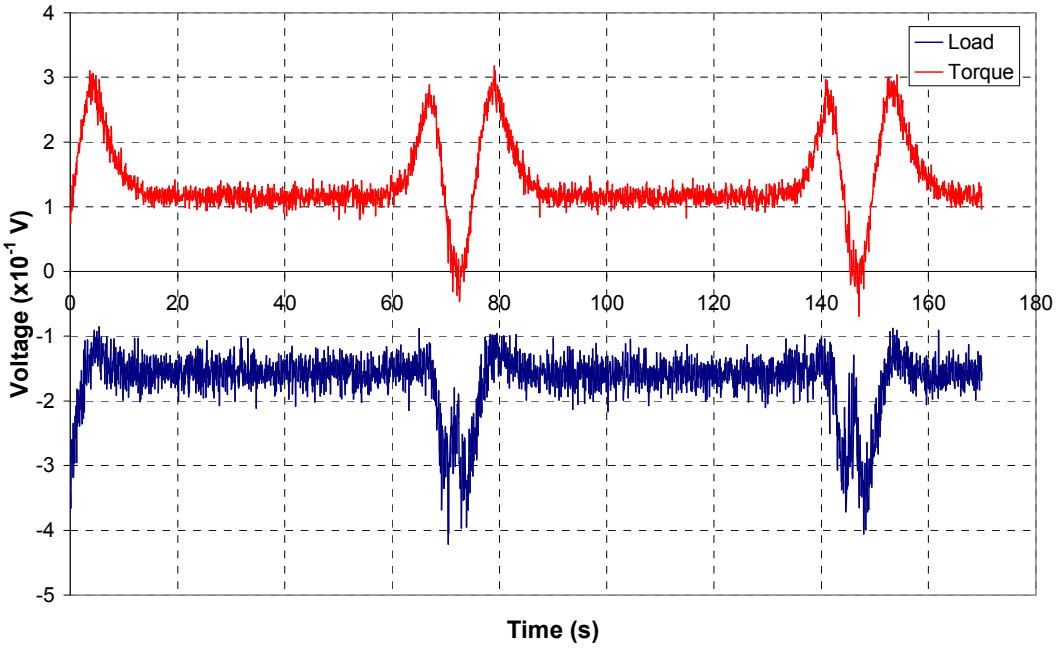

Figure 4-3 A 170 second sample of the load and torque signal showing "beating"

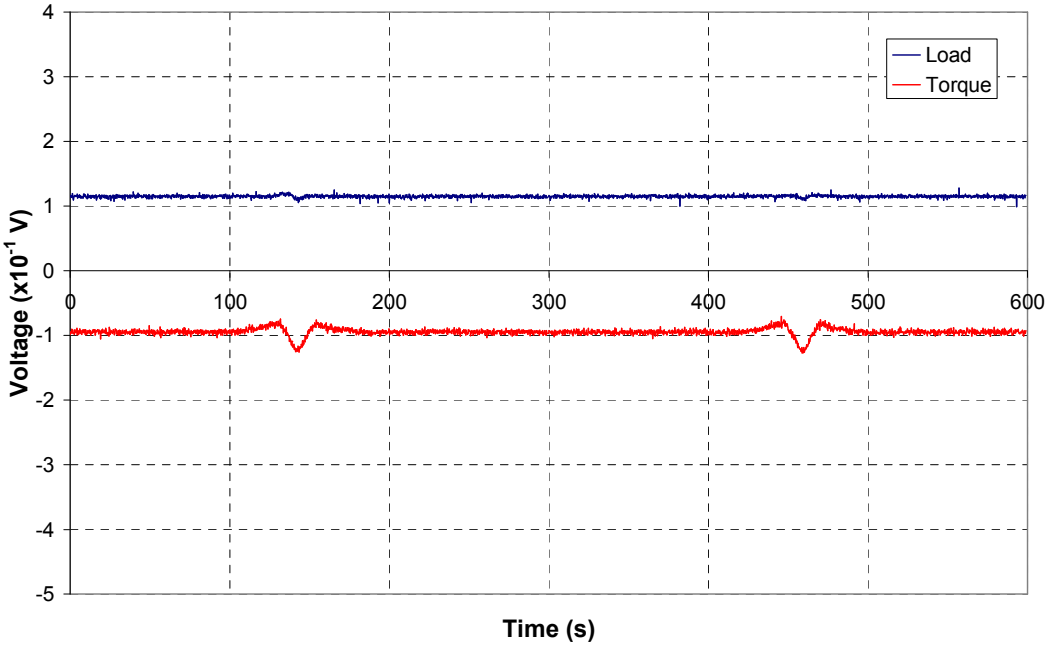

Figure 4-4 A 600 second sample of the load and torque signal with additional filtering showing a significantly reduced beating effect.

4.4 Electrical grounding

Ground is defined as a common reference point of zero potential for all equipment in an earth circuit (Park *et al.* 2003). The initial set-up of the bioreactor earth circuits attempted to keep the instrumentation circuit separate from the equipment circuit.

However, this was not completely possible and there was a degree of coupling between the earthing circuits. This manifested itself as a shift in the voltage output from the load and torque cells of -0.595V and -0.309V respectively when the servo drives were enabled. This was a grounding shift as the zero potential of the instrumentation circuit altered as the drives were enabled. An iterative analytical process was undertaken to identify possible coupling locations and eliminate them where possible or reduce the effect of the coupling if it could not be prevented.

The controller was powered from the same 24V supply as the control circuits of the servo drives. Removing this connection and powering the controller from a separate 24V supply reduced the shift on the sensor signals to -0.386V and -0.222V when the drives were enabled. The next step involved grounding the 0V terminal of the 12V conditioning amplifier power supply to the aluminium case which housed the controller. The case housing the drives was grounded to the aluminium frame of the rig and the housing of the conditioning amplifier was also grounded to the rig. The 12V supply was also grounded to the mains earth in the servo drives case.

One major source of coupling was on the rig itself. Here the equipment and instrumentation earthing circuits became coupled. The frames of the motors were connected to the equipment earth circuit to ensure they do not become electrified due to an internal fault. The frames of the load and torque cells were also connected to the instrumentation circuit. Both the motors and the sensors were mounted on the bioreactor frame and there was electrical continuity between them via the various metal components of the bioreactor.

The motors were removed from the rig to eliminate the transmission of any mechanical vibration but they were connected electrically to the rig via electrical wires. The sensors were also removed and connected via wires in the same way. This allowed a number of combinations of earth connections to be tried and evaluated to further reduce the grounding shift and noise transmission.

Fully isolating the load and torque cells from the bioreactor rig was found to reduce the grounding and noise problems. The mounting method employed to achieve this isolation is shown in Figure 4-5. The two mounting brackets which support the load and torque cells were isolated from the base plate on the linear slide. A thin plastic insulating plate (approximately 1mm thickness) was fixed to the underside of each of the brackets between the brackets and the base plate. It was also necessary to prevent the bolts which

hold the brackets in place from forming an electrical connection. To achieve this, small "top hat" insulators were manufactured to prevent the bolts from making direct contact with the brackets (see Figure 4-5). The diameter of the through holes in the mounting brackets was increased and the "top hats" were fitted.

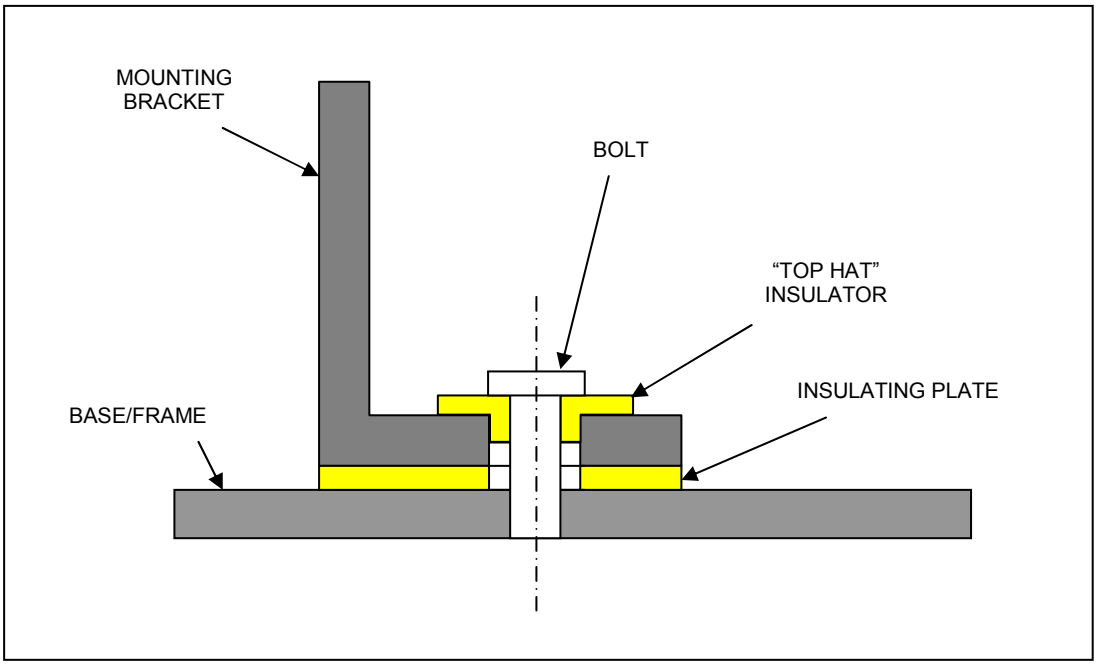

Figure 4-5 Method to electrically insulate a mounting bracket from a base plate or frame

The mounting brackets of the motors contacted the bioreactor frame on both sides of the bioreactor and this may have allowed earth loops to be created. It was found that the grounding shift and noise transmission was improved by isolating the motor mounting brackets from the frame using the same method shown in Figure 4-5. The mounting brackets were then grounded in series to the case which housed the servo drives.

These measures resulted in a grounding shift when the motor servo drives were enabled of 0.067V and 0.128V for the load and torque signals respectively (Figure 4-6). This was an acceptable level of grounding shift for this application.

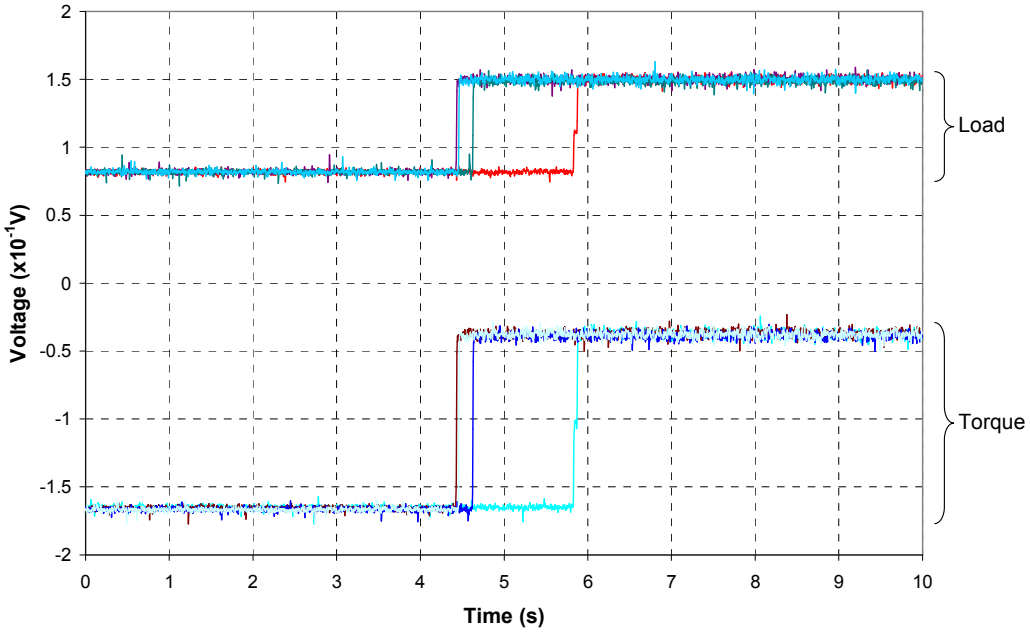

Figure 4-6 Grounding shift of the load and torque signals as the drives are enabled

4.5 Conclusions

Earthing of complex electrical systems can present a lot of challenges to the designer. Standard earthing good practice techniques were followed in the design of the bioreactor electrical system to reduce the noise induced in the instrumentation circuit. The noise signals produced by the motor servo drives were analysed and a beating phenomenon was identified. Further analogue filtering was added to the circuit to filter out more of the induced noise and reduce the effect of beating.

A thorough analysis of the system was also carried out to reduce the grounding shift which occurred when the drives were enabled. An iterative process was conducted to improve the grounding loops for the equipment and instrumentation circuits. The motors and sensors were electrically isolated from the bioreactor rig to limit coupling between the two systems and to prevent earth loops developing due to the multiple mounting points of the motors.

Following this process, the load and torque cell signals experienced a grounding shift of 0.067V and 0.128V when the motor servo drives were enabled and an induced noise level of ±0.016V (0.16%) on the load cell signal and ±0.033V (0.33%) on the torque cell signal. This was an acceptable level of grounding shift and noise for this application.

5 DEVELOPMENT OF CONTROL PROGRAM

A control program was developed to meet the requirements detailed in Section 3.1.

5.1 Program structure

The control program was written using the Mint® programming language to provide motion control of the two Baldor motors and is shown in Appendix C. Mint® is based on the BASIC programming language and incorporates a number of features to allow effective programming.

The Mint® language has multitasking capability to allow a number of control tasks to be carried out concurrently and can have a modular structure with the use of functions and subroutines. Mint can also interact with the analogue and digital inputs and outputs of the controller. A laptop was used to develop the program and act as the user interface to operate the bioreactor. Peer-to-peer data transfer was possible between the laptop and the motion controller via the comms array. The comms array is a section of memory in the controller which could be read or written to via the USB connection.

ActiveX® controls were supplied which allowed access to all the controls in Mint via a front end program. This allowed a user interface to be developed which would be able to interact with the Mint program.

The Mint program was written in the Mint WorkBench environment (Mint WorkBench v5, Baldor UK Limited, Bristol, UK) which was a Mint development front end program compatible with the Baldor controller. Figure 5-1 shows the Mint Workbench program in edit and debug mode. The main window in the centre of the screen allows the program code to be edited and debugged. Commands can be sent directly to the controller via the command window at the bottom of the screen and outputs from the controller can be monitored in the panel above. To the right is the comms watch window which allows the user to monitor and set the values in the comms elements.

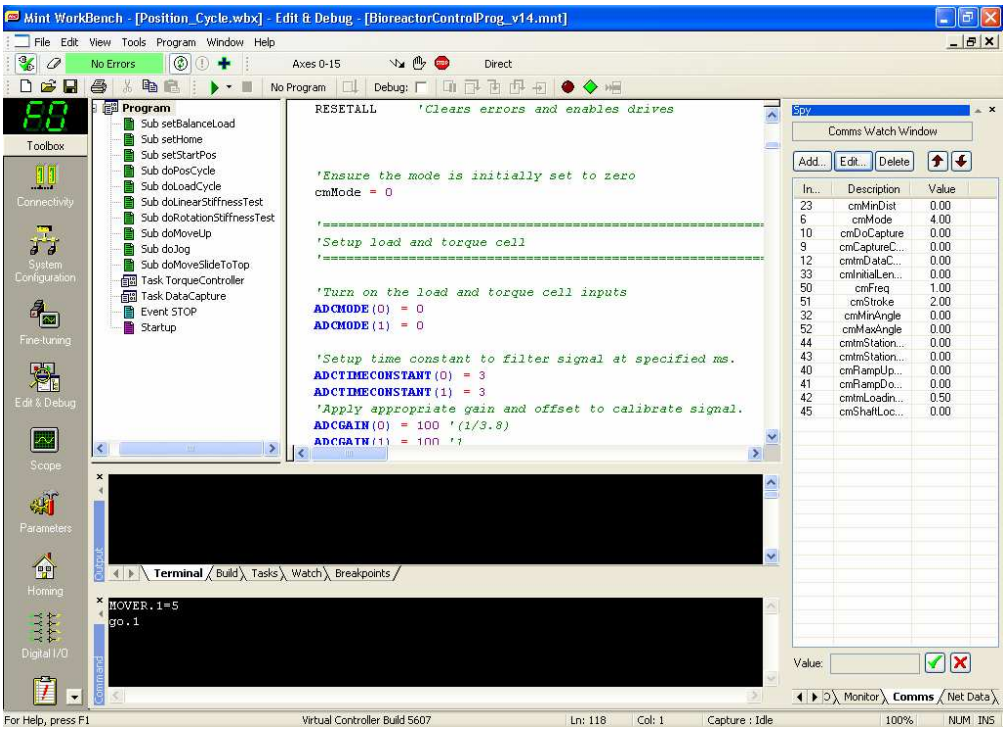

Figure 5-1 Workbench interface in edit and debug mode

Figure 5-2 shows Mint Workbench in scope mode. The panel to the right allows parameters such as position or velocity to be monitored and captured. The captured data is then displayed in the main panel.

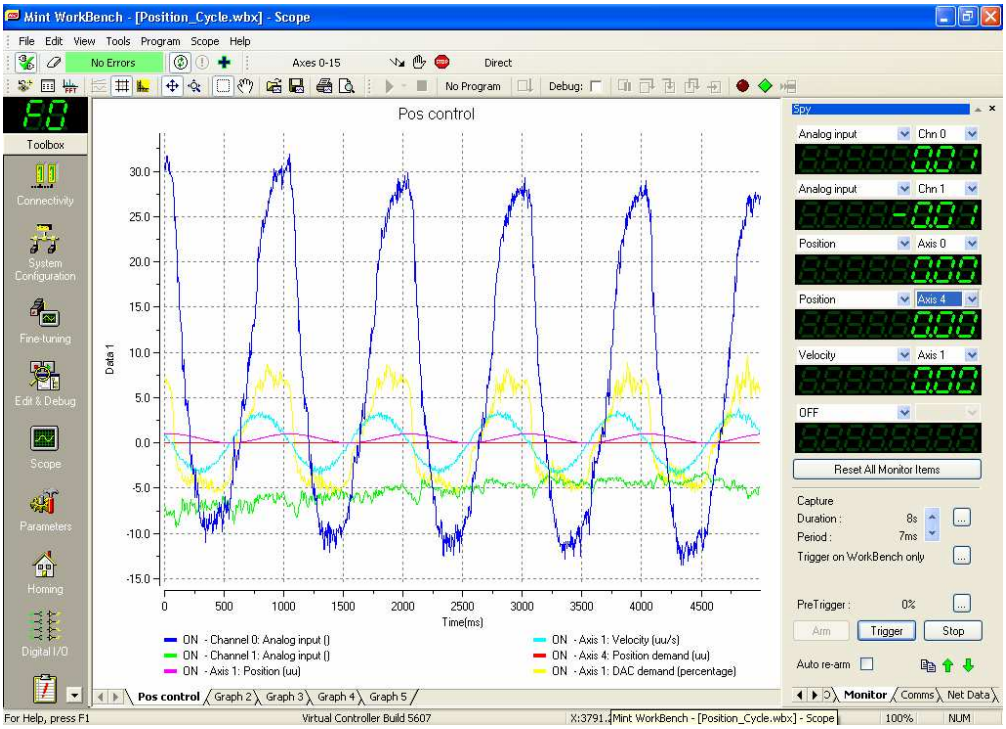

Figure 5-2 Workbench interface in scope mode

5.2 The servo loop

Closed loop motor control was used in the NextMove controller to convert the positional demands into motor demands. Closed loop positional feedback from the motor encoders provided a reduced positional error from the system. The NextMove controller employs a PIDVFA (Proportional, Integral, Derivative, Velocity Feedback, Velocity Feed Forward and Acceleration Feed Forward) control algorithm and the block diagram for the control loop is shown in Figure 5-3.

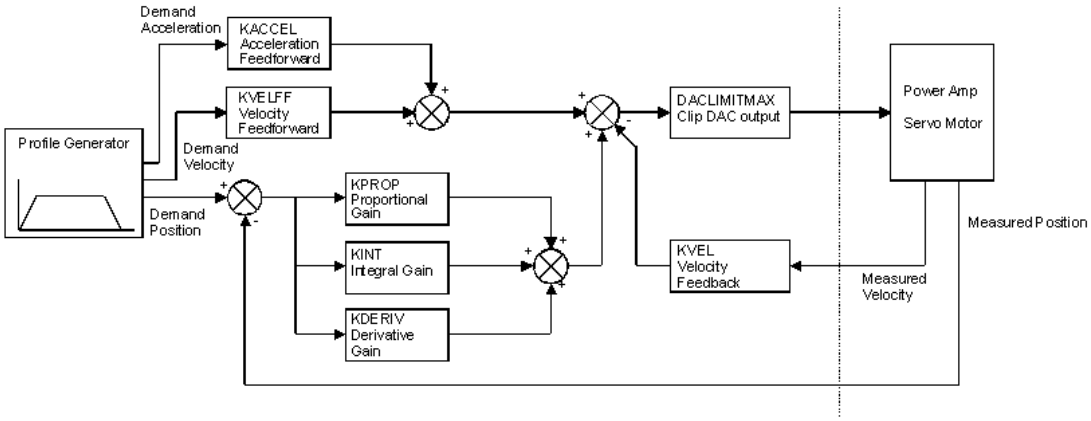

Figure 5-3 Block diagram of the control loop for the NextMove controller (reproduced with permission from Baldor UK Ltd.)

When there is an error between the actual position of the motor and the demanded position, the control loop produces a demand torque to the motor which is proportional to the positional error in the system. The control loop output is the error multiplied by the proportional gain term, KPROP (Figure 5-3), and this signal is amplified before being sent to the motor. Increasing the proportional gain will make the system more resistant to positional error, however, it will also increase the risk of the system overshooting and can cause vibration around the desired position. Very high proportional gains can cause the system to become unstable.

For this reason, a damping term was included in the controller to reduce the risk of instability caused by the proportional gain term. This damping was provided in the NextMove controller in two forms: velocity feedback or a derivative gain. The velocity feedback prevents rapid movements which would be associated with oscillations. Alternatively the derivative gain term (KDERIV, Figure 5-3) is applied to the derivative of the positional error and this provides the same function as the velocity feedback. This is the preferred damping option in a torque control system as was used for the bioreactor.

Small steady state positional errors can occur for which the torque provided by the proportional gain is not sufficient to overcome the static friction in the system. An integrator was included to sum the errors over time and thus gradually increase the torque so the steady state error could be reduced to zero. The speed of the integrator was controller by the integral gain term (KINT, Figure 5-3) which was multiplied by the sum of the errors. However, the integrator reduces the dynamic response of the system, therefore, a software option was provided with the controller which allowed the integrator to be turned off during motion, thus improving the dynamic response. An integration limit was used to limit the effect of the integrator and prevent the accumulation of a very large integral error.

The controller also included a velocity feed forward term which acted to improve the response of the system and reduce any following positional error, and an acceleration feed forward term which was mainly used in a velocity servo system to reduce velocity overshoot when performing high acceleration moves.

The equation for the output demand from the closed loop controller is:

Equation 5-1

$$Demand = KP.e + KD.\frac{\Delta e}{\Delta \tau} - KV.v + KF.V + KI.\sum e + KA.a$$

Where:

KP = proportional gain
KD = derivative gain
KV = velocity feedback gain
KF = velocity feed forward gain
KI = integral gain
KA = acceleration feed forward gain

e = positional error
τ = sample time of servo loop
v = actual axis velocity
V = demand axis velocity
a = acceleration demand

The current output from the amplifier to motors can be limited using the DACLIMITMAX keyword (Figure 5-3).

5.3 Tuning of motors

Tuning of the motors had to be performed to select appropriate gain terms for the motor/encoder combinations and the bioreactor load inertia which were to be applied to the control loop as detailed in the previous section (Section 5.2). The bioreactor had to operate in two modes: position control and load control with feedback from the load and

torque cells. The motors could operate in position control using the control loop built into the controller, however, a separate control loop had to be written to operate the motors in load control and this is described in Section 5.11.1. For both position and load control, it was most appropriate to operate the amplifiers as torque amplifiers as opposed to speed amplifiers. Therefore the derivative was used as the damping term as opposed to velocity feedback. Also, the velocity and acceleration feed forward terms were not required, therefore, the control loop became a standard PID controller and the demand equation was reduced to:

Equation 5-2

$$Demand = KP.e + KD.\frac{\Delta e}{\Delta \tau} + KI.\sum e$$

as: $KV = KF = KA = 0$

Mint WorkBench provided a number of tools to make tuning the motors easier. Firstly there was an Autotune tool. This provided a single parameter, bandwidth, which could be set by the user to describe the required response from the system. The program automatically adjusted the gain terms to achieve the desired response. Increasing the bandwidth provided a faster response which required higher gains. This in turn caused the stiffness of the system to increase whilst reducing the following errors. However, this also increased the risk of overshoot and at very high bandwidths could cause buzzing of the motor due to oscillations at low speed or when stationary.

The bandwidth was adjusted to provide the fastest response whilst limiting overshoot and motor buzzing.

Mint WorkBench also included a Fine-tuning tool which allowed the individual gains to be adjusted to achieve the optimum response from the system. A number of trapezoidal moves were performed to assess the dynamic response of the system and the gains were adjusted where appropriate. The final gain terms were than saved to the Mint program. This fine-tune procedure was performed for both the linear and rotational axes and the final gain terms are shown in Table 5-1:

Table 5-1 Summary of gain terms used for linear and rotational axes

Gain terms	*Linear axis*	*Rotational axis*
Proportional gain (KP)	1.50	1.00
Derivative gain (KD)	7.00	5.00
Integral gain (KI)	0.08	0.02
Integral limit	20.0	20.0

The position of each motor is monitored and fed back by the encoder. Each encoder has 10000 counts per revolution and outputs the number of counts moved. In order to provide a more sensible output for the application, user defined units were specified by applying a scale factor to the encoder output. For example, the units for the rotational axis were revolutions, therefore, a scale factor of 10000 was applied to convert encoder counts to revolutions (10000 counts = 1 rev). The units for the linear axis were millimetres. The leadscrew of the linear slide had a lead of 2mm, meaning one revolution equalled 2mm of displacement. Therefore, a scale factor of 5000 was applied to convert encoder counts to millimetres (5000 counts = 1mm).

5.4 Conditioning of load and torque cell inputs

The amplifiers from the load and torque cells produce a ±10V output and this was connected to the differential analogue inputs on the controller which accept a ±10V signal. This signal is conditioned in the controller through a number of steps as shown in Figure 5-4. Firstly, ADCMODE is set which simply turns the input on or off. The signal then passes through an analogue to digital conversion after which a gain term (ADCGAIN) is applied as a percentage of the full 10V range. An offset can be applied to the signal via the ADCOFFSET keyword again as a percentage of the full range. Finally, the signal is passed through a low pass filter by setting a time constant for the filter with ADCTIMECONSTANT. The final signal is clipped to ±100% of the input range.

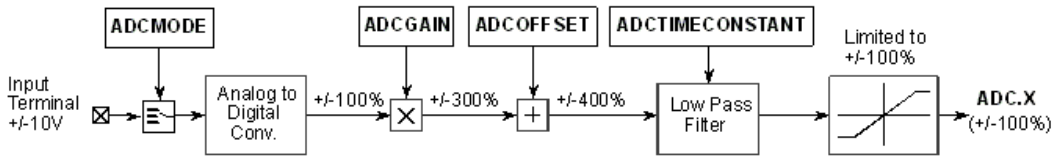

Figure 5-4 Conditioning of analogue input by controller (reproduced with permission from Baldor UK Ltd.)

In the bioreactor control program both the load and torque cell inputs were turned on and the gain was set to 100% to give the full ±10V range. The offset was used to zero the readings from the load and torque cells during the zero load and torque cells subroutine which is described in Section 5.6. A time constant of 3ms was selected to give the optimum filtering as discussed in Section 4.3.

5.5 Safety/protection features

A number of features were built into the bioreactor control program to provide safety to the user and prevent damage to the sensitive components in the bioreactor. Protection limits were set for the load and torque cells using the ADCMAX function. This allowed upper limits for the analogue inputs to be set and if the inputs exceeded these values then an error was generated. The linear and rotational axes were set to monitor both inputs using ADCMONITOR and if an error was generated from either input by exceeding the upper limit then both axes would crash stop and the drives would be disabled. The upper limit for both sensors was set to 90% of the full range.

The current supplied to the motors was limited using DACMAXLIMIT. As the motors were able to produce more torque than was required for most functions their torque was limited to a percentage of their maximum to prevent damaging any other components in the bioreactor. Should, for example, something have jammed in the bioreactor, the motors were not able to produce more torque than was allowed by this limit even if a greater torque was demanded to follow the position profile. This would then generate a following error as the position was too far from the demand position which would crash stop the motor and disable the drive, thus preventing damage to the bioreactor. For the biological test carried out in Section 11 the maximum current for the rotational axis was set to 30% and the maximum current for the linear axis was set to 50%.

An emergency stop button was hard-wired into the system to cut the power to the motors and disable the drives. If the program was in the middle of a move then this would generate a following error and stop the program. However, for some of the moves the following error was disabled, therefore if one of these moves was being executed when the emergency stop was pressed the program would have to be manually stopped. If the program was not stopped and the emergency stop was released, the motor would move rapidly to its demanded position at that time. An emergency stop event was added to the program which would allow a digital stop to be connected to one of the digital inputs on the controller. When the digital input was activated the program event would be executed which would crash stop and disable the axes and stop the program.

5.6 Subroutine to zero the load and torque readings

A subroutine was written to apply an offset to the analogue inputs of the load and torque cells in order to zero the readings. Initially, the offsets were both set to zero and the drives were enabled to ensure any grounding shift due to the drives was present during the zeroing process. The capture function was set up to capture both the analogue inputs for a duration of 10 seconds at the maximum sampling frequency available.

The subroutine was called using a front end LabView program (v7.1, National Instruments, Austin, TX, USA). When the capture was complete the Mint program set one of the comms elements equal to two to act as a flag. The LabView program constantly monitored this comms element and when it was equal to two the LabView program uploaded the captured data. It plotted the captured data for the user and calculated the mean values for the load and torque inputs. It then set two of the comms elements equal to these mean values and set the flag equal to zero again. The Mint program set the offsets for the two analogue inputs equal to the negative of the mean values in the comms elements and a second capture was performed to ensure the inputs had been zeroed correctly. The second capture was again uploaded by the LabView program and plotted for the user to view. If the user was satisfied with the plots then the subroutine could finish or if not the process could be repeated.

The LabView interface is shown in Figure 5-5 and the logic of the subroutine is summarised in Figure 5-6.

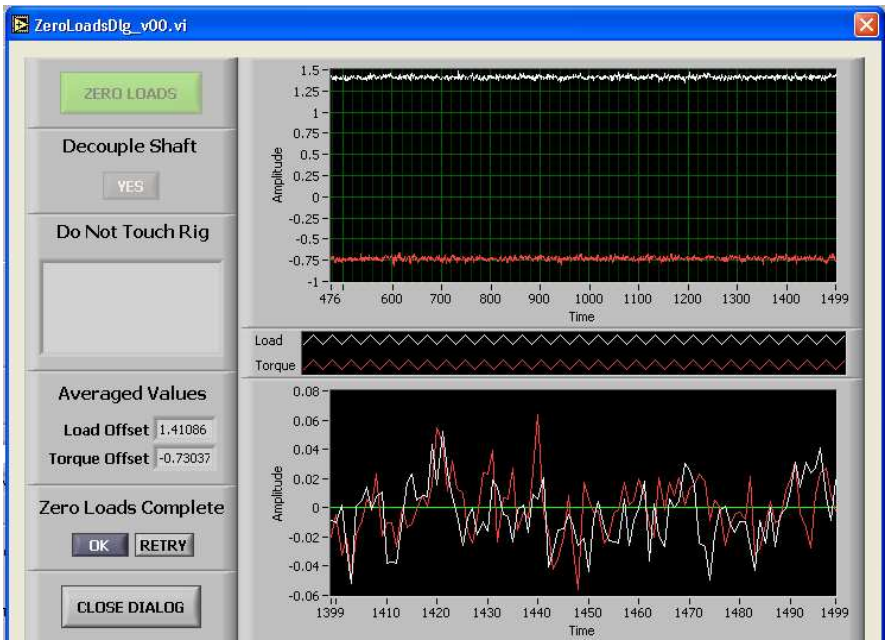

Figure 5-5 LabView interface to zero the load and torque cell readings

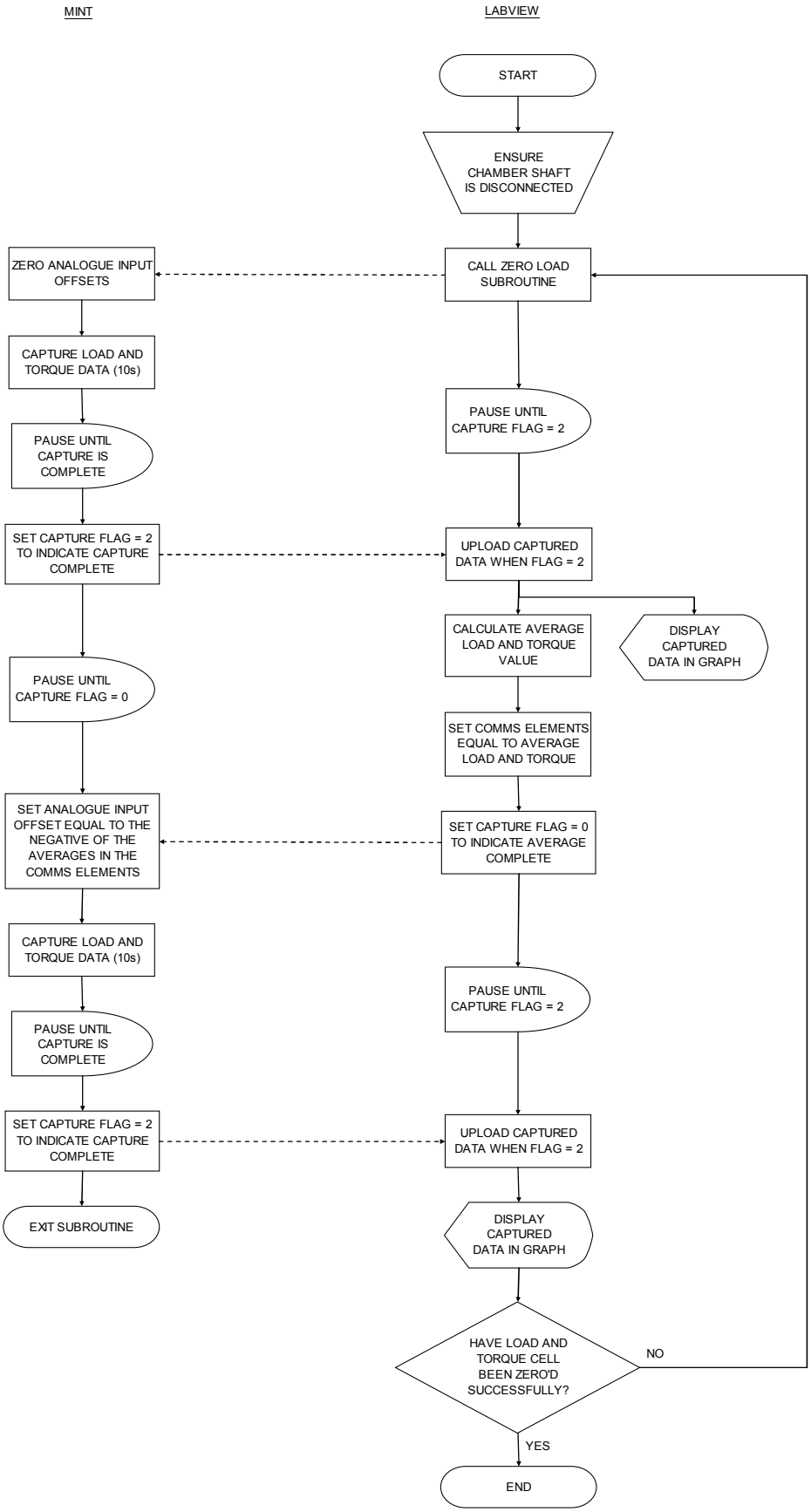

Figure 5-6 Summary of zero load and torque cell logic

5.7 Subroutine to set the 'home' position for a chamber

The motors were fitted with incremental encoders which do not have an absolute reference point. Therefore, it was necessary to reference the motor positions to provide an appropriate zero position. The most appropriate zero position for the linear axis was the position where the ends of the two chamber shafts were touching, hence, the positional reading from the linear axis referred to the distance between the ends of the chamber shafts and the free length of any sample held by the chamber shafts. The most appropriate zero position for the rotational axis was the position where the fibres of the sample were orientated linearly. Therefore, the rotational position referred to the angle of twist of the sample.

Each time the bioreactor controller was turned off it would lose its reference position and when it was turned on again it would reset its position to zero regardless of where it actually was. It would not have been possible to reset the position by measuring the distance between the chamber ends each time because during an experiment the chambers would be sealed with biological tissue clamped into the chamber shafts. Instead, the position between the chamber shafts was measured when the linear axis was moved to the upper stop of the linear slide. This could easily be reset for each chamber before the chamber was inserted into the bioreactor.

A pair of chamber shafts were inserted in the bioreactor without the chamber in place. Vertical motion of the upper bioreactor shaft was prevented using a bolt and bracket positioned temporarily above it. As the linear axis could not move up far enough for the chamber shafts to touch, a precision engineered calibration block of length 25.4mm was positioned between the chamber shafts. The lower chamber shaft was advanced upwards until the calibration block was tight between the two shafts and the position of the axis was set at 25.4mm.

This was achieved in the Mint subroutine by initially limiting the motor torque to 13% using DACMAXLIMIT (Section 5.2) to prevent damage to the bioreactor. In order to prevent an error being generated when the calibration block was secured between the shafts and no more motion was permitted, the following error was disabled. The axis was then moved vertically at a speed of 0.5mm/s until the torque supplied by the motor reached 12% after which the move was stopped. The system was allowed to settle for 200ms and then the current position of the linear axis was set to the calibration block size, 25.4mm.

The program paused until a comms flag was set to indicate that the user was ready to remove the calibration block. The linear axis then moved down 2mm to allow the user to remove the calibration block. The program paused again until the user set the comms flag to indicate the calibration block had been removed. At this point the linear position reading had accurately been set to the distance between the ends of the chamber shafts. The linear axis was then advanced again until it reached the top of the linear slide so an accurate position for the top of the slide could be recorded. The linear axis was moved vertically with a speed of 0.5mm/s until the motor torque reached 12% to indicate the axis was at the top of the slide. The move was then cancelled and again the system was allowed to settle before the position of the linear axis was recorded. The recorded position was the distance between the two chamber shafts when the linear axis was at the top of the linear slide. This position could be set before the chamber was inserted into the bioreactor.

As there were slight differences in the lengths of each of the chamber shafts, this process was repeated for the shafts from each chamber and the position at the top of the slide was recorded for each.

The logic of the home position subroutine is summarised in Figure 5-7.

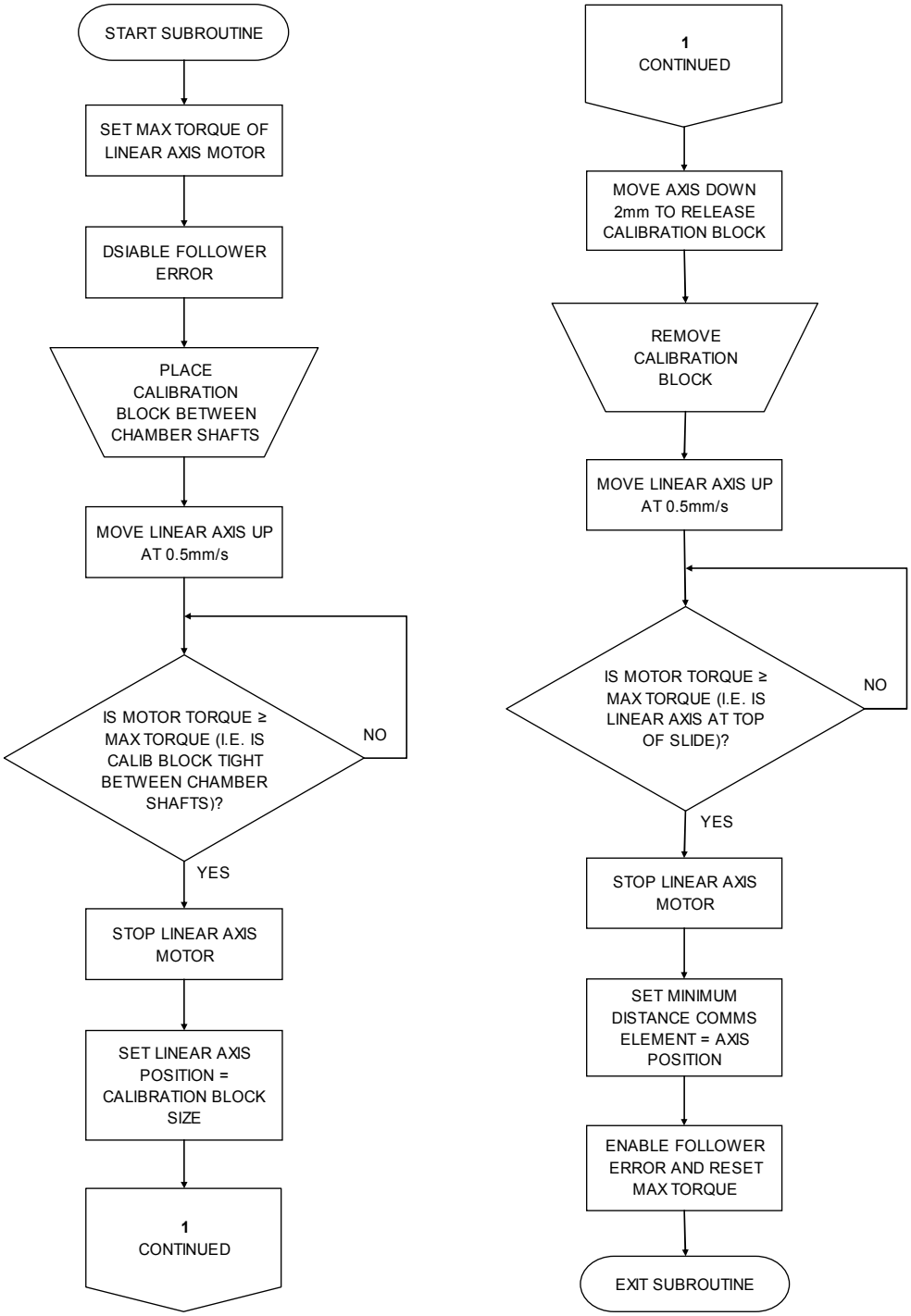

Figure 5-7 Summary of home subroutine logic

5.8 Subroutine to preload the tissue and set the initial positions for a chamber

A subroutine was written to apply a linear preload to the tissue and set the initial positions of the linear and rotational axes. Firstly the zero position for the rotational axis was manually set by vertically aligning the sample fibres. The tissue was then rotated to the initial rotational position as specified by the user if different from zero. If in a particular experiment, it was more appropriate to set the zero rotation as the unstrained position of the tissue, visually set by the operator, regardless of fibre orientation then that was also possible with this algorithm.

In the Mint program, both drives were disabled as was the follower error on the rotational axis. The upper bioreactor shaft could be manually rotated to the most appropriate zero position by the operator. The operator then set a flag in a comms element which allowed the program to clear any errors, enable the drives and follower error, and set the current position on the rotational axis to zero. If an initial rotation other than zero had been set by the operator then the rotational axis would move to that position.

In the linear axis it was necessary to apply a small preload to the tissue to ensure all the slack was removed and strain was applied to a consistent initial length for each tissue sample. The preload had to be applied above any friction, therefore, before the preload procedure could commence the operator had to evaluate the value of dynamic friction in the system. The sources of friction are discussed in Section 9 and the method for evaluating the dynamic friction is discussed in Section 11.1.3. A typical preload curve is shown in Figure 5-8. Upon commencement of motion there is an initial load spike due to static friction which then reduces to a constant level of dynamic friction. The tissue preload is applied above this load level and when the preload level is reached the motion is stopped and the load reduces due to stress relaxation.

In the Mint program the user inputted the desired preload value in Newtons and the measured value of dynamic friction as a percentage of the full load cell range into two of the comms elements. Using the calibration factor for the load cell (Section 6.1), the program then calculated the load cell input value as a percentage of the full range required to apply the desired preload (Equation 5-3):

Equation 5-3

Preload Voltage (%) = [Preload (N) × Load Cell Calibration Factor (% / N)]
+ Friction Voltage (%)

If the current load cell reading was less than the desired preload voltage, the linear axis was advanced downwards at a speed of 0.5mm/s. A pause of 100ms after the move commenced was included in the program so as to ignore the spike due to static friction. When the load cell reading was greater than or equal to the preload voltage the motion was stopped. If the load cell reading was greater than the preload voltage due to initial overshoot the linear axis reversed at a speed of 0.05mm/s until the load cell reading was less than or equal to the preload voltage. The position of the linear axis was recorded as the initial length of the tissue.

This subroutine allowed a small preload to be applied to the tissue and the initial length and rotation to be set and recorded. The logic of the preload subroutine is summarised in Figure 5-9.

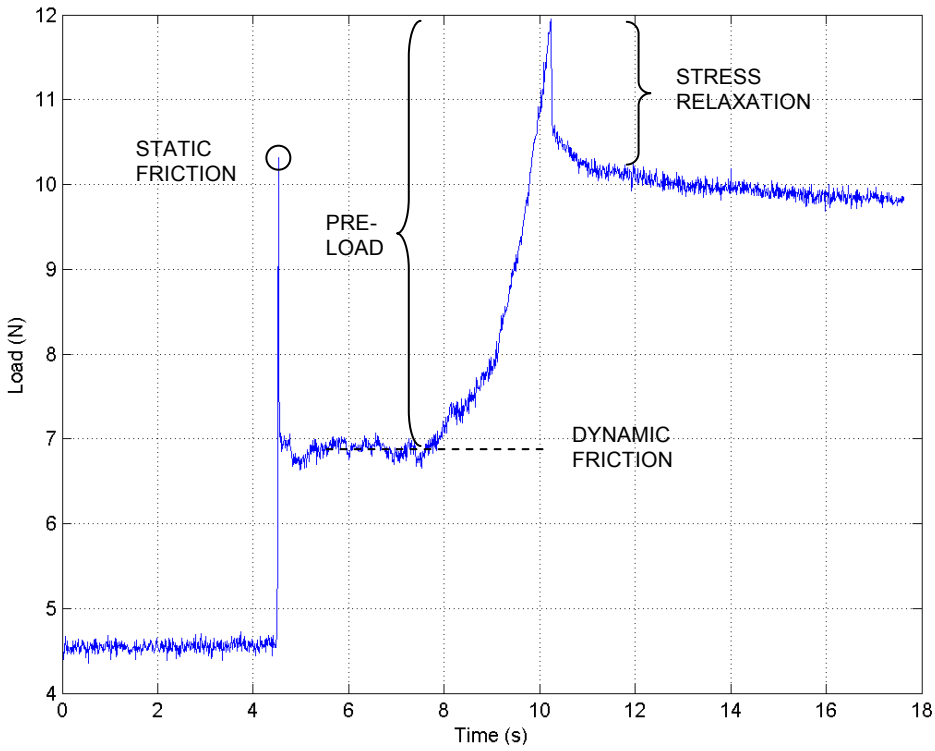

Figure 5-8 Typical preload plot

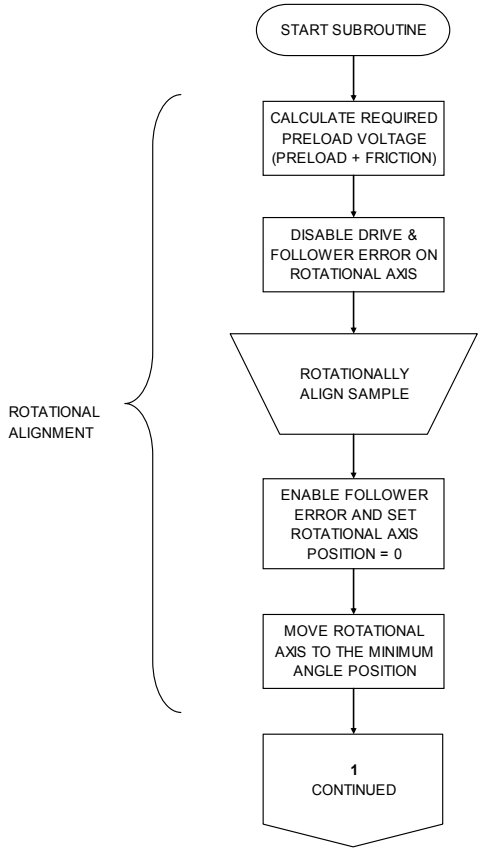

Figure 5-9 Summary of preload subroutine logic

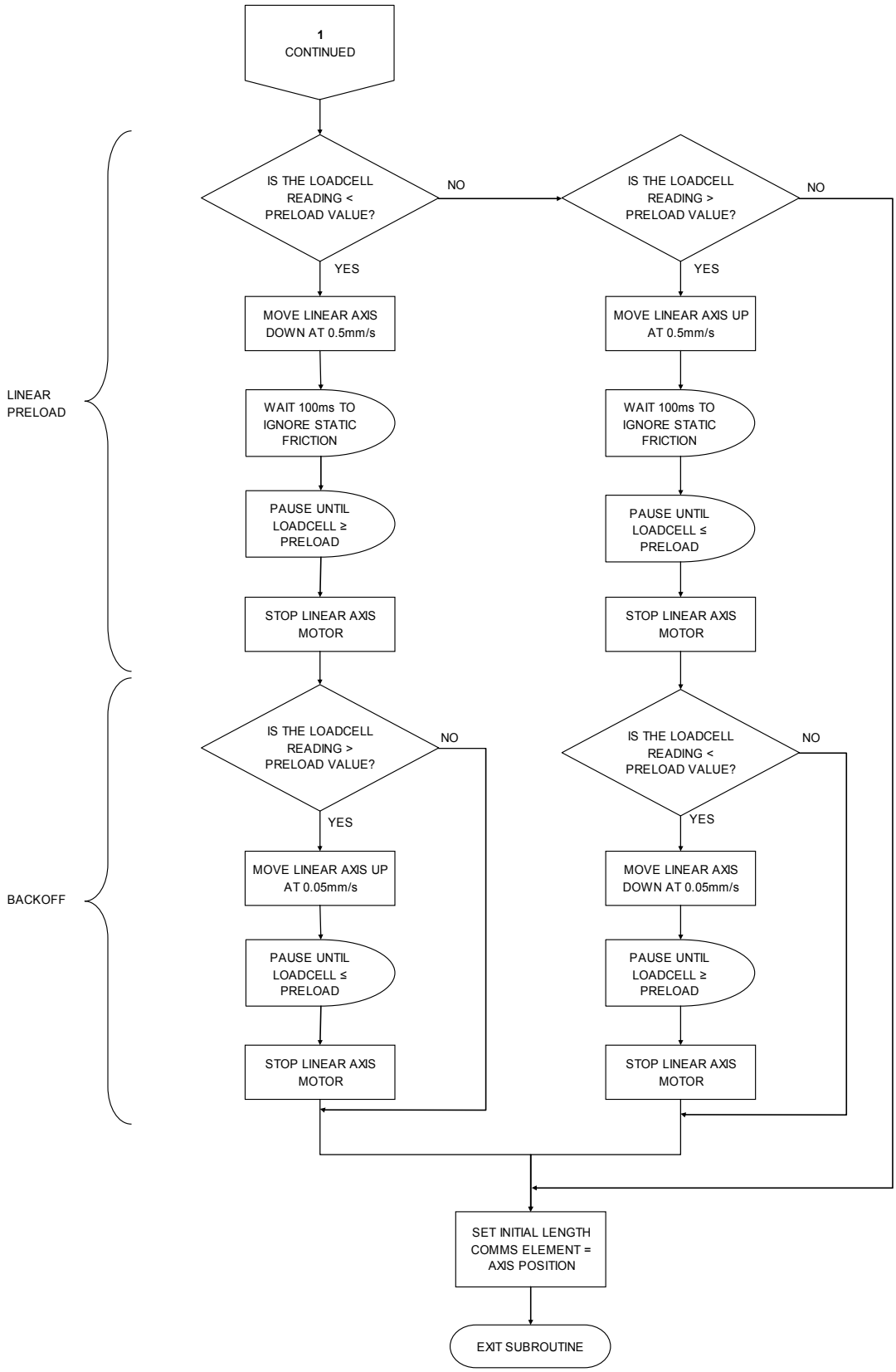

Figure 5-9 Continued. Summary of preload subroutine logic

5.9 Subroutine to cycle the bioreactor in position control

A subroutine was written to enable the motors to perform a cyclic sinusoidal positional profile. The user needed to be able to set the stroke of the linear axis and the maximum and minimum angles of the rotational axis along with the frequency of the cycle. In addition to this it was desirable to include the option to hold the tissue at the beginning and end of the stroke or rotation for a period of time. As discussed in Section 1.9.3, it can be useful to gradually increase the strain applied to a tissue in order to condition the tissue and therefore it was also desirable to include the option to gradually ramp up and ramp down the amplitude of the cycles at the beginning and end of the loading session.

This loading was achieved using the cam profiling feature in Mint. This feature allowed a slave axis to follow a master axis such that the slave axis will move a certain distance for a given movement of the master axis. To achieve this, the position of the slave axis was segmented and stored in a cam array and linear interpolation was performed to provide a constant velocity between each segment. A master distance array specified how far the master axis had to move for each segment of the slave profile (Figure 5-10). The software cam had to be linked to an external source, i.e. the motors, before the profile was executed. The values in the cam array could be either relative, absolute to the cam, i.e. the start of the cam is the zero position, or absolute to the motor position. The cam can be executed as a single cycle or continuously.

In order to achieve a simple sine wave with the cam profile, a slave axis could be created. The sine wave would be segmented evenly and the positional value of each segment would be stored in the cam array. A master axis would also be created using a virtual axis which allows motion to be simulated without moving any physical axis. The master axis could be set up with an equal master distance for each segment of the cam array. If the master axis was moved at a constant velocity then the slave axis would move to the position in each segment of the cam array with a constant time for each segment. Therefore, moving the master axis would cause the slave axis to move with a sinusoidal profile. The frequency of the slave axis motion can be controlled by adjusting the master axis velocity and pauses can be included at the beginning and end of the stroke by increasing the master distance for that segment. A sinusoidal wave was achieved in this case, however, any loading profile could be created for the cam array.

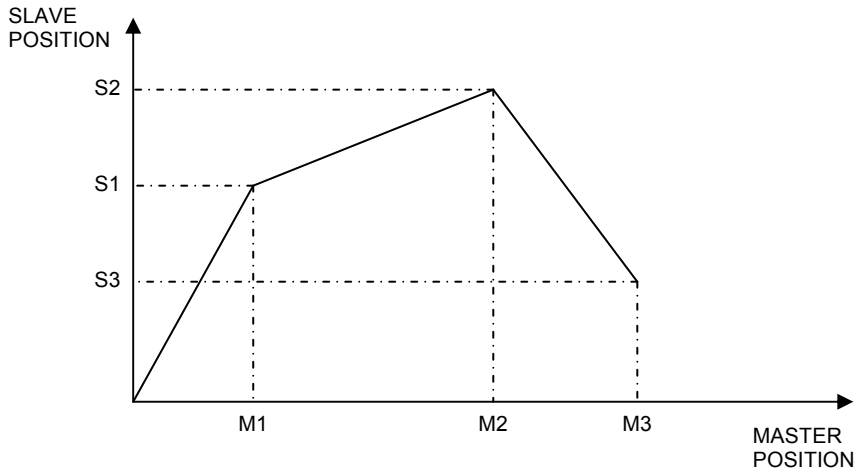

Figure 5-10 Slave and master segmentation

The cam cycle for the linear and rotational motion of the bioreactor is shown in Figure 5-11. It is a sinusoidal profile with a phase and amplitude shift. A cam array was created for the linear axis using the following equation (Equation 5-4) to describe the profile:

Equation 5-4

$$\text{For } i = 1 \text{ To } nDataPoints$$
$$fLinearCamArray(i+1) = cmStroke * (1 + \text{Cos}(180 + i * 360/nDataPoints)) * 0.5$$
$$\text{Next } i$$

Where:

i =	an incremental variable to populate the array
nDataPoints =	the number of data points/segments in the cam array
fLinearCamArray =	the cam array for the linear axis to be populated
cmStroke =	the required stroke supplied by the user in a comms element (mm)

The positional values in the cam array were absolute values to the start of the cam. For the profile shown in Figure 5-11, each of the cam segments are evenly spaced, therefore, that profile would be executed if the master axis moved at a constant speed with a consistent master distance for each segment. The master distance for each segment was set to 10 units and this allowed the required speed of the master axis to be calculated to achieve the frequency specified by the user. The speed of the master axis was calculated as:

Equation 5-5

fMasterAxisSpeed = nBasicMasterDist * nDataPoints * cmFreq

Where:

fMasterAxisSpeed = the calculated speed of the master axis (units/s)

nBasicMasterDist = the master distance of each segment (i.e. 10 units)

nDataPoints = the number of data points or segments in the cam array

cmFreq = the required frequency of the profile supplied by the user in a comms element (Hz)

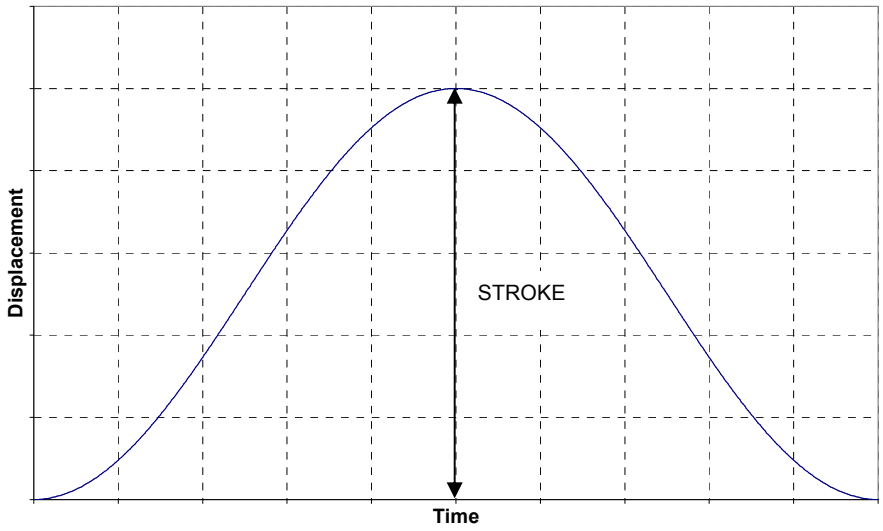

Figure 5-11 Cam cycle for linear and rotational motion

It was also necessary to include a facility to hold the tissue at the start and end of the stroke for a time specified by the user (Figure 5-12). The user inputted these times into the comms element cmtmStationaryHome for the start of the stroke, and cmtmStationaryExt for the end of the stroke. This pause was achieved by increasing the master distance of the segments at the middle (end of the stroke) and end (start of the stroke) of the profile. As the master axis moves at a constant velocity, this will cause the slave axis to pause until moving to the next segment. The master distance array was populated with the basic master distance of 10 units and the end and middle distances were overwritten as follows:

Equation 5-6

fCamMasterDistArray(nDataPoints) = fMasterAxisSpeed * cmtmStationaryHome

fCamMasterDistArray(nDataPoints / 2) = fMasterAxisSpeed * cmtmStationaryExt

Where:

fCamMasterDistArray = the master distance array

nDataPoints = the number of data points/segments in the cam array

fMasterAxisSpeed = the speed of the master axis (units/s)

cmtmStationaryHome = the time required to hold the tissue at the start of the stroke as defined by the user (s)

cmtmStationaryExt = the time required to hold the tissue at the end of the stroke as defined by the user (s)

The inclusion of these holds did not affect the frequency of the profile therefore the period of one cycle was:

Equation 5-7

$$Cycle\ Period = \left({}^{1}\!/_{cmFreq} \right) + cmtmStationaryHome + cmtmStationaryExt\ .$$

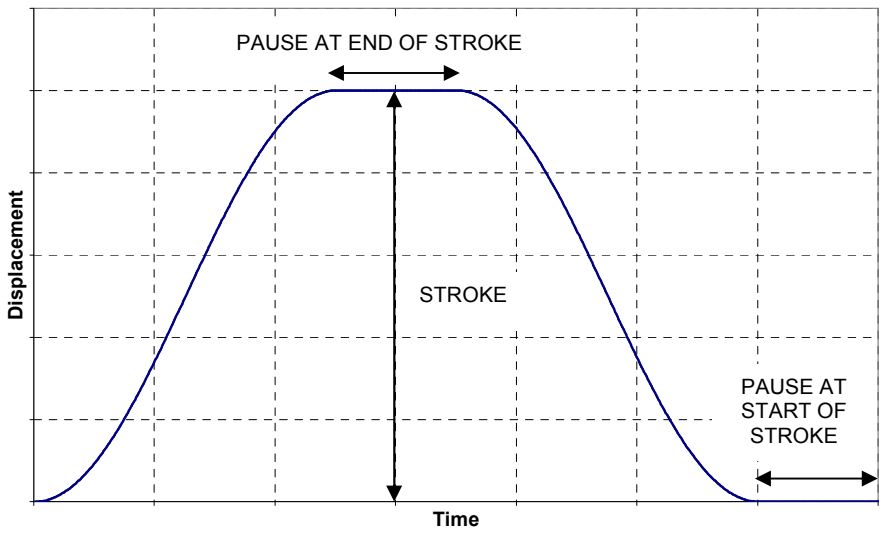

Figure 5-12 Cam profile including user defined pauses at the start and end of the stroke

The final modification required for the profile was to allow the amplitude of the motion to be gradually ramped up at the start of loading and ramped down at the end of loading. The user defined the number of ramp up cycles required and the program calculated the amplitude of each cycle required to linearly increase the amplitude as shown in Figure 5-13. The cam was scaled using the CAMAMPLITUDE keyword and the scaling was calculated as:

Equation 5-8

CAMAMPLITUDE(0) = ((2 * k) - 1) / (2 * cmRampUpCycles)

Where:

CAMAMPLITUDE = the applied scaling factor

k = an incremental variable to indicate the current cycle number

cmRampUpCycles = the number of ramp up cycles as defined by the user in the comms element

Similarly, the amplitude for the ramp down cycles was calculated as:

Equation 5-9

CAMAMPLITUDE(0) = 1 - ((2 * k) - 1) / (2 * cmRampDownCycles)

Where:

cmRampDownCycles = the number of ramp down cycles as defined by the user in the comms element

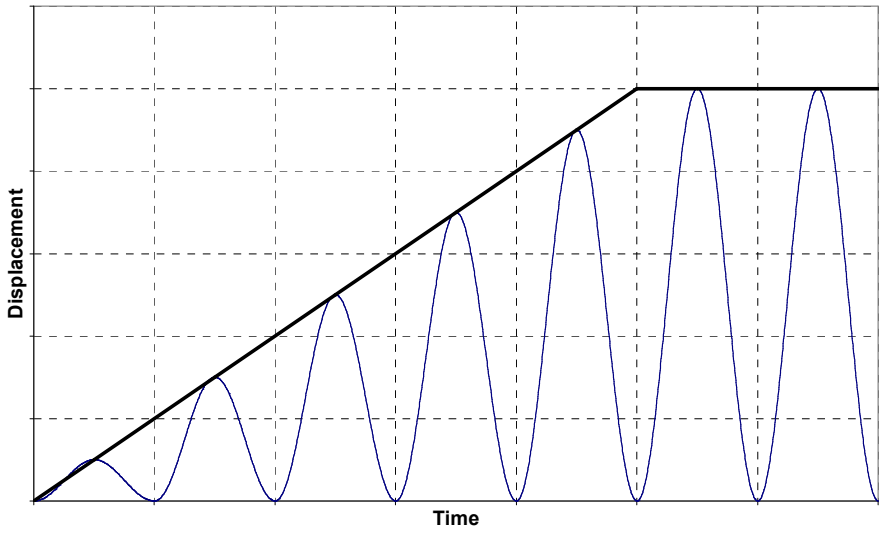

Figure 5-13 Linear ramp up of amplitude in five cycles

The cam outlined above was implemented in the positional cycle subroutine in the Mint program. The subroutine starts by enabling both the motor drives and ensuring the axes are in the initial linear and rotational positions as set by the user in the comms elements. All the necessary elements for the cam are set up including the cam arrays, master distance arrays and the master axis velocity. The master axes for the linear and rotational

cams were configured as virtual axes and the linear and rotational axes were set as the slave axes and linked to the respective master axes.

The master axes were moved at the calculated master axis speed and the time was initialised to zero. If the number of ramp up cycles set by the operator was greater than zero then the program entered a loop to execute a single cam cycle in each iteration of the loop. The cam amplitude was gradually increased during each iteration in accordance with Equation 5-8 until the required number of ramp up cycles had been executed.

A pause was included in the ramp up loop to halt the execution of the program until the linear and rotational axes become idle. This was to ensure both axes had finished moving before executing the next ramp up cam cycle. During the main loading cycle the cams were run continuously. The timer was initialised to zero just before the ramp up cycle was started and a pause was included after the continuous cam was started until the timer reached a specified time. This time was calculated in milliseconds as (Equation 5-10):

Equation 5-10

End time = ((cmtmLoadingDuration * 60) - (cmRampDownCycles/cmFreq)) * 1000

Where:

cmtmLoadingDuration = the total duration of each loading session in minutes as defined by the user in the comms element

cmRampDownCycles = the number of ramp down cycles as defined by the user in the comms element

cmFreq = the required frequency of the profile supplied by the user in the comms element (Hz)

The end time of the continuous cam was calculated as the total duration for the loading session minus the time required to execute the number of ramp down cycles specified by the user. At the end of the continuous cam the axes had to be at their initial positions so the ramp down cycles could commence. However, when the calculated end time had elapsed the axes may be in the middle of a cycle. Therefore, it was necessary for the cycle to finish before the continuous cams were cancelled. To achieve this a further pause was included to wait until the final cam segment was executed. The linear and rotational cams can get slightly out of synchronisation, therefore, if the pause condition

was to wait until the final segments of both cams were executed at the same time then the program may need to go through a number of additional cycles until the cams are once again synchronised. This was undesirable and it was a better option to wait until one of the cams had come to the end of its cycle and then cancel the motion on both axes.

From this point the program executed the ramp down cycles if required as described for the ramp up cycles and using the CAMAMPLITUDE calculated in Equation 5-9. The program ensured the axes were at their initial positions and held here until the user had locked the chamber shafts in place to prevent any motion. The user could then set a flag in one of the comms elements to end the subroutine. The logic of the positional control subroutine is summarised in Figure 5-14.

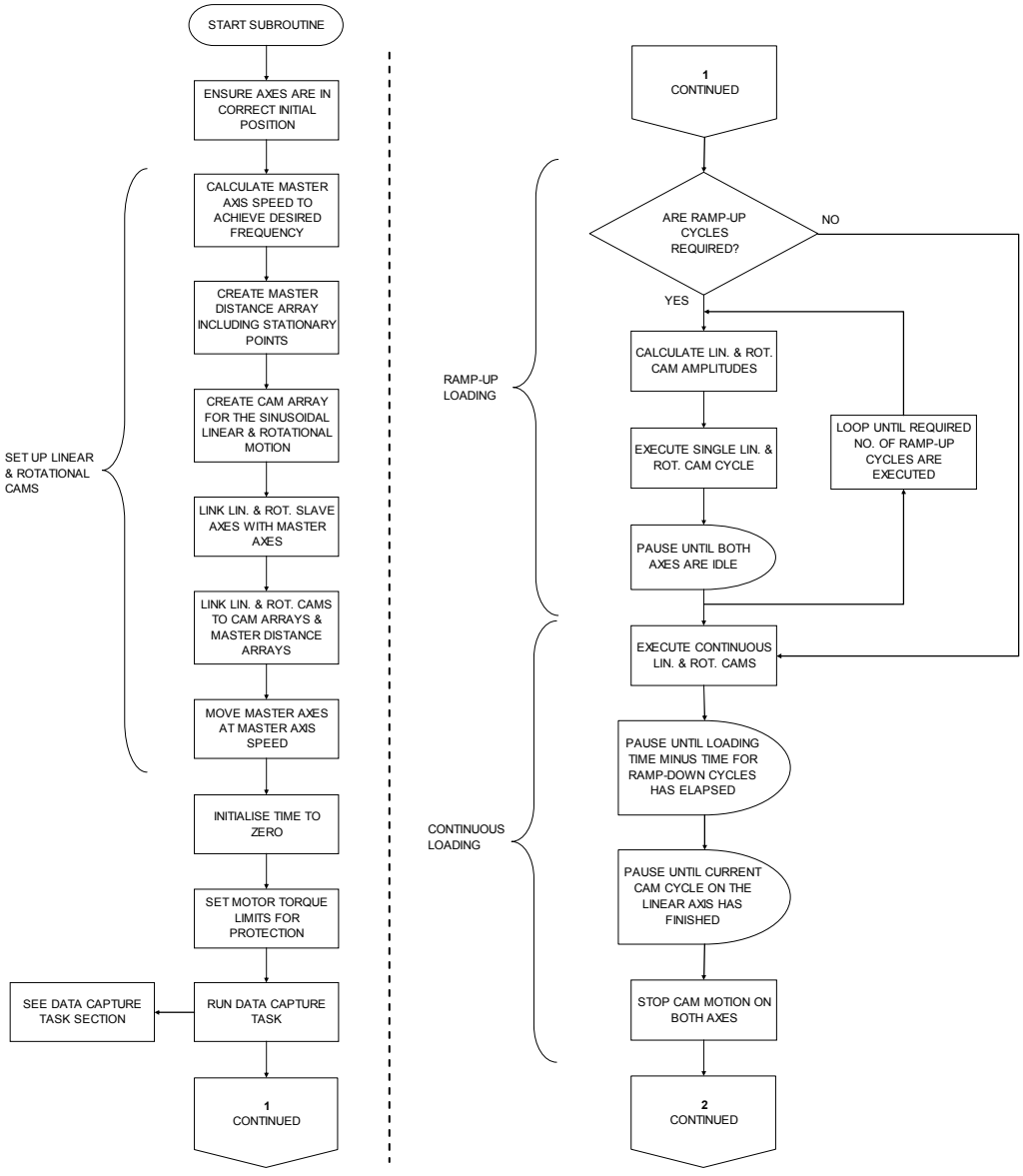

Figure 5-14 Summary of positional control loading subroutine logic

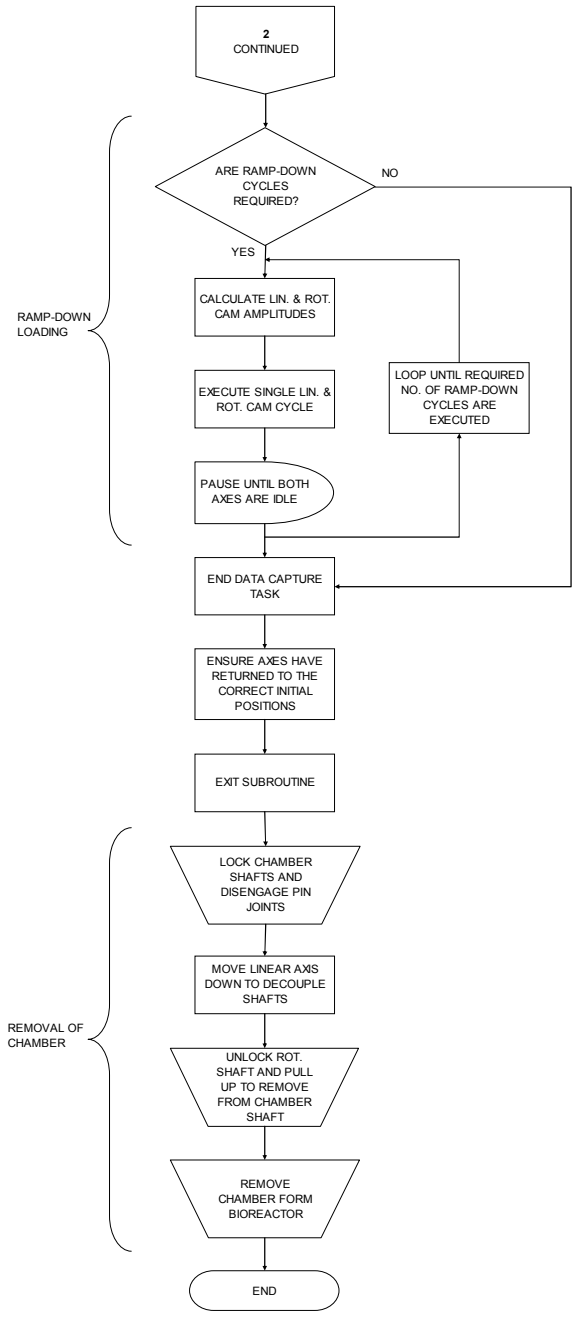

Figure 5-14 Continued. Summary of positional control loading subroutine logic

5.10 Task to capture data from the bioreactor

It was essential for the bioreactor to be able to capture mechanical data from the various sensors to allow the performance to be monitored in real-time and for more detailed analysis to be carried out after the completion of an experiment.

The NextMove controller could capture real-time data and store it in the controller memory. It could acquire up to six channels of data from a large range of parameters. A limited space was allocated in the controller memory for captured data and therefore increasing the number of parameters to be acquired would increase the period between

the individual sample points thus reducing the sample frequency. Similarly, increasing the duration of the capture period would also reduce the sample frequency. A finer sampling resolution could be achieved by either reducing the number of parameters being acquired or reducing the duration of the capture session.

A number of capture modes were possible with the controller including single capture, continuous capture and duration capture. The most useful mode for this application was the duration capture. This allowed the capture parameters and the duration of the capture to be specified and the sampling interval was automatically calculated to make the best use of the available memory.

A data capture task was created so it could be executed alongside the main loading task. This task was called from the positional control and load control subroutines just prior to the commencement of loading. After the completion of loading the subroutines terminated the data capture task. The user specified the number of cycles to be acquired in each capture session and the time interval between each capture session in minutes. The number of capture cycles was used together with the frequency and the stationary time at the start and end of the stroke to calculate the capture duration in milliseconds:

Equation 5-11

$$Capture\ Duration = \left(\left({}^{1}\!/_{cmFreq} \right) + cmtmStationaryHome + cmtmStationaryExt \right) * 1000 * cmCaptureCycles$$

Where:

cmCaptureCycles = the number of cycles to be captured in each capture session specified by the user

cmFreq = the required frequency of the profile supplied by the user in the comms element (Hz)

cmtmStationaryHome = the time required to hold the tissue at the start of the stroke as defined by the user (s)

cmtmStationaryExt = the time required to hold the tissue at the end of the stroke as defined by the user (s)

The parameters to be acquired were set up. The two analogue inputs from the load and torque cell were captured and during positional control loading the measured position of the linear and rotational axes were also captured. If the bioreactor was operated in load

control the positional output from the motors was not available as the axes were not configured as servo axes (see Section 5.11 for details). In this case the encoder values had to be acquired which had been scaled to the appropriate user units in the load control subroutine (Section 5.11).

The capture task then entered a continuous loop to perform each capture session until the task was terminated. The duration capture was started and the task was paused until the capture had finished i.e. when the CAPTURE keyword returned a value of zero. A comms flag was set to a value of two to indicate that the capture session was complete and the data could be uploaded by the LabView program. A pause was included in the task to waited until the interval between capture sessions had elapsed before it returned to the start of the loop to begin the next capture.

The data capture LabView program allowed data to be uploaded and saved automatically. Before running the position control subroutine, the user was required to start the LabView program and specify the directory in which the data was to be saved. The program then constantly monitored the capture flag until it had a value of two. When that condition was met the program uploaded the data from the controller. It displayed the data in a graph for the user to see in real-time and saved it to a file in the specified directory. The program reset the capture flag to zero and continued to monitor it until it was set to two once again by the capture task. The program could be ended by pressing the quit button. The LabView interface is shown in Figure 5-15 and the logic for the data capture task and LabView capture program is summarised in Figure 5-16.

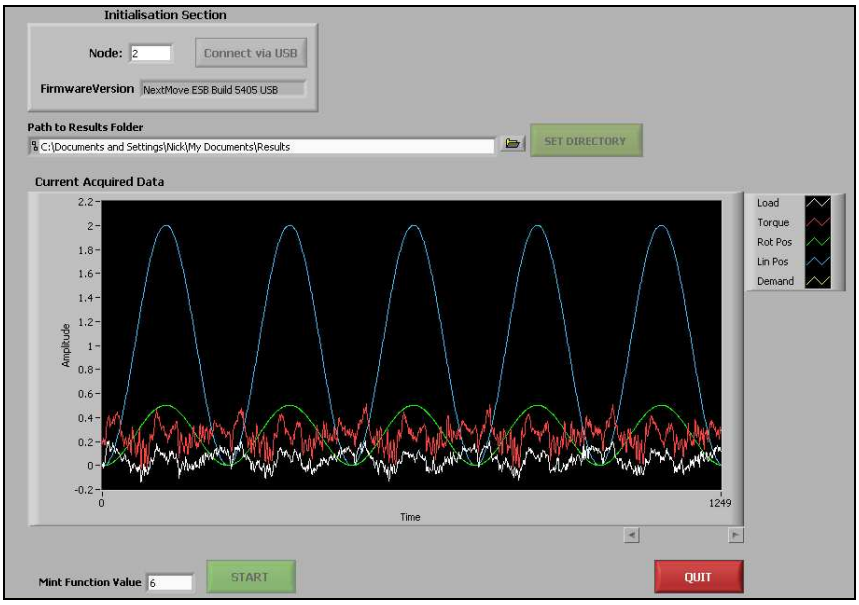

Figure 5-15 LabView interface for the data capture program

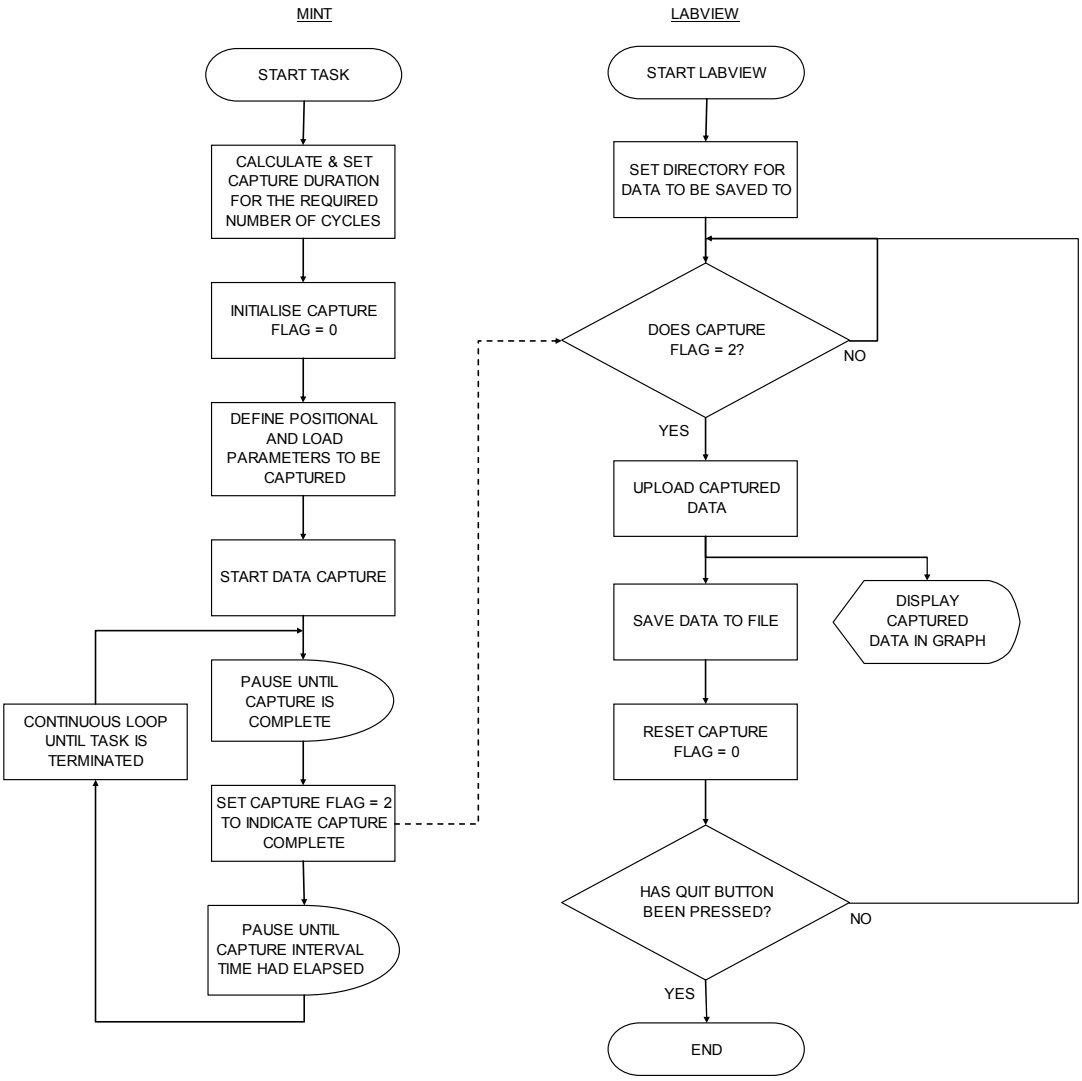

Figure 5-16 Summary data capture task logic

5.11 Operating the bioreactor in load control

In some applications it might be necessary to operate the bioreactor in load control utilising closed loop feedback provided by the load and torque cells. The in-built servo loop in the controller could not provide this function, therefore, a separate control loop had to be written to enable this mode of operation.

5.11.1 Task to operate the motors in load control

The load control loop was programmed in a separate task which would run simultaneously with the main task. The load control loop is shown in Figure 5-17 and the output demand equation is shown in Equation 5-12.

The controller was a standard PID controller. A load demand was provided from a cam in the main task similar to the cam used in the positional control subroutine. The error between the demanded load and feedback load was evaluated and multiplied by the

proportional gain term to provide a proportional component to the output demand. The derivative of the error was found by evaluating the difference between the current and previous error and this was multiplied by the derivative gain term (the difference did not need to be divided by the control loop sample time as this was a constant). The errors were also summed and multiplied by the integral gain term to reduce steady state errors. The integrator was capped to prevent very large or small values accumulating and impairing the function of the control loop. The PID terms were summed to provide the output demand (see Equation 5-12) and this was capped to prevent excessively large torques being provided by the motors.

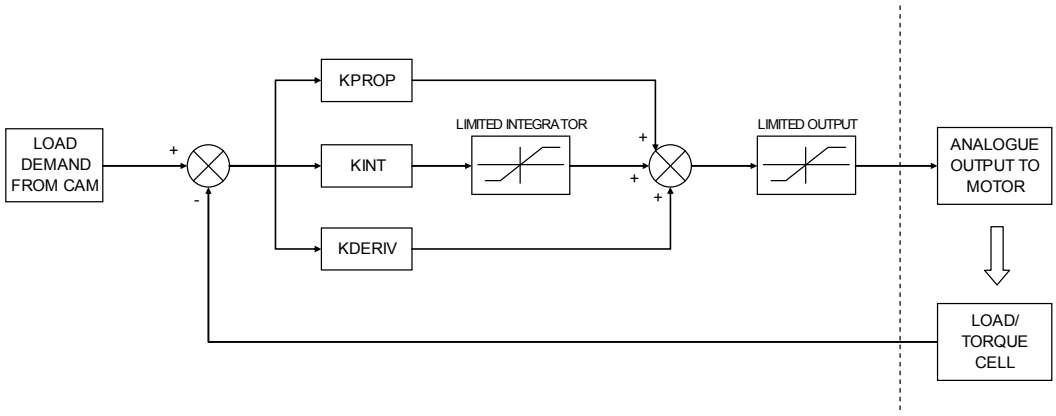

Figure 5-17 Block diagram of load controller

Equation 5-12

$$Output\ Demand = KP.e + KD.\Delta e + KI\sum e$$

A main load control subroutine was used to generate the demand load profile and call the load control task. Initially the motor servo axes were configured to off to enable the controller to provide the current demands to the motors. As the motors no longer operated in servo mode the only positional outputs were encoder counts and scale factors were applied to provide user unit outputs, i.e. millimetres and revolutions for the linear and rotational axes respectively. Cam arrays were generated for the demanded load and torque cycles in the same way as described for the positional control cycle (Section 5.9). The profile cycled between a maximum and minimum load and torque as specified by the user through the respective comms elements. In this operational mode, both the master and slave axes for each cam were virtual axes, however, these slave axes provided the load demands for the load controller. Limits to the motor torques were set to protect the bioreactor and the load controller and data capture tasks were executed.

The same process of ramp up cycles adjusting the amplitude of the cam, continuous running of the cam, and then ramp down cycles was implemented as described for the positional control subroutine in Section 5.9. The only difference in this section was that the cam arrays and cams were absolute to the true zero position. The positional cams were absolute to the position of the motor at the start of the cam, i.e. the motor position at the start of the cam was taken to be zero and the demand positions in the cam array were relative to this base position. However, the load control cams were relative to the absolute zero load. For example, assume the bioreactor was to cycle the load between 20N and 50N and the current load was 5N. Using the cam method in the positional control cycle would provide the loading cycle relative to the start load, i.e. it would cycle between 25N and 55N, however, using a cam relative to the true zero position would cause the system to cycle between 20N and 50N as desired.

Finally, the load controller and data capture tasks were terminated and the motor axes were reconfigured to servo axes.

5.11.2 Tuning of load controller

Preliminary tuning of the linear axis in the load controller was performed to demonstrate that the controller operated as desired. An extension spring with a stiffness of 1.5N/mm was loaded into the bioreactor to allow the tuning to be carried out. A continuous cyclic motion was initiated with the demand cycling between 25N and 35N. The controller gains were dynamically modified and the measured load was compared to the demanded load.

A proportional gain of 8, derivative gain of 0.8 and integral gain of 0 were selected and the measured and demanded loads are shown in Figure 5-18. The trace of the measured load follows approximately the same path as the demanded load with a slight time lag. Also, the upper measured load is slightly lower than the demanded maximum load.

The demanded load range was increased to cycle between 25N and 40N (Figure 5-19). The measured load range increased and exhibited the same lag and maximum load characteristics as those observed for Figure 5-18.

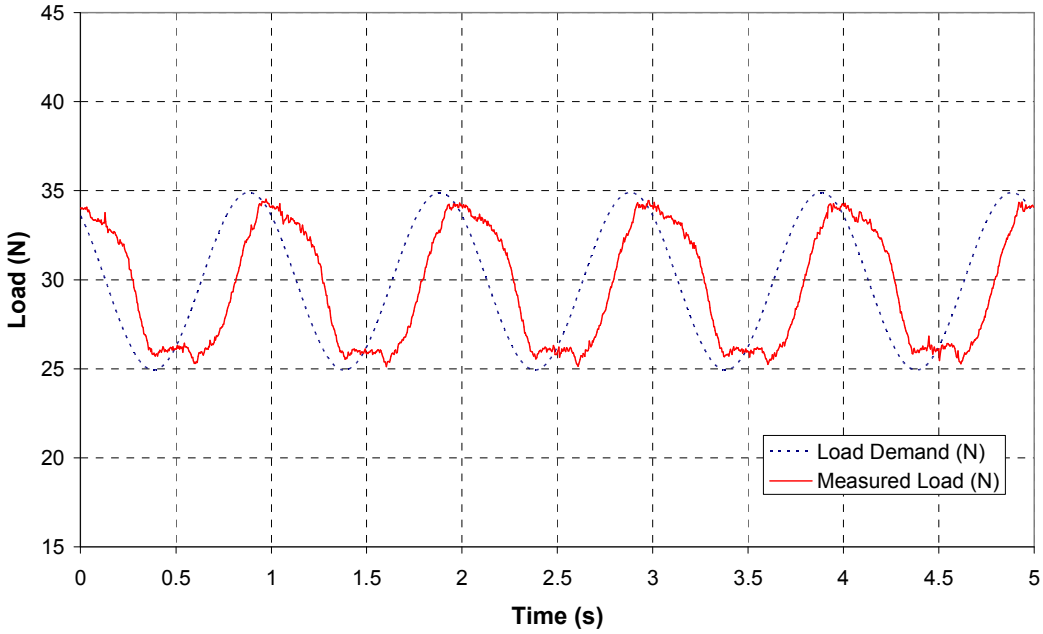

Figure 5-18 Bioreactor operating in load control between 25N and 35N

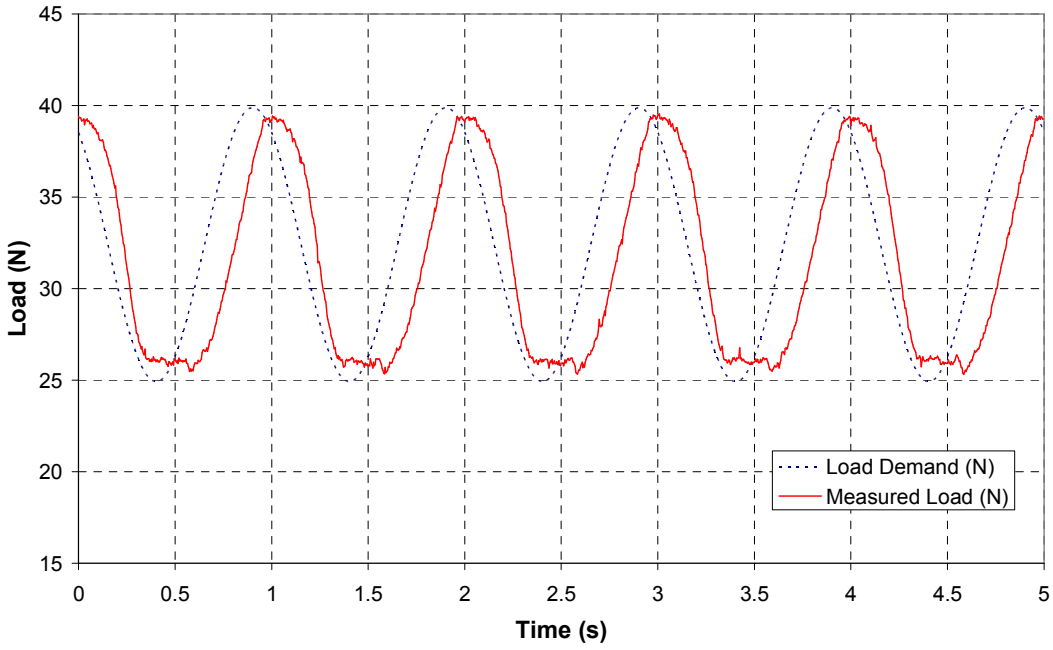

Figure 5-19 Bioreactor operating in load control between 25N and 40N

This demonstrated that the load control system could be tuned and operated successfully. The measured load approximately followed the load demand, however, this could be improved by optimisation of the controller gains. Appropriate tuning of the controller is dependent on the stiffness of the sample, therefore, re-tuning would be required if a sample of a different stiffness was used. Finally, safety features are required when operating the bioreactor in load control. Displacement limits are essential to prevent excessive motion should, for example, the sample break or slip out of the clamps. Also,

the motor demand should be limited to prevent excessive torque being produced in the event of sample failure or a problem with the load cell output.

5.12 Conclusions

A control program was successfully developed in the Mint programming language to meet all the relevant requirements listed in Section 3.1 and achieve Objective 7. The motors for the linear and rotational axes were tuned to provide the best stiffness and dynamic response whilst minimising any oscillations or instabilities.

Safety features were built into the control program to protect both the user from injury and the sensitive components in the bioreactor from damage. These include safety limits in the software and a hard-wired emergency stop button.

A number of subroutines were written in the Mint program to zero the load and torque readings, set the home position for the chamber, preload the sample and set the initial positions, cyclically load the sample in position control, and cyclically load the sample in load control. In addition to these subroutines, separate tasks were written to capture relevant load and positional data during a cyclic loading experiment and to provide a control loop to operate the motors in the load control mode.

LabView user interfaces were developed to zero the load and torque readings and save the captured data to file for further analysis.

6 CALIBRATION AND CHARACTERISATION OF LOAD AND TORQUE CELLS

6.1 Calibration of load cell

A 500N Interface Super Mini universal load cell (Model –SM-500N-38, Interface Force Measurements Ltd., Berkshire, U.K.) was included in the bioreactor to monitor the load applied to the tissue and provide feedback for the load control loop (Figure 6-1). The load cell signal was conditioned through a d.c. amplifier manufactured in-house and then passed to the analogue input of the NextMove controller.

The amplifier provided the load cell with an excitation voltage of 10V and the load cell outputted a maximum voltage of ±30mV at the maximum load of 500N. This output was then amplified via the d.c. amplifier to provide an output range of ±10V to the controller. The gains and offset of the amplifier were adjusted to scale the ±30mV load cell output to the ±10V amplifier output.

The load cell had to be calibrated to determine the relationship between the amplifier output voltage and the applied load. Although the load cell operated in a dynamic environment, a static calibration of the load cell was performed. It was felt this was acceptable as the moving mass of the system was small compared to the expected loads.

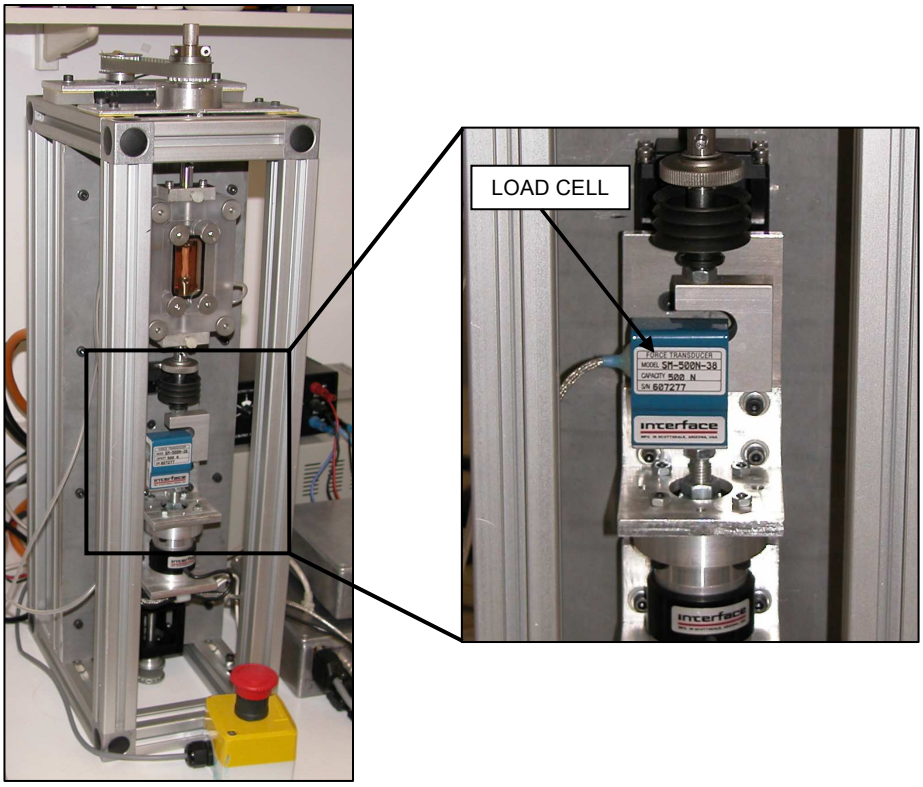

Figure 6-1 Position of load cell in bioreactor

6.1.1 Methods and materials

The load cell was calibrated using the set-up shown in Figure 6-2. A threaded rod was fitted to the top of the load cell and secured in place with a locking nut. This rod was held in the upper clamp of a 5kN materials testing machine (Model 3365, Instron, High Wycombe, UK) suspending the load cell. The clamp was fitted with V-shaped serrated jaws to securely grip the rod and align it vertically.

A threaded hook was fitted to the bottom of the load cell and again this was secured in place using a locking nut. From this a weight hanger was suspended and this allowed weights to be added and removed.

Weights were added to the hanger in 5kg intervals up to approximately 50kg (500N) and the load cell was then unloaded in the same way. At each loading and unloading point the hanger was allowed to settle and the voltage received by the controller was captured for two seconds. The corresponding load measured by the materials testing machine was recorded. The accuracy of the load output from the materials testing machine was shown to be within ±0.35% of the recorded load during a UKAS accredited calibration.

This sequence of loading and unloading was repeated an additional four times with the load cell removed and replaced between each repetition. This produced five independent calibrations of the load cell.

An algorithm was written in MatLab (The Mathworks Inc., Natick, MA, USA) to calculate the mean loading and unloading gradients for the five calibrations. The statistical software package, SPSS (SPSS Inc., Chicago, USA), was used to determine if the loading and unloading groups were normally distributed and also determine if there was a significant difference between the means of each group using an independent samples t-test. Finally, a MatLab algorithm calculated the weighted mean loading gradient for the load cell based on the five calibrations. Details of these statistical calculations are shown in Appendix D.

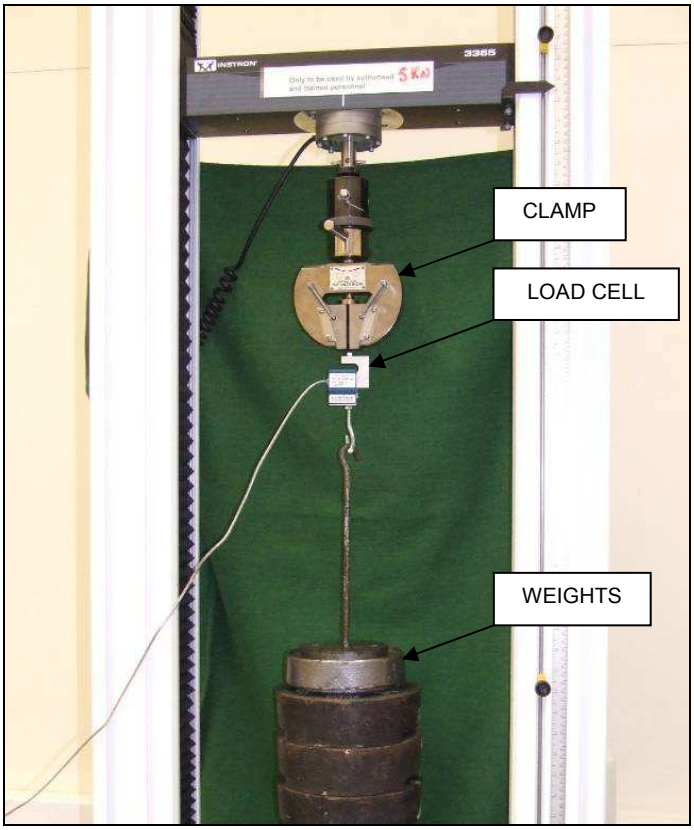

Figure 6-2 Load cell calibration set-up

6.1.2 Results

The five calibration plots are shown in Figure 6-3 and the mean gradients of the loading and unloading sections of the calibration are shown in Figure 6-4 and Figure 6-5 respectively.

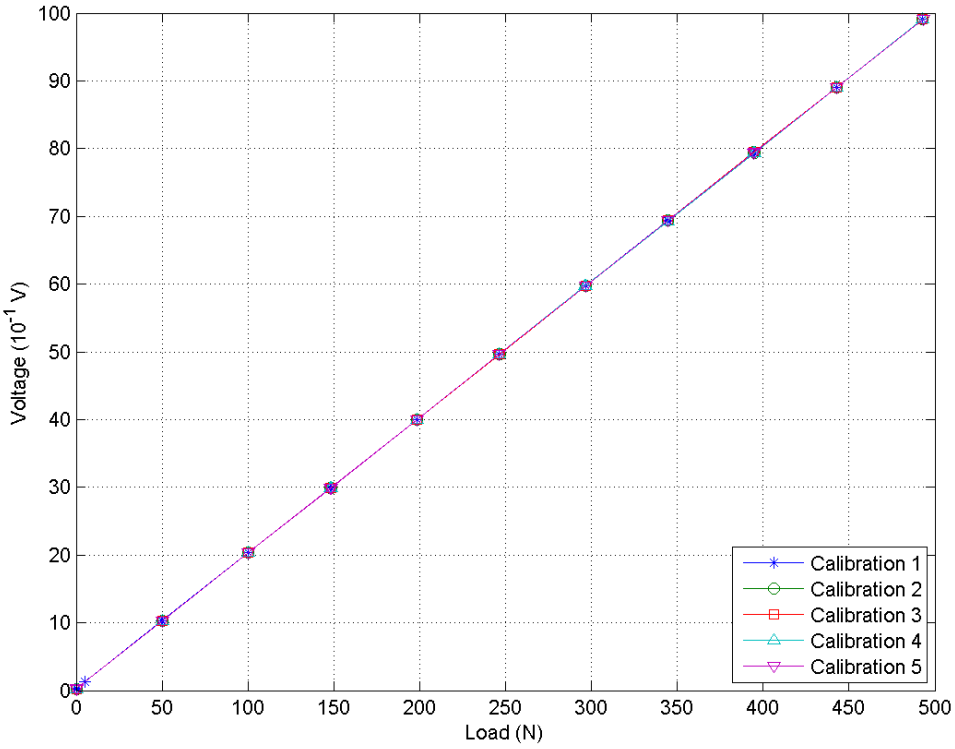

Figure 6-3 Five independent calibration of the load cell

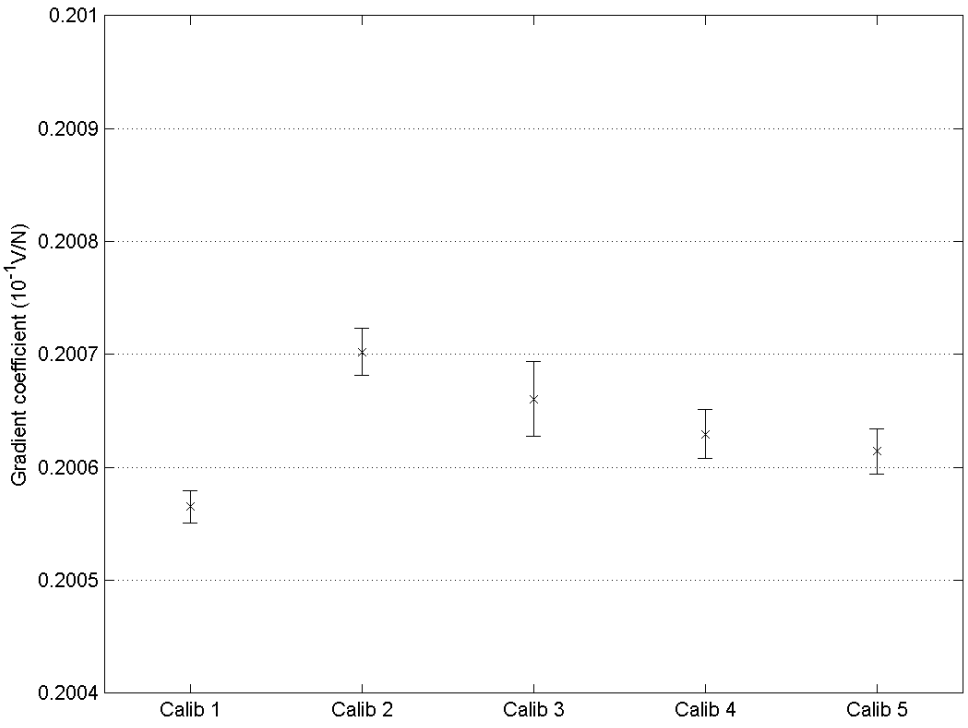

Figure 6-4 Mean loading gradient for the five load cell calibrations ± standard deviation

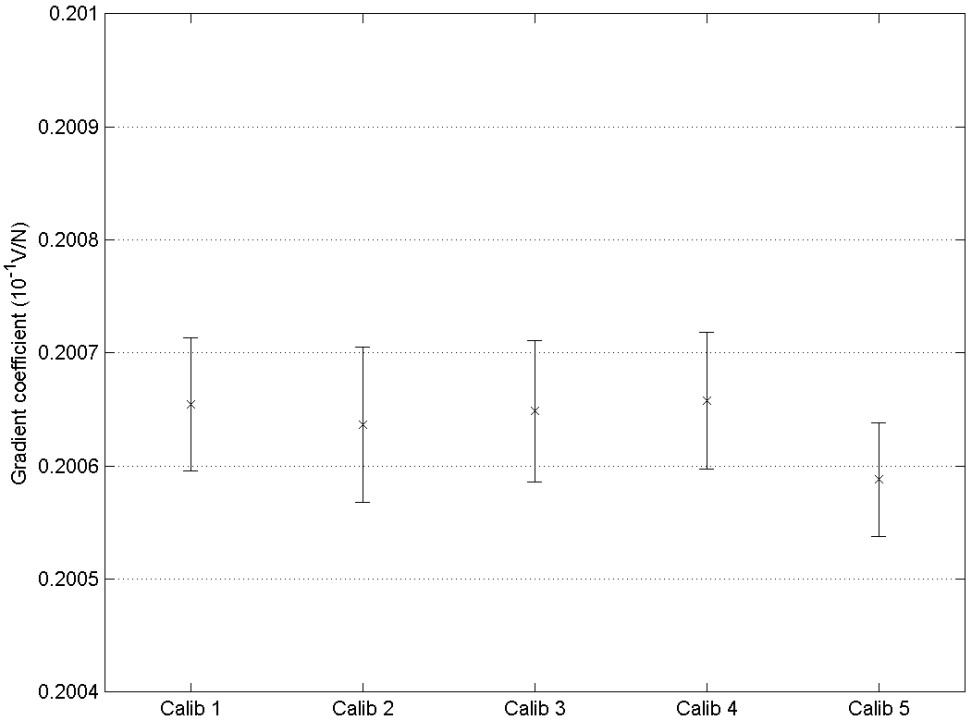

Figure 6-5 Mean unloading gradient for the five load cell calibrations ± standard deviation

The distributions of the loading and unloading load cell gradients were tested for normality using the Shapiro-Wilk test. The results were not significant indicating that the distributions of both groups were normal.

An independent samples t-test was performed to compare the loading and unloading groups. A p-value of 0.917 was calculated indicating there was no significant difference between the means of the two groups.

Consequently, the loading data was selected to calculate a weighted average for the calibration gradient. The gradient was evaluated as 0.2006 ± 0.000 x10^{-1}V/N (mean ± standard deviation) and a calibration factor of 0.2006 was used in the bioreactor control program to convert applied load to the load cell to output voltage read by the controller.

6.2 Calibration of torque cell

A 2Nm capacity Interface MRT Miniature Reaction Torque Cell (Model –MRT-2.0NM, Interface Force Measurements Ltd., Berkshire, U.K.) was included in the bioreactor to provide feedback for the load control loop and torque monitoring (Figure 6-6). The torque cell signal was conditioned through a d.c. amplifier manufactured in-house and then passed to the analogue input of the NextMove controller.

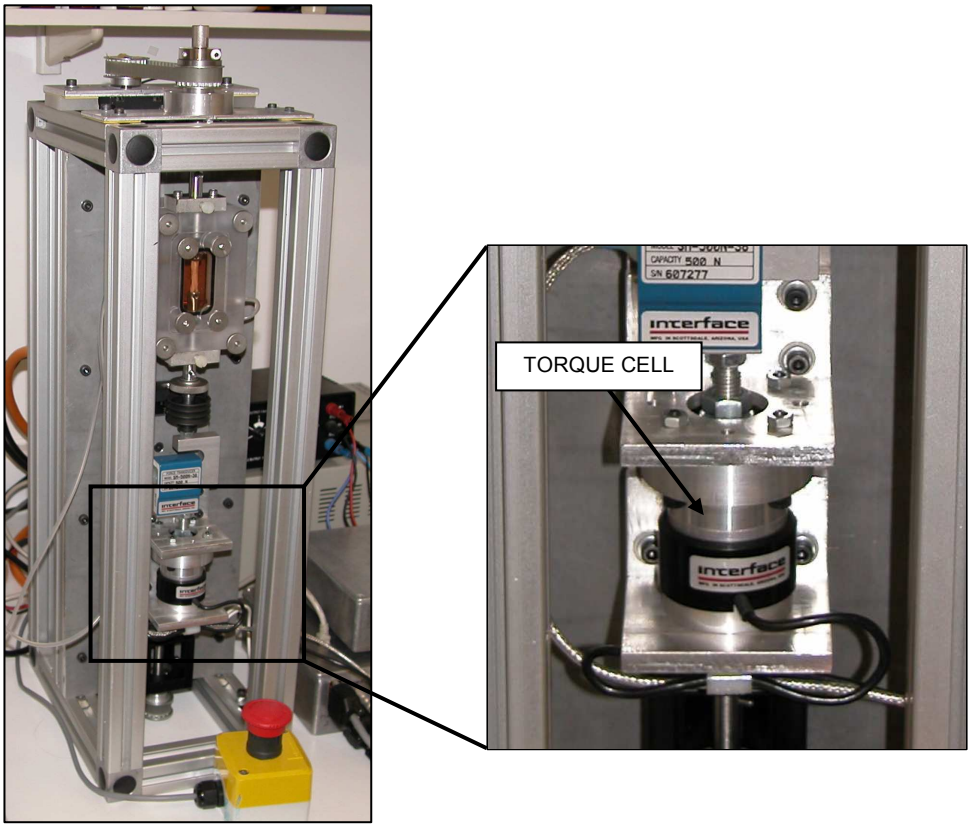

Figure 6-6 Position of torque cell in bioreactor

As with the load cell, the amplifier provided the torque cell with an excitation voltage of 10V and the torque cell outputted a maximum voltage of ±20mV at the maximum torque of 2Nm. This output was then amplified via the d.c. amplifier to provide an output range of ±10V to the controller. The gains and offset of the amplifier were adjusted to scale the ±20mV torque cell output to the ±10V amplifier output, corresponding to an input torque of ±2Nm.

The torque cell had to be calibrated to determine the relationship between the amplifier output voltage and the applied torque. Although the torque cell operated in a dynamic environment, a static calibration was performed. It was felt this was acceptable as the rotational inertia of the system was very small.

6.2.1 Methods and materials

The calibration equipment was set-up as shown in Figure 6-7. The bioreactor was laid on its back and a thin aluminium lever arm was fitted horizontally between the torque cell and the torque cell shaft. The lever was secured via two holes: one located on the portion of the torque cell shaft passing through the central hole of the torque cell, and the

other located on one of the bolts which secure the torque cell shaft to the torque cell and through which the torque was transmitted (see Figure 6-8A & B). The calibration was performed with the load cell *in situ* so as to allow for any effects due to electrical grounding or noise and also so that the bearing above the torque cell will support it and prevent cantilever loading of the torque cell.

A weight hanger was suspended from a hole in the end of the lever arm and the centre of this hole was approximately 207mm from the centre of the torque cell. 1N weights were added to the hanger one at a time up to a maximum torque of 1.988Nm and the voltage output from the torque cell was captured for two seconds via the controller. The corresponding torque was recorded for each voltage capture. The weights were then removed one at a time and the voltages and torques were again recorded.

This loading and unloading sequence was repeated an additional four times to provide five complete sets of data. The hanger was removed between each repetition but the lever arm was not removed.

As with the calibration of the load cell, an algorithm was written in MatLab (The Mathworks Inc., Natick, MA, USA) to calculate the mean loading and unloading gradients for the five calibrations. The statistical software package, SPSS (SPSS Inc., Chicago, USA), was used to determine if the loading and unloading groups were normally distributed and also determine if there was a significant difference between the means of each group using an independent samples t-test. Finally, a MatLab algorithm calculated the weighted mean loading gradient for the torque cell based on the five calibrations. Details of these statistical calculations are shown in Appendix D.

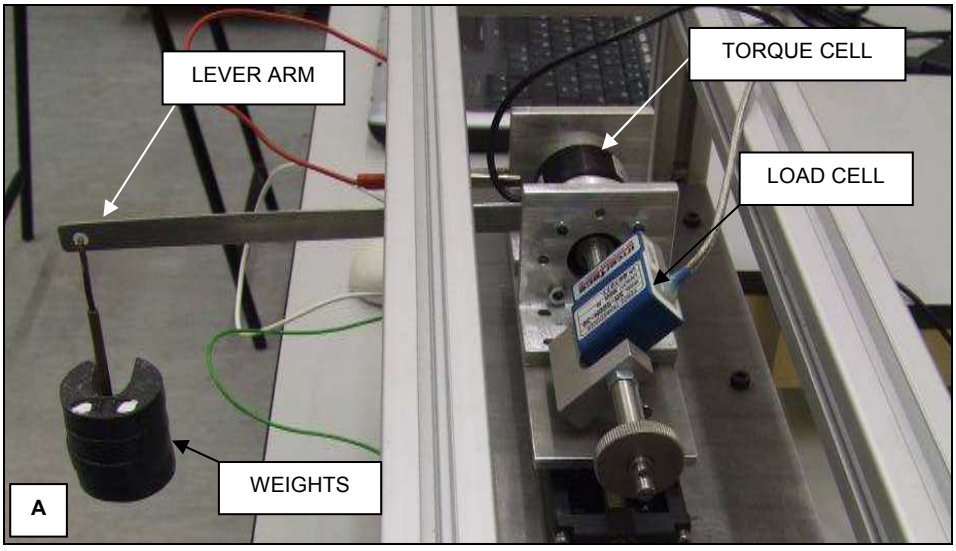

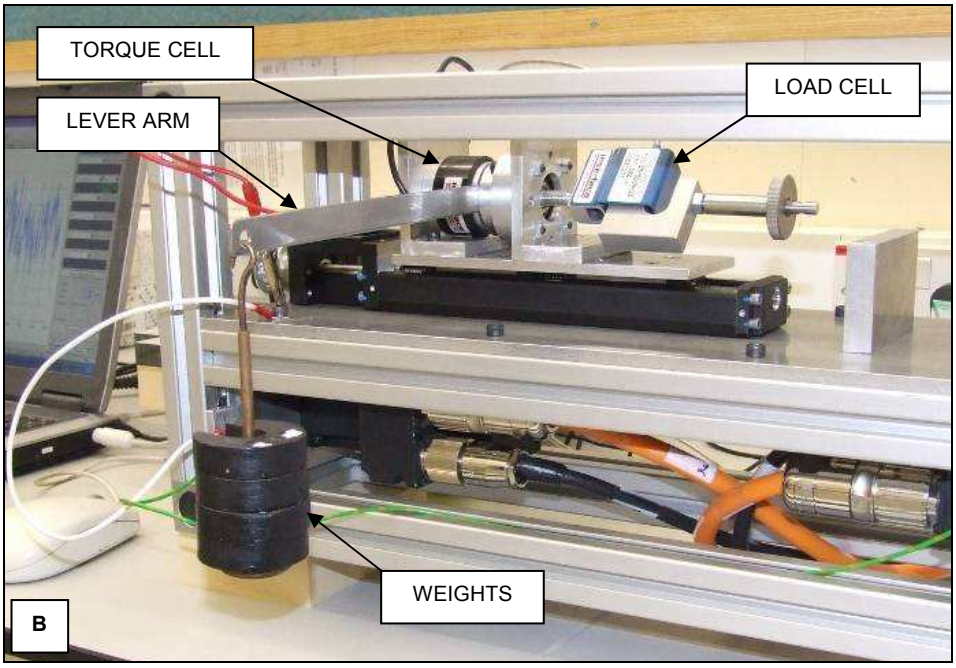

Figure 6-7 Top (A) and side (B) view of the torque cell calibration setup

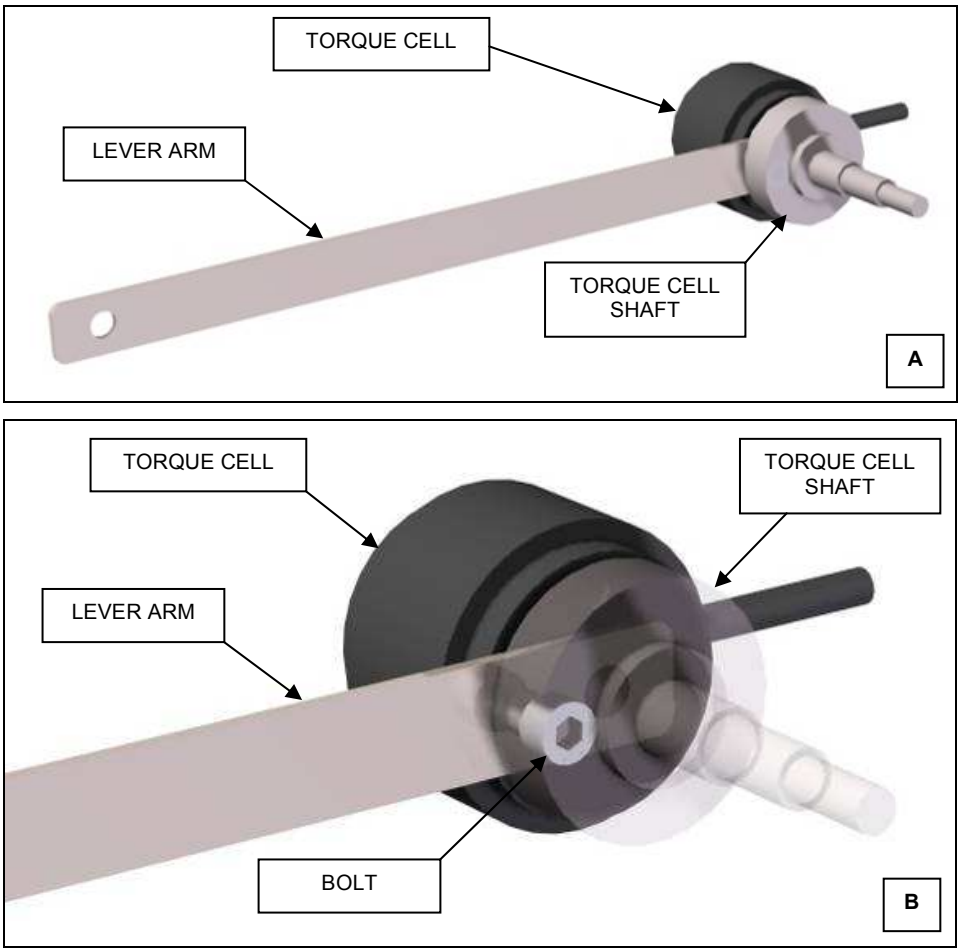

Figure 6-8 Diagram of lever arm attachment showing the complete lever arm (A) and a zoomed view of the attachment (B)

6.2.2 Results

The five torque cell calibration plots are shown in Figure 6-9 and the mean gradients of the loading and unloading sections of the calibration are shown in Figure 6-10 and Figure 6-11 respectively.

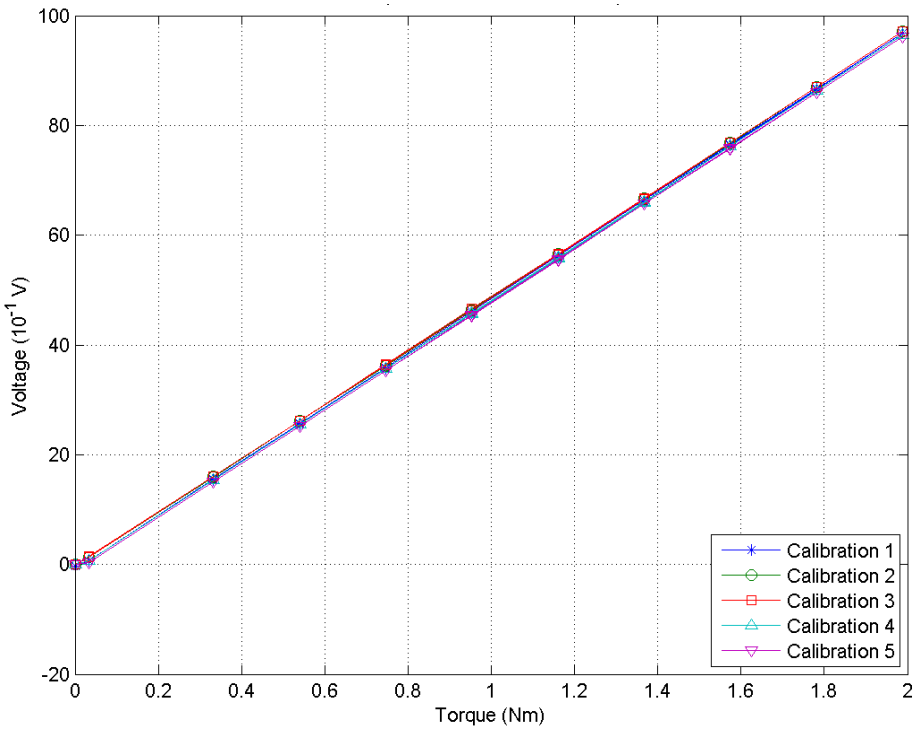

Figure 6-9 Five independent calibrations of torque cell

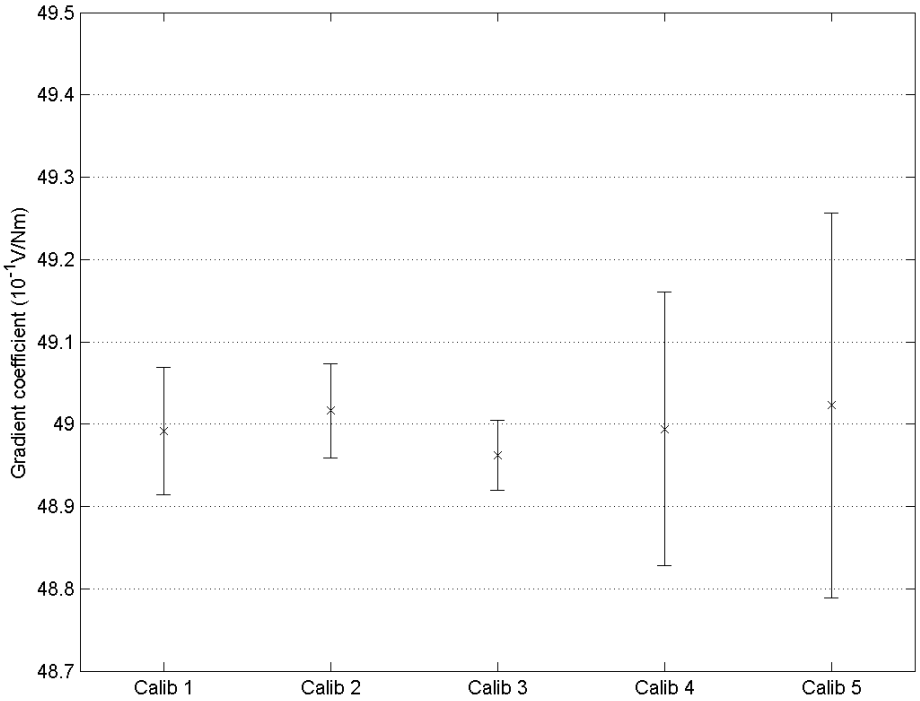

Figure 6-10 Mean loading gradient for the five torque cell calibrations ± standard deviation

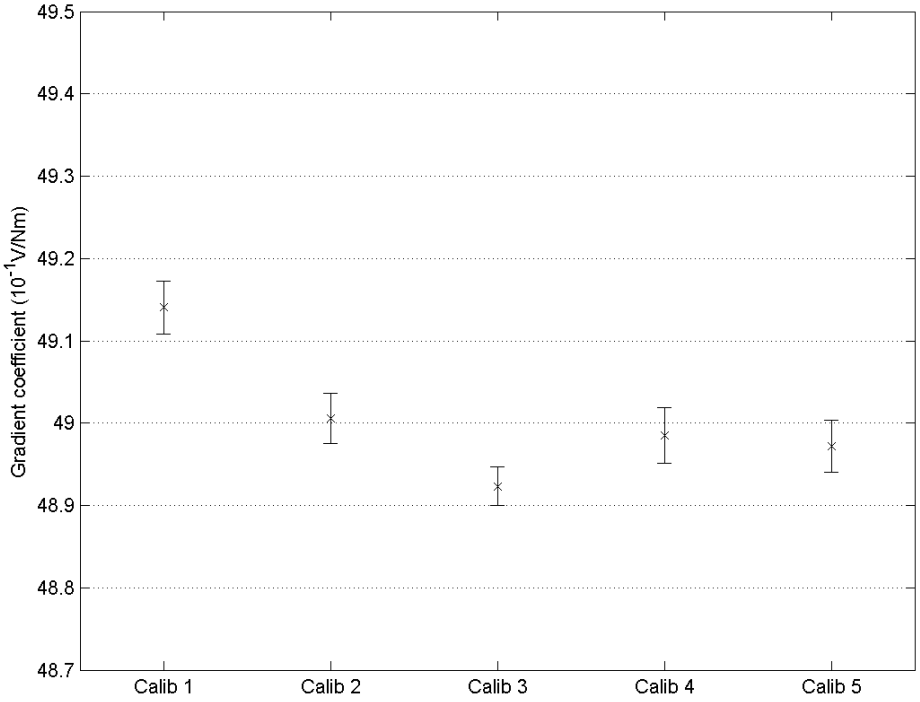

Figure 6-11 Mean unloading gradient for the five torque cell calibrations ± standard deviation

The distributions of the loading and unloading torque cell gradients were tested for normality using the Shapiro-Wilk test. The results were not significant indicating that the distribution of both the groups was normal.

An independent samples t-test was performed to compare the loading and unloading groups. A p-value of 0.842 was calculated indicating there was no significant difference between the means of the two groups.

Consequently, the loading data was selected to calculate a weighted average for the torque cell calibration gradient. The gradient was evaluated as 48.98 ± 0.03 $x10^{-1}$V/Nm (mean ± standard deviation) and a calibration factor of 48.98 was used in the bioreactor control program to convert applied torsion at the torque cell to output voltage read by the controller.

6.3 Characterisation of load and torque cells

The load and torque cells were characterised to evaluate any drift which may occur in the output of the sensors. Also, the sensors are mounted in such a way that it is possible for loading in one axis to affect the output of the sensor monitoring the other axis. This cross-talk between the two sensors was also evaluated.

6.3.1 Drift

Drift describes a change to the static characteristics of measuring equipment due to changes in the ambient conditions (Morris 2001a). Zero drift is the effect where the zero point of an instrument is modified by a constant due to changes in the ambient conditions and this is illustrated in Figure 6-12.

In the bioreactor, the conditioning card for the load and torque cells contains a number of electrical components. When power is supplied to the card these components are energised and heat up to a constant level. The zero drift caused by this change in temperature was quantified and the time at which equilibrium was reached was identified.

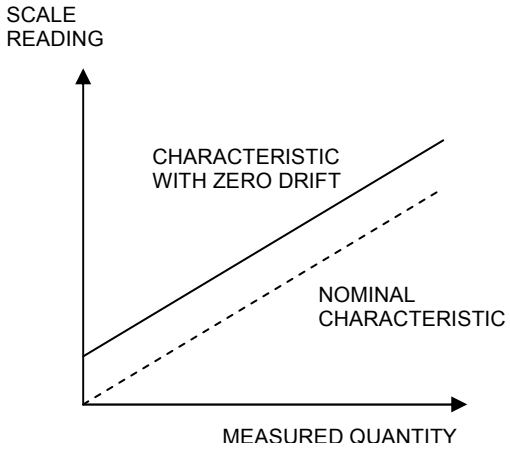

Figure 6-12 Effect of zero drift (adapted from Morris (2001a))

6.3.1.1 Methods and materials

After the bioreactor had been turned off for the previous night, the motor drives, controller and laptop were switched on but the conditioning card for the sensors was not powered. With no sample in the bioreactor, the position cycle subroutine was set up to run with no displacement of the linear and rotational axes. This was to allow the long-term data capture to be performed using the capture task in the program (see Section 5.10). Data from the load and torque cells were to be captured for a duration of 30 minutes. Each individual capture session was to last for 299 seconds with a one second interval between subsequent captures. The labView capture program was initiated to allow the captured data to be uploaded and saved during the one second capture interval. The data was captured at a sampling frequency of 5Hz.

With all the necessary programs running, the sensor conditioning card was powered up and the data capture was initiated simultaneously.

This data capture was repeated at the start of five different days after the bioreactor had been turned off for the previous night.

An algorithm was written in MatLab to evaluate the drift of the load and torque cells. The initial value for each repetition was calculated as the mean of the first 100 points. The final value was calculated as the mean of the final 100 points. The drift for each repetition was evaluated by subtracting the initial value from the final value. Finally, the mean drift value and standard deviation for the load and torque cells were calculated from the results for the five repetitions.

6.3.1.2 Results

The five repetitions of the drift analysis for the load and torque cells are shown in Figure 6-13 and Figure 6-14 respectively. These plots have been magnified to allow any drift to be visible.

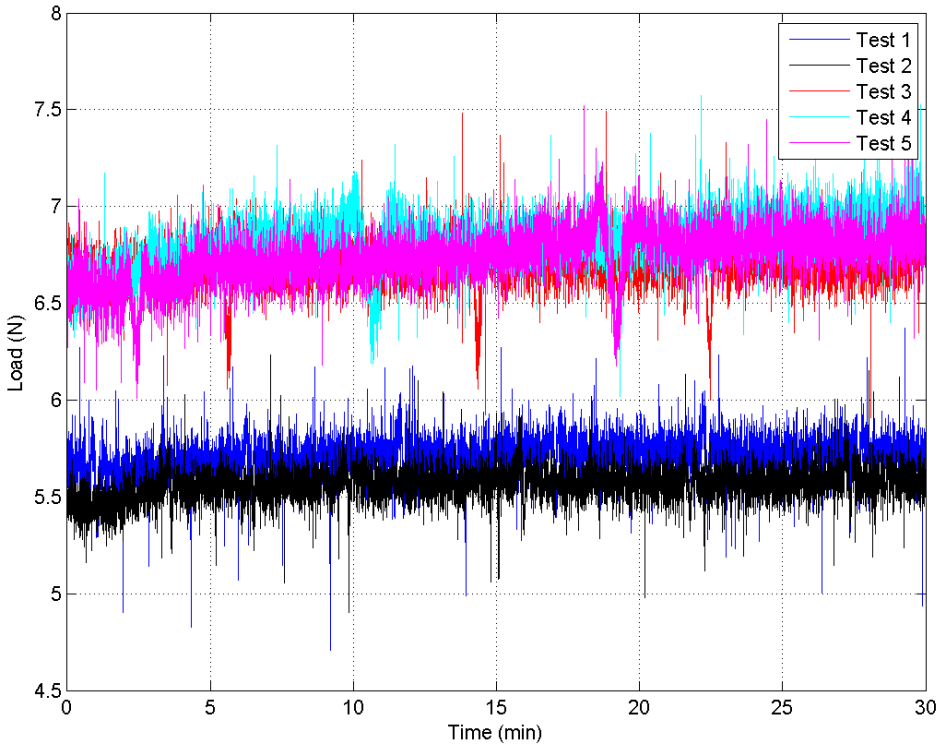

Figure 6-13 The zero drift of the load cell measured in five independent tests (magnified view)

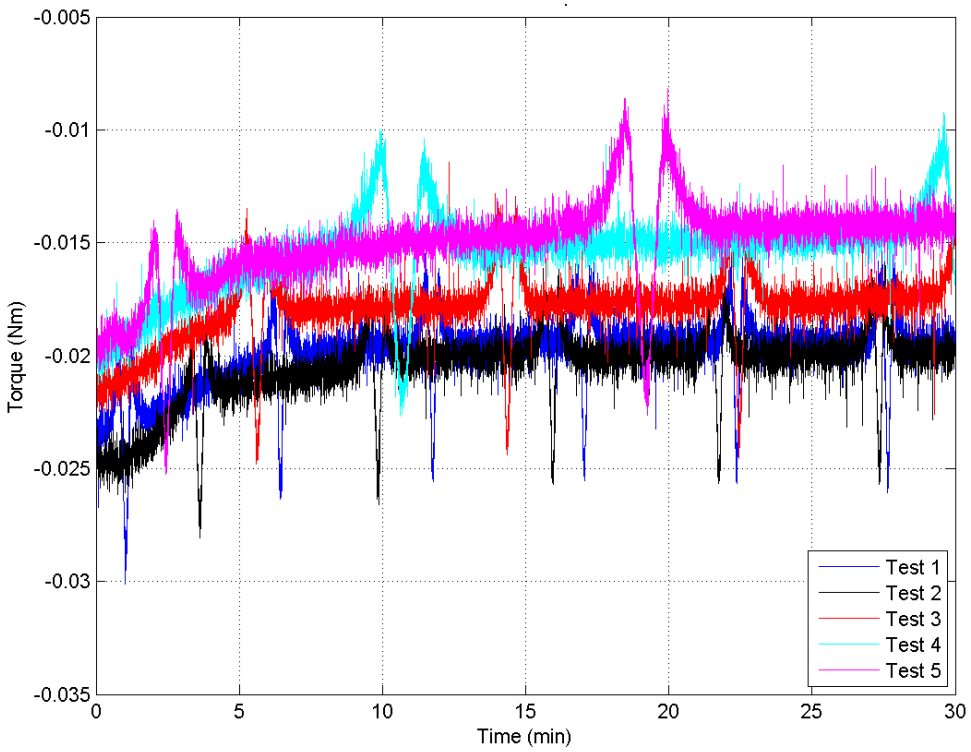

Figure 6-14 The zero drift of the torque cell measured in five independent tests (magnified view)

The load cell drift was calculated as 0.18 ± 0.13 N (mean ± standard deviation) and the torque cell drift was calculated as 0.005 ± 0.001 Nm (mean ± standard deviation).

6.3.2 Cross-talk between load and torque cells

Cross-talk can occur as a variation in the load cell reading due to a torque imposed by the bioreactor or as a variation in the torque cell reading due to a linear load from the bioreactor. Therefore, the cross-talk between the two sensor was evaluated in two directions. Firstly, zero torque was applied to a rigid sample. The axial load was increased incrementally up to a maximum value of 308.30 ± 4.09N (mean ± standard deviation) and the torsion reading was recorded. Secondly, zero linear load was applied to the sample. The torque applied to the sample was then increased incrementally up to a maximum value of 1.060 ± 0.012Nm (mean ± standard deviation) and the load reading from the load cell was recorded.

6.3.2.1 Methods and materials

A steel shaft (10mm diameter, 170mm long) was loaded into the bioreactor to act as a rigid sample. It was attached to the upper rotational shaft and the lower load cell shaft

using the pin joints which were normally used to secure the upper and lower chamber shafts and the locking nuts were tightened (Figure 6-15).

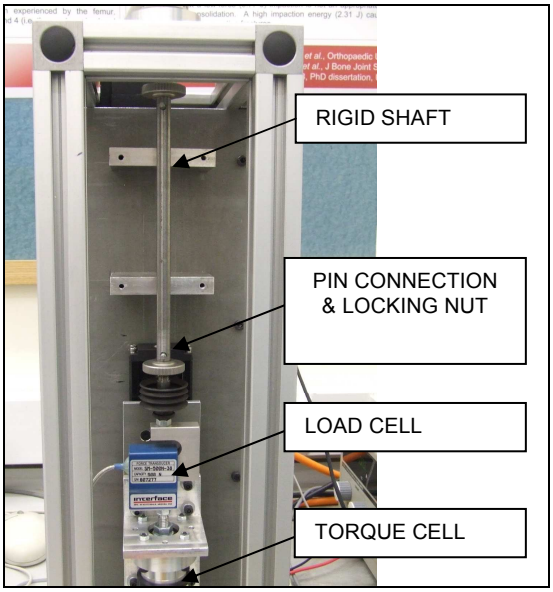

Figure 6-15 Bioreactor set-up with rigid shaft sample

A Mint subroutine was written to increase the torque applied by the linear axis motor in ten increments up to a maximum specified by the user in a comms element (see Section 5 for details of comms elements and Mint subroutines). The torque produced by the motor was converted to a linear load through the ballscrew and slide unit which could be measured with the load cell. The subroutine initialised the position of the linear and rotational axes to zero and enabled both the axes. A number of parameters were set up to be captured and these were: the analogue readings from the load and torque cells, the positions of the linear and rotational axes and the demanded torque as a percentage of the motor peak torque. A capture duration of two seconds was set. The capture flag was initialised to zero and the torque output of the linear axis motor was also set to zero. The data was acquired after two seconds to allow the system to settle. The capture flag was then set to equal two upon completion of the acquisition.

The LabView capture program detailed in Section 5.10 was run and monitored the comms element which was used as the capture flag. When the capture flag had a value of two, the LabView program uploaded the acquired data and saved it to a data file. When this was complete it reset the flag to zero and continued to monitor it until it had a value of two once again.

In the Mint subroutine a 'for' loop was employed to increase the torque provided by the motor up to the maximum motor torque specified by the user in ten equally spaced increments. Within the loop the motor torque was set, the system was allowed to settle for two seconds and the data was captured. When the capture was complete the capture flag was set to two and the data was uploaded and saved by the LabView capture program. The Mint program continued in the loop until the maximum motor torque was applied. The linear axis was loaded to a maximum of 20% of the maximum torque output from the linear axis motor. This equated to a maximum load of 308.3 ± 4.09N (mean ± standard deviation) through the load cell.

Five repetitions of the incremental linear loading were performed. The sample was removed and repositioned between each repetition.

The data analysis was performed in MatLab (The Mathworks Inc., Natick, MA, USA). The data was read into the MatLab program and the mean load and torque were calculated for the two second sample at each load interval. The data was adjusted so that the initial torque reading of each repetition was zero to account for any initial preload or offset. The measured torque from the torque cell was plotted against the applied axial load measured by the load cell and is shown in Figure 6-16.

A similar method was used to evaluate the variation of the load cell reading with applied torque. A subroutine was written to apply an increasing torque to the sample in the same way as that described above for the linear axis. The LabView capture program was used to capture and save the data. The sample was loaded up to a torque of 50% of the maximum rotational axis motor torque. This was equivalent to 1.060 ± 0.012Nm (mean ± standard deviation). Data analysis was again performed in MatLab. The data was adjusted such that the initial load reading of each repetition was zero to account for any initial preload or offset. The measured load from the load cell was plotted against the applied torsion measured by the torque cell and is shown in Figure 6-17.

6.3.2.2 Results

The cross-talk measured on the torque cell due to the application of linear load is shown in Figure 6-16 and the cross-talk measured on the load cell due to the application of a torque is shown in Figure 6-17.

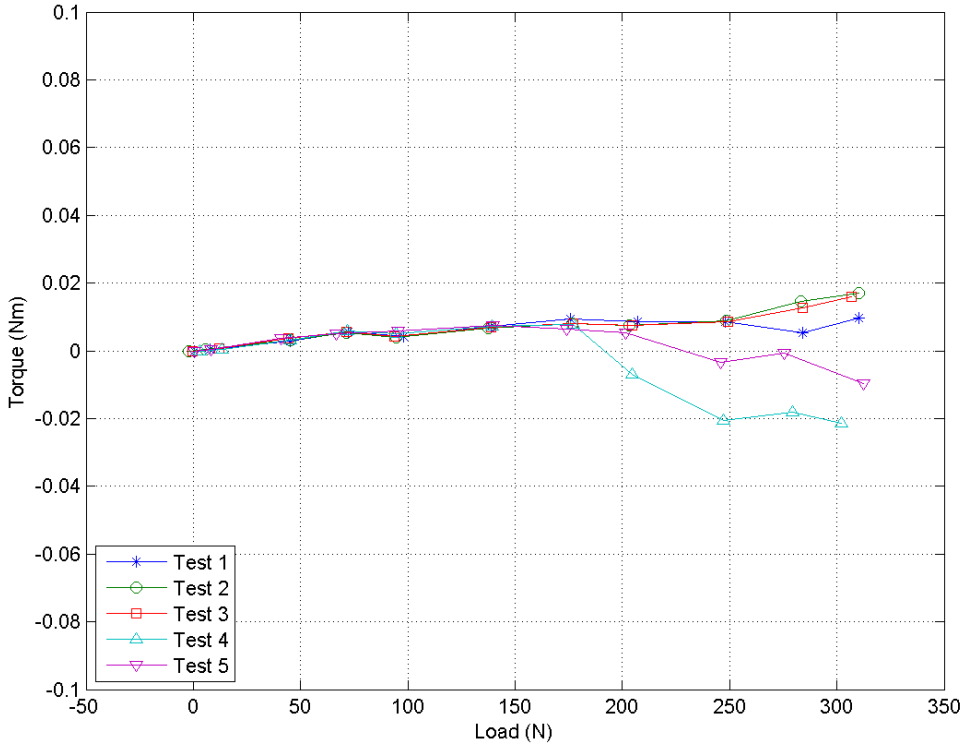

Figure 6-16 Variation of measured torque with tensile load

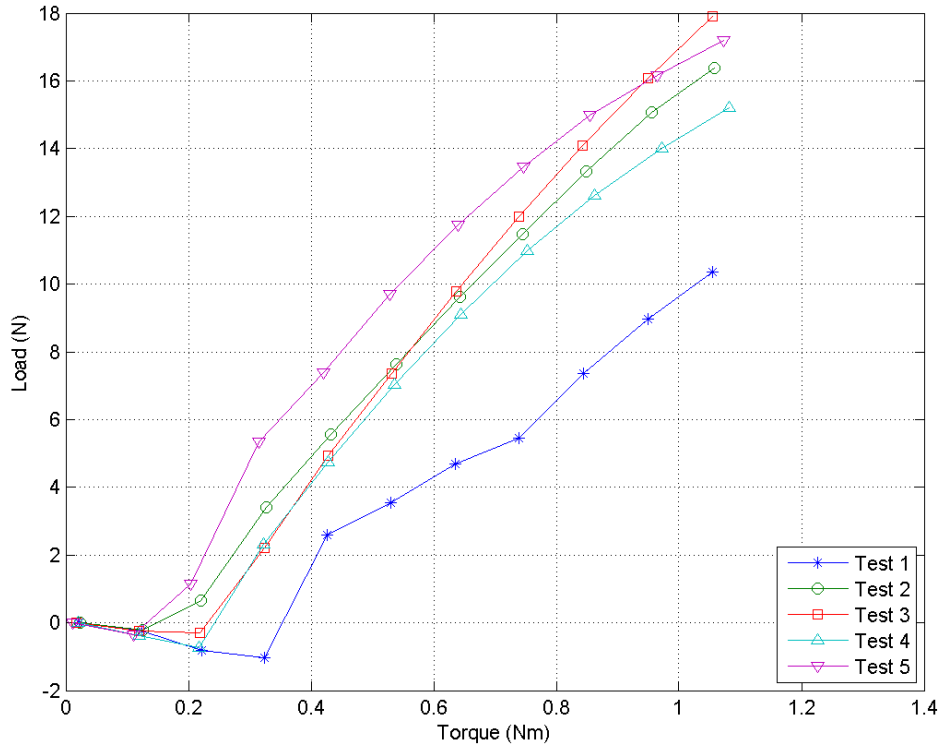

Figure 6-17 Variation of measured axial load with applied torque

6.4 Discussion

Five calibrations of the load and torque cells were performed and a weighted average calibration gradient was calculated for each. The calibration gradients were used to convert the output voltage from the load and torque cells read by the controller to the load and torque applied to the sensors. The standard deviation associated with the calibration factors were very small indicating that the results had high repeatability.

The 30 minute load cell drift readings are shown in Figure 6-13. The readings were not zeroed before the start of the capture to ensure the data was captured as soon as the conditioning card was powered. For this reason the readings all have a slightly different offsets. The load cell drift was measured as 0.18 ± 0.13 N (mean ± standard deviation). By observation, the mean gradient of the load cell readings after 20 minutes was approximately zero indicating that the drift took place within the first 20 minutes of powering up the conditioning card. Also, the measured drift was 0.04% of the load cell full scale.

Figure 6-14 shows the torque cell drift which was calculated as 0.005 ± 0.001Nm (mean ± standard deviation). Again, the drift appeared to take place within the first 20 minutes of powering up the conditioning card, after which a constant reading was recorded. The measured drift was 0.27% of the torque cell full scale.

Drift has a very small effect on the load and torque cell readings, however, allowing the conditioning card to heat up for approximately 20 minutes before using the bioreactor would eliminate this effect.

Figure 6-16 shows that there was little variation due to cross-talk in the torque cell reading (<0.01Nm) with increasing axial load up to approximately 150N. Above this, the torque reading deviated up to ±0.02Nm at approximately 300N of axial load. The torque cell was mounted in such a way as to prevent transmission of axial load. Figure 6-18 shows a cross section of the load and torque cell assembly and the axial load path is shown in Figure 6-19. Axial load was applied to the sample and this was transmitted through the load cell to the torque cell shaft. The torque cell shaft was mounted on a double row angular contact ball bearing to transfer the axial load to the mounting bracket and then on to the base plate which was fixed to the linear slide. This was the ideal load path and prevented the transmission of any axial load to the torque cell. However, at high loads this ideal load path was not achieved. The torque cell shaft was securely

bolted to the torque cell to ensure torque was transmitted from the sample to the torque cell without any hysteresis due to clearance in the holes of bolts or dowels. The torque cell was also bolted securely to the torque cell mounting bracket. At high loads it is possible for the bearing mounting bracket to flex slightly, allowing a small vertical displacement of the torque cell shaft. As the torque cell is rigidly fixed to the torque cell shaft, axial load is transmitted through the torque cell to prevent vertical displacement of the load cell shaft. This load path is shown in Figure 6-19.

At torques of less than 0.1Nm the load cell appeared not to be affected by the applied torque (Figure 6-17). Above a torque of approximately 0.2Nm the measured axial load increased with increasing torque and at torque greater than 0.3Nm the measured load increased at a rate of 18.19 ± 0.28 N/Nm. The torque path through the load and torque cell assembly is shown in Figure 6-20. Torque was applied to the sample and was transmitted through the chamber shaft, load cell and torque cell shaft to the torque cell. In this configuration the total torque was transferred through the load cell to the torque cell. This configuration was used to simplify the design and reduce equipment costs and is discussed fully in Section 3.

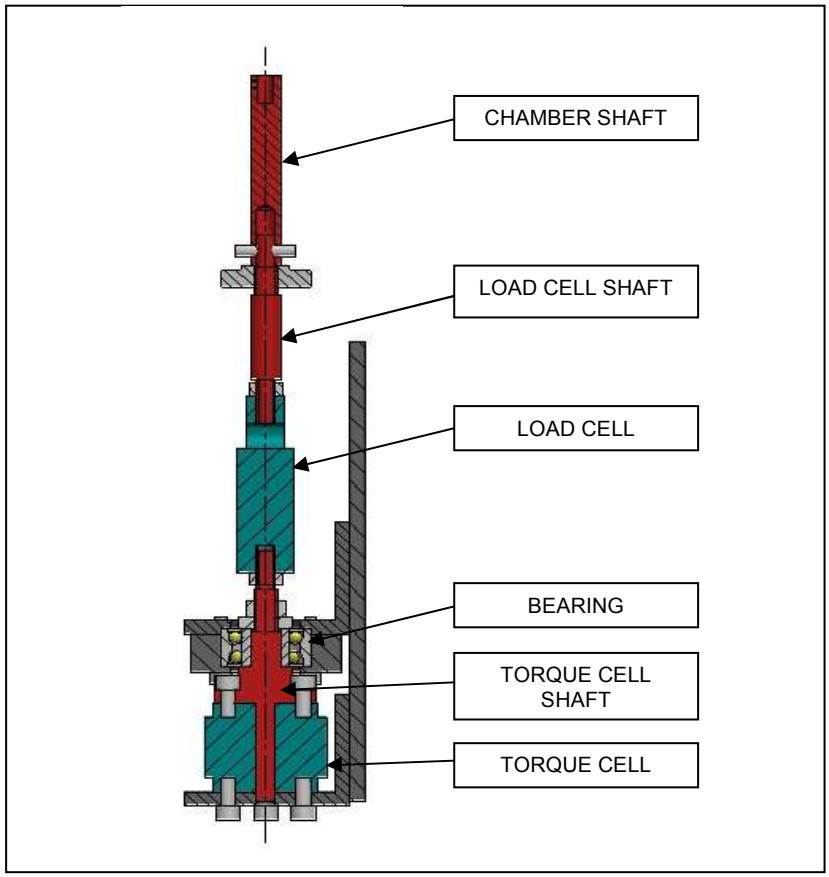

Figure 6-18 Cross section of load and torque cell assembly

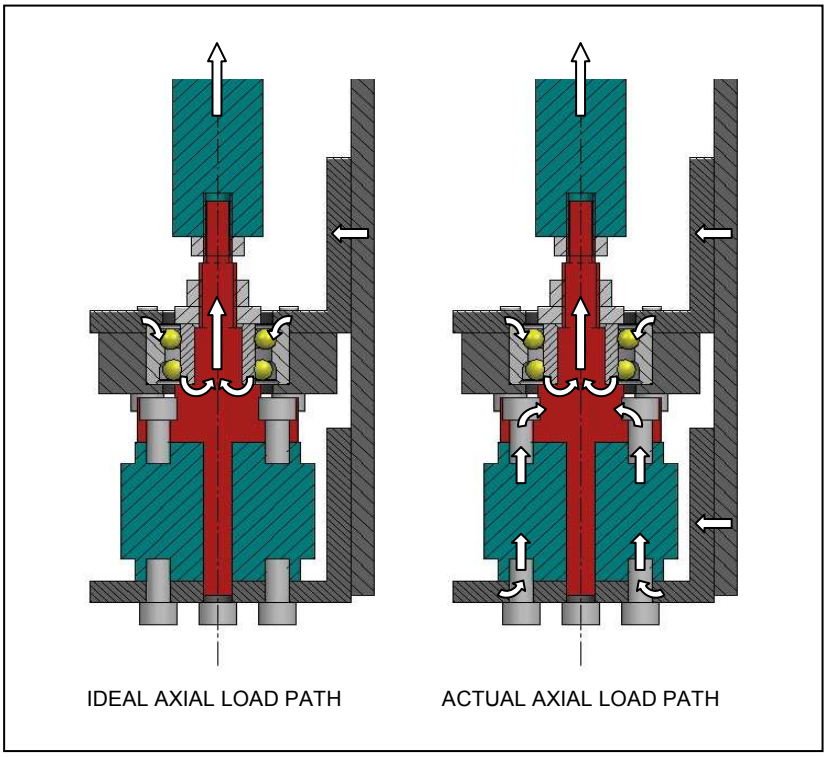

Figure 6-19 Axial load path through load and torque cell assembly

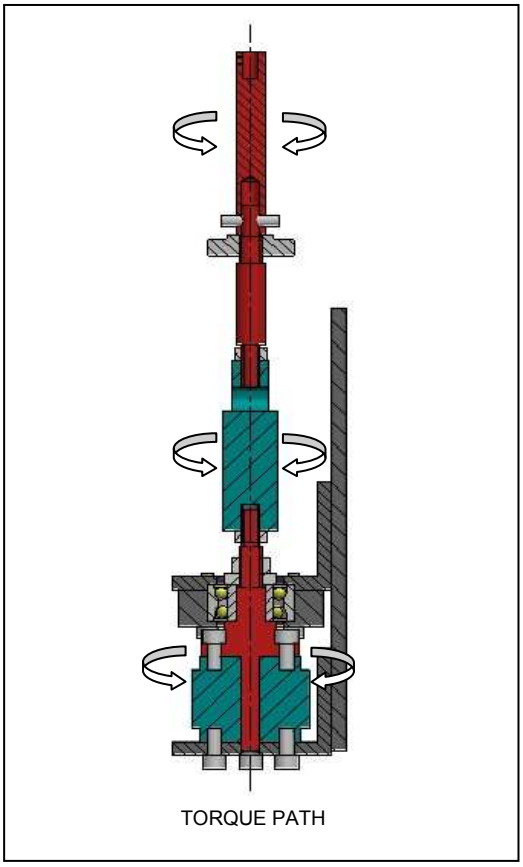

Figure 6-20 Torque path through load and torque cell assembly

6.5 Conclusions

The load and torque cells have been calibrated and fully characterised to understand and quantify any errors associated with drift and cross-talk between the load and torque.

Calibrations of the load and torque cells were performed. Calibration factors were evaluated from the results with small standard deviations associated with them indicating good repeatability. The calibration factors were used in the bioreactor control program to convert the applied load and torsion to the load and torque cell output voltages read by the controller.

The drift of the load and torque cell readings associated with the heating up of components in the conditioning card at power up was evaluated. A drift of 0.04% and 0.27% of the full scale for the load and torque cells respectively was measured. Therefore, drift has a very small effect on the output from the sensors in the bioreactor. However, the drift appeared to take place within the first 20 minutes of powering up the conditioning card for both sensors. Therefore, allowing the conditioning card to heat up for approximately 20 minutes before using the bioreactor would eliminate any error due to zero drift of the load and torque cells.

Cross-talk between the load and torque cells was evaluated. The mounting of the load and torque cells were designed to protect the torque cell from experiencing axial load. At axial loads less than 150N this was achieved and minimal deviation from the zero torque reading was observed. However, at load greater than 150N deviation from the zero torque reading was observed up to ±0.02Nm at approximately 300N of axial load. This was due to flexion of the bearing bracket causing axial load to be transmitted to the torque cell.

The application of torques less than 0.1Nm caused little variation in the load reading from the load cell. Above a torque of approximately 0.2Nm the measured axial load increased with increasing torque and at torque greater than 0.3Nm the measured load increased at a rate of 18.19 ± 0.28 N/Nm. The configuration of the load and torque cells was such that the total torque was transferred through the load cell to the torque cell and this was the reason for the coupling of applied torque and load reading. This configuration was used to simplify the design and reduce equipment costs as detailed in Section 3.

The calibration and characterisation of the load and torque cells have contributed to the successful achievement of Objective 8.

7 VALIDATION OF POSITIONAL OUTPUT

The positional data obtained from the bioreactor for the linear and rotational displacement imposed on the tissue is based on the encoder output of the motors driving the two axes. For the rotational axis, the encoder count read by the controller from the motor is scaled to revolutions of the rotational shaft (10,000 encoder counts per rotational shaft revolution) as there is a gearing ratio of one between the motor and the rotational shaft of the biological chamber. For the linear axis the encoder count is scaled to millimetres using a scaling factor of 5,000 as the linear slide has a lead of 2mm and therefore one revolution equals 2mm displacement (see Section 5.3). The drive of the motors is transmitted to the chamber shafts through toothed belt drives. As with most drive systems there will be a level of hysteresis associated with a change in direction as the slack in the belt is taken up and also in the linear slide when the screw drives the nut on the opposite side of the thread. To determine the accuracy of the positional data from the bioreactor it was necessary to validate the positional output from the motors and also evaluate the level of hysteresis in the system.

7.1 Methods and materials

7.1.1 Linear axis

A linear variable differential transformer (LVDT) (Schaevitz PCA 117-050, Measurement Specialities Inc., Hampton, VA, USA) was used to measure the linear displacement of the lower chamber shaft. The voltage output from the LVDT was passed through an amplifier card and acquired on a separate computer with an acquisition program written in HP VEE (Hewlett-Packard Visual Engineering Environment, Version 5.01, Hewlett-Packard Co., Palo Alto, California, USA). The maximum amplified output from the LVDT was ±10V and the gains were adjusted on the amplifier card for this maximum range to be provided at approximately ±2.5mm.

The LVDT was calibrated using a 'V' block and single-ended micrometer with graduations of 0.001" (25.4μm) as shown in Figure 7-1. The micrometer was advanced from a position of 0.13" (3.30mm) to 0.33" (8.38mm) in 0.02" (0.51mm) increments providing 11 calibration points. At each point the voltage output from the amplifier card was recorded. At the end of the calibration the micrometer was returned to zero and the process was repeated. Five calibrations were performed without repositioning.

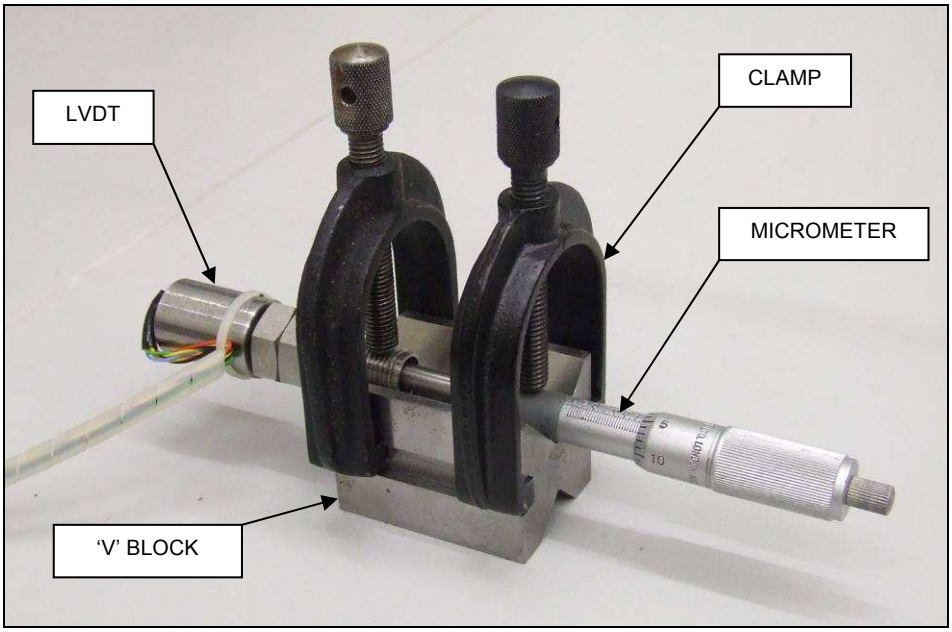

Figure 7-1 LVDT calibration set-up

The LVDT was spring loaded and mounted vertically on the frame of the bioreactor such that its displacement shaft was loaded against the bearing bracket on the linear slide which is rigidly attached to the lower chamber shaft (Figure 7-2). A plastic isolator was located between the LVDT mounting bracket and frame and a plastic bolt was used to secure the LVDT mounting bracket in place. This was to reduce the transmission of electrical noise from the bioreactor to the LVDT similar to the procedure detailed in Section 4.

With the drive to the linear axis motor disabled, the linear slide was manually adjusted such that the reading from the LVDT was 0V. At this point the position for the linear axis was set to 0mm. The linear axis was moved to a position of -1.5mm using the motor control program and the output voltage from the LVDT was recorded using the acquisition program for 10s at a frequency of 250Hz. The position was increased in steps of 0.5mm up to +1.5mm (seven sample positions) and the LVDT output voltage was recorded at each position. As the positive direction of the linear axis is vertically down, increasing the position of the linear axis caused the linear slide to move down. The positive direction of the LVDT was also vertically down. The linear axis was then returned to the position of -1.5mm and the experiment was repeated a further four times.

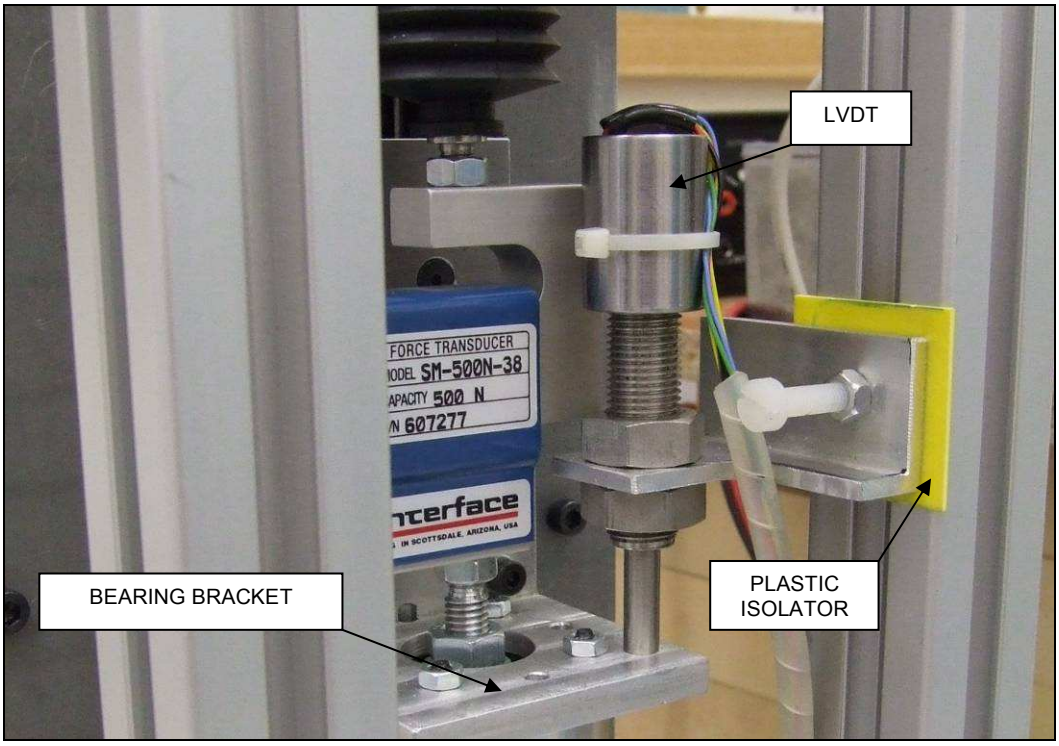

Figure 7-2 LVDT set-up on bioreactor

Hysteresis occurs when the direction of motion changes and as the bioreactor will perform a cyclic position profile it was necessary to evaluate the magnitude of hysteresis in the linear system. The LVDT was mounted to the bioreactor frame and the zero position of the linear axis was set as outlined above. The linear axis was moved to the position of +1mm. The voltage output from the LVDT was sampled for 2s at 250Hz. The axis was then moved to -1mm and again back to +1mm. The voltage output from the LVDT was sampled at each position. This was repeated to provide 5 readings at +1mm and 5 readings at -1mm.

7.1.2 Rotational axis

A similar procedure was carried out for the rotational axis. A rotational potentiometer (P2701A502, Novotechnik, Southborough, MA, USA) was used to measure the rotational displacement of the upper chamber shaft. The voltage output from the potentiometer was passed through an amplifier card and acquired using the same system detailed above for the LVDT. The maximum amplified output from the potentiometer was ±10V and the gains were adjusted on the amplifier card for this maximum range to be provided at approximately ±170°.

The potentiometer was calibrated using a calibrated turntable with graduations of 0.1° as shown in Figure 7-3. Initially, the turntable was set to 0° and the potentiometer was manually rotated within the chuck of the turntable to give a voltage reading of 0V. The turntable was then rotated from a position of -170° to +170° in 20° increments providing 18 calibration points. At each point the voltage output from the amplifier card was recorded. At the end of the calibration the chuck was released and the zero position was manually reset. Five calibrations were performed.

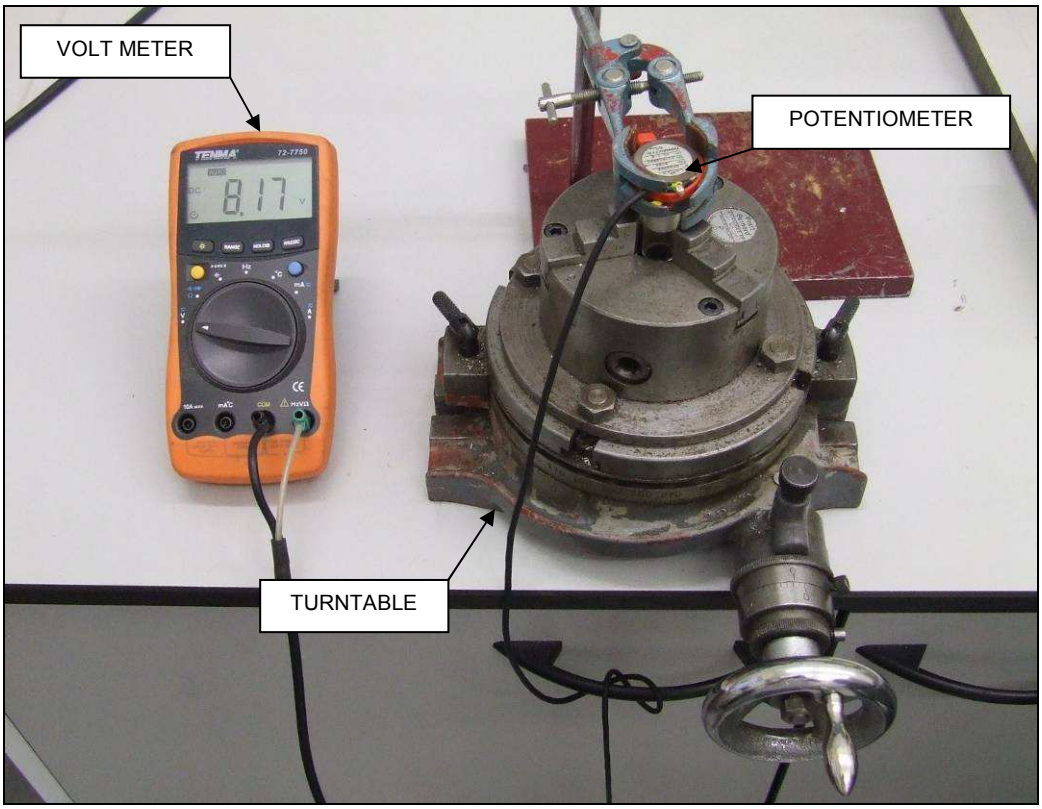

Figure 7-3 Potentiometer calibration set-up

The potentiometer was mounted on the bioreactor frame so that it was positioned directly above the upper rotational shaft and was coupled to this shaft via a short piece of plastic tubing (Figure 7-4). The rotational shaft is rigidly attached to the upper chamber shaft. A plastic isolator was located between the potentiometer mounting bracket and frame and a plastic bolt was used to secure the mounting bracket in place. As with the LVDT, this was to reduce the transmission of electrical noise from the bioreactor to the potentiometer following a similar procedure as that illustrated in Section 4.

With the drive to the rotational axis motor disabled, the upper rotational shaft was manually adjusted so that the reading from the potentiometer was approximately 0V. At this point the position for the rotational axis was set to 0°. The rotational axis was moved to a position of -90° using the motor control program and the output voltage from

the potentiometer was recorded using the acquisition program for 10s at a frequency of 250Hz. Seven samples were taken at -90°, -54°, -18°, 0°, +18°, +54° and +90° and the potentiometer output voltage was recorded at each position. The positive direction of the rotational axis was clockwise when looking from above and the positive direction of the potentiometer was also set to be clockwise. The rotational axis was then disabled and the zero position was manually reset. The experiment was repeated a further four times.

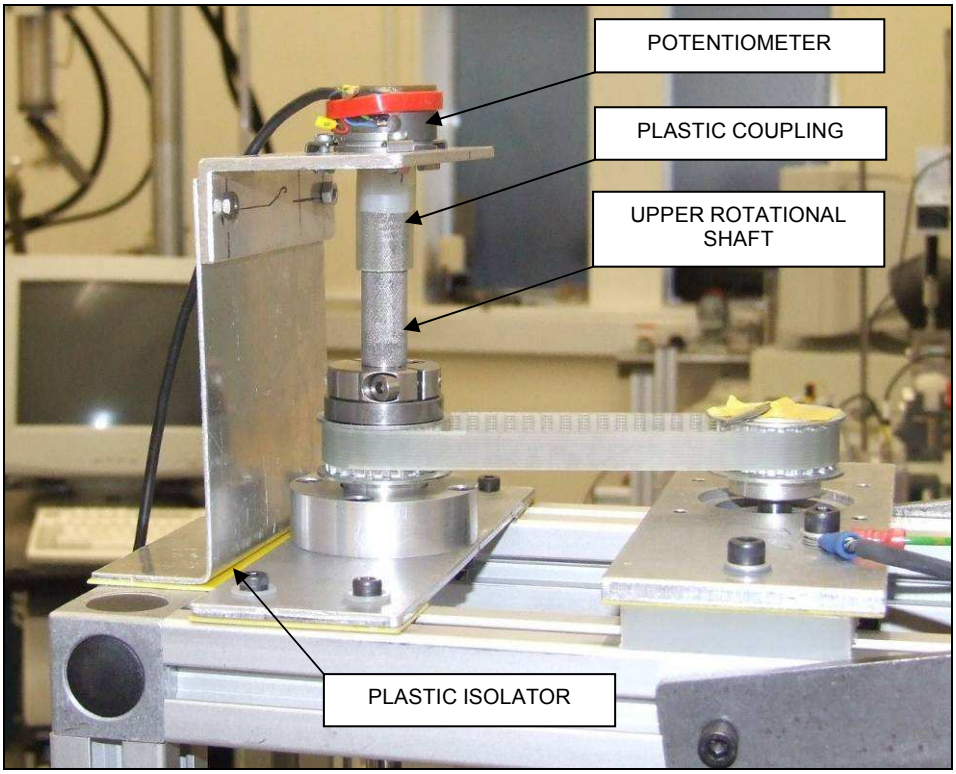

Figure 7-4 Potentiometer set-up on bioreactor

The bioreactor will perform a cyclic position profile in the rotational axis so it was necessary to evaluate the magnitude of hysteresis in the rotational system. The potentiometer was mounted to the bioreactor frame and the zero position of the rotational axis was set as outlined above. The rotational axis was moved to the position of -36°. The voltage output from the LVDT was sampled for 2s at 250Hz. The axis was then moved to +36° and again back to -36°. The voltage output from the potentiometer was sampled at each position. This was repeated to provide 5 readings at -36° and 5 readings at +36°.

7.2 Results

7.2.1 LVDT calibration

The plot of the five calibrations of the LVDT is shown in Figure 7-5 below. The data for each calibration was fitted to a straight line using the least-squares method and the mean gradients were calculated (Figure 7-6). The standard deviations were also calculated and are shown in Figure 7-6. The weighted average of the gradient for the calibrations was calculated (see Appendix D), again with its standard deviation. The LVDT calibration had a weighted average gradient of -3.765 ± 0.009 V/mm (mean ± SD). The intercept was not relevant as the zero graduation on the micrometer was no aligned with the zero reading of the LVDT because the micrometer could not move in the negative direction.

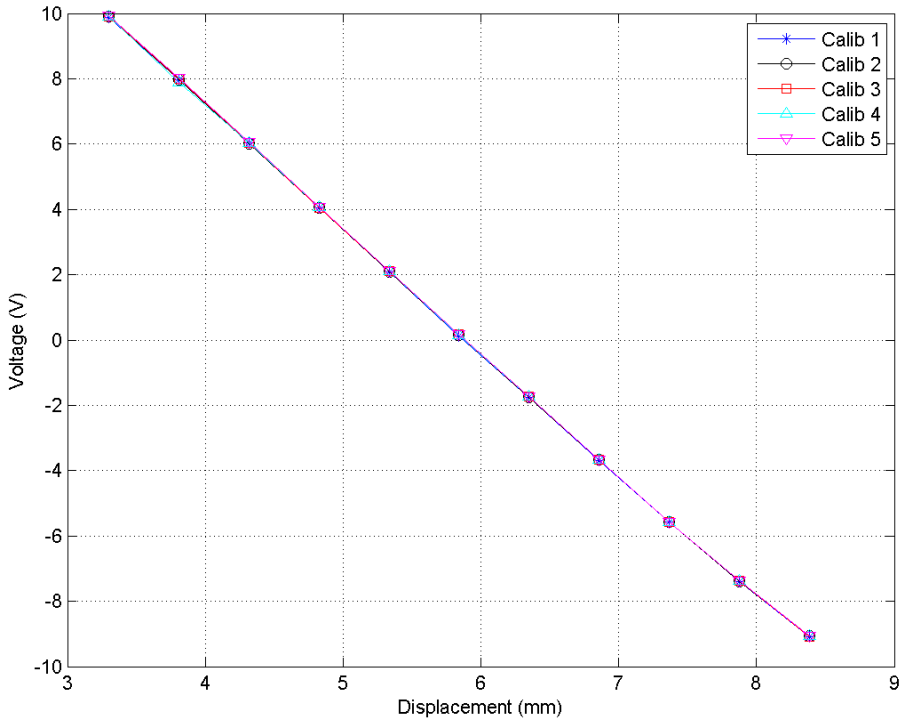

Figure 7-5 The five calibrations for the LVDT

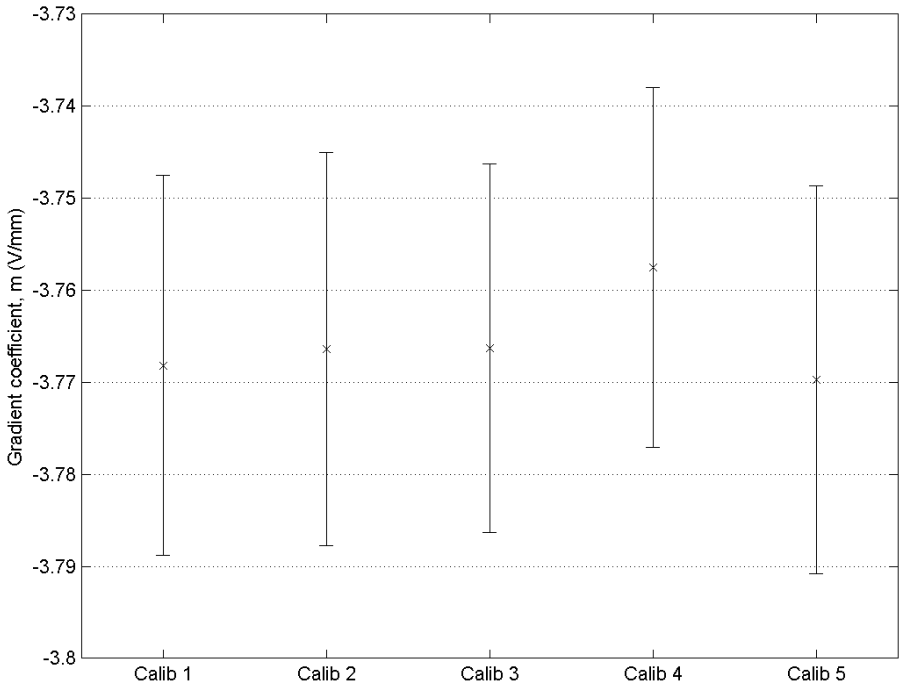

Figure 7-6 The mean gradient, m, for the five LVDT calibrations +/- standard deviation

7.2.2 Linear position validation

Following the linear position validation experiment, the motor axis position was plotted against the measured LVDT position which was converted to millimetres using the calibration gradient previously determined (Figure 7-7). Again, the mean gradients and intercepts for the five repetitions were calculated (Figure 7-8 and Figure 7-9) and the weighted averages of these constants were determined (see Appendix D). The correlation between the motor axis position and the measured LVDT position had a mean gradient of 1.011 ± 0.002 and a mean intercept of 0.000 ± 0.002 mm (mean ± SD).

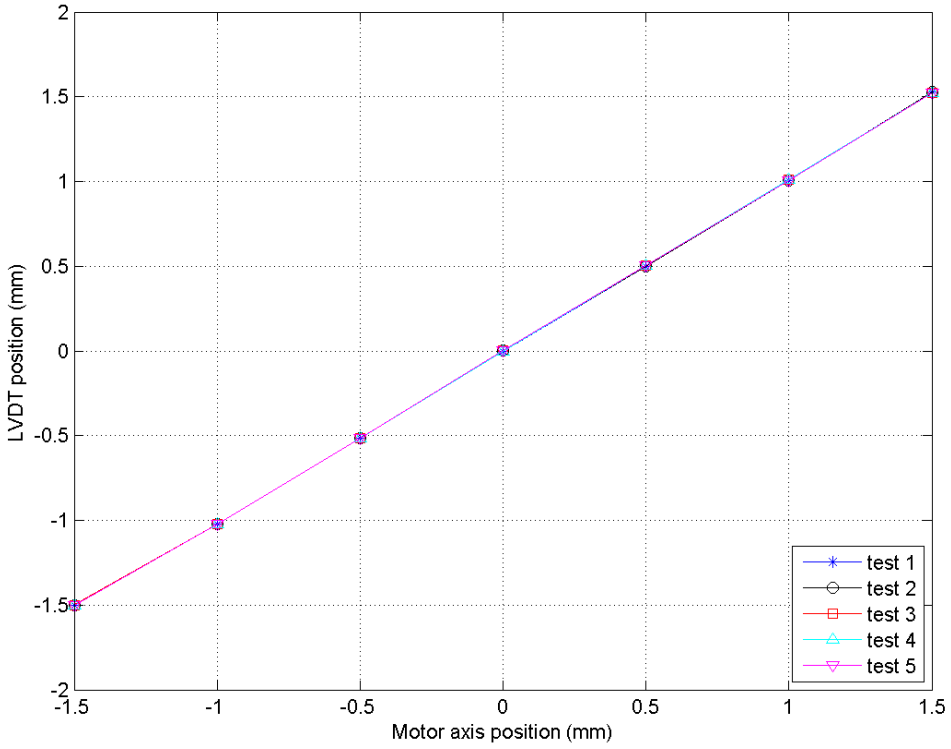

Figure 7-7 The five validation tests of the linear position

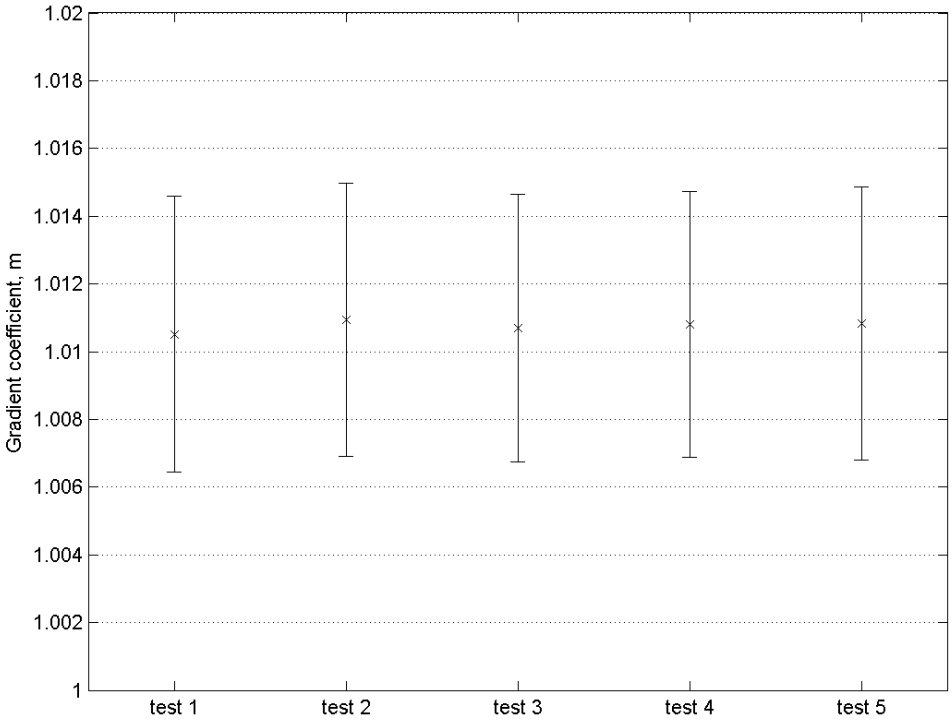

Figure 7-8 Mean gradient, m, for the five linear position validation tests +/- standard deviation

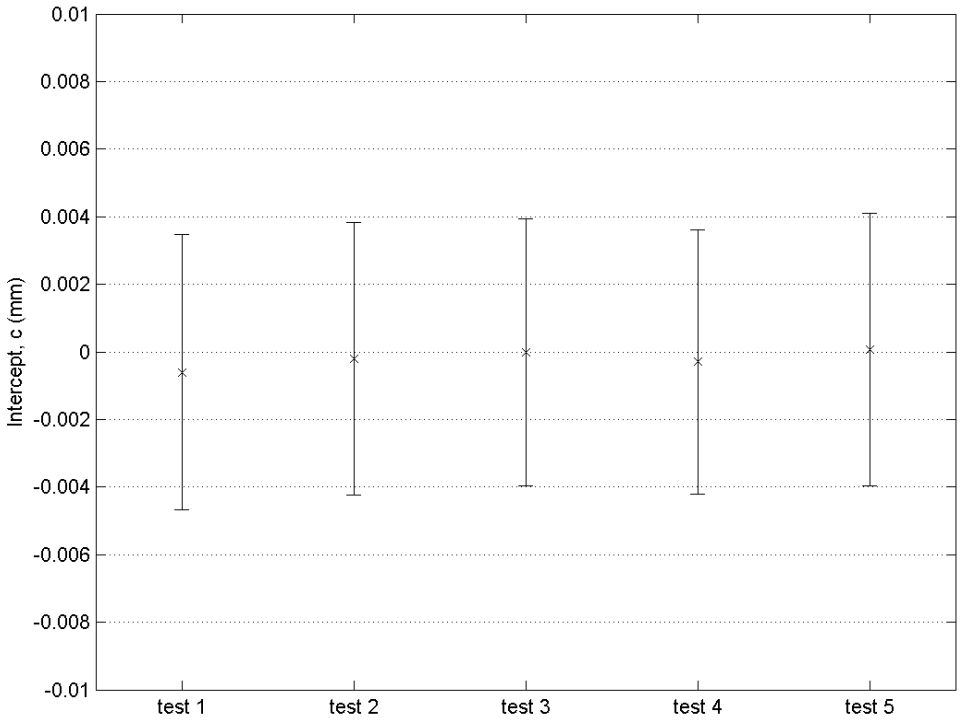

Figure 7-9 Mean intercept, c, for the five linear position validation tests +/- standard deviation

7.2.3 Linear hysteresis

The motor axis position and the measured LVDT position were recorded during the linear hysteresis investigation and are displayed in Figure 7-10 below. To enable the small hysteresis at the graph peaks to be seen a magnified view of the first upper and lower peaks are shown in Figure 7-11. The hysteresis was calculated as the difference between the motor axis position and the LVDT position and a positive hysteresis value represents an overshoot of the system compared to the positional output from the motor encoder. The mean hystereses at the upper and lower peaks were calculated along with their standard deviations. The mean hysteresis at the upper peaks was 0.905 ± 1.590µm whereas the mean hysteresis at the lower peaks was 20.049 ± 1.175µm (mean ± SD) (Figure 7-12).

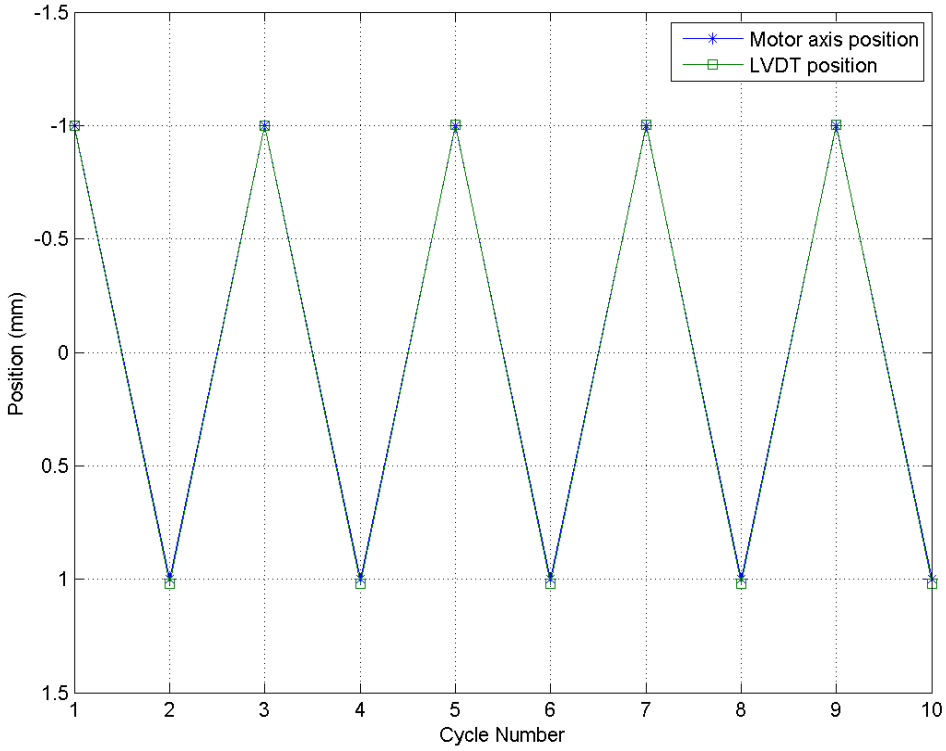

Figure 7-10 Linear hysteresis plot showing the motor axis position and the measured LVDT position

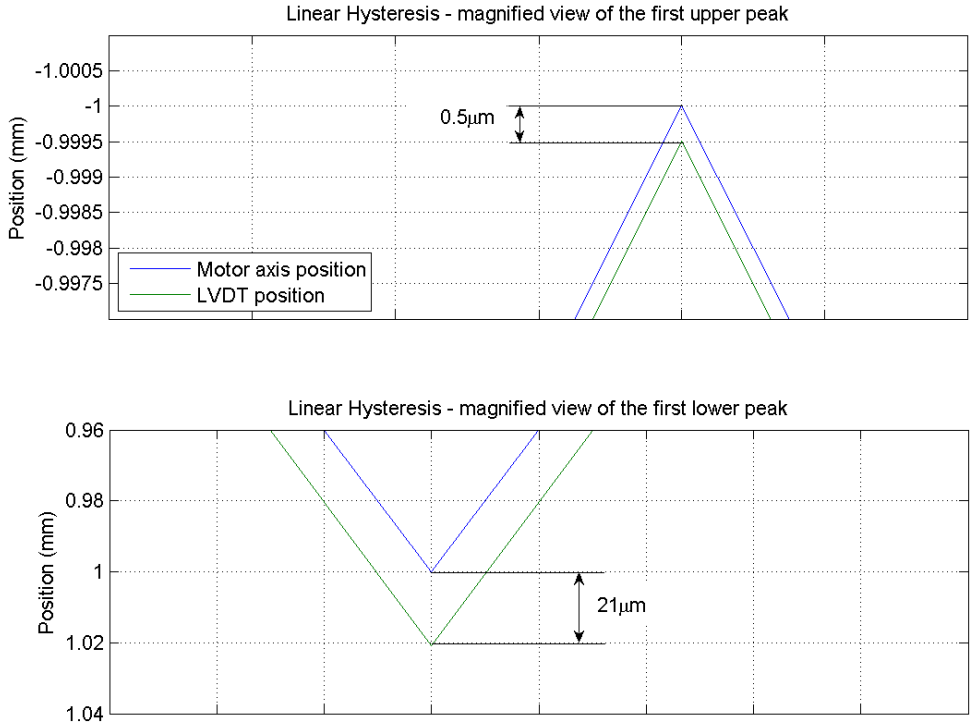

Figure 7-11 Magnified view of the first upper and lower peaks of the linear hysteresis plot showing the motor axis position and the measured LVDT position

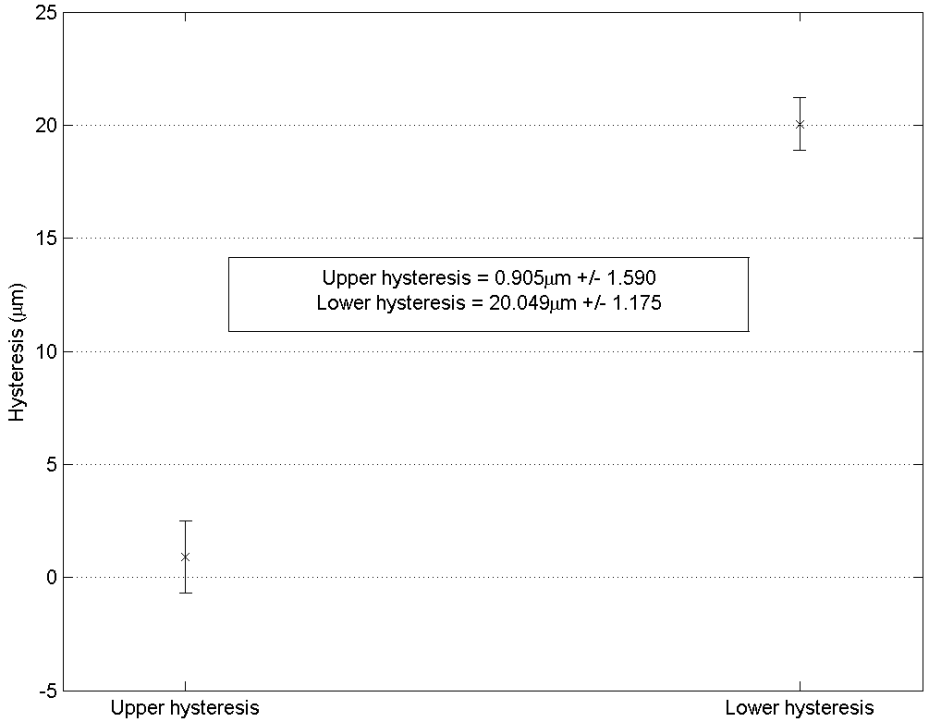

Figure 7-12 The mean hysteresis at the upper and lower peaks on the linear axis hysteresis graph, +/- standard deviation

7.2.4 Rotational potentiometer calibration

The plot of the five calibrations of the rotational potentiometer is shown in Figure 7-13. As with the LVDT, the data for each calibration was fitted to a straight line using the least-squares method and the mean gradients and intercepts were calculated. The standard deviations of these constants were calculated and are shown in Figure 7-14 and Figure 7-15. The weighted averages of the gradient and intercept for the calibrations were calculated, again with their standard deviations (see Appendix D). The rotational potentiometer calibration had a gradient of -0.059 ± 0.000 V/deg and an intercept of -0.012 ± 0.005 V (mean ± SD).

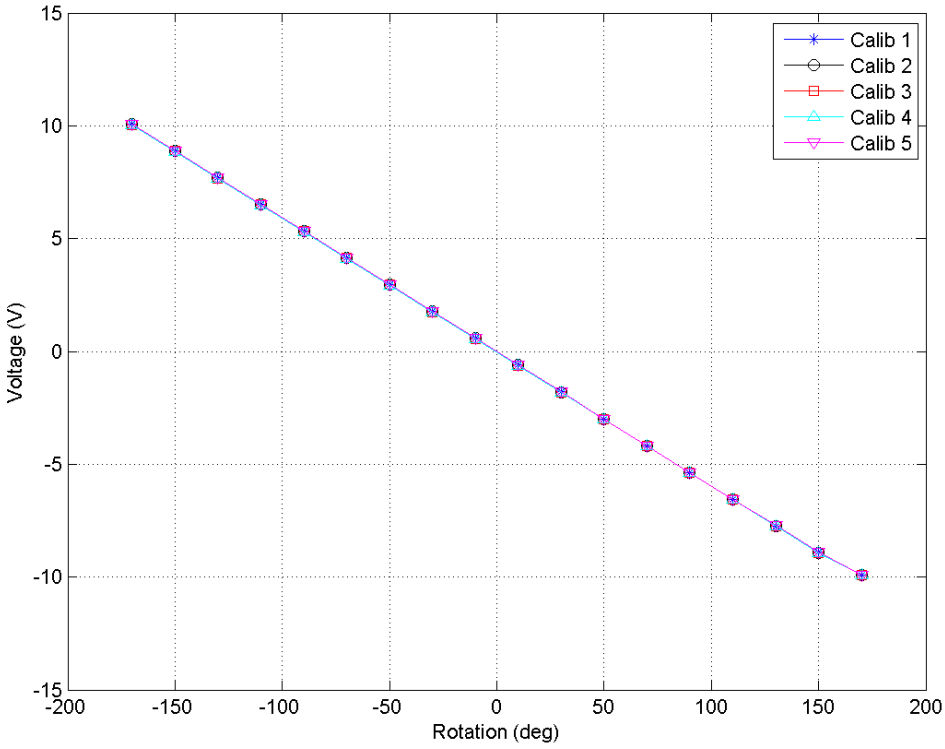

Figure 7-13 The five calibrations for the rotational potentiometer

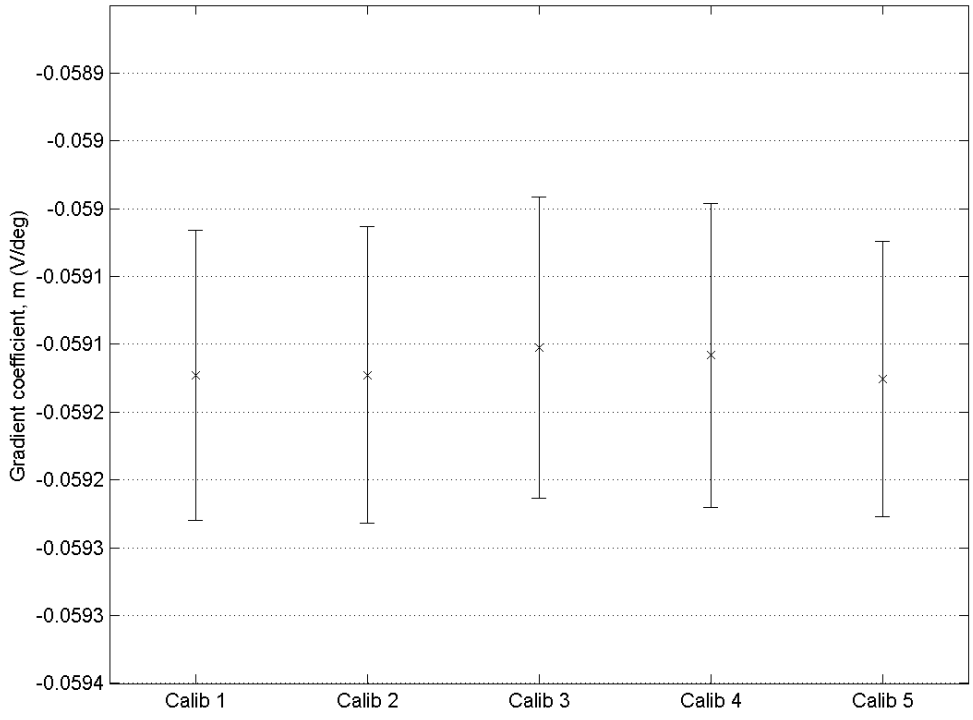

Figure 7-14 The mean gradient, m, for the five rotational potentiometer calibrations +/- standard deviation

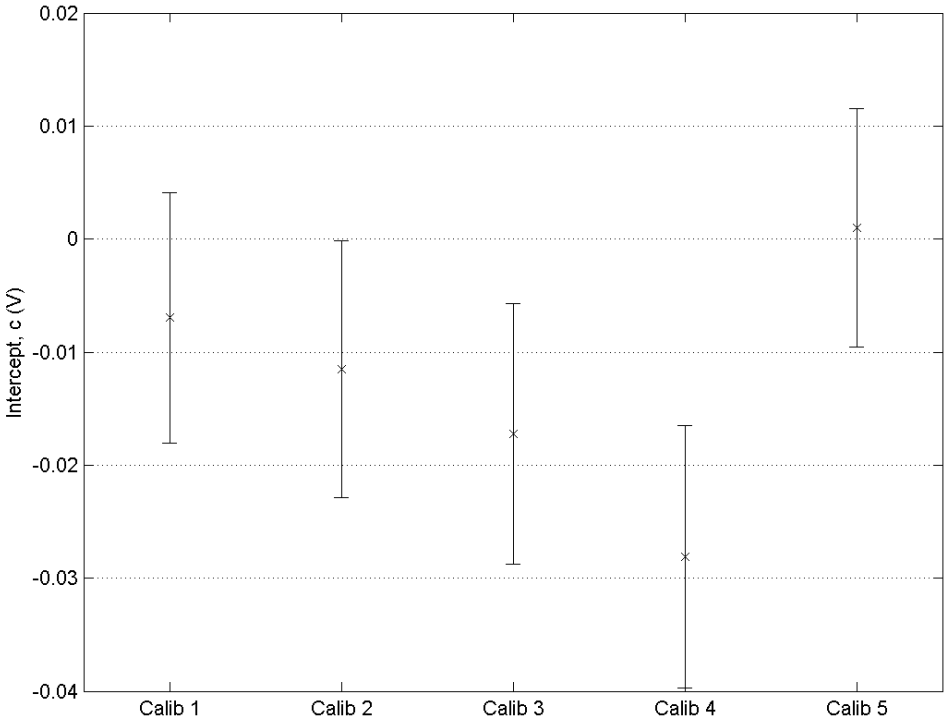

Figure 7-15 The mean intercept, c, for the five rotational potentiometer calibrations +/- standard deviation

7.2.5 Rotational position validation

Following the rotational position validation experiment, the motor axis position was plotted against the measured rotational potentiometer position which was converted to degrees using the calibration gradient previously determined (Figure 7-16). The mean gradients and intercepts for the five repetitions were calculated (Figure 7-17 and Figure 7-18) and the weighted averages of these constants were determined. The correlation between the motor axis position and the measured potentiometer position had a mean gradient of 1.005 ± 0.000 and a mean intercept of 0.213 ± 0.011 deg (mean ± SD).

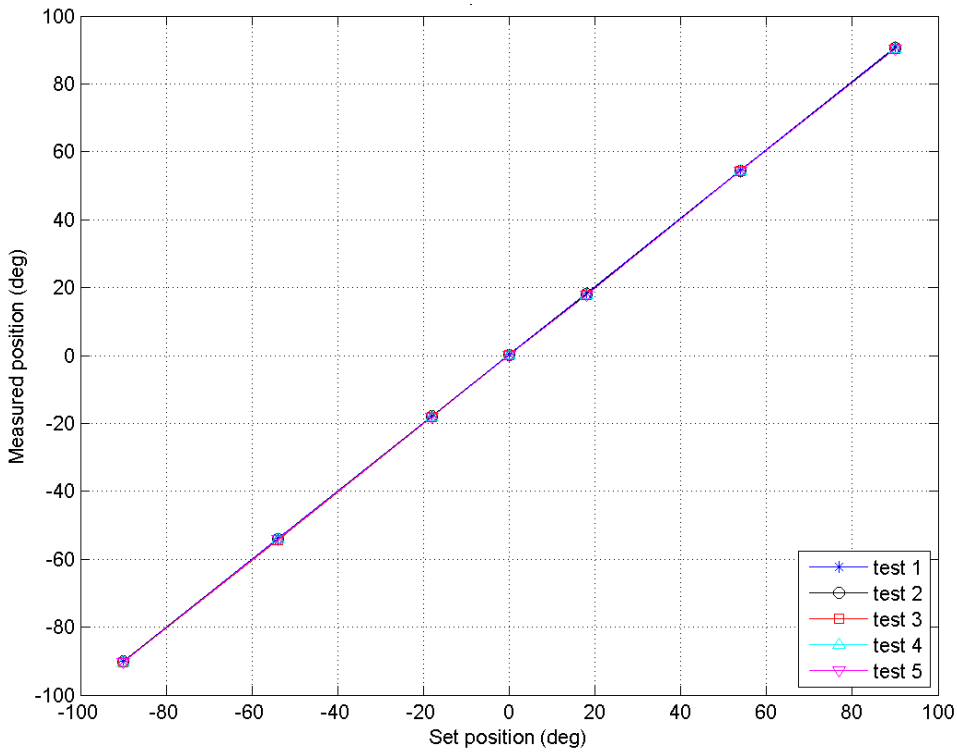

Figure 7-16 The five validation tests of the rotational position

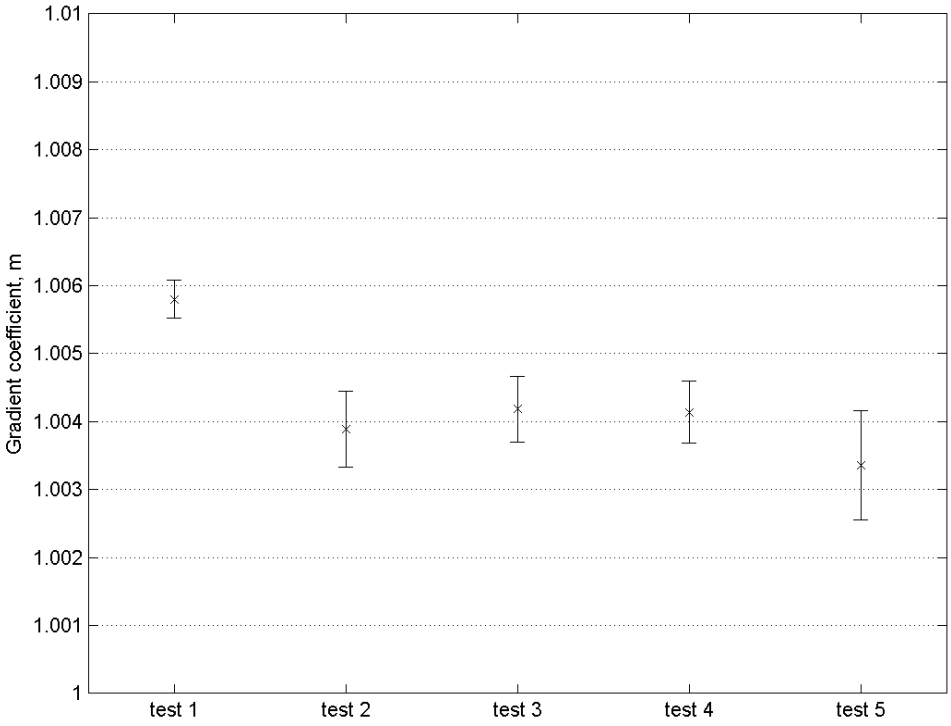

Figure 7-17 Mean gradient, m, for the five rotational position validation tests +/- standard deviation

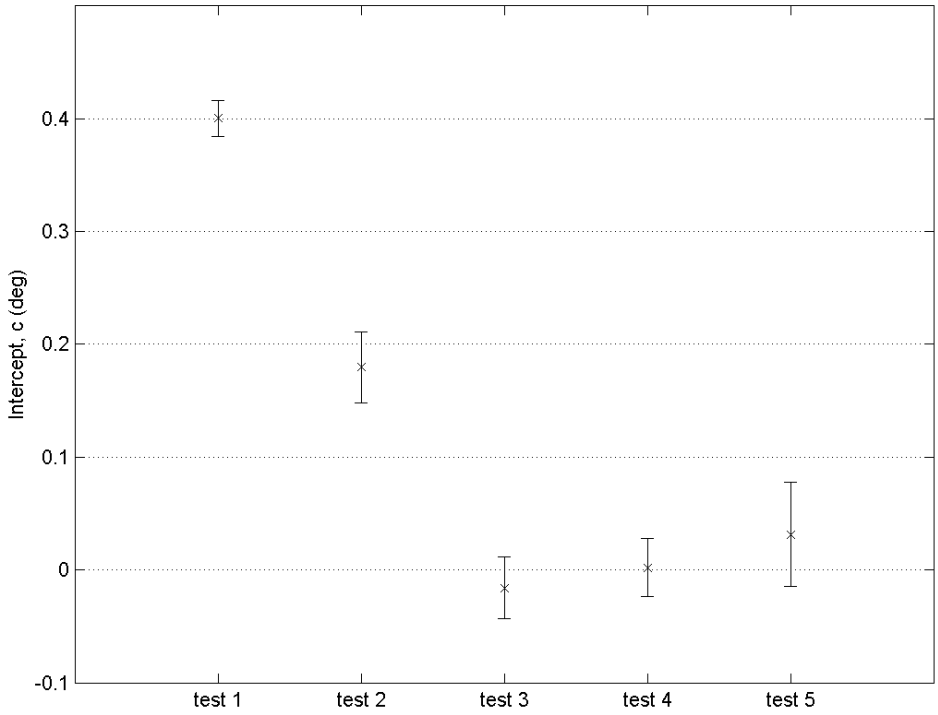

Figure 7-18 Mean intercept, c, for the five rotational position validation tests +/- standard deviation

7.2.6 Rotational hysteresis

The motor axis positions and the measured rotational potentiometer positions were recorded during the rotational hysteresis investigation and are displayed in Figure 7-19. To enable the small hysteresis at the graph peaks to be seen a magnified view of the first upper and lower peaks are shown in Figure 7-20. The hysteresis was calculated as the difference between the motor axis position and the potentiometer position and, as with the linear hysteresis experiment, a positive hysteresis value represents an overshoot of the system compared to the positional output from the motor encoder. The mean hystereses at the upper (clockwise) and lower (anticlockwise) peaks were calculated along with their standard deviations (Figure 7-21). The mean hysteresis at the upper peaks was 0.206 ± 0.063 deg whereas the mean hysteresis at the lower peaks was 0.134 ± 0.026 deg (mean ± SD).

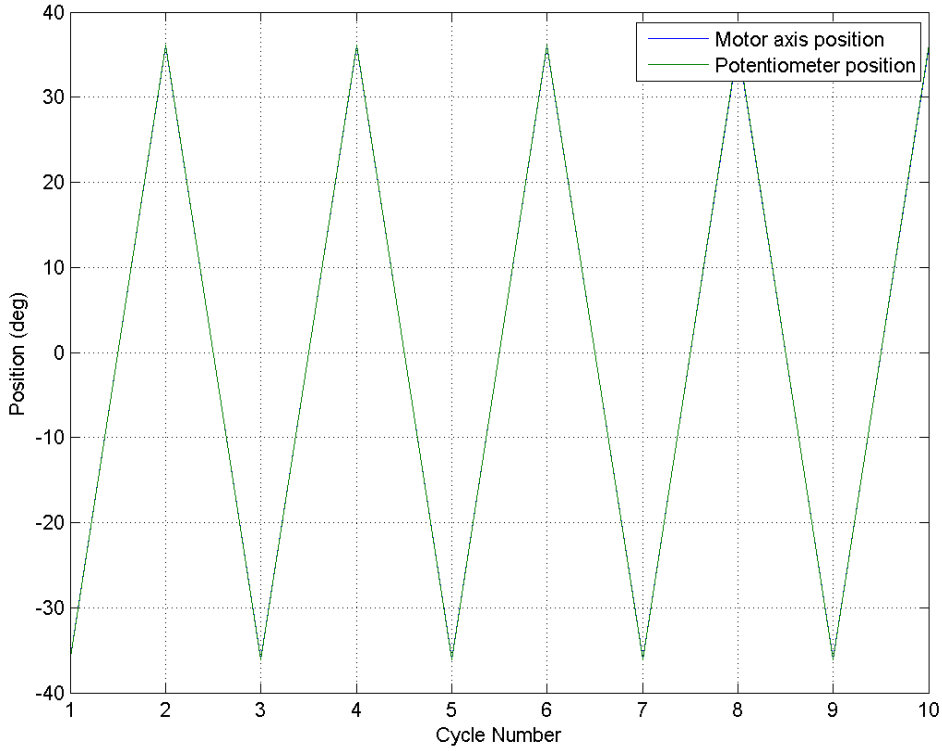

Figure 7-19 Rotational hysteresis plot showing the motor axis position and the measured potentiometer position

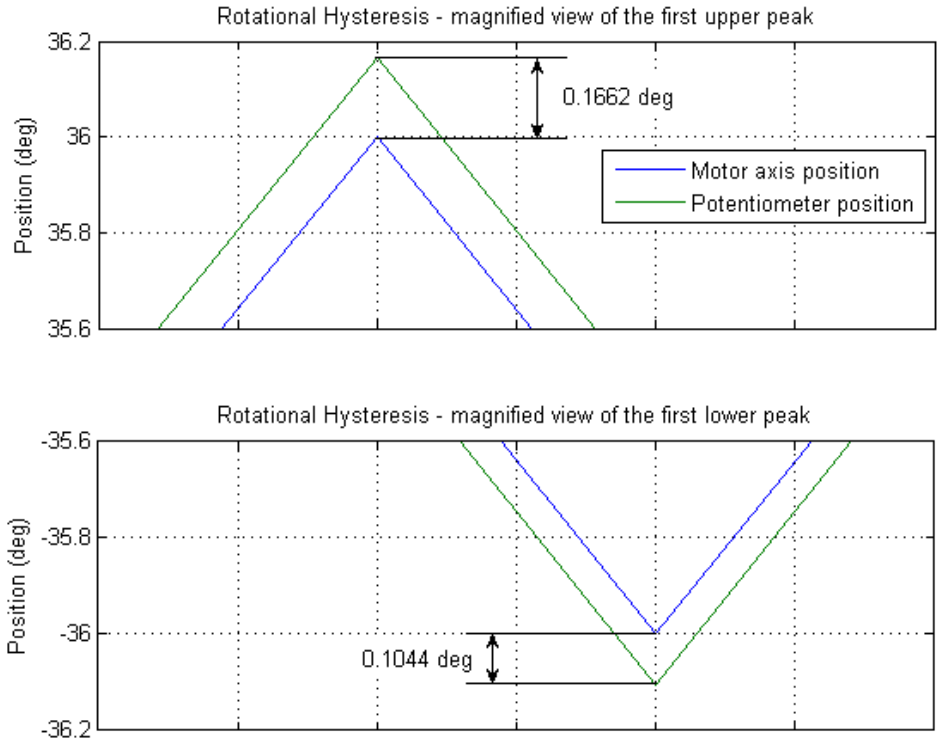

Figure 7-20 A magnified view of the first upper and lower peaks of the rotational hysteresis plot showing the motor axis position and the measured potentiometer position

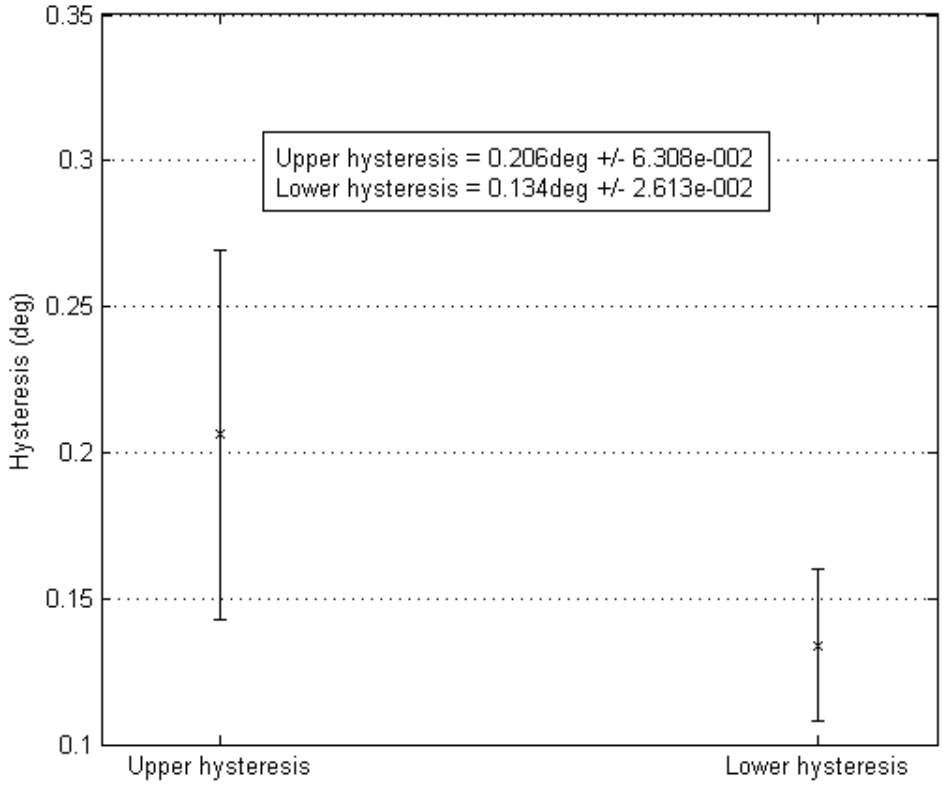

Figure 7-21 The mean hysteresis at the upper and lower peaks on the rotational axis hysteresis graph, +/- standard deviation

7.3 Discussion

The calibration of the LVDT (Figure 7-5) showed that the transducer was linear and a calibration gradient was calculated for use in the linear position validation and linear hysteresis experiments. The calibration gradient was shown to be repeatable and fell within a small standard deviation showing that it represented a suitable estimate to use in the subsequent experiments (Figure 7-6).

In the linear position validation experiment there was good linear correlation between the motor axis position as set by the motor controller and the measured LVDT position (Figure 7-7). The intercept position (Figure 7-9) was approximately zero and fell within small standard deviations showing that the manual set-up of the zero position of the LVDT was good. The gradient of the positional data was 1.011 ± 0.002 (Figure 7-8), therefore for every 1mm moved by the motor axis, the linear slide moves 1.011mm. This represents a 1.1% positional error. This error could be due to manufacturing tolerances in the ballscrew pitch or the pulley diameters. The maximum cyclic displacement expected for the bioreactor is ±2mm which would result in a maximum error of ±22µm. This is within the acceptable accuracy of the bioreactor.

The measured hysteresis with the linear system was 0.905 ± 1.590 μm at the top of the stroke whereas the mean hysteresis at the bottom of the stroke was 20.049 ± 1.175 μm (mean ± SD) (Figure 7-10 – Figure 7-12). There is an order of magnitude difference between these two values and this is most probably caused by the vertical orientation of the slide. As the motor moves the slide to the upper position the leadscrew nut will be loaded on the upper face of the leadscrew thread. In this experiment the move velocity was 20mm/s and the acceleration and deceleration were 200mm/s^2. Due to the high velocity and deceleration, when the motor stops, the inertia of the slide and the components mounted on it could cause it to continue to move vertically until the nut is loaded on the lower face of the screw. If the slide and components have even further momentum, they could drive the screw and take up any slack which may exist in the non-drive side of the timing belt. This would result in the maximum hysteresis within the system. However, as the slide is orientated vertically, gravity would cause the slide and components to move back down so that the nut would again be loaded on the upper face of the leadscrew thread and the slack in the timing belt would be returned. As this transient motion would happen in a fraction of a second, it would be in this final steady state that the positional reading would have been taken.

Similarly, as the slide was moved downwards with a high velocity, the nut would have been loaded against the lower face of the leadscrew thread. As the motor would come to a stop, the inertia and gravitational forces would cause the slide and components to continue to move downwards so as the nut is loaded on the upper face of the leadscrew thread and these forces drive the leadscrew to take up the slack in the timing belt. Due to gravity, the slide would remain in this position which is where the readings were taken.

If the motor drives the linear system at a low velocity with low decelerations then the nut will remain loaded on the upper face of the leadscrew thread and one side of the timing belt will remain loaded, not allowing the slack to be used. Therefore, this experiment has shown the best case scenario where low velocities and decelerations would result in negligible hysteresis as shown at the top of the stroke, and the worst case scenario, where high velocities and decelerations would result in the maximum hysteresis (±20.049μm ± 1.175) as shown at the lower end of the stroke.

The calibration of the rotational potentiometer (Figure 7-13) showed that the transducer was linear and calculated a calibration gradient for use in the rotational position

validation and rotational hysteresis experiments. The calibration gradient (Figure 7-14) was shown to be repeatable and fell within a small standard deviation showing that it was a suitable estimate to use in the other experiments. The value of the intercept (Figure 7-15) showed more variability and this was because the zero position of the potentiometer was manually set between each calibration.

In the rotational position validation experiment there was good linear correlation between the motor axis position as set by the motor controller and the measured LVDT position (Figure 7-16). There was some variability in the intercept position (Figure 7-18) due to the zero position being reset between each experiment. There was much greater correlation between the mean gradients (Figure 7-17) and the weighted average gradient of the positional data was calculated to be 1.005 ± 0.000. Therefore for every 1° rotated by the motor axis, the bioreactor chamber shaft rotates 1.005°. This represents a 0.5% rotational positional error. This error could be caused by manufacturing tolerances in the pulley diameters. The maximum cyclic rotation expected for the bioreactor is ±45° which would result in a maximum error of ± 0.225°. Again, this is within the acceptable accuracy of the bioreactor.

As with the linear hysteresis experiment, the rotational hysteresis experiment was performed with high velocities (10 revolutions/s) and decelerations (300 revolutions/s^2) to record the maximum hysteresis in the system (Figure 7-19 & Figure 7-20). The inertia of the upper rotational shaft and pulley would have caused the shaft to continue to rotate, after the motor had stopped, until the slack in the non-driving side of the timing belt had been taken up. The mean hysteresis when turning from clockwise to anticlockwise was 0.206° ± 0.063 whereas the mean hysteresis when turning from anticlockwise to clockwise was 0.134° ± 0.026 (mean ± SD) (Figure 7-21). There is no significant difference between the hystereses found in either direction ($p>0.05$).

7.4 Conclusion

The positional output from the linear and rotational axis has been validated. The positional errors associated with the linear and rotational axes have been quantified as 1.1% and 0.5% respectively. The maximum hystereses were evaluated as ±20.049 ± 1.175μm and ±0.206 ± 0.063 deg for the linear and rotational axes. The errors associated with the positional outputs are within the acceptable accuracy of the bioreactor.

The validation of the positional output from the bioreactor has contributed to the successful achievement of Objective 8.

8 EVALUATION OF RIG STIFFNESS

The stiffness of the bioreactor rig was evaluated to determine what proportion of the displacement measured by the motors was associated with deflection of the rigid structures in the rig. Both the linear and rotational stiffnesses of the rig were evaluated.

8.1 Linear stiffness

8.1.1 Methods and materials

The stiffness of the rig was measured by loading a rigid sample into the bioreactor and applying a load or torque. Assuming that there was no deformation of the sample, the displacement measured was due to deflection of the structures in the rig and this deflection was used to calculate the stiffness.

A 10mm diameter solid steel shaft, approximately 170mm long, was loaded into the bioreactor to act as a rigid sample. It was attached to the upper rotational shaft and the lower load cell shaft using the pin joints which were normally used to secure the upper and lower chamber shafts and the locking nuts were tightened (Figure 6-15, p.154).

The Mint subroutine described in Section 6.3.2.1 was also used to evaluate the linear stiffness. The algorithm increased the torque applied by the linear axis motor in ten increments up to a maximum specified by the user in a comms element (see Section 5 for details of comms elements and the Mint subroutines). This torque was converted to an axial load through the linear slide and was measured by the load cell. The subroutine initialised the position of the linear and rotational axes to zero and enabled both the axes. A number of parameters were set up to be captured and these were: the analogue readings from the load and torque cells, the positions of the linear and rotational axes and the demanded torque as a percentage of the motor peak torque. A capture duration of two second was set. The capture flag was initialised to zero and the torque output of the rotational axis motor was also set to zero. The data was acquired after two seconds to allow the system to settle. The capture flag was then set to equal two upon completion of the acquisition.

The LabView capture program detailed in Section 5.10 was running and monitoring the comms element which was used as the capture flag. When the capture flag had a value of two, the LabView capture program uploaded the captured data and saved it to a data

file. When this was complete it reset the flag to zero and continued to monitor it until it had a value of two once again.

In the Mint subroutine a loop increased the torque provided by the linear axis motor up to the maximum torque specified by the user in ten equally spaced increments. Within each iteration of the loop the torque was increased, the system was allowed to settle for two seconds and the data was captured. When the capture was complete the capture flag was set to two and the data was uploaded and saved by the LabView capture program. The Mint program continued to repeat the loop until the maximum torque was applied. The linear axis was loaded to a maximum of 20% of the maximum torque output from the linear axis motor. This equated to a tensile load of approximately 300N through the load cell.

Five repetitions of the incremental linear loading were performed. The sample was removed and repositioned between each repetition.

The data was read into MatLab (The Mathworks Inc., Natick, MA, USA) and the mean load, torque and linear position were calculated for the two second sample at each torque interval. The measured linear displacement was plotted against the applied load which was measured by the load cell and is shown in Figure 8-1.

8.1.2 Results

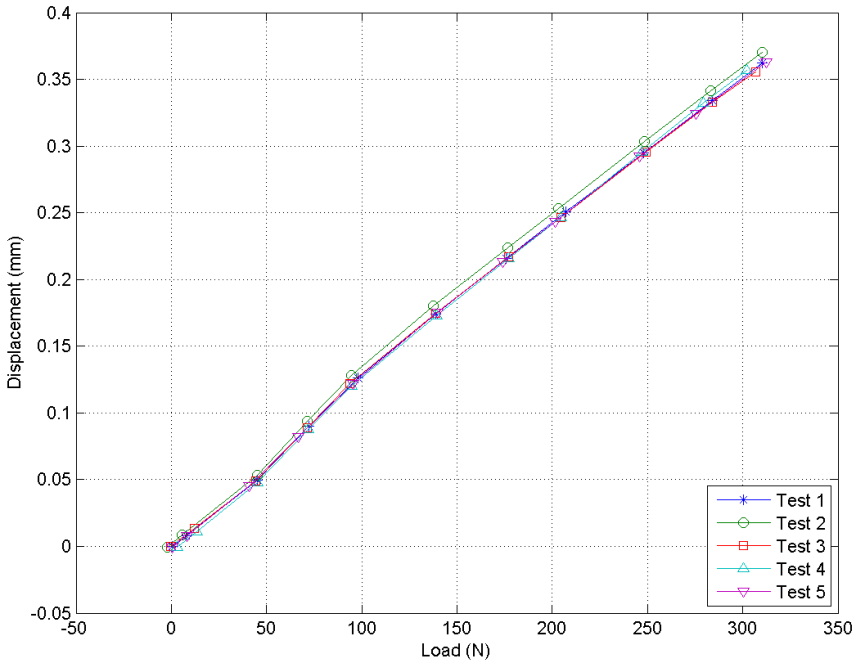

Figure 8-1 Linear stiffness of rig

The procedure detailed in Appendix D was used to calculate the mean linear stiffness of the bioreactor by calculating the weighted mean inverse gradient of the five tests shown in Figure 8-1. A stiffness of 841.67 ± 5.27 N/mm (mean ± standard deviation) was calculated.

8.1.3 Discussion

For most soft tissue applications the axial load would not be expected to exceed 150N. This load would produce a displacement of approximately 0.2mm due to flexion of the bioreactor structures. If this load was achieved at a maximum displacement of 2mm of the tissue then the displacement from the bioreactor structures would represent a positional error of 10%.

The maximum deflection in the bioreactor was observed at the upper mounting plate which supported the rotational shaft (see Figure 8-2). This plate reacted the total axial load which was put through the sample. The plate was only 3mm in thickness and if it was deemed to be too compliant the plate could easily be replaced with one of 5mm thickness. This would significantly increase the stiffness of the bioreactor and reduce any positional error associated with the linear stiffness.

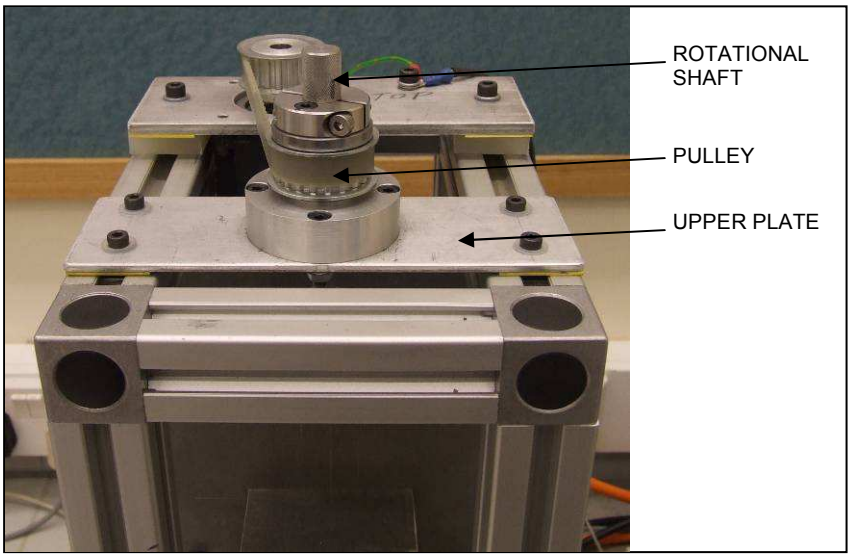

Figure 8-2 Upper plate supporting rotational shaft

8.2 Rotational stiffness

8.2.1 Methods and materials

The same set-up shown in Figure 6-15 and described in Section 8.1.1 was used to evaluate the rotational stiffness of the bioreactor. A Mint subroutine was written to incrementally increase the torque applied by the rotational axis motor in the same way as that described for the linear stiffness subroutine (Section 8.1.1). The rotational axis was loaded to a maximum of 50% of the maximum torque output from the rotational axis motor. This equated to a torque of 1.06 ± 0.01Nm through the torque cell. The LabView capture program was used to capture the data and save it to file.

Five repetitions of the incremental rotational loading were performed. The sample was removed and repositioned between each repetition.

The data was read into MatLab (The Mathworks Inc., Natick, MA, USA) and the mean load, torque and rotational displacement were calculated for the two second sample at each load interval. The measured rotation was plotted against the applied torque which was measured by the torque cell and is shown in Figure 8-3.

8.2.2 Results

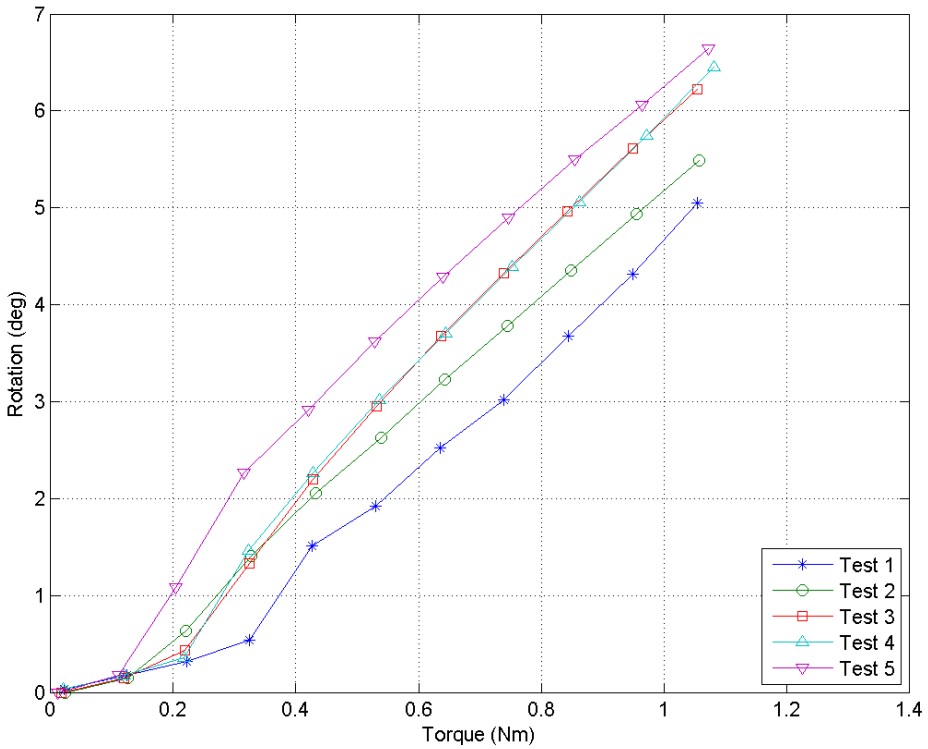

Figure 8-3 Rotational stiffness of rig

The procedure detailed in Appendix D was used to calculate the mean torsional stiffness of the bioreactor by calculating the weighted mean inverse gradient of the five tests shown in Figure 8-3. A stiffness of 0.164 ± 0.002 Nm/deg (mean ± standard deviation) was calculated.

8.2.3 Discussion

A number of areas were identified which contributed to the rotational stiffness of the bioreactor. Firstly, there was some limited stretching in the timing belt used to transmit the torque from the motor to the upper rotation shaft. Rotation also occurred between the load cell and the thread of the shaft connecting the load cell to the torsion cell. During construction this thread was secured with threadlocking compound (Loctite®, Henkel Ltd, Hemel Hempstead, UK) to minimise any rotation caused by large torques and there was no method to reduce this rotation further without a major redesign of the load and torque cell mountings. Finally, rotation was identified at the pin joints which connect the rigid sample to the upper rotational shaft and the lower load cell shaft. This was caused by the clearance between the connecting pin and the holes in the mating shafts. This is illustrated in Figure 8-4. Without the application of any torsion, the locking nut is tightened to push the rigid sample shaft or chamber shaft up so as to tighten down on the pin. However, when the torsion is applied, it is possible for the nut to loosen slightly, allowing the sample/chamber shaft to move down a small distance. Due to the clearance between the pin and holes in the shafts, this small vertical displacement permits relative rotation between the sample/chamber shaft and the load cell/rotation shaft. The effect of this was minimised by ensuring the locking nut was secured very tightly. If the application was demanding a large torque to be transmitted through the bioreactor which was sufficient to loosen the locking nut then a spring washer included between the locking nut and sample/chamber shaft was found to prevent nut loosening.

A rotation of 5.97 ± 0.68 degrees (mean ± standard deviation) was recorded at a maximum torque of 1.06 ± 0.01Nm (mean ± standard deviation).

Should the bioreactor be used for mechanical stimulation of a ligament by rotation about the longitudinal axis, the torque would be expected to be quite low. For the purposes of this study, the maximum torsional resistance exerted by a ligament was expected to be 0.2Nm and this would result in a rotation of approximately 1.2° at the maximum rotational stroke due to the mechanical components in the bioreactor. If a torque of 0.2Nm was achieved at a maximum rotation of 90° then a positional error at the

maximum stroke of approximately 1.4% would occur due to the stiffness of the bioreactor. This estimate is within the acceptable accuracy of the bioreactor.

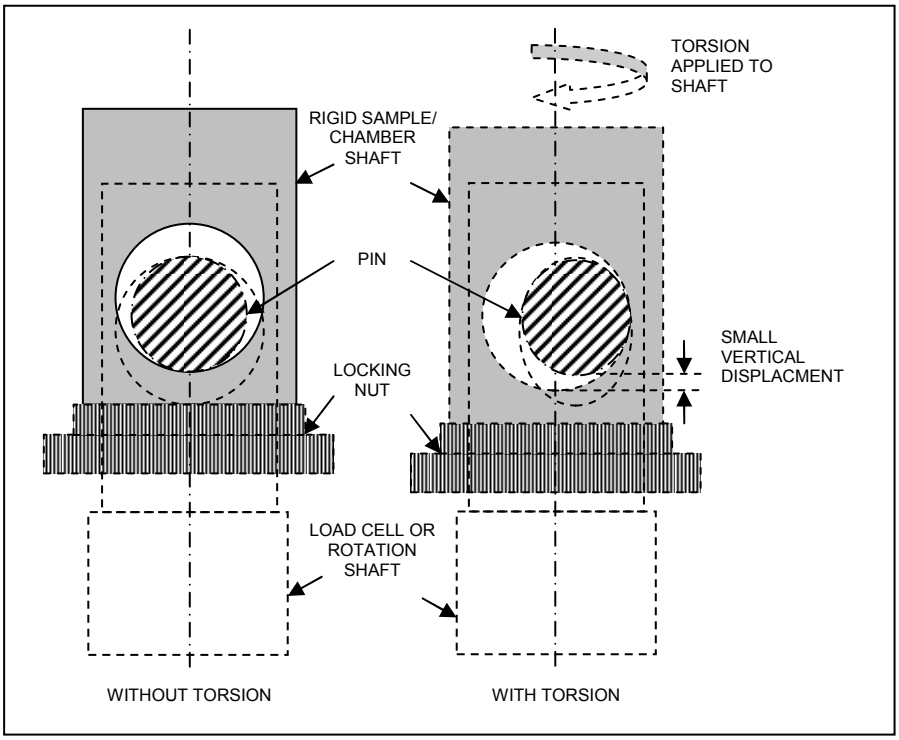

Figure 8-4 Effect of clearance in shaft pin joint when torque is applied.

8.3 Conclusions

The linear and rotational stiffness of the bioreactor has been evaluated. A linear stiffness of 841.67 ± 5.27 N/mm and rotational stiffness of 0.164 ± 0.002 Nm/deg (mean ± standard deviation) were calculated. The compliant structures within the bioreactor were identified. The linear stiffness could be increased by manufacturing a 5mm thick upper mounting plate for the rotational shaft in place of the 3mm plate currently in operation. Under particularly high torques which could cause the locking nut to loosen, a spring washer could be used to prevent rotation at the pin joint.

The evaluation of the bioreactor stiffness contributed to the successful achievement of Objective 8.

9 EVALUATION OF LINEAR AXIS FRICTION WITHIN THE CHAMBER

The lower chamber shaft was designed to move with a reciprocating motion into and out of the chamber. The chamber shaft was sealed using a PTFE spring-loaded variseal (Trelleborg Sealing Solutions, Solihull, UK) to permit the reciprocating motion whilst preventing leaks and the ingress of infection. The shaft also passed through the stainless steel insert which held the seal in place.

A cyclic test was performed to determine the friction within the linear axis due to the seal and stainless steel insert. A chamber was assembled and loaded into the bioreactor without any fluid inside it and with no sample between the chamber shafts. Spring washers were used in the pin joints of the chamber shafts to ensure a secure coupling. A positional cycle was performed at 1Hz with a stroke of 1.5mm for 10 minutes and the load measured by the load cell was recorded. A capture of 20 cycles from the test is shown in Figure 9-1 and a maximum load of 44.4N was recorded for that sample.

This level of friction was much higher than expected from the seal alone. Therefore, the experiment was repeated using the same method as described above except the seal from the lower chamber shaft was removed. This allowed the friction between the chamber shaft and the stainless steel insert to be quantified. Figure 9-2 shows the load output from this experiment and a maximum load of 34.2N was recorded. The load is symmetric about the x-axis indicating that the load is indeed a measure of friction as opposed to an artefact, for example, created by load cell misalignment.

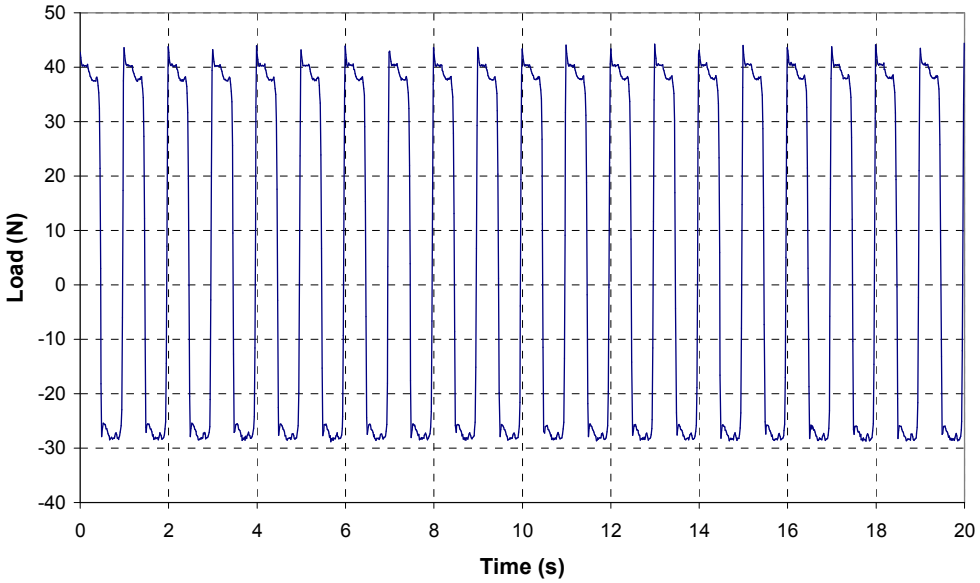

Figure 9-1 Recorded axial load with a seal in place and no sample

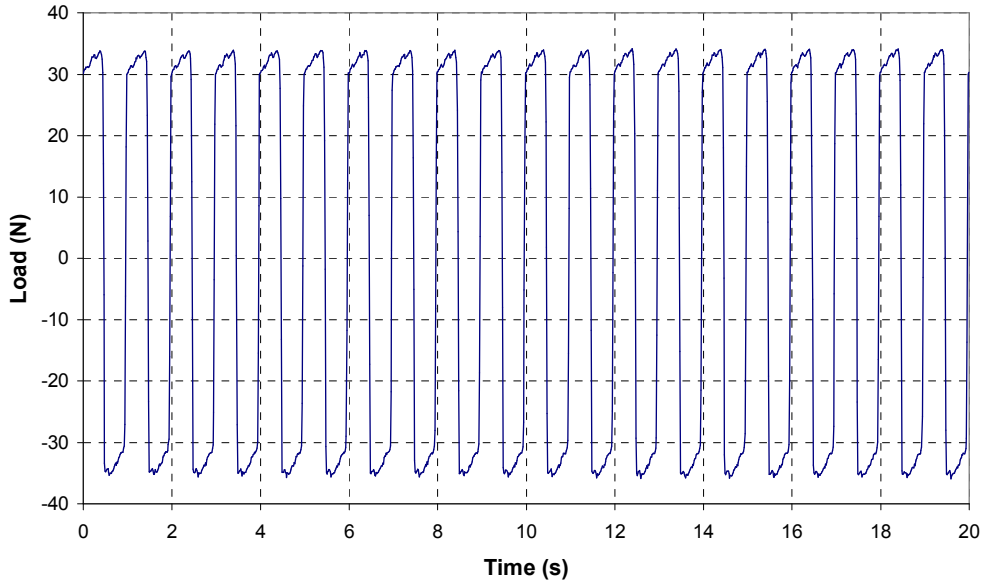

Figure 9-2 Recorded axial load with no sample or seal in place

A number of factors were identified which contributed to this high friction load. A split spring washer was used between the chamber shaft and the locking nut to ensure a secure coupling and prevent hysteresis as described in Section 8. There was a small clearance between the bore in the chamber shaft and the mating load cell shaft. When the split spring washer was compressed it imposed a moment on the chamber shaft and this caused a small angular misalignment due to the clearance in the coupling (Figure 9-3).

The connecting pin through holes in the chamber shafts were filed using a needle file to ensure the pin could be easily inserted through the chamber shaft and load cell shaft. This filing process created asymmetric hole clearances on either side of the chamber shaft. Therefore, when the chamber shaft was loaded against the pin by tightening the locking nut the asymmetric hole clearances combined with the clearance between the bore in the chamber shaft and the mating load cell shaft to again cause a small angular misalignment (Figure 9-4).

This angular misalignment of the chamber shaft caused undesirable loading between the shaft and the stainless steel insert. A number of improvements were made to reduce the axial load due to friction at this interface. Firstly, the coefficient of friction between the two components was reduced by lapping the two together using a fine abrasive paste (Valve grinding compound 360 fine, Carborundum Abrasives G.B. Ltd., Manchester, UK). Also, the split spring washer was deemed not appropriate due to the shaft misalignment it created.

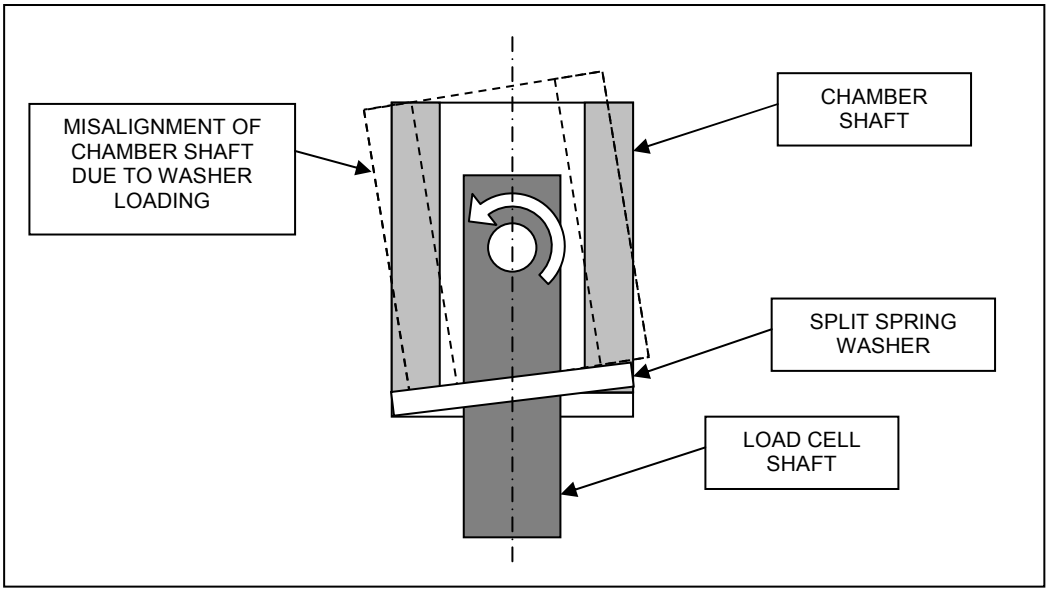

Figure 9-3 Misalignment of chamber shaft due to asymmetric loading from spring washer

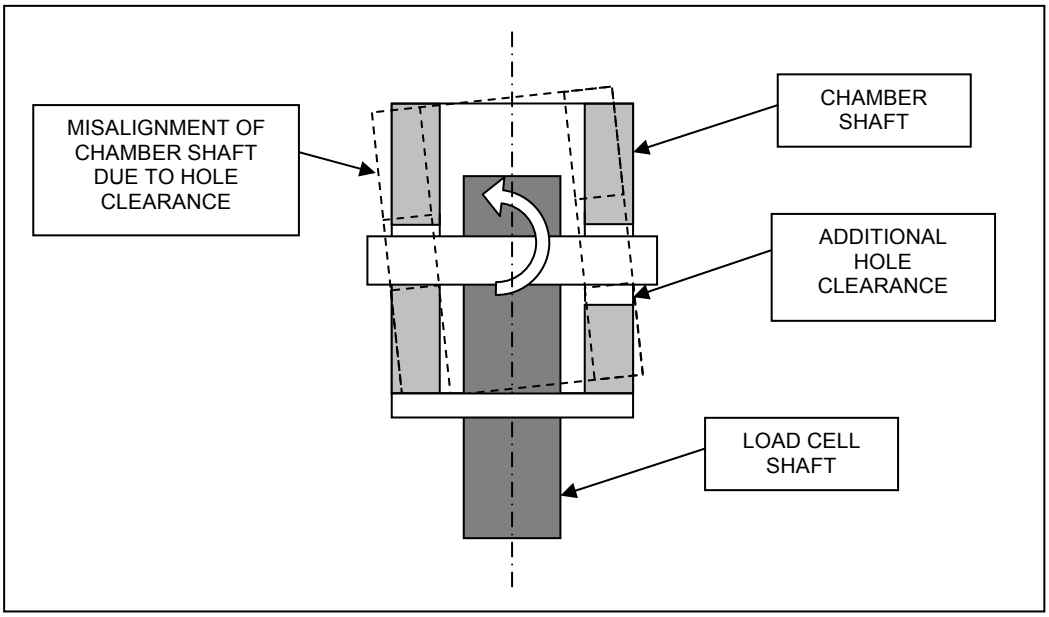

Figure 9-4 Misalignment of chamber shaft due to asymmetric hole clearance

With these measures in place the chamber friction was evaluated. The seal friction within the chamber was quantified without any misalignment by performing a number of pull-out tests using a materials testing machine. Three chambers were fully assembled and filled with water to ensure the seals were lubricated. Appropriate tubing was connected to the ports of each chamber and this was open to the atmosphere to reduce any fluid pressure effects. The chamber was mounted in a vice on the bed of a materials testing machine (Model 3365, Instron, High Wycombe, UK) fitted with a 100N load cell. The chamber shaft was centrally aligned with the load cell above and a rod was used to

connect the chamber shaft to the load cell (Figure 9-5). The rod was rigid axially but would permit limited rotation to reduce the effect of any misalignment.

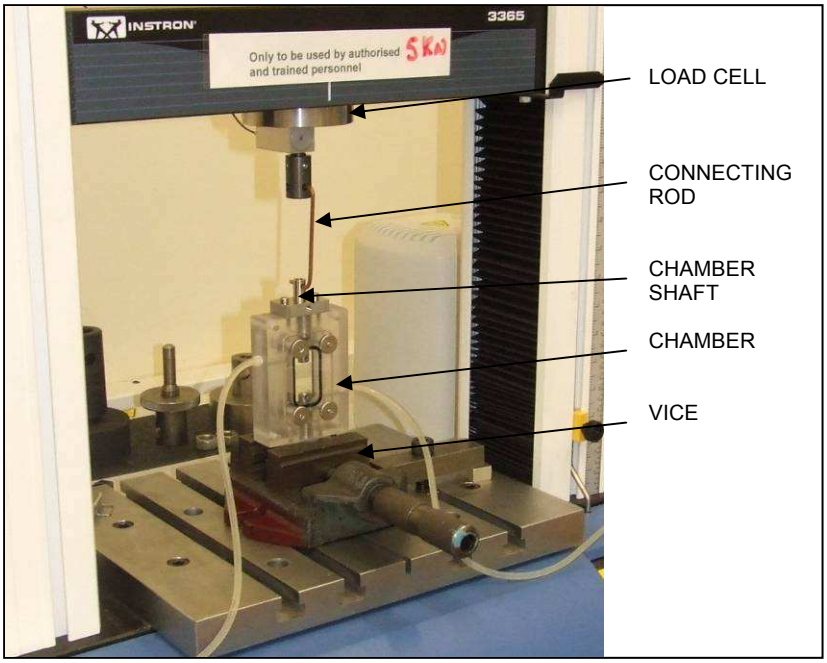

Figure 9-5 Set-up of seal friction test in the materials testing machine

The chamber rod was withdrawn at 10mm/min and the load was measured. The withdrawal was repeated five times for each seal with repositioning of the chamber rod and the connecting rod between each repetition. The friction from both seals of each chamber was measured, providing data relating to six seals in total. The maximum load measured from each pull-out test is shown in Figure 9-6. The loads in seal five appear particularly high compared to the other seals suggesting either the seal was damaged or there was a large misalignment in the set-up of that chamber. The maximum frictional load, excluding seal five, ranged from 8.16N – 15.64N.

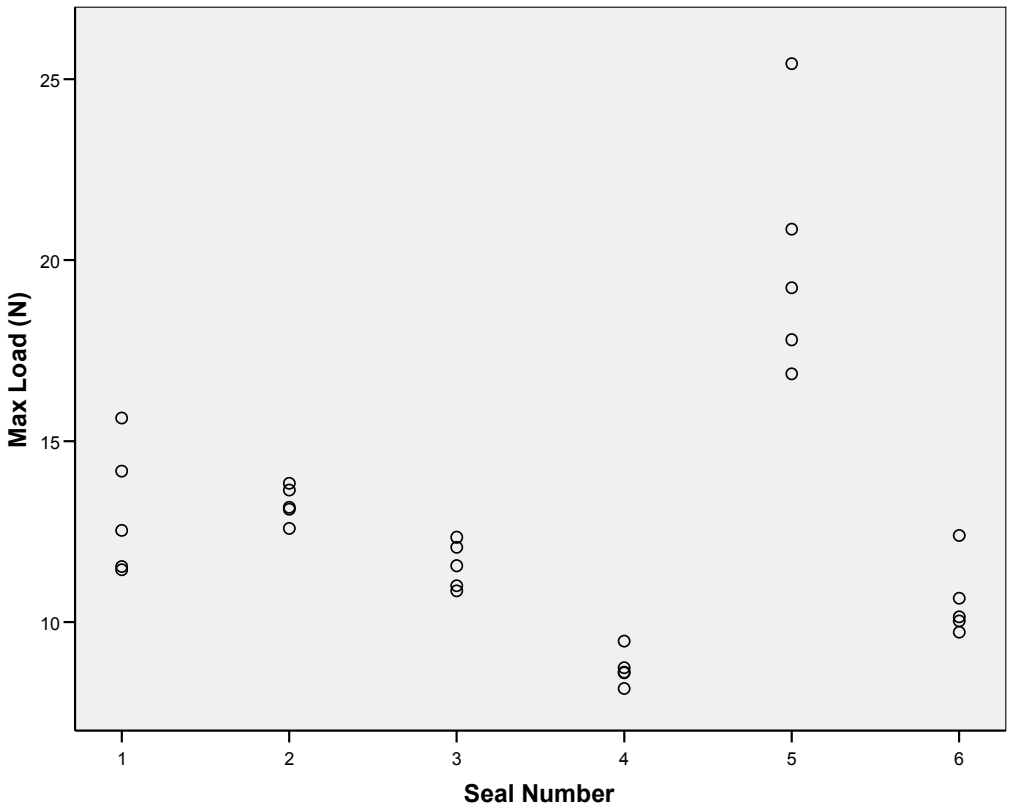

Figure 9-6 Maximum load achieved during pull-out tests of six seals

The chambers were then loaded into the bioreactor to repeat the experiment. A move of 2mm was performed at 10mm/min and the load was recorded. This was repeated ten times for each chamber and the position of the chamber shaft was returned to zero between each repetition. Only the lower seal of each chamber was tested.

The pull-out was performed with the pin joint locking nut loosely secured. A further ten repetitions were performed with the locking nut tightly secured to evaluate the effect of locking nut tightness on the measured friction load. Figure 9-7 shows the load during one displacement cycle with the locking nut loosely and tightly secured and the results from the three chambers are summarised in Figure 9-8.

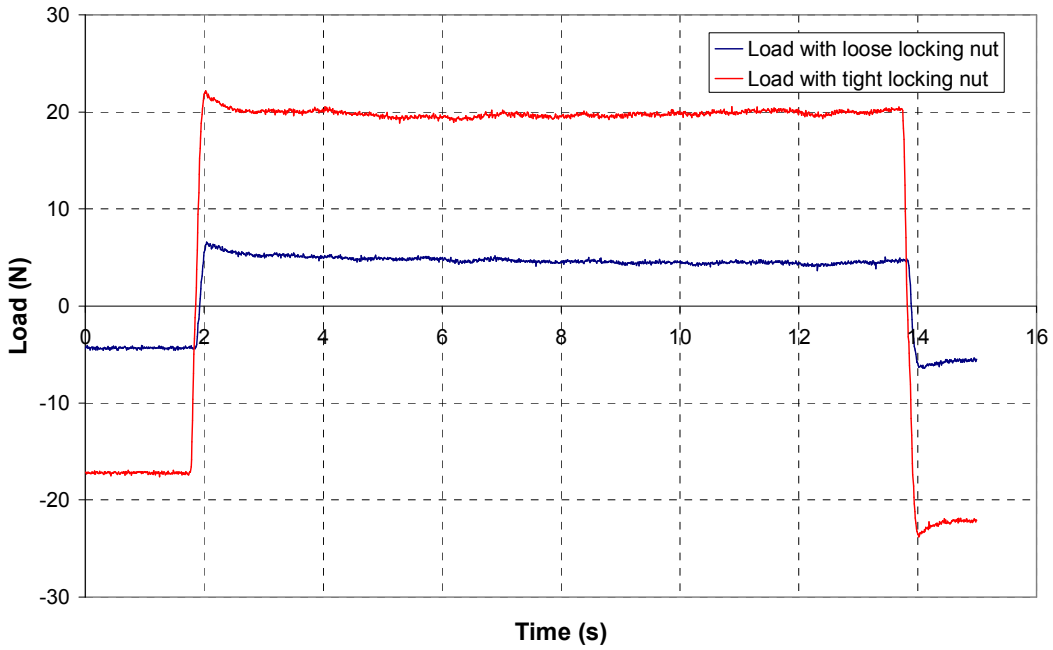

Figure 9-7 Load during one displacement cycle with the locking nut loose and tight

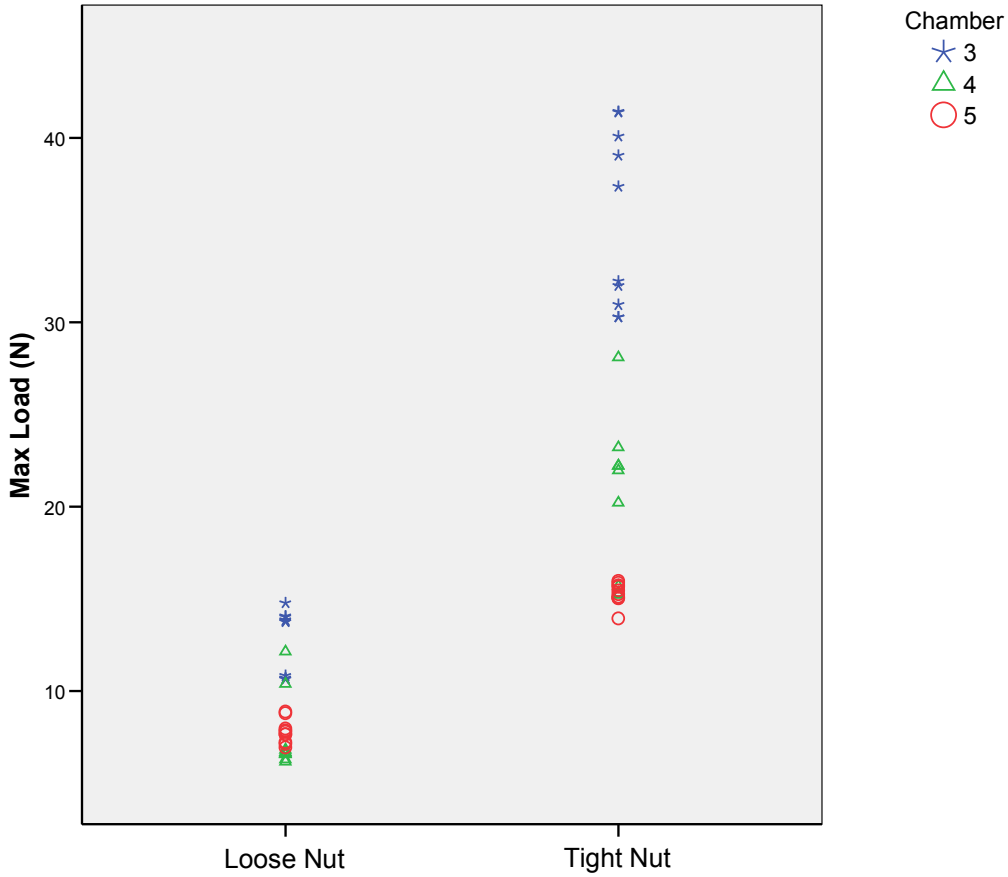

Figure 9-8 The effect of the locking nut tightness on the maximum friction load

The measured maximum frictional loads with the nut loosely secured ranged from 6.17N – 14.78N, whereas the frictional load ranged from 13.93N – 41.44N with the locking nut

fully tightened. The maximum load which was measured was due to the initial static friction between the components and then this reduced to the dynamic friction level. Tightening the locking nut increased the friction measured in each of the chambers and it also increased the spread of the recorded frictional values. For this reason, it was most appropriate to lightly secure the locking nut during biological experiments.

A number of improvements could be made to the biological chamber design to reduce the effect of misalignment of the chamber shaft. The stainless steel chamber insert could be replaced with a low friction polymer such as PTFE or nylon to reduce the coefficient of friction between the chamber shaft and the insert.

The friction is a consequence of over constraining the chamber shaft, with alignment defined at both the pin joint and through the insert. Removing one of these constraints would significantly reduce the friction created in the linear axis. This could be achieved by modifying the sealing method at the lower chamber shaft. A custom-made bellow-type seal could be designed to seal the shaft within a bore with sufficient clearance to prevent any contact between the chamber shaft and the chamber body or any insert required to restrain the seal.

Modification of the coupling between the chamber shaft and the load cell shaft could reduce the misalignment of the chamber shaft generated with the pin joint. It would be possible to connect the shafts using, for example a three-piece rigid shaft coupling.

The evaluation of friction within the biological chamber has contributed to the successful achievement of Objective 8.

10 FINAL BIOREACTOR DESIGN SPECIFICATION

A bioreactor was designed and manufactured to provide combined tensile and torsional stimulation to tissue engineered anterior cruciate ligaments. The design incorporated a fully sealed biological chamber to house the developing tissue. This comprised a main chamber body machined from polycarbonate with two clear polycarbonate windows on the front and back of the chamber. Two shafts passed into the chamber from the top and bottom and the tissue was supported at either end by these shafts. They were sealed with spring-loaded PTFE seals. Tensile loading was provided to the lower chamber shaft by a d.c. servo motor through a ballscrew and linear slide unit while torsional loading was provided to the upper chamber shaft via another d.c. servo motor.

Load and torque cells were included in the design to monitor the loading applied to the tissue and also provide closed loop feedback to the control system. A control program was developed to operate the bioreactor. This allows the load and torque cells to be zeroed and a preload to be applied to the tissue. The bioreactor is capable of operating in position and load control. The positional control loop was fully tuned to provide the optimal dynamic response. The load control loop was initially tuned to demonstrate that the bioreactor can operate in the load control mode. However, further tuning is required to achieve the required dynamic response. A variable loading profile can be applied to the tissue through a number of user defined parameters. The control system can capture load and positional data to allow real-time diagnostics of the tissue loading and ensure the user has sufficient data to make decisions on the progress of an experiment.

A suitable method of tissue clamping was developed to allow the load to be transmitted to the tissue. Also, a recirculating flow system was designed to ensure the tissue was provided with sufficient nutrients and waste products were removed from the chamber.

The bioreactor was fully characterised and the final design specification is summarised in Table 10-1. This meets the initial requirements detailed in Section 3.1.

Table 10-1 Bioreactor design specification

Mechanical loading - Cyclic Tension	
Loading method	d.c. servo motor (0.19 kW) Ballscrew & linear slide unit (2 carriages)
Transmission	Timing belt drive
Gearing ratio	2mm : 1 rev
Max stroke	38mm
Positional feedback/ monitoring	Incremental encoder (10000 counts/rev)
Linear positional error	1.1%
Max linear positional hysteresis	20.049 ± 1.175μm
Load feedback/ monitoring	500N S-beam load cell
Load cell drift	0.18 ± 0.13N (<20mins after start up)
Variation in load reading due to cross-talk	<0.1Nm : negligible >0.3Nm: 18.19 ± 0.28 N/Nm
Load error due to electrical noise	± 0.80N (0.016V)
Linear axis friction	Ranged from 6.17 – 14.78N with the lower locking nut loosely tightened
Mechanical loading – Cyclic Torsion	
Loading method	d.c. servo motor (0.36 kW)
Transmission	Timing belt drive
Gearing ratio	1 : 1
Positional feedback/ monitoring	Incremental encoder (10000 counts/rev)
Rotational positional error	0.5%
Max rotational positional hysteresis	0.206 ± 0.063°
Torque feedback/ monitoring	2Nm reaction torque cell
Torque cell drift	0.005 ± 0.001 Nm (<20mins after start up)

Table 10-1 cont. Bioreactor design specification

Variation in torque reading due to cross-talk	<150N : <0.01Nm variation ~300N : ± 0.02Nm variation
Torque error due to electrical noise	± $6.73e^{-3}$ Nm (0.033V)
Control program	
Zero load and torque cells	Can zero the reading from the load and torque cells
Preload	Can apply a preload to the tissue
Operating mode	Capable of operating in position or load control with closed loop feedback
Loading waveform	Sinusoidal, with the facility to program custom waveforms.
User defined loading parameters	Frequency Amplitude Pauses at the start and end of the stroke Ramp-up and ramp-down cycles Loading duration
Data capture	Can capture and save positional and load data from the bioreactor and display it in real-time.
User defined capture parameters	Number of cycles to capture Time interval between capture sessions
Biological Chamber	
Chamber volume	15 ml
Chamber dimensions	Can accommodate a sample size of 17 – 32mm long.
Tissue fixation	Tissue was clamped within the chamber using a grub screw and small plate to distribute the load. Could withstand tensile loads of 84.6 – 218.0N.
Other design requirements	The chamber was sealed to prevent contamination. The chamber was easy to assemble. The chamber was able to be removed from the bioreactor. The sides of the chamber were clear to permit optical analysis. The design allowed for the changing of medium and cleaning of components.
Medium Flow	
Flow type	Intermittent recirculating flow through the chamber
Flow rate	> 45ml per day
Other flow requirements	Was capable of supplying up to eight chambers with medium.

Table 10-1 cont. Bioreactor design specification

Cytotoxicity / Contamination	
Materials	All materials in the chamber and flow system were biocompatible. All materials in the chamber were able to be sterilised by autoclave. All materials in the flow system were able to be sterilised by autoclave or soaking in ethanol.
Other requirements	
Experimental Duration	Bioreactor was capable of operating for long-term with an intermittent loading cycle.
Physical requirements	Bioreactor was able to fit within a standard incubator (600mm high).

11 VALIDATION OF SYSTEM WITH BIOLOGICAL TISSUE

An experiment was carried out to validate the suitability of the bioreactor for use with biological tissue. The aim of this investigation was to demonstrate that the application of sinusoidal loading to tissue maintained within the bioreactor would not result in increased cell apoptosis (i.e. programmed cell death). Live porcine tendons were loaded into the bioreactor and stimulated on five of the eight days of culturing. After completion of the loading, histology was performed on the tissue to determine the variation in the cell numbers of the loaded tissue compared to the cell numbers of the original tissue (the baseline) and the unloaded control tissue.

11.1 Methods and materials

11.1.1 Preparation of tissue

Porcine superficial digital flexor tendons were harvested within 3 hours of slaughter. The tendons were harvested from both hind limbs and one of the fore limbs. The tendons were briefly washed in ethanol to sterilise them and then soaked in medium (Minimum Essential Medium Eagle (MEM) Alpha Modification with L-Glutamine and ribonucleosides, E15-862, PAA Laboratories Ltd, Yeovil, UK). Each tendon was sectioned into quarters by cutting longitudinally and transversely to provide 12 tendon samples. Each sample was then trimmed, if necessary, to ensure it fitted comfortably into the recess in the chamber shafts and returned to the medium. The samples measured approximately 40mm x 3mm x 3mm.

Four random tendon samples were selected and frozen to provide a baseline measurement for the tissue. Each sample was suspended in individual cylindrical aluminium foil moulds which were then filled with LAMB OCT embedding medium (Raymond A Lamb Limited, Eastbourne, UK). The moulds were submerged in liquid nitrogen to freeze the tissue and embedding medium and were stored frozen for subsequent histological investigation.

11.1.2 Tissue culture

The tissue was cultured in Minimum Essential Medium Eagle (MEM) Alpha Modification with L-Glutamine and ribonucleosides (E15-862, PAA Laboratories Ltd, Yeovil, UK) supplemented with 10% foetal bovine serum standard quality, EU approved (A15-101, PAA Laboratories Ltd, Yeovil, UK) and 2% antibiotic-antimycotic solution (P11-002, PAA Laboratories Ltd, Yeovil, UK). The medium was pumped through the bioreactor chambers for one minute, ten times a day, which resulted in more than three

volume changes per day per chamber. Each reservoir, which served two chambers, contained approximately 280ml of medium and this was changed after 5 days.

11.1.3 Bioreactor set-up

The bioreactor set-up previously described (Section 3) was used for this experiment with eight biological chambers which were to be kept in an incubator at 37°C and 5% CO_2. The peristaltic pumps had a maximum operating temperature of 30°C and could not be placed inside the incubator. There was a port on the side of the incubator (approximately 25mm diameter) through which the supply tubes from the reservoirs and the tubes returning from the pumps could be passed. In total, 12 tubes needed to pass through the port: four tubes from the reservoirs and eight inlet tubes to the chambers (Figure 11-1). It was important to seal this port effectively to prevent heat and CO_2 escaping. The chambers needed to be inserted into the bioreactor once a day so the sealing method had to allow each chamber pair to be removed from the incubator individually and had to be easy to reseal. A number of options were considered. The first idea was to seal the port with modelling clay, however, it may have been difficult to get a good seal around all the tubes. The second option was to use a rubber bung and drill 12 holes for the tubes and also cut it into quarters to allow the tubes for each chamber pair to be separated. This would seal well, however, when drilling and cutting rubber the drill or blade tends to move off course hence it would be very difficult to manufacture this stopper. Some tubing could be set in silicone rubber in a tapered mould with thin separators dividing the mould into quarters. Again this would be difficult to manufacture and ensure the tubing and dividers stayed in the appropriate position. The final option was to manufacture a tapered nylon stopper, drill 12 holes for the tubes and cut it into quarters. Although, the drill or blade could move off course when drilling or cutting nylon, it is a much more reliable material to work with than rubber. For this reason a nylon stopper was manufactured and a diagram is shown in Figure 11-2. 80mm lengths of hard tubing (3mm outside diameter) were inserted into the holes in the stopper and they were sealed to the stopper using silicone sealant. Each quarter was wrapped in PTFE tape to aid sealing. The nylon stopper fulfilled all the requirements and was used in the biological experiments.

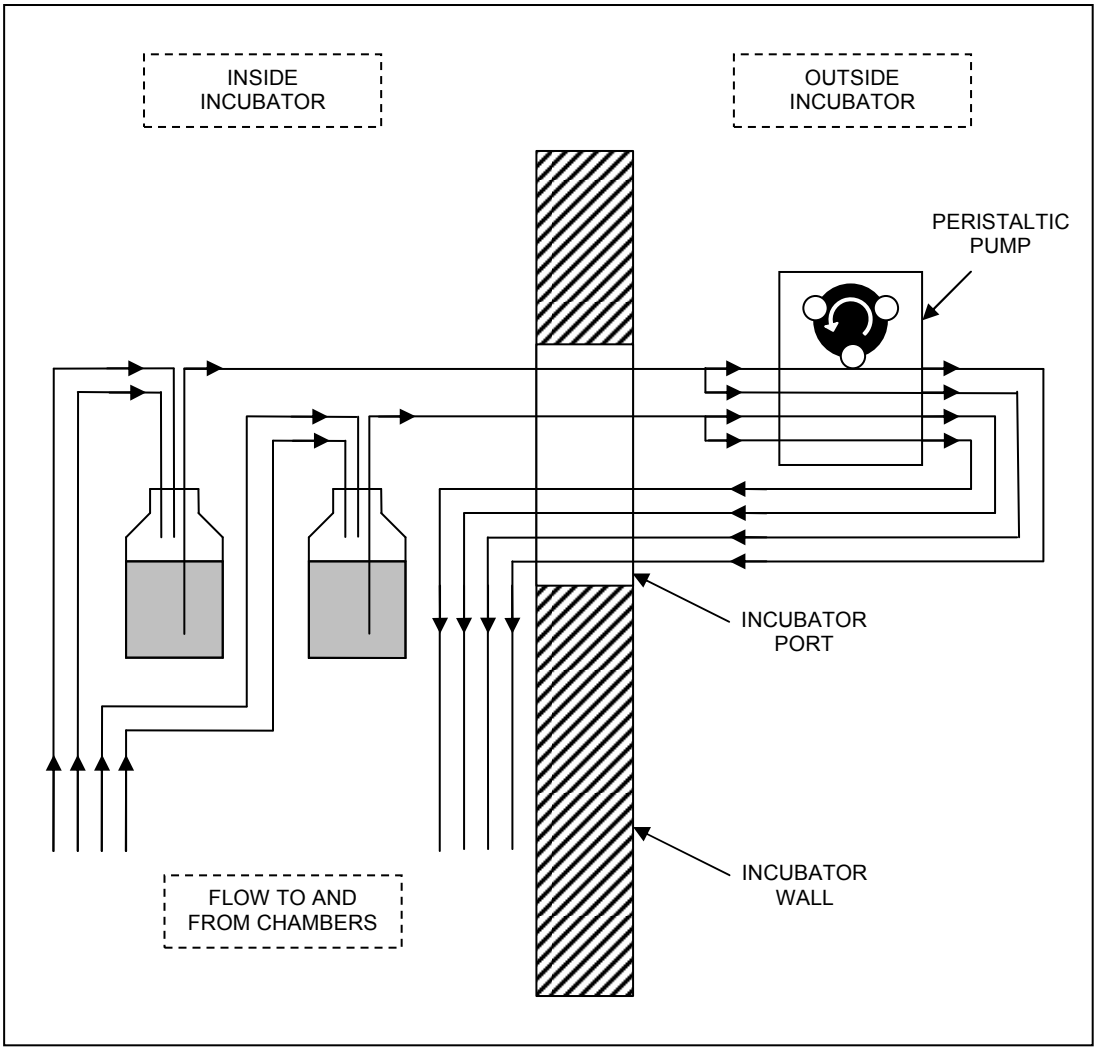

Figure 11-1 Flow paths through the incubator port (flow paths for one pump only is shown)

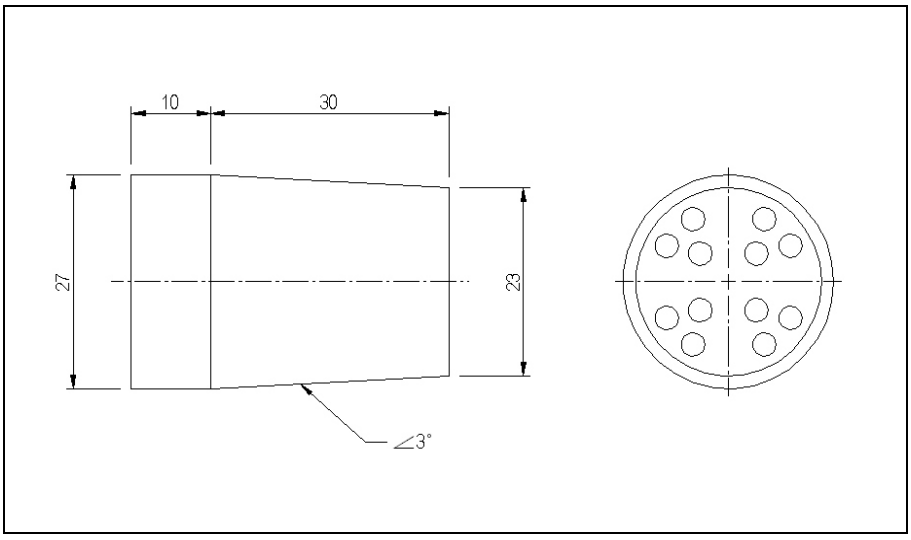

Figure 11-2 Nylon stopper for incubator port

Eight chambers were set-up with their associated recirculating flow systems (Figure 11-3A) (see Section 3.7 for details). Four chambers were mechanically loaded and four chambers acted as controls. The chambers were dismantled and all parts were autoclaved. The chambers were then reassembled in aseptic conditions. All the flow components were autoclaved with the exception of the 3-way valves and the incubator stopper which were soaked in ethanol for more than three hours. The flow systems were assembled and connected to the chambers. To reduce the possibility of leaks, all the tubing connections were wrapped in laboratory Parafilm. Each quarter of the incubator stopper was wrapped in PTFE thread seal tape to provide an air tight seal in the incubator port.

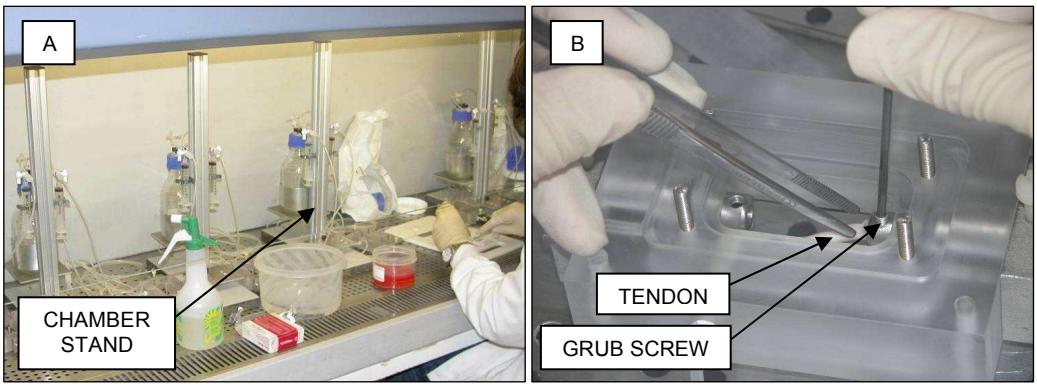

Figure 11-3 (A) The four chamber pairs set-up in the hood ready for the tissue to be inserted and (B) the tendon inserted into the upper chamber shaft and clamped in place by the grub screw

The tissue was loaded into the chambers with the front cover removed (Figure 11-3B). The position of the upper chamber shaft was set and the sample was inserted into the recess in the chamber shaft along with a polycarbonate plate to distribute the clamping load (see Section 3.6). Approximately 10mm of the tendon sample was inserted and a grub screw was tightened down on the polycarbonate plate to securely clamp the tendon. The other end of the tissue was inserted into the lower chamber shaft and clamped in the same way to leave approximately 20mm of the tendon free between the two chamber shafts. Each chamber was sealed and filled with medium using the syringe and 3-way valve as described previously in Section 3.7.

The chambers were mounted in their stands (Figure 11-4A) and the stands were placed in the incubator (Figure 11-4B). The tubing and stopper quarters were passed through the incubator port and the stopper was fitted to tightly seal the incubator port (Figure 11-5A). The tubing was loaded into the peristaltic pumps and clamped in place using the tubing

clamps described in Section 3.7 (Figure 11-5B). The 3-way valves were checked to ensure they were all in a position such that the syringe port was blocked off and flow was permitted from the chamber outlet through to the reservoir. The pumps were switched on and the return tubes in the reservoirs were observed to ensure medium was flowing through the systems. Also, each pump was checked to ensure the clamps were tightened sufficiently and the tubes were not being drawn into the pump head, and to ensure all four tubes were central on the tubing bed and not likely to slip off the edge. The electrical socket timers were enabled to control the pumps.

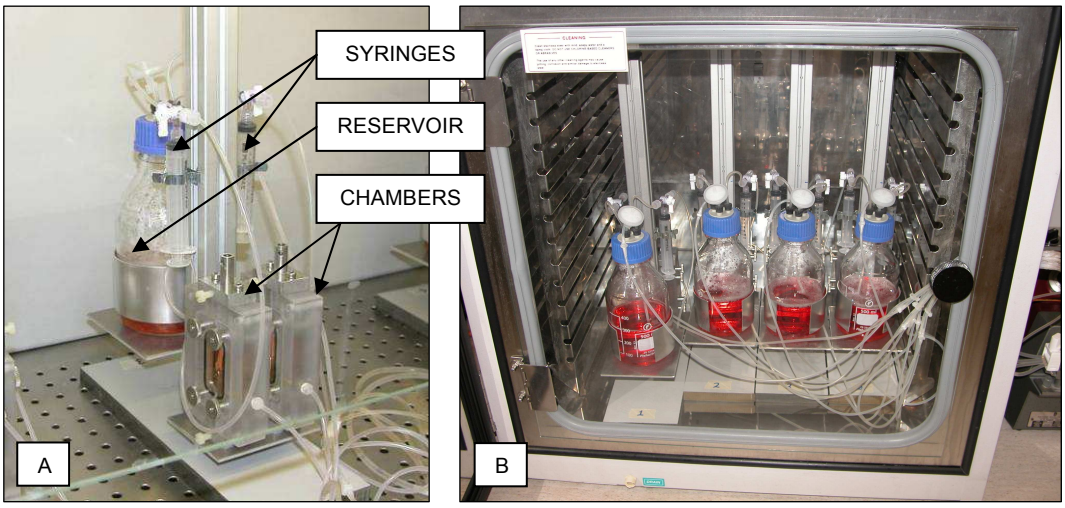

Figure 11-4 (A) The chambers mounted on the stand and filled with media and (B) the chambers positioned in the incubator

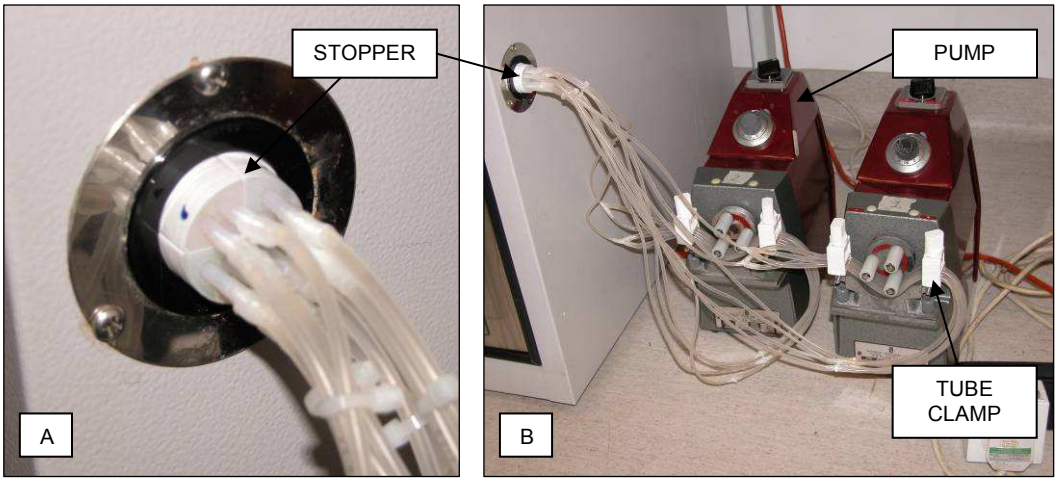

Figure 11-5 (A) The incubator stopper wrapped in PTFE tape and in place and (B) the tubing connected to the peristaltic pumps outside the incubator

11.1.4 Loading regime

The tissue was not subject to mechanical stimulation on day 1 to allow it to acclimatise to its new environment. On day 2 the tissue was preloaded. The peristaltic tubing was

removed from the pumps and the incubator stopper was removed from the port. The tubing and stopper were passed through the port into the incubator and the original bung was returned to the incubator port. The first stand containing chambers 1 and 2 was removed from the incubator and the 3-way valve for each chamber was turned to block the outlet port from the chambers and prevent any flow.

The output from the load and torque cells in the bioreactor were zeroed using the control program as previously described (Section 5.6). The linear axis was moved to the top of the linear slide and the minimum distance for chamber 1 was set (see Section 5.8 for details). The position of the linear axis was then moved to 40mm to allow chamber 1 to be inserted. Chamber 1 was loaded into the bioreactor and the four positional bolts were loosely inserted to hold the chamber in place. The nylon bolts which locked the chamber shafts in place were tightened to ensure the shafts did not move as they were being connected to the bioreactor. The upper chamber shaft was coupled to the upper rotational shaft via the pinned connection and the locking nut was tightened to ensure a secure coupling. The linear axis was gradually advanced towards the chamber and the load cell shaft was inserted into the lower chamber shaft as the operator ensured the two shafts were correctly aligned. Again, the shafts were coupled with the pinned connection and the locking nut was loosely tightened to prevent excessive friction during linear axis motion due to misalignment of the axis (see Section 9). The four positional bolts holding the chamber were tightened to hold the chamber in place (Figure 11-6).

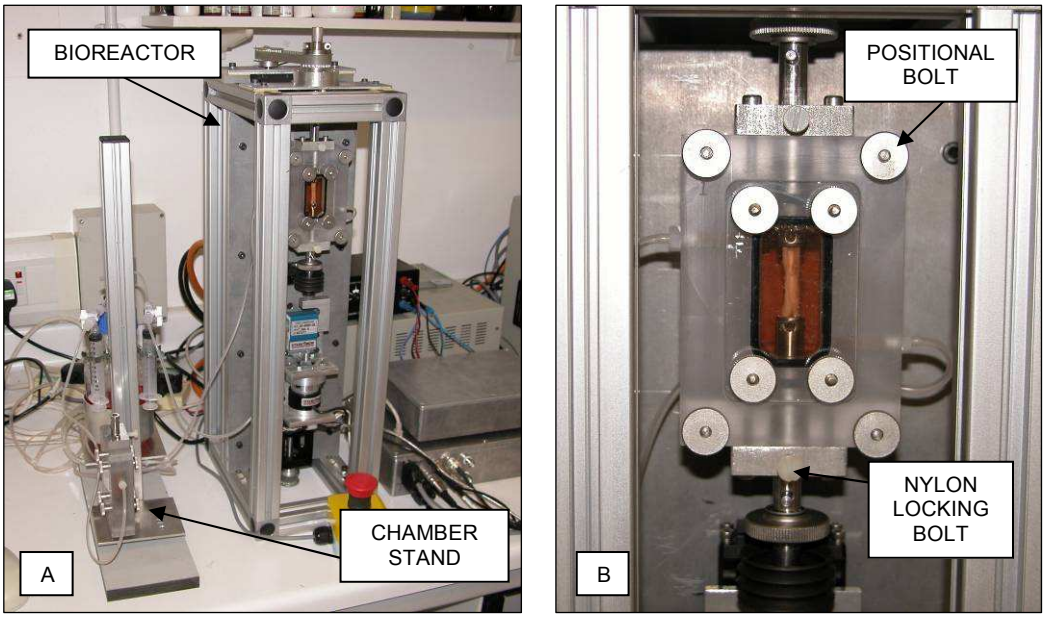

Figure 11-6 (A) A chamber loaded into the bioreactor and (B) a zoomed view of the chamber

The nylon bolt on the lower chamber shaft was released and, with the tissue slack, a 0.5mm displacement was performed at 0.5mm/s to measure the friction in the linear system. The load data was captured and an estimate for the dynamic friction was made. This process was repeated a number of times when necessary to try to ensure a consistent friction value was recorded. This value was inputted into the control program and a preload of 5N was applied to the tissue above this frictional load (see Section 5.8 for details of the algorithm used). The load data for the preloading of the tissue was captured and the final position of the linear axis was recorded as the initial length for the tissue.

The tissue was then mechanically loaded in positional control. A cyclic 5% strain was applied to the tissue at 1Hz with a sinusoidal waveform for ten minutes. The strain was ramped up linearly for the first 5 cycles of each loading session. The tendon used in this experiment would experience pure tensile loading *in vivo*, therefore, no rotational displacement was applied to the tissue. No stationary time was included in the mechanical loading regime, either at the extreme or home position, and the strain was not ramped down at the end of the loading.

The load, torque and position of the linear and rotational axes were captured at set intervals. 15 cycles were acquired in each capture session and there was an interval of 45 seconds between each capture session. Therefore, the first 15 cycles of every minute were acquired for the duration of the ten minute loading session.

When the mechanical stimulation was complete, the nylon bolts were tightened to lock the chamber shafts in place. The lower chamber shaft was decoupled and the linear axis was moved to a position of 40mm to allow the chamber to be removed. The upper shaft was decoupled and the chamber was unbolted from the bioreactor and removed.

The preload procedure detailed above was repeated for all the chambers. Chambers 3, 5 and 7 were mechanically loaded after the preload procedure in the same way as chamber 1. Chambers 2, 4, 6 and 8 were control chambers and the tissue was not cyclically loaded. In order to isolate the effect of only the mechanical loading in the experiment, the control chambers were inserted into the bioreactor and coupled to the upper rotational shaft as described for chamber 1. The lower chamber shafts were not coupled to the load cell shaft and the load cell shaft was positioned below the chamber shafts so that there was no contact with the lower chamber shafts. The linear axis was cycled from this

position with a stroke length of 5% of the initial length of the tissue. After this cyclic motion the control chambers were removed from the bioreactor.

Each stand held one loaded and one control chamber and they were inserted into the bioreactor in sequence and returned to the incubator when finished. The chambers were mechanically loaded 5 times in total on days 2, 3, 6, 7 and 8. When all the chambers had been loaded for that day the tubing was fed through the incubator port and inserted into the pumps. The port was sealed with the stopper, the 3-way valves were rotated to permit flow once again and the pumps were operated to ensure there were no problems with the flow system.

The chambers were loaded in the bioreactor at room temperature causing a reduction in the tissue temperature and this is discussed in Section 11.3.1.

A summary of the loading parameters used in this experiment is shown in Table 11-1.

Table 11-1 Summary of loading parameters

Loading Parameters	
No. of loading sessions	5
Loading duration (mins)	10
Strain (%)	5
Frequency (Hz)	1
Stationary time at extreme (s)	0
Stationary time at home (s)	0
No. of ramp-up cycles	5
No. of ramp-down cycles	0
Rotational angle (revs)	0
No. of cycles to capture	15
Capture interval (s)	45

On day 9 the tissue was removed from the chambers and stored frozen, using the technique detailed in section 11.1.1, for further histological examination.

11.1.5 Data analysis

Data analysis was performed using MatLab (R2007a, The Mathworks Inc, Natick, MA, USA). Algorithms were written to calculate the magnitude of the tensile load applied to the tissue and the stiffness of the tissue and plot the raw and analysed data.

A typical load cycle against time plot is shown in Figure 11-7. The steep increase in load at the start of the cycle was due to the change in linear velocity from negative to positive. As this happened the frictional force in the system also changed direction to cause a

discontinuity in the measured load. The point at the top of this step change in load was where loading of the tissue started and was an important point to identify. After this the load decreased to a minimum due to the difference between static and dynamic friction in the system. This minimum load point was the value of the dynamic friction which was superimposed on the load results. From this point the tissue was strained to a maximum load at the maximum displacement before the velocity changed from positive to negative and a step reduction in the load occurred. The difference between the maximum and minimum load points which were identified is equal to the load applied to the tissue.

Each capture sequence consisted of 15 loading cycles, therefore the data was split into each individual cycle to be analysed. This was done by identifying the minima in the positional data where the cycle start point (P_n) satisfies the following condition:

$$P_{n-1} \geq P_n < P_{n+1}, P_{n+2}$$

With the data separated into the individual cycles, the maximum load for each cycle was identified.

The point at the start of loading of the tissue was characterised by a change from a large positive gradient to a small positive or negative gradient. The gradient was evaluated over three points (L_{n+1} - L_{n-1}) to ensure the large step change was identified. Sampling was performed at a fixed timestep therefore it was not necessary to divide the load difference by the corresponding time difference. The level of friction in the system could change quite significantly due to the installation of the chamber into the bioreactor and the tightness of the pin joint locking nut, therefore, the magnitude of the load difference to identify the step change was set at greater than 40% of the maximum load. The point after this step change where the load difference changed to be less than 10% of the maximum load was identified as the point at the start of loading. If the point at the start of loading was identified as occurring after the maximum load point in the cycle then an error was recorded for that cycle. This may occur if the tissue was not loaded and the maximum was due to the static friction at the start of the cycle, or if the gradients in that cycle were too low to register the correct loading start point.

The minimum load was identified between the point at the start of loading and the maximum load point. The applied load was calculated as the difference between the maximum and minimum loads.

The stiffness of the tissue was evaluated by applying a linear fit to the data between the minimum and maximum load points on the load-displacement plot (Figure 11-8) using the least-squares method. The 20 data points leading up to the maximum load point were used for the curve fitting as the more linear portion occurred closer to the maximum point. If there were 10 to 20 points between the minimum and maximum load points then all the points were used to fit the curve. If there were less than 10 points between the minimum and maximum load points then no value for the stiffness was recorded as there were insufficient points to get a good estimate for stiffness. The coefficient of determination (r^2) was calculated to measure the correlation of the data and all measures of stiffness with a coefficient of determination less than 0.85 were rejected.

This method was also applied to the preload data to calculate an initial stiffness for the tissue; in this case the 40 points leading up to the maximum were used to fit the line.

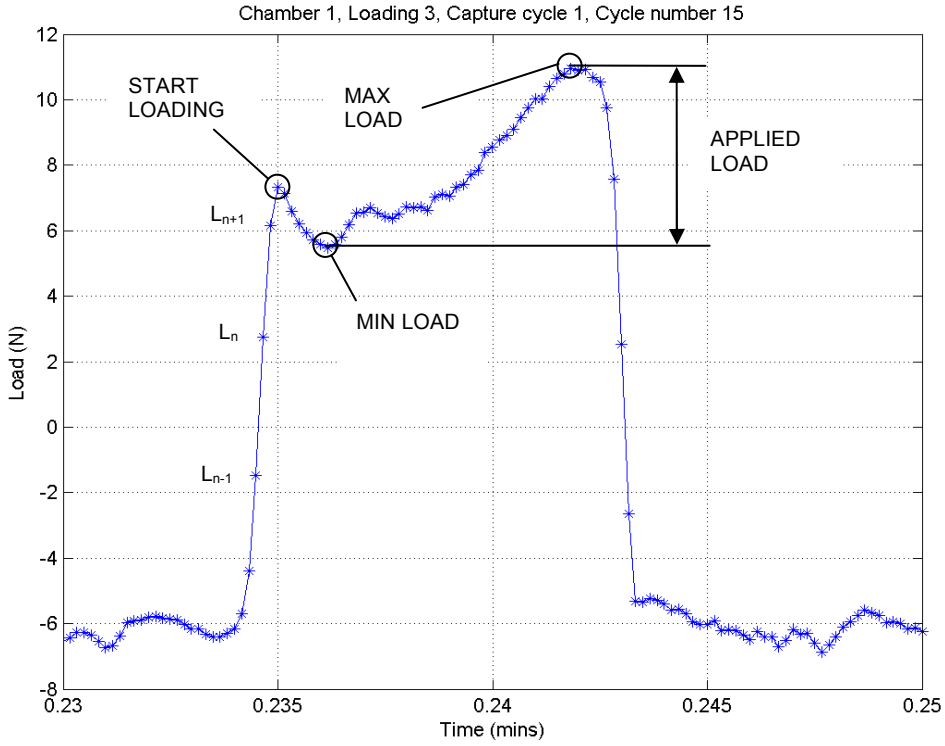

Figure 11-7 Typical loading curve for one cycle

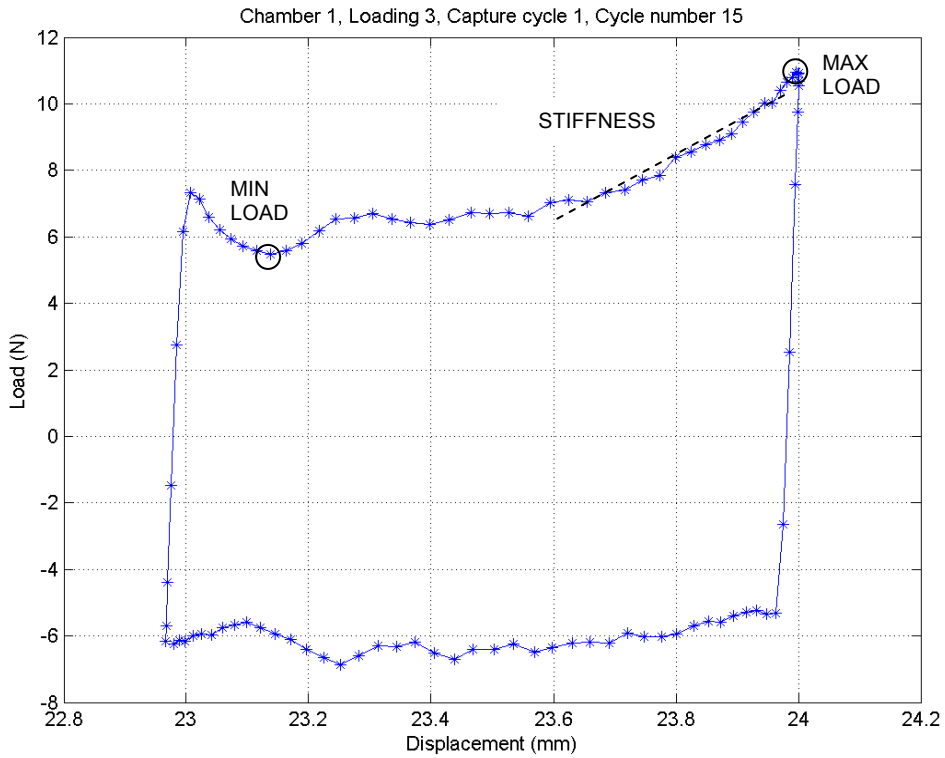

Figure 11-8 Typical load-displacement plot for one cycle

11.1.6 Histology

The histological study involved taking a number of sections along the length of each tendon. Each slice was transferred to a slide and was fixed with a hardest DAPI stain to label cell nuclei that were alive when the tissue was frozen. The sections were then viewed under a fluorescent microscope and the live cells were counted.

An embedded tendon was fixed to a cylindrical holder by setting the end in more OCT embedding medium and freezing it to the end of the holder in liquid nitrogen. The holder was loaded into the chuck of a Bright 5030 cryostat (Bright Instrument Company Ltd, Huntingdon, UK) (Figure 11-9). A diagram of the embedded tendon is shown in Figure 11-10. The ends of the tendon had been compressed when clamped within the bioreactor chamber. Therefore, the tissue at the ends was discarded as not suitable for the purpose of this study. Consecutive slices of the embedded tissue were taken until the cross section of the tendon appeared more rounded indicating the compressed end had been removed. At this location eight slices were taken and transferred to four Superfrost Plus Microscope Adhesion Slides (MNJ-700-010N, Fisher Scientific UK Ltd, Loughborough, UK), i.e. two slices per slide. Each slice was 7 – 8 μm in thickness. 3mm of tissue were then removed along the length of the tendon prior to obtaining a

further eight slices. This was repeated along the length of the tendon with eight slices taken every 3mm as indicated in Figure 11-10.

The slices were air dried and then sealed in parafilm before being stored frozen. All twelve tendon specimens were prepared in this way.

One slide from each slice location was defrosted and stained. The slides were washed by applying a few drops of tap water to dissolve the embedding medium. The excess water was removed and the slide was dried around the tissue sections. Two or three drops of Vectashield Hardset Mounting Medium with DAPI (H-1500, Vector Laboratories Ltd, Peterborough, UK) were applied to each slide and cover slips were placed over the sections. The slides were left to dry for approximately 15 minutes and then wrapped in aluminium foil and stored in a fridge.

Figure 11-9 A tendon mounted in the cryostat

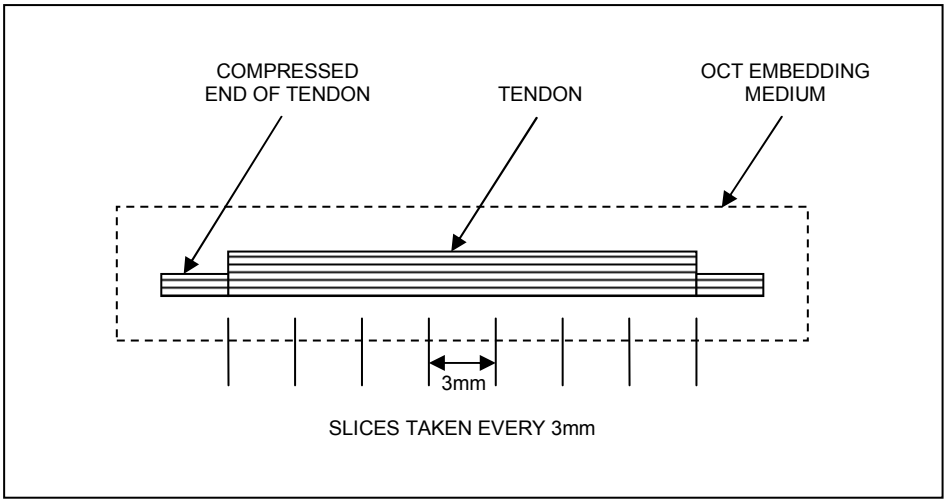

Figure 11-10 Diagram of embedded tendon

The sections from the centre of the tendons were of most interest because that was the area of tendon least affected by the clamps. The central portion of each section was the area with the poorest nutrient supply and therefore the influence of mechanical loading would be most apparent here. Also the core was least affected by fluid shear caused by the flow of media around the tendons. Consequently, the central portions of the central sections of the tendon samples were selected for imaging.

The sections were viewed under a fluorescent microscope (Leica BMRB, Leica Microsystems (UK) Ltd, Milton Keynes, UK) equipped with a Colorview XS digital camera (Soft Imaging System GmbH, Münster, Germany). The appropriate filter was used to view DAPI stain and the camera settings were adjusted to optimise the image contrast.

The section was viewed on 5X magnification to centralise the tissue section in the vision field. The power was then increased to 10X magnification and an image of the central portion of the section was captured using the acquisition software for the microscope (AnalySIS Imager v3.2, Soft Imaging System GmbH, Münster, Germany). Each slide from the centre of the tendons had two sections on it from that location. An image from each section was captured. In total this resulted in 24 images available for data analysis (two images from each tendon: four baseline, four loaded and four control), and a typical image is shown in Figure 11-11.

The image analysis software (Image Pro MC v6.0, Media Cybernetics, Inc., Bethesda, MD, USA) was used to evaluate the number of cells visible in the images. Each image was converted to a greyscale 8 image and the contrast was optimised automatically. The numbers of cells were estimated using the *clusters* function within the software. This estimated the number of cells in a large cluster based on the size of individual cells elsewhere in the image.

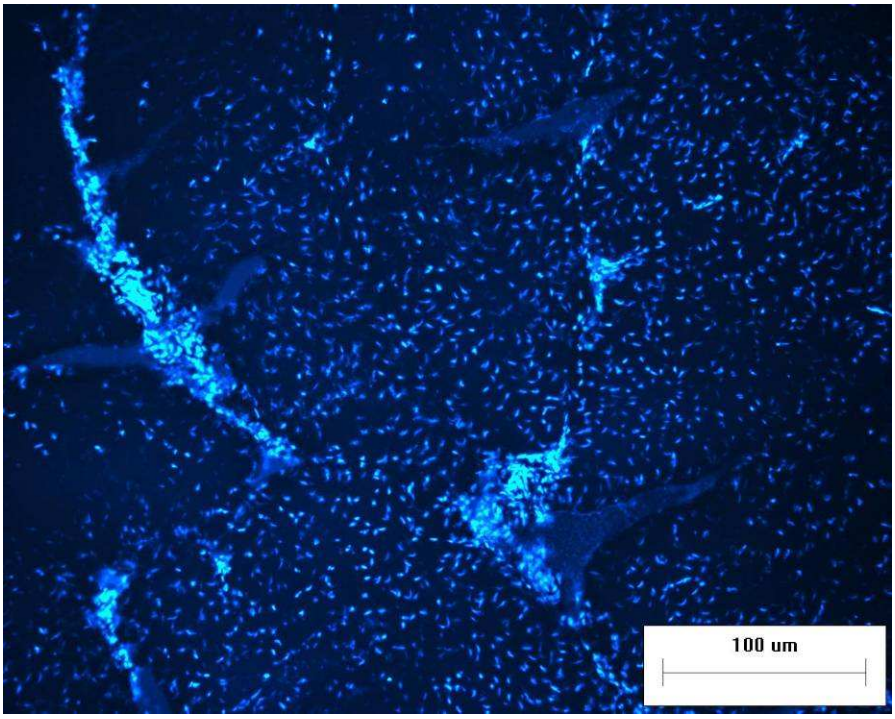

Figure 11-11 Typical image captured from the fluorescent microscope

11.2 Results

A selection of the results from this experiment is presented and discussed below. A more exhaustive set of results can be found in Appendix E.

11.2.1 Friction

The results of the measured friction in the linear axis for chamber 4 are shown in Figure 11-12. This showed a consistent level of dynamic friction and therefore two measurements were sufficient to make a good estimate of this parameter. The friction recorded for chamber 7 was less consistent (Figure 11-13) and it was necessary to take four measurements to determine an approximate level of dynamic friction which could be used in the preload routine.

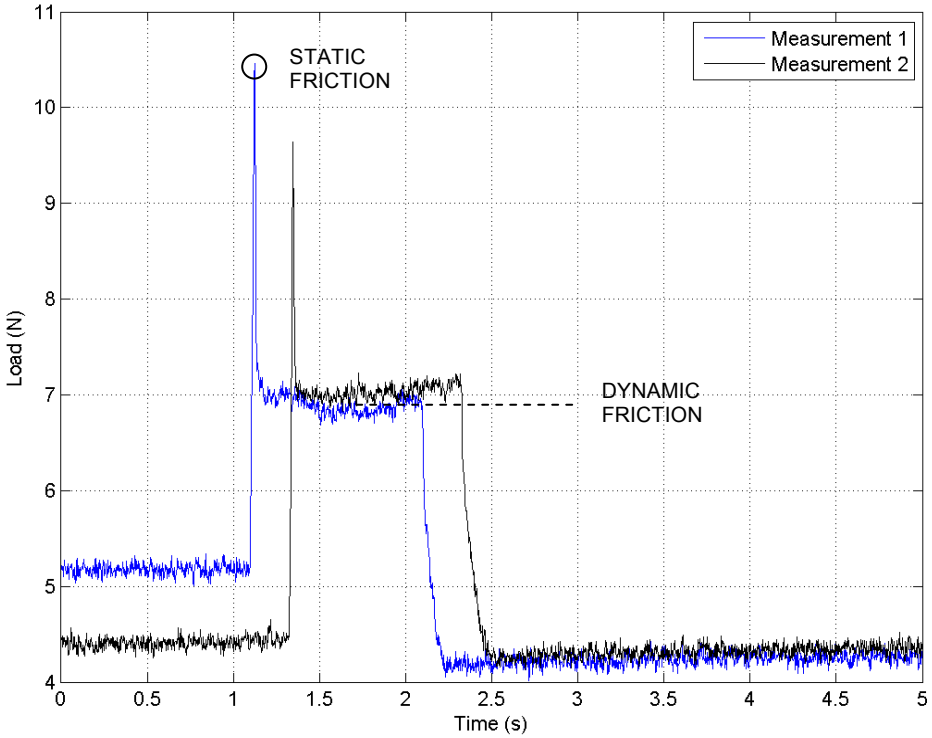

Figure 11-12 The friction measurements for chamber 4

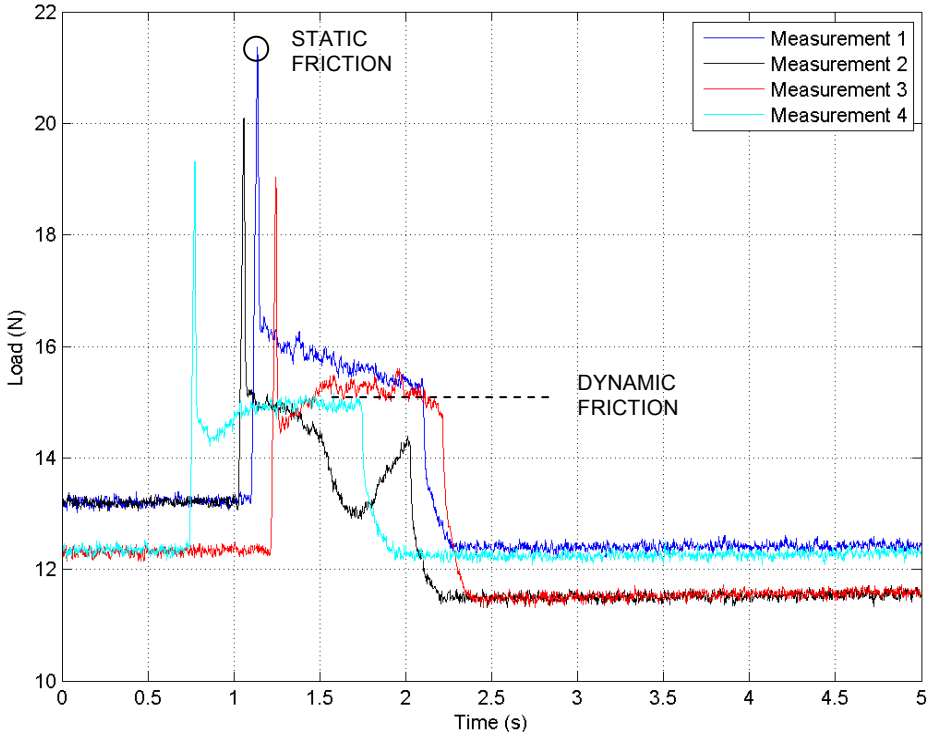

Figure 11-13 The friction measurements for chamber 7

11.2.2 Preload

The load data captured during the preload of the tissue in chambers 4 and 5 are shown in Figure 11-14 and Figure 11-15 respectively. Table 11-2 lists the initial stiffness and their corresponding r^2 values of the tissue from the preload data. The stiffness was not calculated for chambers 5, 6 and 7 because they showed substantial disruptions in the preload graph due to slippage within the tissue clamps.

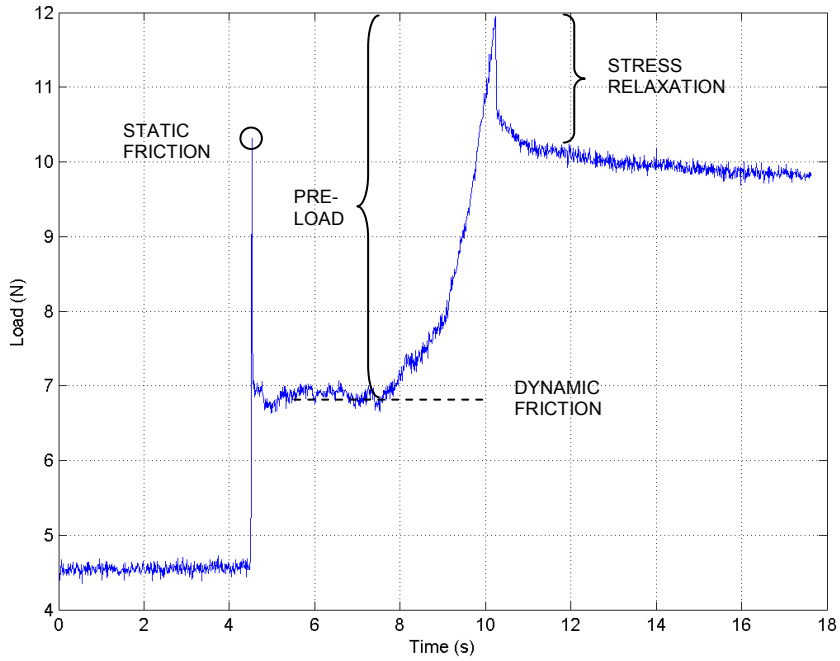

Figure 11-14 The preload of chamber 4

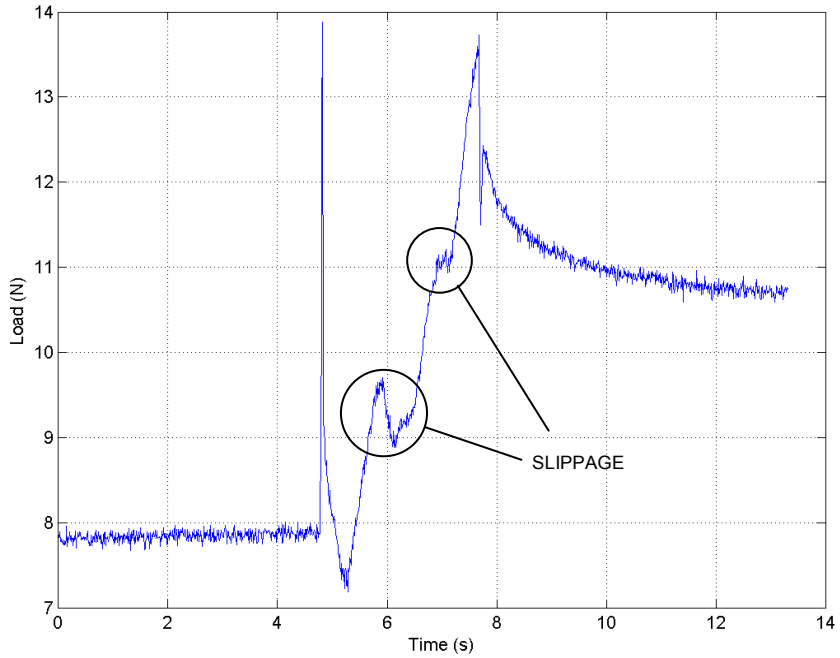

Figure 11-15 The preload of chamber 5

Table 11-2 Initial stiffness from the preload procedure for the chambers which did not show any slippage

Chamber	*Stiffness (N/mm)*	r^2
Chamber 1	11.32	0.99
Chamber 2	12.32	0.99
Chamber 3	6.31	0.95
Chamber 4	8.21	0.97
Chamber 8	11.41	0.98

11.2.3 Displacement

The displacement profile imposed on the tissue in chamber 3 during the first loading session is shown in Figure 11-16. 15 cycles were captured at the start of every minute of the loading session and Figure 11-16 shows the first five capture cycles during the loading session. It also shows the first five cycles ramping up to the full displacement amplitude.

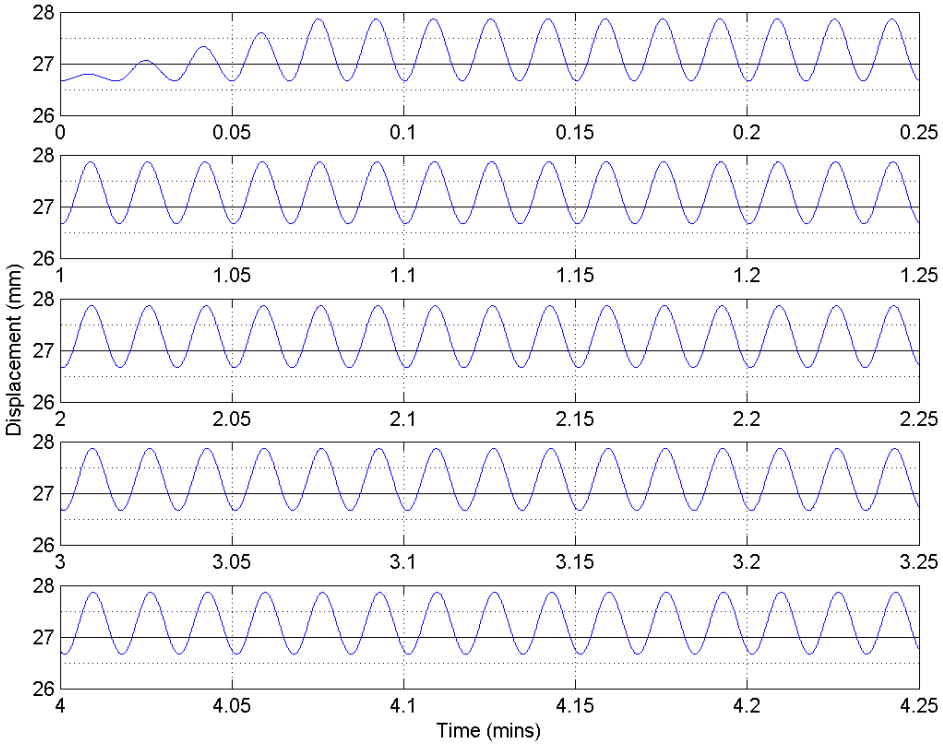

Figure 11-16 Displacement data of the first five capture cycles for the first loading session of chamber 3

11.2.4 Loading

Figure 11-17 and Figure 11-18 show the first five load capture cycles for the third loading sessions of chambers 1 and 7. The load profiles in Figure 11-17 follow the typical load profile previously discussed, however, Figure 11-18 shows a more square profile.

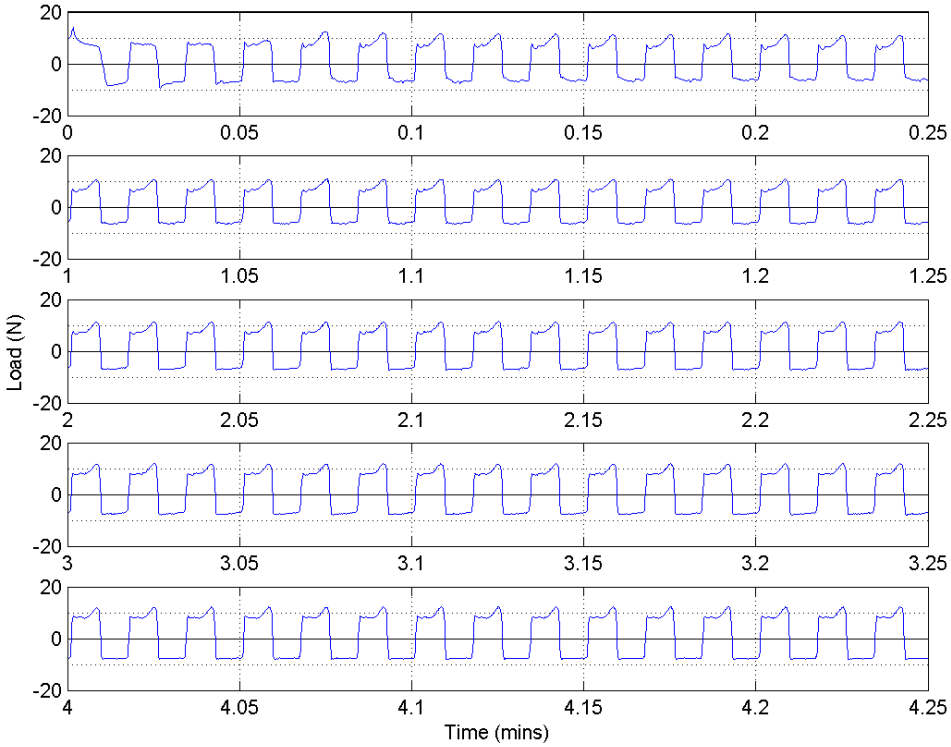

Figure 11-17 Load data of the first five capture cycles for the third loading session of chamber 1

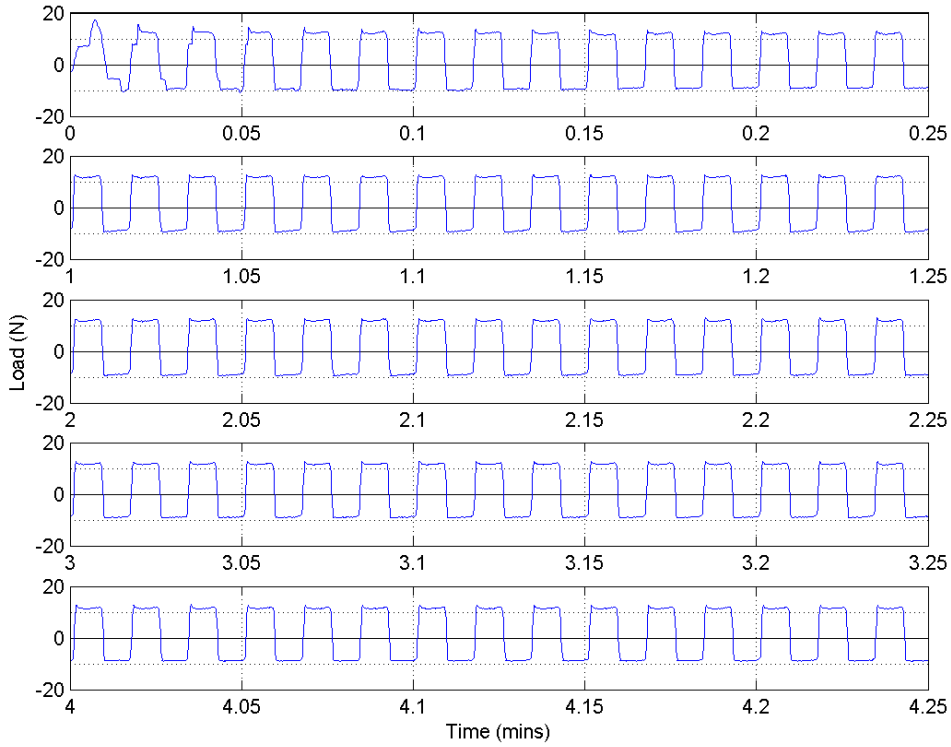

Figure 11-18 Load data of the first five capture cycles for the third loading session of chamber 7

11.2.5 Applied load

The applied load was calculated using the algorithm described previously. All valid results where the maximum load occurred after the loading start point (see Section 11.1.5) have been plotted and Figure 11-19 shows the loads applied to the tissue in chamber 3 during loading session 3.

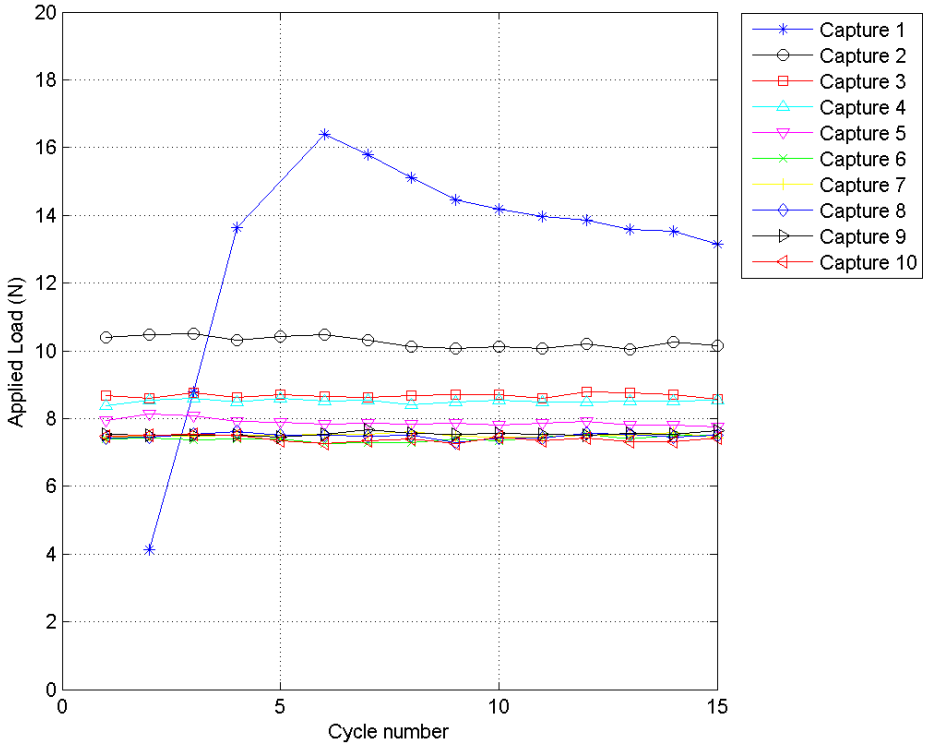

Figure 11-19 The load applied to the tissue during the first loading session of chamber 3

11.2.6 Load-Displacement

The load was plotted against displacement for all the captured data, and capture cycles six to ten of loading session three for chambers 1 and 7 are shown in Figure 11-20 and Figure 11-21 respectively.

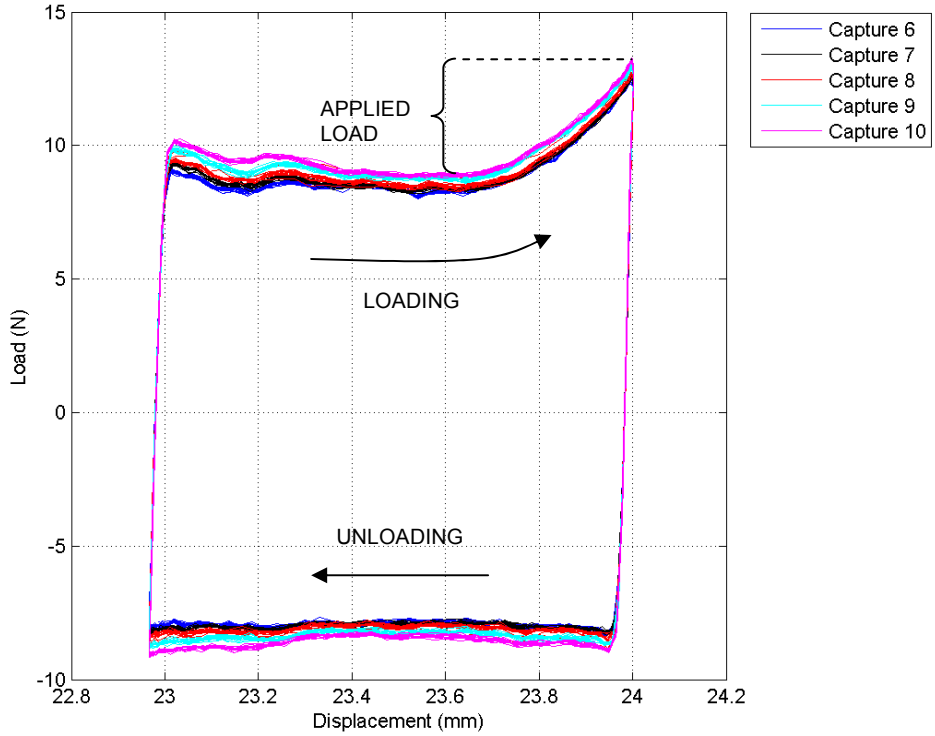

Figure 11-20 Load-displacement plot of the last five capture cycles for the third loading session of chamber 1

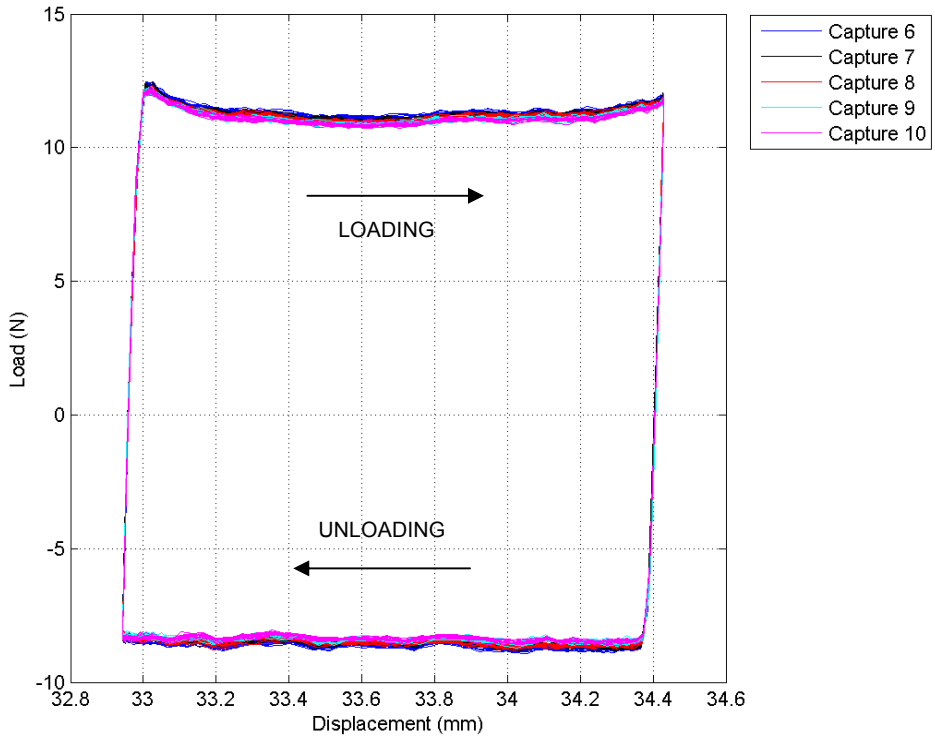

Figure 11-21 Load-displacement plot of the last five capture cycles for the third loading session of chamber 7

11.2.7 Stiffness

The tissue stiffness was calculated using the algorithm previously described. All valid stiffness values, where the linear fit was applied to 10 points or more and the coefficient of determination exceeded 0.85 (see Section 11.1.5), were calculated and the results for the tissue in chamber 3 during loading session two are shown in Figure 11-22.

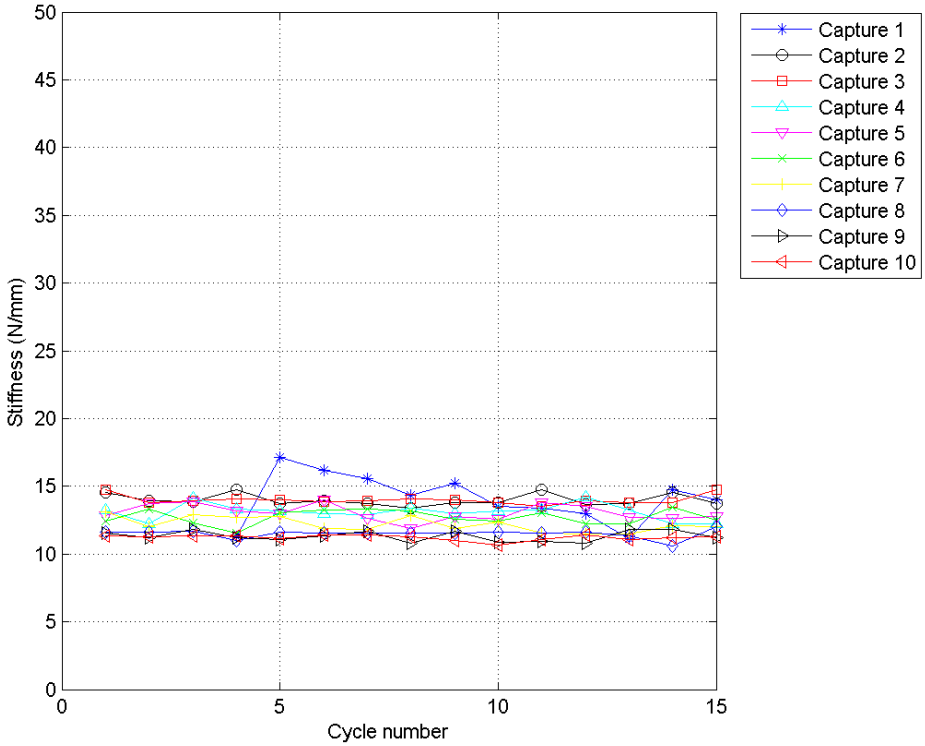

Figure 11-22 The tissue stiffness calculated during the second loading session of chamber 3

11.2.8 Histology

The numbers of cells in the central portion of the section from the mid-point of the tendon samples were counted and are shown in Figure 11-23. The cell numbers are categorised into the baseline representing the native tissue, the loaded and the control tissue and the results are summarised in Table 11-3.

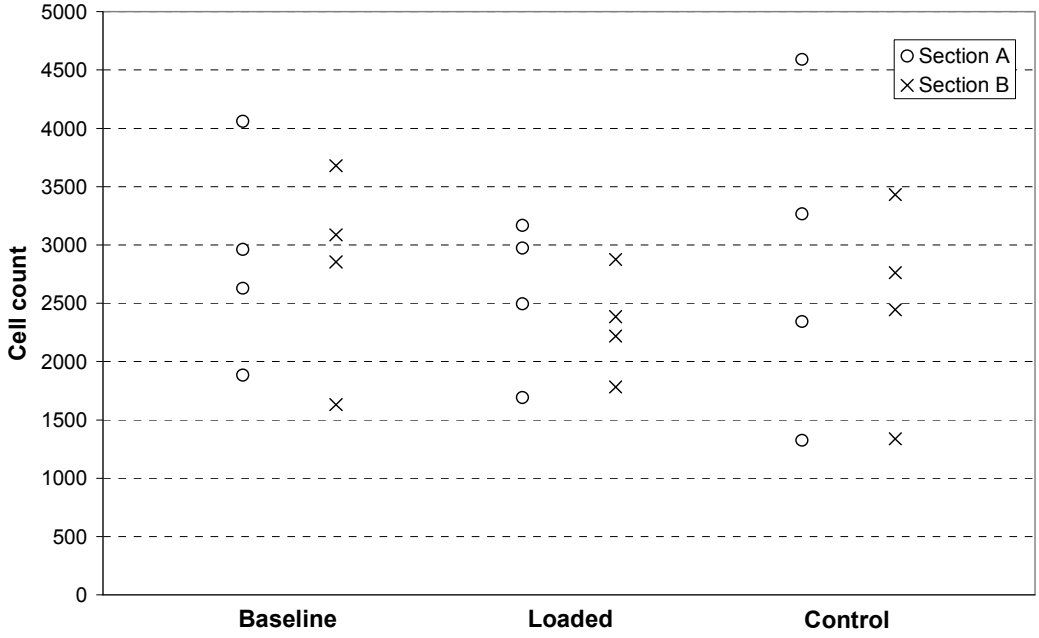

Figure 11-23 Cell counts from the central area of the sections taken from the mid-point of the baseline, loaded and control tissues. Sections A and B are separated by less than 100µm.

Table 11-3 Summary of cell count results

Tissue name	*Tissue type*	*Cell count*	
		Section A	*Section B*
Baseline 1	Baseline	1884	1631
Baseline 2	Baseline	2629	2854
Baseline 3	Baseline	4060	3679
Baseline 4	Baseline	2962	3086
Chamber 1	Loaded	2495	2876
Chamber 2	Control	3266	3432
Chamber 3	Loaded	3167	1782
Chamber 4	Control	1325	1338
Chamber 5	Loaded	1692	2218
Chamber 6	Control	4591	2762
Chamber 7	Loaded	2974	2385
Chamber 8	Control	2343	2444

The baseline cell count was evaluated as 2848 ± 818 (mean ± standard deviation), the loaded cell count was 2383 ± 718 (mean ± standard deviation) and the control cell count was 2687 ± 1093 (mean ± standard deviation).

11.3 Discussion

11.3.1 Experimental procedure

The tissue was clamped by compressing it between the inner wall of the chamber shaft and the polycarbonate insert using a grub screw against the polycarbonate insert. All

efforts were made to ensure the polycarbonate insert remained flat as it was clamped against the tendon, however, on some occasions this was not possible and the insert compressed against the tissue at an angle as is illustrated in Figure 11-24. This compromised the tissue clamping as not all the load from the grub screw was used to directly compress the tissue and the insert was not distributing the load effectively. Also, it allowed the tissue to bulge out and wrap around the insert. This meant that less tissue was clamped and also caused the tendon to curl up thus shortening the free length of the tendon. This shortening of the tendon as the tissue was clamped made it difficult to ensure a sufficient length of tendon was clamped by the polycarbonate insert.

Impingement of the insert on the inner wall of the chamber shaft could occur if the insert was slightly too wide or if the tendon samples were cut slightly too thin as is shown in Figure 11-25. This impingement would limit the compression of the tissue and impair the effectiveness of the tissue clamping.

Compromised clamping due to an angled insert, insufficient clamped length of tendon or impingement of the insert on the chamber shaft wall are individually or in combination likely to be the cause of the clamping failures seen in chambers 5, 6 and 7 in this experiment.

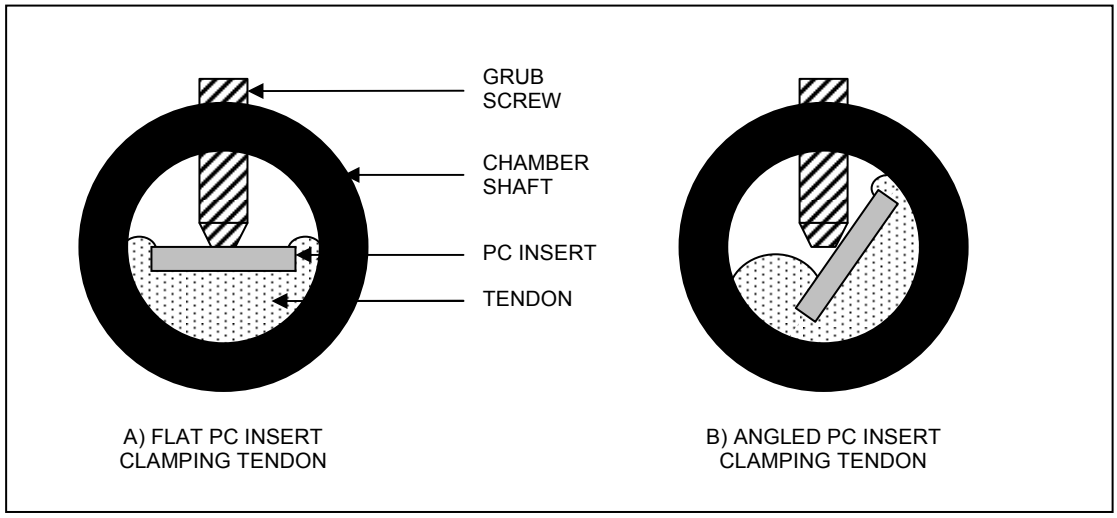

Figure 11-24 Cross-sectional view showing effect of insert orientation on clamping of tendon

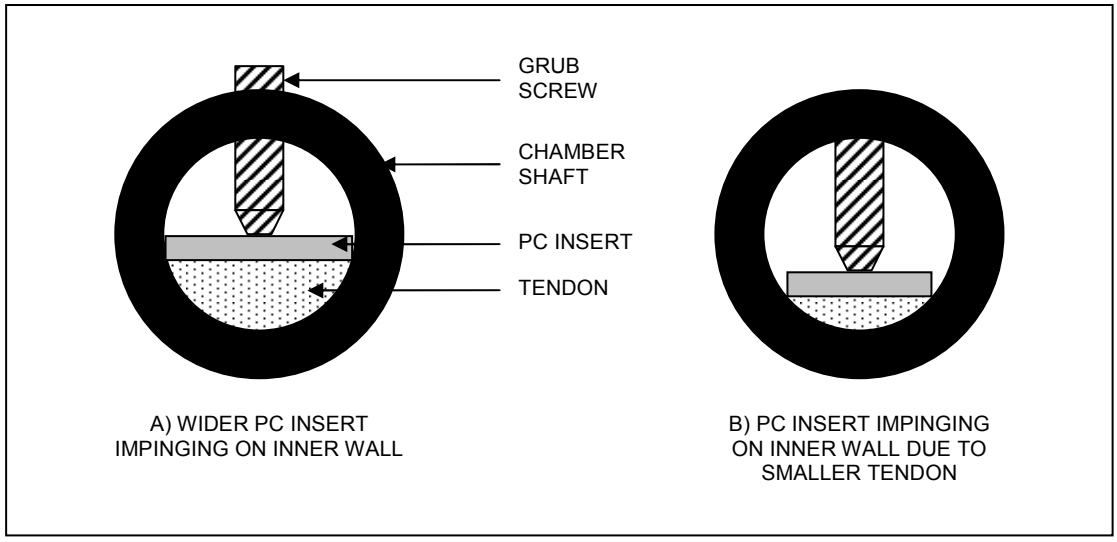

Figure 11-25 Cross-sectional view showing effect of insert impingement on clamping of tendon

The bioreactor was designed to fit within an incubator to allow long-term loading to be carried out at 37°C. For this experiment only short-term loading of 10 minutes per chamber per day was required. Constantly opening and closing the incubator door to load and remove the chambers from the bioreactor would have reduced the incubator temperature to close to room temperature, therefore, it was deemed appropriate for this experiment to run the bioreactor at room temperature on the laboratory bench. Each chamber pair was out of the incubator for approximately 30 minutes while each chamber was loaded. In that time the temperature of the chamber, media and tissue reduced (the chamber temperature after 30 minutes was approximately 28°C), however, this was considered acceptable for this experiment.

It was possible for an infection to develop in the media which would have had a serious detrimental effect on the development of the tissue and would have ruined any biological results from the experiment. Infection could be either fungal or bacterial and would be visible in the solution as small floating fibres (fungal) or turning the solution cloudy (bacterial) combined with a yellowing of the solution associated with a change in pH due to the increased metabolic activity of the infection. A number of steps were taken to reduce the risk of developing an infection. All but two of the components of the chamber and flow system were sterilised by autoclave. The materials used in the stopper and 3-way valves made them unsuitable for sterilisation by autoclave and therefore they were soaked in 70% ethanol for more than three hours. The chambers and flow systems were assembled under an environmental hood in aseptic conditions. Standard aseptic protocol was followed for the dissection and loading of the tissue, and filling of the

system with media, until the system was fully sealed. All tubing connections were wrapped in laboratory Parafilm to prevent any fluid leaks and ingress of infection. Finally, the media solution was supplemented with 2% antibiotic-antimycotic solution to prevent the spread of any bacterial or fungal infection which may have entered the system. At the end of the experiment there were no visible leaks from any of the chambers and none of the media solution showed sign of infection.

The recirculating flow system was set-up as previously described in Section 3.7. On occasions there was some variation between the flow rates to each chamber, however, the pumps were able to consistently provide a minimum flow rate to each of the chambers. Each reservoir supplied two chambers: one control chamber and one loaded chamber. Each reservoir cap had four ports: one for a pressure relief air filter, two for the return lines from each chamber to allow the flow through each chamber to be monitored, and one for the supply line to the chambers. This supply line was split with a 'Y' connector before the pump to allow medium to be individually pumped to each chamber. When the chambers were installed in the bioreactor, both 3-way valves were turned to prevent flow through the return lines from each chamber. This prevented media draining from the chambers when they were in the bioreactor as they were positioned above the reservoir and had a greater pressure head. As the lower shaft in the loaded chamber was moved into and out of the chamber the volume in the chamber changed and caused media to flow back up the supply line to the reservoir as the pump was no longer occluding the peristaltic tubing. However, due to the 'Y' connector, the control chamber also experienced a cycle fluid pressure. There was always a small amount of air in the return line from the chambers between the chamber and the valve and this was compressed by the pressure fluctuation to allow a small amount of cyclic fluid flow into the control chamber. The cyclic pressurisation and fluid flow in the control chamber may have provided some mechanical stimulation to the control tissue and therefore compromised the control. In future experiments the supply line of the control chamber should be clamped to prevent this cyclic pressurisation and flow.

The load cell has a resolution of ±0.80N due to interference from electrical noise as has been discussed in Section 4. Therefore, care must be taken when identifying trends or characteristics from the load data that they do not lie within this resolution and could therefore be an artefact of the electric signal.

11.3.2 Measure of linear axis friction

Coulomb friction occurred at the interfaces between the lower chamber shaft and the PTFE seal and between the lower chamber shaft and the stainless steel insert which retained the seal in place. The normal force between the surfaces was provided by the small misalignment of the linear axis due to machining tolerances. This misalignment was very sensitive to the tightness of the nut which secured the pin joint of the lower chamber shaft as discussed in Section 9. The coefficient of friction between the chamber shaft and stainless steel insert was reduced by lapping the two components together, however, the friction remained a significant load which could vary each time the chamber was installed into the bioreactor.

The friction had to be evaluated before the preload could be applied to the tissue. Figure 11-12 and Figure 11-13 show the load results for chambers 4 and 7 for a one second move at 0.5mm/s. The load cell was balanced before the experiment and the tissue remained slack, therefore, the increase in load was due to the friction in the system. Figure 11-12 shows that initially there was a large load spike when motion was initiated and this reduced to a constant friction level for the remainder of the motion, after which the load reduced further when the motion had finished. The value of static coefficient of friction, when there is no relative motion between the two surfaces, is generally larger than the value of the dynamic coefficient of friction, when there is relative motion between the two surfaces. The static coefficient of friction is responsible for the initial load spike visible at the onset of motion. The constant level of friction (the dynamic friction) which follows the spike is proportional to the dynamic coefficient of friction. Only the dynamic friction needed to be measured for the preload procedure as the static friction at the beginning of the motion is overcome as the move is initiated.

The dynamic friction loads measured for chamber 4 (Figure 11-12) were very consistent therefore only two measurements were necessary. The friction loads measured for chamber 7 were initially less consistent therefore four measurements were necessary to obtain a good estimate for the dynamic friction in the system. A number of factors could be responsible for this initial variation. This was the first movement of the lower chamber shaft since the tissue was installed into the chamber and it was filled with fluid. Some slight repositioning of the seal was possible as it bedded in as there was some axial clearance in the gap where the seal was located. Also, the first one or two moves would have allowed lubrication of the seal interface and this would have changed the dynamic

friction. Finally, there may have been slight movement of the chamber to change the axial misalignment, and this would in turn have affected the dynamic friction.

11.3.3 Preload of tissue

A small preload of 5N was applied to all the tissue samples to remove any slack and allow the initial length of the sample to be measured. The preload routine, described in Section 5.8, applied the 5N preload above the measured value of dynamic friction for that chamber and ignored the initial static friction spike. Figure 11-14 and Figure 11-15 show the acquired load data for the preload of chambers 4 and 5 respectively.

As motion is initiated the static and dynamic friction can be seen clearly in Figure 11-14. The bioreactor continued to load the tissue to provide the desired preload of 5N. The motion stopped when the preload was achieved and then the load reduced due to stress relaxation within the tissue. Stress relaxation is the reduction in load which occurs in viscoelastic materials, such as tendons, when the material is maintained under a constant strain. Figure 11-14 shows that there were no problems during the preload of the tissue in chamber 4.

However, the preload data for chamber 5 shown in Figure 11-15 shows significant disruptions to the loading curve which were most likely caused by slippage at the clamped ends of the tissue. The preload value was still achieved, however, this slippage indicated that the clamps may not have been holding the tissue securely and this may have led to problems during the loading of the tissue. This data was available to the operator in real-time which allowed a decision to be made as to what was the appropriate action if any. A number of options were available including opening the chamber and tightening the clamps, reinsert the tissue, inserting a different tissue sample or remove the chamber from the experiment altogether. For this experiment it was decided that no action would be taken if the tissue was loaded to the preload value. Chambers 5, 6 and 7 showed signs of slippage during the preload procedure.

After the experiment the initial stiffness of the tissue was calculated for chambers 1 – 4 and 8 as shown in Table 11-2. These stiffnesses may be useful for comparison with the stiffness calculated from the loading profile. However, caution must be exercised when using this data to describe the true initial stiffness of the tendon samples. On the preload graphs the samples do appear to have a tail region as the tendon stiffens followed by a linear region of constant stiffness consistent with that presented earlier in Section 1.2.2

as the typical loading curve for a ligament or tendon. However, the preload occurred at very low loads therefore the apparent linear region on the preload plot may in fact be a zoomed in view of part of the toe region visible when a tendon is loaded to failure.

11.3.4 Loading of the tissue

A sinusoidal strain of 5% of the initial length was imposed on the loaded tissue at a frequency of 1Hz. The strain amplitude was ramped up linearly in the first five cycles of each loading session as recommended by Butler *et al.* (2003) (see Section 1.9.3). This is clearly shown in Figure 11-16 which plots the displacement from the first 5 capture cycles during the first loading session of chamber 3. Figure 11-16 also demonstrates that there is excellent repeatability of the positional profile which is imposed on the tissue. Each loaded tissue was stimulated at 1Hz for 10 minutes per day on days 2, 3, 6, 7 and 8 which resulted in 600 loading cycles per day. If ligaments and tendons responded to mechanical stimulation in a similar way to bone then the work by Rubin and Lanyon (1984) would suggest that this number of loading cycles would be sufficient to stimulate the tissue (see Section 1.9.3).

The load profile for the third loading session of chamber 1 is shown in Figure 11-17. The first four load cycles of the first capture follow a slightly different profile because the strain level was being ramped up, however, the remaining cycles are quite consistent with the typical load profile shown in Figure 11-7. The step change associated with the change in direction of friction and the more gradual ramping up of the load consistent with tissue loading are both clearly visible from Figure 11-17. This is in contrast with the load profile from chamber 7 shown in Figure 11-18. Again, the frictional step change is apparent, however, no tensile loading of the tissue occurred. This is consistent with the preload data which suggested that there was slippage in the clamps which may inhibit the transfer of load to the tissue. Similar load profiles were available for chamber 5 and this demonstrates that the preload data is a good indicator of the effectiveness of the clamps and can highlight any problems at an early stage. As with the preload data, the load and displacement data was available to the operator in real-time which allowed the operator to constantly assess the progress and effectiveness of the experiment and make any decisions accordingly.

The load which was applied to the tissue was calculated using the algorithm described previously. It would be possible to incorporate the algorithm into the program used to capture the data if real-time applied load data was deemed necessary however, in this

experiment the applied load was calculated after the end of the experiment. The first few cycles of each loading session did not always produce valid results for the applied load and, if they did, the applied loads were often quite different to the loads evaluated during subsequent captures through the loading session. This was due to the initial ramping-up cycles producing load profiles which differed from the typical load profile used to develop the algorithm. Also, the load profiles for chambers 5 and 7 differed from the typical load profile as the tissue was not loaded. Therefore, often no valid load was calculated and those that were calculated were due to unexpected load profiles as opposed to load actually transferred to the tissue. However, the applied load plots for chambers 1 and 3 (see Figure 11-19) which did load the tissue, and therefore have a load profile similar to that shown in Figure 11-7, allow trends to be identified such as a gradual reduction in applied load over time due to stress relaxation or slippage of the clamps.

The load-displacement curves in Figure 11-20 and Figure 11-21 show a number of features of the loading of the tissue in chambers 1 and 7. They show the hysteresis in the loading system and confirm that this was due to friction as the step change in load occurred at the extreme positions when the linear axis changed the direction of motion. They also show the consistency of the loading cycles of the two chambers. The load that was applied to the tissue is clearly visible in Figure 11-20, whereas Figure 11-21 shows that the tissue in chamber 7 was not loaded. There was no reduction in the load associated with unloading of the tissue in chamber 1 (i.e. the unloading line in Figure 11-20 is straight) due to stress relaxation within the tissue. Also, no loading occurs in the initial 60% of displacement in the loading path of Figure 11-20. This is because the viscoelastic tissue has undergone stress relaxation since the preload was applied. In future experiments it may be appropriate to carry out some conditioning cycles after the initial preload to allow stress relaxation to reach a steady state. The preload procedure could then be repeated to ensure the tissue would be loaded throughout the cycle. This is in line with the procedure used by Banes *et al.* (1999) detailed in Section 1.9.3.

The load-displacement data allowed the stiffness of the tissue to be calculated. The 10 to 20 points leading up to the maximum were used to fit the line and only those with a coefficient of determination greater than 0.85 were recorded as valid stiffnesses. Again, no valid stiffness results were calculated for chambers 5 and 7 as the tissue was not loaded. However, Figure 11-22 demonstrates that consistent stiffnesses can be calculated for loaded tissue. Any trends over time can be identified and the stiffnesses can be compared with the initial stiffness of the samples identified either by previous

experiments or calculated from the preload data. For example, the calculated stiffnesses from the second loading session of chamber 3 (Figure 11-22) was approximately 10 – 15N/mm. The cross-sectional area of the tissue was approximately 3x3mm and, based on the ACL diameter and linear stiffness data in Table 1-1, this would equate to a stiffness in the linear region of the load elongation curve of approximately 43.3N/mm for the tissue. The lower measured stiffness indicates that the tissue was being loaded within the toe region of the loading profile.

The capture system is sufficiently versatile to allow the operator to identify the loading features of most interest. For example, if the operator is interested in identifying the general profiles and checking the repeatability of the position or load profile then the number of cycles in each capture can be increased, thus reducing the sampling frequency. However, if the operator requires more detail in each loading cycle to identify parameters such as tissue stiffness then the number of cycles in each capture can be reduced thus increasing the sampling frequency and providing more data points for the calculations.

11.3.5 Histology

The cell numbers in sections from the central portions of the tendon samples were evaluated to determine the effect of loading the tissue in the bioreactor. The cell numbers in the three groups (baseline, loaded and control) appear to be consistent with each other (Figure 11-23). This indicates that loading of the tissue within the bioreactor did not have a detrimental effect on the number of live cells within the core of the tissue. Evaluating the number of live cells in the tissue is a basic indicator of the success of the experiment and is an appropriate measure for this initial investigation. There are a number of other markers which could be used to highlight changes such as collagen content. These would be useful for future experiments but they were not deemed appropriate for this initial proof of principle. It has already been shown that mechanical loading is essential for successful functional tissue engineering therefore this investigation shows that the bioreactor can perform that function and does not have an additional detrimental effect.

During the sectioning process some of the sections mounted on the slides were slightly torn. Also, as the DAPI mount was applied it was possible for some air bubbles to get trapped between the sections and the cover slips. These two problems would affect the

number of cells counted by the image analysis software, therefore, when imaging the slides a central area with the least bubbles or tears was selected.

The tissue sections were 7 – 8μm in thickness and this compares to a typical fibroblast diameter of 10 – 15μm (Bhattarai *et al.* 2004). The cell nuclei measured by the image analysis software had a mean area of 3.57μm^2 for all the sections which would equate to a mean diameter of 2.13μm if the area was assumed to be circular. These nuclei were dispersed throughout the thickness of the tissue and due to the depth of field of the camera it was not possible to focus on all the cell nuclei. The cells that were less focussed had poor contrast and therefore were not counted by the software. However, this error was consistent for all tissue sections which were imaged and therefore would not affect the results as they were used to compare the cell numbers between the groups.

11.4 Conclusions

This investigation has demonstrated that the bioreactor can be used to stimulate biological tissue. Tissue samples can be clamped in the biological chambers and load can be transmitted to the tissue. Leaks and infection were prevented and the flow system successfully maintained an appropriate environment for the tissue to be cultured.

The dynamic friction was evaluated for the linear axis of each chamber and a preload was applied. The load data from the preload procedure was captured and allowed any problems, such as poor clamping, to be identified and appropriate action could be taken.

Cyclic loading was successfully provided by the bioreactor to the tissue and a repeatable positional profile was observed. The load profile enabled the load applied to the tissue to be measured and allowed any slippage identified in the preload stage to be confirmed. The stiffness of the tissue could be calculated from the load-displacement data and at low loads this tended to be within the toe region of a typical tendon loading curve.

The positional and load data was captured successfully and modification of the duration of each capture session would enable the user to identify the loading features of most interest by adjusting the sampling frequency.

The histological investigation demonstrated that the bioreactor was capable of keeping the tissue alive as the cell numbers were maintained. This analysis was appropriate for this initial investigation and more detailed analysis could be carried out for future experiments.

A number of limitations and potential improvements to the bioreactor and experimental procedure have been identified including clamping, the flow system and preconditioning of the tissue.

The bioreactor was successfully validated with biological tissue and Objective 9 was achieved.

12 DISCUSSION AND CONCLUSIONS

The anterior cruciate ligament (ACL) is a major ligament within the knee joint and it is vital to provide stability and maintain the physiological kinetics and kinematics of the joint. ACL injuries are common as a result of sporting and traffic accidents and current therapeutic options do not fully restore the joint kinetics and kinematics. Graft tissue can become scar-like with an associated change in mechanical properties and the tissue can creep altering graft tension and joint stability. As such, patients often suffer from increased joint laxity and joint pain following an ACL reconstruction and this can lead to secondary problems such as osteoarthritis.

Tissue engineering has the potential to provide functional tissue to repair or replace injured or diseased tissues in the patient. The ACL is a tissue which could benefit from such developments and thus improve the success of the reconstruction. However, the ACL is a complex structure made up of a highly orientated collagen hierarchy which experiences three dimensional loading *in vivo*. For an engineered tissue to be functional it is necessary for this orientated structure to be replicated.

Successful tissue engineering requires an appropriate cell source to populate the tissue, a scaffold to provide structural support to the cells, appropriate biochemicals to stimulate cell differentiation along the particular lineage and mechanical loading similar to that experienced *in vivo* to facilitate orientated cell matrix production. To achieve this the developing tissue should be housed within a bioreactor to culture the tissue and apply mechanical loading. Replication of the *in vivo* ACL strain pattern requires combined tensile and torsional loading. Current custom-made and commercially available bioreactors have not been able to fully replicate this motion with the necessary feedback and monitoring of mechanical parameters.

The aim of this project was to develop a bioreactor for the tissue engineering of an anterior cruciate ligament. A requirement specification was developed based on a thorough literature review. From this an iterative design process was conducted to meet the requirements. Appropriate mechanical loading systems were selected with monitoring of both position and load/torque. A sealed biological chamber was designed to support the tissue and permit the loading to be applied through two stainless steel chamber shafts. A flow system was included to circulate medium through the chamber to provide a constant supply of nutrients and prevent the build up of waste material. All

materials in contact with the tissue or medium were biocompatible and able to be sterilised.

A control program was developed to cyclically stimulate the tissue in either position or load control with closed loop feedback. The program also enabled a number of loading features to be imposed on the tissue including the application of a preload, ramping up of the cyclic amplitude and holding the tissue at the start or end of the stroke. Load and position data was captured in real-time for diagnostic purposes and analysis.

The bioreactor was fully validated and any errors associated with the position and load data were evaluated. Possible improvements were identified to reduce any errors.

A multi-chamber system was developed and an investigation was conducted as a proof of principle to validate the bioreactor for use with biological tissue. Porcine digital flexor tendons were harvested and cultured in the bioreactor to demonstrate that it could keep tissue alive. The tissue was successfully mounted in the chambers and preloaded. The preload data was used to identify any problems with the clamping of the tissue within the chambers. The tissue was cyclically loaded in position control and the data was analysed to identify loading characteristics such as the applied load and the stiffness of the tissue. The flow system operated successfully and no leaks or infection were identified. A histological study showed that there was no reduction in the cell numbers in the central portion of the tissue due to the bioreactor.

A number of bioreactors have been developed for the tissue engineering of anterior cruciate ligaments, however, there are limitations associated with all of them. The majority of bioreactors apply simple tensile loading to the tissue which does not replicate the complex three dimensional loading experienced by the ACL *in vivo*. Bose have recently developed a system capable of applying tension and torsion however rotation is limited to ± 15 degrees (Burke 2009) which is significantly less than the rotation of the ACL *in vivo*. The bioreactor developed by Altman *et al.* (2002b) did not include any load or torque measurement and therefore they could not be sure that the tissue was loaded as intended. For example, any stress relaxation or slippage in the clamps could not be identified. Also, their multi-station system provided the same displacement to all samples regardless of any variation in initial length, therefore, the strain applied to the samples could vary.

The bioreactor developed through this research addresses these limitations. The advantages associated with this device are that the sealing arrangement allows unlimited rotation of the tissue thus ensuring that the physiological rotation can be replicated. The load and torque cells included in the system allow for a greater understanding of the loading experienced by the tissue and enables loading features and potential problems to be identified. In addition, the sensors allow the system to operate in load control with closed loop feedback which is a facility not included in the other systems. Finally, the bioreactor is a single-station multi-chamber device which allows a consistent strain to be applied to all the samples regardless of variation in sample length.

The bioreactor which has been developed is a novel research tool which allows the effect of a number of parameters to be investigated in a 3-D loading environment. It can be used for the engineering of connective tissues such as ligaments and tendons and has the potential to be adapted for use with other musculoskeletal tissues such as bone. It could also be used for basic science to understand the processes involved in the growth and development of tissues.

13 FURTHER WORK

The validation and evaluation process carried out on the bioreactor identified a number of areas in which the bioreactor could be improved and further work which could be conducted.

The area of tissue fixation could be improved. Methods such as setting the tissue ends in epoxy resin or using cryoclamps were not appropriate as was discussed in Section 3.6. It may be possible to tightly bind the ends in suture to compress the tendon ends into a tight cylinder which would be easier to insert into the chamber shaft and easier to position the polycarbonate plate. Another option would be to develop flat clamps for the end of the chamber shafts which would allow for a more secure fixation.

For future experiments the sourcing of a multi-channel syringe or peristaltic pump would improve the fluid flow system and eliminate the variability introduced into the experiment using the existing method. It would also allow continuous flow to occur which would reduce the flow rate and fluid shear on the tissue. If the current system was to be used, the supply line to the control chamber should be clamped to prevent cyclic pressurisation of the media surrounding the control tissue when the loaded tissue was being stimulated.

The biological chamber design could be modified to reduce the effect of misalignment of the lower chamber shaft. The stainless steel chamber insert could be replaced with a low friction polymer such as PTFE or nylon to reduce the coefficient of friction between the chamber shaft and the insert.

The additional constraint on the lower chamber shaft from the chamber could be removed and therefore allow a limited amount of misalignment without increasing the friction in the system. This could be achieved by modifying the sealing method at the lower chamber shaft. A custom-made bellow-type seal could be designed to seal the shaft within a bore with sufficient clearance to prevent any contact between the chamber shaft and the chamber body or any insert required to restrain the seal.

Modification of the coupling between the chamber shaft and the load cell shaft could reduce the misalignment of the chamber shaft generated with the pin joint. It would be possible to connect the shafts using, for example a three-piece rigid shaft coupling.

Finally, cyclic pressurisation could be included in the bioreactor to simulate the pressurisation of the synovial fluid within the knee capsule. This would allow the effect of cyclic pressurisation on mass transfer and mechanical stimulation to be investigated.

14 REFERENCES

Ageberg, E., Roos, H. P., Silbernagel, K. G., Thomee, R., & Roos, E. M., 2009. Knee extension and flexion muscle power after anterior cruciate ligament reconstruction with patellar tendon graft or hamstring tendons graft: a cross-sectional comparison 3 years post surgery. *Knee Surgery Sports Traumatology Arthroscopy*, 17(2), pp. 162-169.

Altman, G. H., Horan, R. L., Lu, H. H., Moreau, J., Martin, I., Richmond, J. C., & Kaplan, D. L., 2002a. Silk matrix for tissue engineered anterior cruciate ligaments. *Biomaterials*, 23(20), pp. 4131-4141.

Altman, G. H., Horan, R. L., Martin, I., Farhadi, J., Stark, P. R. H., Volloch, V., Richmond, J. C., Vunjak-Novakovic, G., & Kaplan, D. L., 2001. Cell differentiation by mechanical stress. *Faseb Journal*, 15(14).

Altman, G. H., Lu, H. H., Horan, R. L., Calabro, T., Ryder, D., Kaplan, D. L., Stark, P., Martin, I., Richmond, J. C., & Vunjak-Novakovic, G., 2002b. Advanced bioreactor with controlled application of multi-dimensional strain for tissue engineering. *Journal of Biomechanical Engineering-Transactions of the ASME*, 124(6), pp. 742-749.

An, K. N., 2003. In vivo force and strain of tendon, ligament, and capsule. In: F. Guilak et al., eds. *Functional tissue engineering*, 1st edn, New York: Springer-Verlag, pp. 96-105.

Bancroft, G. N., Sikavitsas, V. I., & Mikos, A. G., 2003. Design of a flow perfusion bioreactor system for bone tissue-engineering applications. *Tissue Engineering*, 9(3), pp. 549-554.

Banes, A. J., Wall, M., Garvin, J., & Archambault, J., 2003. Cytomechanics: signalling to mechanical load in connective tissue cells and its role in tissue engineering. In: F. Guilak et al., eds. *Functional tissue engineering*, 1st edn, New York: Springer-Verlag, pp. 318-334.

Banes, A. J., Weinhold, P., Yang, X., Tsuzaki, M., Bynum, D., Bottlang, M., & Brown, T., 1999. Gap junctions regulate responses of tendon cells ex vivo to mechanical loading. *Clinical Orthopaedics and Related Research*(367), p. S356-S370.

Bell, E., 2000. Tissue engineering in perspective. In: R. P. Lanza, R. Langer, & J. Vacanti, eds. *Principles of tissue engineering*, 2nd edn, San Diego: Academic Press, p. xxxv-xli.

Beynnon, B., Howe, J. G., Pope, M. H., Johnson, R. J., & Fleming, B. C., 1992. The Measurement of Anterior Cruciate Ligament Strain In vivo. *International Orthopaedics*, 16(1), pp. 1-12.

Bhattarai, S. R., Bhattarai, N., Yi, H. K., Hwang, P. H., Cha, D. I., & Kim, H. Y., 2004. Novel biodegradable electrospun membrane: scaffold for tissue engineering. *Biomaterials*, 25(13), pp. 2595-2602.

Botchwey, E. A., Dupree, M. A., Pollack, S. R., Levine, E. M., & Laurencin, C. T., 2003. Tissue engineered bone: Measurement of nutrient transport in three-dimensional matrices. *Journal of Biomedical Materials Research Part A*, 67A(1), pp. 357-367.

Bruder, S. P. & Caplan, A. I., 2000. Bone regeneration through cellular engineering. In: R. P. Lanza, R. Langer, & J. Vacanti, eds. *Principles of tissue engineering*, 2nd edn, San Diego: Academic Press, pp. 683-696.

Burke, D, (Darren_Burke@bose.com), 8 Apr. 2009. *Tension/torsion bioreactor.* Email to Mitchell, M. S. (M.S.Mitchell@bath.ac.uk).

Bursac, N., Papadaki, M., Cohen, R. J., Schoen, F. J., Eisenberg, S. R., Carrier, R., Vunjak-Novakovic, G., & Freed, L. E., 1999. Cardiac muscle tissue engineering: toward an in vitro model for electrophysiological studies. *American Journal of Physiology-Heart and Circulatory Physiology*, 277(2), p. H433-H444.

Butler, D. L., Dressler, M., & Awad, H., 2003. Functional tissue engineering: assessment of function in tendon and ligament repair. In: F. Guilak et al., eds. *Functional tissue engineering*, 1st edn, New York: Springer-Verlag, pp. 213-226.

Caplan, A. I., 2005. Mesenchymal stem cells: Cell-based reconstructive therapy in orthopedics. *Tissue Engineering*, 11(7-8), pp. 1198-1211.

Chen, H. C., Lee, H. P., Sung, M. L., Liao, C. J., & Hu, Y. C., 2004. A novel rotating-shaft bioreactor for two-phase cultivation of tissue-engineered cartilage. *Biotechnology Progress*, 20(6), pp. 1802-1809.

Chen, R., Curran, S. J., Curran, J. M., & Hunt, J. A., 2006. The use of poly(L-lactide) and RGD modified microspheres as cell carriers in a flow intermittency bioreactor for tissue engineering cartilage. *Biomaterials*, 27(25), pp. 4453-4460.

Clark, J. M. & Sidles, J. A., 1990. The Interrelation of Fiber-Bundles in the Anterior Cruciate Ligament. *Journal of Orthopaedic Research*, 8(2), pp. 180-188.

Cooper, J. A., Jr., Bailey, L. O., Carter, J. N., Castiglioni, C. E., Kofron, M. D., Ko, F. K., & Laurencin, C. T., 2006. Evaluation of the anterior cruciate ligament, medial collateral ligament, achilles tendon and patellar tendon as cell sources for tissue-engineered ligament. *Biomaterials*, 27(13), pp. 2747-2754.

Cooper, J. A., Lu, H. H., Ko, F. K., Freeman, J. W., & Laurencin, C. T., 2005. Fiber-based tissue-engineered scaffold for ligament replacement: design considerations and in vitro evaluation. *Biomaterials*, 26(13), pp. 1523-1532.

Cowin, S. C., 2003. How does nature build a tissue? In: F. Guilak et al., eds. *Functional tissue engineering*, 1st edn, New York: Springer-Verlag, pp. 3-16.

Curran, S. J. & Black, R. A., 2005. Oxygen transport and cell viability in an annular flow bioreactor: Comparison of Laminar couette and Taylor-Vortex flow regimes. *Biotechnology and Bioengineering*, 89(7), pp. 766-774.

Cushner, F. D., La Rosa, D. F., Vigorita, V. J., Scuderi, G. R., Scott, W. N., & Insall, J. N., 2003. A quantitative histologic comparison: ACL degeneration in the osteoarthritic knee. *Journal of Arthroplasty*, 18(6), pp. 687-692.

Danylchuk, K. D., Finlay, J. B., & Krcek, J. P., 1978. Microstructural Organization of Human and Bovine Cruciate Ligaments. *Clinical Orthopaedics and Related Research*(131), pp. 294-298.

Danzig, L. A., Hargens, A. R., Gershuni, D. H., Skyhar, M. J., Sfakianos, P. N., & Akeson, W. H., 1987. Increased transsynovial transport with continuous passive motion. *Journal of Orthopaedic Research*, 5(3), pp. 409-413.

Department of Health. Hospital episode statistics - Primary diagnosis: 3 character 2007-08. http://www.hesonline.nhs.uk . 2009. London, Department of Health.
Ref Type: Electronic Citation

Donahue, T. L. H., Howell, S. M., Hull, M. L., & Gregersen, C., 2002. A biomechanical evaluation of anterior and posterior tibialis tendons as suitable single-loop anterior cruciate ligament grafts. *Arthroscopy-the Journal of Arthroscopic and Related Surgery*, 18(6), pp. 589-597.

Dye, S. F. & Cannon, W. D., 1988. Anatomy and Biomechanics of the Anterior Cruciate Ligament. *Clinics in Sports Medicine*, 7(4), pp. 715-725.

Enderle, J., Blanchard, S., & Bronzino, J., 2000. *Introduction to biomedical engineering.* San Diego: Academic Press.

Frank, C., Amiel, D., Woo, S. L. Y., & Akeson, W., 1985. Normal Ligament Properties and Ligament Healing. *Clinical Orthopaedics and Related Research*(196), pp. 15-25.

Frank, C. B. & Jackson, D. W., 1997. Current concepts review - The science of reconstruction of the anterior cruciate ligament. *Journal of Bone and Joint Surgery-American Volume*, 79A(10), pp. 1556-1576.

Frank, E. H., Jin, M., Loening, A. M., Levenston, M. E., & Grodzinsky, A. J., 2000. A versatile shear and compression apparatus for mechanical stimulation of tissue culture explants. *Journal of Biomechanics*, 33(11), pp. 1523-1527.

Freeman, M. A. R. & Pinskerova, V., 2005. The movement of the normal tibio-femoral joint. *Journal of Biomechanics*, 38(2), pp. 197-208.

Garvin, J., Qi, B., Maloney, M., & Banes, A. J., 2003. Novel system for engineering bioartificial tendons and application of mechanical load. *Tissue Engineering*, 9(5), pp. 967-979.

Goh, J. C. H., Ouyang, H. W., Teoh, S. H., Chan, C. K. C., & Lee, E. H., 2003. Tissue-engineering approach to the repair and regeneration of tendons and ligaments. *Tissue Engineering*, 9 p. S31-S44.

Goulet, F., Rancourt, D., Cloutier, R., Germain, L., Poole, A. R., & Auger, F. A., 2000. Tendons and ligaments. In: R. P. Lanza, R. Langer, & W. L. Chick, eds. *Principles of tissue engineering*, London: Academic Press, pp. 711-722.

Gray, H., 2001. *Gray's anatomy: a facsimile.* Kent, UK: Grange books.

Hannafin, J. A., Arnoczky, S. P., Hoonjan, A., & Torzilli, P. A., 1995. Effect of stress deprivation and cyclic tensile loading on the material and morphologic properties of canine flexor digitorum profundus tendon: An in vitro study. *Journal of Orthopaedic Research*, 13(6), pp. 907-914.

Hardin-Young, J., Teumer, J., Ross, R. N., & Parenteau, N. L., 2000. Approaches to transplanting engineered cells and tissues. In: R. P. Lanza, R. Langer, & J. Vacanti, eds. *Principles of tissue engineering*, 2nd edn, San Diego: Academic Press.

Harner, C. D., Janaushek, M. A., Kanamori, A., Yagi, M., Vogrin, T. M., & Woo, S. L. Y., 2000. Biomechanical analysis of a double-bundle posterior cruciate ligament reconstruction 1. *American Journal of Sports Medicine*, 28(2), pp. 144-151.

Hart, D. A., Shrive, N. G., & Goulet, F., 2005. Tissue engineering of ACL replacements. *Sports Medicine and Arthroscopy Review*, 13(3), pp. 170-176.

Herrington, L., Wrapson, C., Matthews, M., & Matthews, H., 2005. Anterior Cruciate Ligament reconstruction, hamstring versus bone-patella tendon-bone grafts: a systematic literature review of outcome from surgery. *Knee*, 12(1), pp. 41-50.

Hildebrand, K. A., Gallant-Behm, C. L., Kydd, A. S., & Hart, D. A., 2005. The basics of soft tissue healing and general factors that influence such healing. *Sports Medicine and Arthroscopy Review*, 13(3), pp. 136-144.

Hubbell, J. A., 1995. Biomaterials in Tissue Engineering. *Bio-Technology*, 13(6), pp. 565-576.

Janssen, F. W., Oostra, J., van Oorschot, A., & van Blitterswijk, C. A., 2006. A perfusion bioreactor system capable of producing clinically relevant volumes of tissue-engineered bone: In vivo bone formation showing proof of concept. *Biomaterials*, 27(3), pp. 315-323.

Johnston, D. R., Baker, A., Rose, C., Scotland, T. R., & Maffulli, N., 2003. Long-term outcome of MacIntosh reconstruction of chronic anterior cruciate ligament insufficiency using fascia lata. *Journal of Orthopaedic Science*, 8(6), pp. 789-795.

Kahn, C. J. F., Vaquette, C., Rahouadj, R., & Wang, X., 2008. A novel bioreactor for ligament tissue engineering. *Bio-Medical Materials and Engineering*, 18(4-5), pp. 283-287.

Kastelic, J., Galeski, A., & Baer, E., 1978. Multicomposite Structure of Tendon. *Connective Tissue Research*, 6(1), pp. 11-23.

Khatod, M. & Amiel, D., 2003. Ligament biochemistry and physiology. In: R. A. Pedowitz, J. J. O'Connor, & W. Akeson, eds. *Daniel's knee injuries : ligament and cartilage structure, function, injury, and repair*, 2nd edn, Philadelphia: Lippincott Williams & Wilkins.

Konan, S. & Haddad, F. S., 2009. A clinical review of bioabsorbable interference screws and their adverse effects in anterior cruciate ligament reconstruction surgery. *Knee*, 16(1), pp. 6-13.

Lee, C. H., Shin, H. J., Cho, I. H., Kang, Y. M., Kim, I. A., Park, K. D., & Shin, J. W., 2005. Nanofiber alignment and direction of mechanical strain affect the ECM production of human ACL fibroblast. *Biomaterials*, 26(11), pp. 1261-1270.

Lu, H. H., Cooper, J. A., Manuel, S., Freeman, J. W., Attawia, M. A., Ko, F. K., & Laurencin, C. T., 2005. Anterior cruciate ligament regeneration using braided biodegradable scaffolds: *in vitro* optimization studies. *Biomaterials*, 26(23), pp. 4805-4816.

Lyon, R. M., Akeson, W. H., Amiel, D., Kitabayashi, L. R., & Woo, S. L. Y., 1991. Ultrastructural Differences Between the Cells of the Medial Collateral and the Anterior Cruciate Ligaments. *Clinical Orthopaedics and Related Research*(272), pp. 279-286.

Martin, Y. & Vermette, P., 2005. Bioreactors for tissue mass culture: Design, characterization, and recent advances. *Biomaterials*, 26(35), pp. 7481-7503.

Martini, F. H., 2001. *Fundamentals of anatomy and physiology.* 5th edn. New Jersey: Prentice-Hall Inc..

Maskarinec, S. A. & Tirrell, D. A., 2005. Protein engineering approaches to biomaterials design. *Current Opinion in Biotechnology*, 16(4), pp. 422-426.

Meyer, U., Buchter, A., Nazer, N., & Wiesmann, H. P., 2006. Design and performance of a bioreactor system for mechanically promoted three-dimensional tissue engineering. *British Journal of Oral & Maxillofacial Surgery*, 44(2), pp. 134-140.

Mol, A., Driessen, N. J. B., Rutten, M. C. M., Hoerstrup, S. P., Bouten, C. V. C., & Baaijens, F. P. T., 2005. Tissue engineering of human heart valve leaflets: A novel bioreactor for a strain-based conditioning approach
1. *Annals of Biomedical Engineering*, 33(12), pp. 1778-1788.

Morris, A. S., 2001a. Instrument types and performance characteristics. In: *Measurement and Instrumentation Principles. Measurement and Instrumentation Systems*, 1 edn, Oxford: Elsevier Science & Technology, pp. 12-31.

Morris, A. S., 2001b. Measurement noise and signal processing. In: *Measurement and Instrumentation Principles. Measurement and Instrumentation Systems*, 1 edn, Oxford: Elsevier Science & Technology, pp. 73-101.

Moskowitz, R. W., Altman, R. D., Buckwalter, J. A., Goldberg, V. M., & Hochberg, M. C., 2006. *Osteoarthritis: diagnosis and medical/surgical management.* 4th edn. Philadelphia: Lippincott, Williams & Wilkins.

National Institute for Clinical Excellence (NICE), 2001. *Guidance on the use of cyclo-oxygenase (Cox) II selective inhibitors, celecoxib, rofecoxib, meloxicam and etodolac for osteoarthritis and rheumatoid arthritis*. London: NICE, (Technology appraisal no. 27, report no. N0016).

Nerem, R. M., 2000. The challenge of imitating nature. In: R. P. Lanza, R. Langer, & J. Vacanti, eds. *Principles of tissue engineering*, 2nd edn, San Diego: Academic Press, pp. 9-18.

Neuenschwander, S. & Hoerstrup, S. P., 2004. Heart valve tissue engineering. *Transplant Immunology*, 12(3-4), pp. 359-365.

Nordin, M. & Frankel, V. H., 2001. Biomechanics of the knee. In: M. Nordin & V. H. Frankel, eds. *Basic Biomechanics of the musculoskeletal system*, 3rd edn, Maryland: Lippincott Williams & Wilkins, pp. 176-201.

Office of National Statistics, 2003. *Chronic sickness: rate per 1000 reporting selected longstanding conditions, by sex and age (table 7.15)*. UK: Office of National Statistics, (LIB0715).

Pain, H. J., 2005. Simple Harmonic Motion. In: *The Physics of Vibrations and Waves*, 6 edn, Chichester: John Wiley & Sons, Ltd, pp. 1-35.

Park, J., Mackay, S., & Wright, E., 2003. Electrical noise and interference. In: *Practical Data Communications for Instrumentation and Control*, 1st edn, Oxford: Elsevier Newnes, pp. 124-144.

Pearsall, A. W., Hollis, J. M., Russell, G. V., & Scheer, Z., 2003. A biomechanical comparison of three lower extremity tendons for ligamentous reconstruction about the knee. *Arthroscopy-the Journal of Arthroscopic and Related Surgery*, 19(10), pp. 1091-1096.

Pedowitz, R. A., Gershuni, D. H., Crenshaw, A. G., Petras, S. L., Danzig, L. A., & Hargens, A. R., 1989. Intraarticular Pressure During Continuous Passive Motion of the Human Knee. *Journal of Orthopaedic Research*, 7(4), pp. 530-537.

Peperzak, K. A., Gilbert, T. W., & Wang, J. H. C., 2004. A multi-station dynamic-culture force monitor system to study cell mechanobiology. *Medical Engineering & Physics*, 26(4), pp. 355-358.

Raif, E. M. & Seedhom, B. B., 2005. Effect of cyclic tensile strain on proliferation of synovial cells seeded onto synthetic ligament scaffolds - an in vitro simulation. *Bone*, 36(3), pp. 433-443.

Reddi, A. H., 2000. Morphogenesis and tissue engineering. In: R. P. Lanza, R. Langer, & J. Vacanti, eds. *Principles of tissue engineering*, 2nd edn, San Diego: Academic Press, pp. 81-92.

Renstrom, P., Arms, S. W., Stanwyck, T. S., Johnson, R. J., & Pope, M. H., 1986. Strain Within the Anterior Cruciate Ligament During Hamstring and Quadriceps Activity. *American Journal of Sports Medicine*, 14(1), pp. 83-87.

Riemersa, D. J. & Schamhardt, H. C., 1982. The Cryo-Jaw, A Clamp Designed for Invitro Rheology Studies of Horse Digital Flexor Tendons. *Journal of Biomechanics*, 15(8), pp. 619-620.

Rubin, C. T. & Lanyon, L. E., 1984. Regulation of Bone-Formation by Applied Dynamic Loads. *Journal of Bone and Joint Surgery-American Volume*, 66A(3), pp. 397-402.

Rumian, A. P., Draper, E. R. C., Wallace, A. L., & Goodship, A. E., 2006. A new understanding of structural adaptation of tendon to mechanical load. In: *1st joint meeting of the bone research society and the british orthopaedic research society*, 5-6 July 2006 Southampton. Southampton: p. 26.

Sales, K. M., Salacinski, H. J., Alobaid, N., Mikhail, M., Balakrishnan, V., & Seifalian, A. M., 2005. Advancing vascular tissue engineering: the role of stem cell technology. *Trends in Biotechnology*, 23(9), pp. 461-467.

Shamblott, M. J., Edwards, B. E., & Gearhart, J. D., 2000. Pluripotent stem cells. In: R. P. Lanza, R. Langer, & J. Vacanti, eds. *Principles of Tissue Engineering*, 2nd edn, San Diego: Academic Press, pp. 369-382.

Sharkey, N. A., Smith, T. S., & Lundmark, D. C., 1995. Freeze Clamping Musculotendinous Junctions for *In-Vitro* Simulation of Joint Mechanics. *Journal of Biomechanics*, 28(5), pp. 631-635.

Simmons, C. A. & Mooney, D. J., 2003. Regulation of cellular response to mechanical signals by matrix design. In: F. Guilak et al., eds. *Functional tissue engineering*, 1st edn, New York: Springer-Verlag, pp. 291-304.

Simon, S. R., Alaranta, H., An, K. N., Cosgarea, A., Fischer, R., Frazier, J., Keading, C., Muha, M., Perry, J., Pope, M. H., & Quesada, P., 2000. Kinesiology. In: J. A. Buckwalter, T. A. Einhorn, & S. R. Simon, eds. *Orthopaedic basic science: biology and biomechanics of the musculoskeletal system*, 2 edn, Rosemont: American Academy of Orthopaedic Surgeons, pp. 731-827.

Skyhar, M. J., Danzig, L. A., Hargens, A. R., & Akeson, W. H., 1985. Nutrition of the Anterior Cruciate Ligament - Effects of Continuous Passive Motion. *American Journal of Sports Medicine*, 13(6), pp. 415-418.

Smith, B. A., Livesay, G. A., & Woo, S. L. Y., 1993. Biology and Biomechanics of the Anterior Cruciate Ligament. *Clinics in Sports Medicine*, 12(4), pp. 637-670.

Sodian, R., Lemke, T., Loebe, M., Hoerstrup, S. P., Potapov, E. V., Hausmann, H., Meyer, R., & Hetzer, R., 2001. New pulsatile bioreactor for fabrication of tissue-engineered patches. *Journal of Biomedical Materials Research*, 58(4), pp. 401-405.

Stegemann, J. P., Hong, H., & Nerem, R. M., 2005. Mechanical, biochemical, and extracellular matrix effects on vascular smooth muscle cell phenotype. *Journal of Applied Physiology*, 98(6), pp. 2321-2327.

Svendsen, K. H. & Thomson, G., 1984. A New Clamping and Stretching Procedure for Determination of Collagen Fiber Stiffness and Strength Relations Upon Maturation. *Journal of Biomechanics*, 17(3), pp. 225-229.

Taylor, J. R., 1997. *An introduction to error analysis - The study of uncertainties in physical measurements.* 2nd edn. Sausalito, CA: University science books.

Toyoda, T., Matsumoto, H., Fujikawa, K., Saito, S., & Inoue, K., 1998. Tensile load and the metabolism of anterior cruciate ligament cells. *Clinical Orthopaedics and Related Research*(353), pp. 247-255.

van Dijk, R., 1983. *The behaviour of the cruciate ligaments in the human knee.* Thesis (PhD). Catholic University, Nijmegen, Netherlands.

Vance, J., Galley, S., Liu, D. F., & Donahue, S. W., 2005. Mechanical stimulation of MC3T3 osteoblastic cells in a bone tissue-engineering bioreactor enhances prostaglandin E-2 release. *Tissue Engineering*, 11(11-12), pp. 1832-1839.

von Porat, A., Roos, E. M., & Roos, H., 2004. High prevalence of osteoarthritis 14 years after an anterior cruciate ligament tear in male soccer players: a study of radiographic and patient relevant outcomes. *Annals of the Rheumatic Diseases*, 63(3), pp. 269-273.

Wartella, K. A. & Wayne, J. S., 2009. Bioreactor for Biaxial Mechanical Stimulation to Tissue Engineered Constructs. *Journal of Biomechanical Engineering-Transactions of the ASME*, 131(4).

Weiss, J. A., Gardiner, J. C., & Bonifasi-Lista, C., 2002. Ligament material behavior is nonlinear, viscoelastic and rate-independent under shear loading. *Journal of Biomechanics*, 35(7), pp. 943-950.

Wieloch, P., Buchmann, G., Roth, W., & Rickert, M., 2004. A cryo-jaw designed for in vitro tensile testing of the healing Achilles tendons in rats. *Journal of Biomechanics*, 37(11), pp. 1719-1722.

Wohl, G. R., Shymkiw, R. C., Matyas, J. R., Kloiber, R., & Zernicke, R. F., 2001. Periarticular cancellous bone changes following anterior cruciate ligament injury. *Journal of Applied Physiology*, 91(1), pp. 336-342.

Woo, S. L. Y., Abramowitch, S. D., Kilger, R., & Liang, R., 2006. Biomechanics of knee ligaments: injury, healing, and repair. *Journal of Biomechanics*, 39(1), pp. 1-20.

Woo, S. L. Y., Abramowitch, S. D., Loh, J. C., Musahl, V., & Wang, J. H. C., 2003. Ligament healing: present status and the future of functional tissue engineering. In: F. Guilak et al., eds. *Functional tissue engineering*, 1st edn, New York: Springer-Verlag, pp. 17-34.

Woo, S. L. Y., Chan, S. S., & Yamaji, T., 1997. Biomechanics of knee ligament healing, repair and reconstruction. *Journal of Biomechanics*, 30(5), pp. 431-439.

Woo, S. L. Y., Hollis, J. M., Adams, D. J., Lyon, R. M., & Takai, S., 1991. Tensile Properties of the Human Femur-Anterior Cruciate Ligament-Tibia Complex - the Effects of Specimen Age and Orientation. *American Journal of Sports Medicine*, 19(3), pp. 217-225.

World Health Organisation, 2003. *The burden of musculoskeletal conditions at the start of the new millenium*. Geneva: World Health Organisation, (technical report series no. 919).

Yarlagadda, P. K. D. V., Chandrasekharan, M., & Shyan, J. Y. M., 2005. Recent advances and current developments in tissue scaffolding. *Bio-Medical Materials and Engineering*, 15(3), pp. 159-177.

Ye, H., Das, D. B., Triffitt, J. T., & Cui, Z. F., 2006. Modelling nutrient transport in hollow fibre membrane bioreactors for growing three-dimensional bone tissue. *Journal of Membrane Science*, 272(1-2), pp. 169-178.

Zavatsky, A. B. & O'Connor, J. J., 1994. Three-dimensional geometrical models of human knee ligaments. *Proceedings of the Institution of Mechanical Engineers, Part H: Journal of Engineering in Medicine*, 208(H4), pp. 229-240.

Zhu, X. H., Tabata, Y., Wang, C. H., & Tong, Y. W., 2008. Delivery of Basic Fibroblast Growth Factor from Gelatin Microsphere Scaffold for the Growth of Human Umbilical Vein Endothelial Cells. *Tissue Engineering Part A*, 14(12), pp. 1939-1947.

APPENDIX A. REVIEW OF BIOREACTORS

A review of custom-made bioreactors was performed to compare the different cell source and scaffold combinations which have been used in experiments, the size of the engineered tissue, the duration of experiments, the method of mass transfer used in the bioreactor and the mechanical loading which was applied. The results of this review are summarised in Table A-1. Commercially available bioreactors have also been reviewed and their features and limitations have been summarised in Table A-2.

Table A-1 Review of custom-made bioreactors (in order of tissue relevance)

Author	*Research group*	*Study*	*Tissue*	*Cell/tissue source*	*Scaffold*	*Scale & duration*	*Mass transfer*	*Loading*	*Results/ conclusions*
Toyoda *et al.* (1998)	Keio Univ., Tokyo; National Defence Med. College, Saitama, Japan; Tokyo Women's Med. College.	Effect of loading on metabolism of ACL cells.	ACL	Rabbit cells from the ACL and synovium.	Flexible rubber base of wells (Flexcell Int.)	Well dia. 25.4mm. 24hr cyclic loading.	-	Cyclic tensile loading (80mm Hg vacuum force; 3sec on, 3sec off)	ACL cells with the largest loading became spindle shaped and aligned. ACL cells' metabolism increased (collagen synthesis), however, synovium cells' metabolism did not.
Altman *et al.* (2002b)	Tufts Univ.; Harvard Medical School; Univ. Hospital Basel, Switzerland; New England Medical Centre; MIT.	Development of bioreactor for ACL TE.	ACL	Human bone marrow stromal cells (hBMSC) from bone marrow aspirates.	Silk rope matrix, collagen gel in previous study (Altman *et al.* 2001)	30mm gauge length, ~6mm dia. Duration: 21 days.	Perfusion and annular flow.	Cyclic loading: 0.0167Hz (1 cycle/min), 2mm (linear), 90° (torsional).	System supported cell growth and proliferation on silk matrix. Also supported cell differentiation into ligament-like cells.
Kahn *et al.* (2008)	Nancy-University, Vandoevre, France	Novel bioreactor for ligament tissue engineering.	ACL	Rat (Wistar) bone marrow stem cells.	Polycaprolactone (PCL) scaffold	Scaffold size unknown. Scaffold seeded with $5x10^5$ cells. Duration: 2 weeks.	Chamber flow included in design but not used during experiment. Chamber medium was changed every 3 days.	Bioreactor can impose tension (0-10mm) and torsion (0-90°) at 0.0167-1Hz. Loading during experiment is unclear.	A bioreactor was designed capable of applying mechanical stimulation suitable for tissue engineering of an ACL.
Raif and Seedhom (2005)	Leeds School of Medicine	Effect of cyclic tensile strain on cell proliferation on synthetic scaffold.	Ligament	Bovine synovial cells from synovium of metatarso-phalangeal joint.	Polyester open weave (Leeds-Keio). Max tensile strength 320N, average stiffness 15N/mm.	Unknown dimensions of the scaffold. Short term tests (24hrs), and medium term tests (5 weeks).	In medium well, no flow.	Cyclic tensile loading via motor-driven cam shaft. Variable frequency and strain amplitude (tested 1%-4.5%)	Increased cell proliferation with increased loading. A lower threshold of 1% strain below which no sig. increase in cell proliferation.

Author	*Research group*	*Study*	*Tissue*	*Cell/tissue source*	*Scaffold*	*Scale & duration*	*Mass transfer*	*Loading*	*Results/ conclusions*
Lee *et al.* (2005)	Inje Univ., South Korea; Ajou Univ., S. Korea.	Effect of nanofibre alignment and strain direction on ECM production.	Ligament	Human ACL fibroblasts	Polyurethane nanofibres (aligned and unaligned)	10 x 10 x 1mm (unloaded), 35 x 4 x 0.5mm (loaded). Duration <7 days.	No flow.	Nanofibre sheet attached to Flexcell plate. 5% strain at 0.2Hz for 24hrs.	Cells on aligned fibres were more morphologically similar to ACL fibroblasts and had increased ECM production.
Cooper *et al.* (2006)	Drexel Univ., Philadelphia; Univ. of Virginia, Charlottesville.	Evaluation of ACL, MCL, Achilles tendon & patella tendon as cell source for ligament TE.	Ligament	Cells from ACL, MCL, AT & PT of NZ white rabbits.	PLLA braided scaffold	Intraarticular zone: 23 x 2.7 x 2.7mm Duration: 7, 14, 21 days	In medium, no flow.	No loading	PT & AT were shown to have the fastest cellular proliferation, however, ACL cells have the highest expression of matrix markers. Concluded that ACL matrix producing cells would be the most suitable for ligament TE.
Banes *et al.* (1999)	Dept. of Orthopaedics, Univ. of North Carolina; Univ. of Iowa, USA.	How gap junctions regulate the response of tendon cells to loading.	Tendon	Avian digital flexor tendon (chicken) +	—	40mm gauge length, 4mm wide (double notch wound model – 2mm wide). Duration: 3 days.	In medium bath, no flow.	Custom-made tensile loading device: 1Hz, 0.65%, 8hrs active, 16 hrs rest.	DNA & collagen synthesis increased with loading. Gap junction blocker (octanol) significantly reduces DNA & collagen synthesis =>
				Tendon cells from human digital flexor tendon.	Polyester foam	Foam construct: 35 x 8 x 2mm Duration: 3 weeks.		Flexcell loading unit, same regime as above.	communication between cells is important for wound healing.
Garvin *et al.* (2003)	Univ. of North Carolina; Flexcell Int., North Carolina.	Novel system for tendon TE and load application.	Tendon	Avian tendon internal fibroblasts (ATIFs) from chicken digital flexor tendon.	Collagen gel	Gel matrix: 25 x 3 x 3mm	In medium bath, no flow.	Flexcell loading unit: 1hr/day, 1%, 1Hz.	—
Peperzak *et al.* (2004)	Univ. of Pittsburgh Medical Centre	Study of cell mechano-biology	Non-specific	Human patellar tendon fibroblasts	Collagen gel	Scaffold: 70 x 30 x 10mm. 3-30 mins.	No flow. Not clear if gel is in a medium well or not.	Cyclic tension via linear actuator. Sine and triangular waveforms, 0.05Hz, 3-5mm amplitude.	Developed a system to apply loading and can accurately measure forces due to applied loading and cell contraction.

Author	*Research group*	*Study*	*Tissue*	*Cell/tissue source*	*Scaffold*	*Scale & duration*	*Mass transfer*	*Loading*	*Results/ conclusions*
Frank *et al.* (2000)	MIT; Georgia Inst. Of Technology, Atlanta	Development of shear & compression bioreactor.	Cartilage	Explant of bovine cartilage disks.	None	Disk dimensions: 3mm dia., 1.1mm thick. Duration: 24hrs	In culture well, no flow.	Cyclic loading: 10% compressive strain, 0.4-1.6% shear strain, 0.01-1Hz	Bioreactor was validated against previous studies for the viscoelastic properties of the cartilage explants.
Chen *et al.* (2004)	National Tsing Hua Uni., Taiwan.	Cartilage TE	Cartilage	Chondrocytes from rat articular cartilage.	PLGA porous scaffold discs.	Disc dimension: 7.5mm dia., 3.5mm thickness. Duration: 4 weeks	Perfusion, cyclic immersion in medium.	Cyclic shear due to rotation into and out of medium.	Showed the maintenance of chondrocyte phenotype and formation of cartilage-like constructs.
Wartella & Wayne (2009)	Orthopaedic Research Laboratory, Virginia Commonwealth University, Richmond, USA.	Bioreactor for biaxial mechanical stimulation to tissue engineered constructs.	Cartilage, meniscus	Bone marrow cells from primary hip replacement patients.	Collagen type I scaffold	Scaffold: 10 x 20 x 1.5 mm^3. Duration: 2 – 3 weeks static culture followed by 4 days of mechanical stimulation.	Bioreactor has "portal for media exchange".	Biaxial loading. 3.8% tension and 5% compression.	Strain measured at mid-substance was lower than grip-to-grip strain. SEM showed mechanical loading increased the number of cells and matrix components.
Ye *et al.* (2006) (+ ref. an abstract)	Oxford Univ.	Bone TE	Bone	Rat bone marrow fibroblasts.	Hollow fibre membrane (unknown material) + rat tail collagen gel. Also polycaprolactone scaffold implanted into mice muscles.	Fibre length of 30mm. Unknown fibre dia, overall dia, interfibre space.	Continuous flow through hollow fibre.	No loading	Improved cell viability with continuous perfusion, calcification of implanted scaffold.
Bursac *et al.* (1999)	MIT; Boston Univ., USA.	Cardiac muscle TE	Cardiac muscle	Cardiac myocytes from rats + rat ventricular tissue (as control).	PGA fibre mesh (13μm fibres, 97% porosity)	Disc dimension: 5mm dia., 2mm thickness. Duration: 7days	Magnetic stir bar for tissue culture studies. In culture bath with continuous flow (60-120ml/min) for for electro-physiological study.	Stimulation with electrical pulse for electro-physiological study.	3D cardiac muscle constructs can be engineered with appropriate structural and electro-physiological properties for in vitro studies.

Author	*Research group*	*Study*	*Tissue*	*Cell/tissue source*	*Scaffold*	*Scale & duration*	*Mass transfer*	*Loading*	*Results/ conclusions*
Sodian *et al.* (2001)	German Heart Inst. Berlin; Baylor College of Medicine, Houston; University Hospital, Zurich.	TE of cardio-vascular patch	Cardio-vascular patch	Vascular cells (unknown source)	Polymeric patch scaffold (polyhydroxyalcanoid)	Patch dia. 40-45mm (unknown thickness). Test duration: 4 days.	Continuously recirculating pulsatile flow with 600ml reservoir.	Combined fluid shear stress (pulsatile surface flow producing shear stress approx. 0.2-10 dyne/cm^2) and biomechanical stress (pulsatile pressure caused patch to arch between the two fluid chambers).	Preliminary results showed cell ingrowth into pores and formation of multiple cell layers on side exposed to flow.
Mol *et al.* (2005)	Eindhoven Univ. of Tech., Netherlands; Univ. Hospital, Zurich.	Bioreactor for TE of a human heart valve leaflet.	Heart valve	Human saphenous vein cells.	Acrylic stent, PGA leaflets (cut from non-woven meshes) coated with thin layer of poly-4-hydroxybutyrate. Cells were seeded using a fibrin carrier.	Leaflet thickness: 1mm Duration: 2, 3, 4 weeks	Continuous medium flow (4ml/min)	Prestrain due to constrain by the stent (3-5%) and dynamic strain from pressure differential (1Hz, <80mm Hg)	Bioreactor showed no contamination or biocompatibility issues. Dynamic strain appeared to produce a more homogenous and densely packed tissue. Dynamic strain and/or prestrain produced improved mechanical properties.

Table A-2 Review of commercially available bioreactors

Manufacturer	*Product*	*Features*	*Limitations*
Synthecon (www.synthecon.com)	Rotating cell culture systems.	Rotating wall vessel(s)	Incubator required, no environmental control, no mechanical control.
Synthecon (www.synthecon.com)	Perfused culture system.	Rotating wall vessel, medium perfusion.	Incubator required, no environmental control, no mechanical control.
Flexcell International (www.flexcellint.com)	FX-4000T	Tension via vacuum pressure to rubber membrane, <30% elongation, <5Hz.	Incubator required, no environmental control, no perfusion, no torsion.
Flexcell International (www.flexcellint.com)	FX-4000C	Compression via pneumatic piston, <62N (14lbs)	Incubator required, no environmental control, no perfusion, no torsion, limited loading.
Flexcell International (www.flexcellint.com)	FlexFlow, Streamer, Osci-Flow	Shear stress via fluid flow. Flow can be laminar and/or pulsatile.	Incubator required, no environmental control, no mechanical control.
Bose Corporation (www.bose-electroforce.com)	Vascular BioDynamic system	Can combine pulsatile flow with tension/ compression. <200N, <6.35mm stroke. Autoclavable, vertical or horizontal setup, can be banked into a multi-station system.	Incubator required, no environmental control.
Bose Corporation (www.bose-electroforce.com)	Orthopaedic BioDynamic system	Tension/compression and perfusion flow. <200N, <6.35mm stroke. Torsional add-on: ±2.8Nm, ±15°. Autoclavable, vertical or horizontal setup, can be banked into a multi-station system.	Incubator required, no environmental control, limited rotation.
Tissue Growth Technologies (www.tissuegrowth.com)	LigaGen Bioreactor System	Tension/compression. 20N or 40N linear motor. Single (23ml) or four sample (80ml) chamber options.	Incubator required, no environmental control, no perfusion, no torsion.

APPENDIX B. BIOREACTOR GENERAL ASSEMBLY

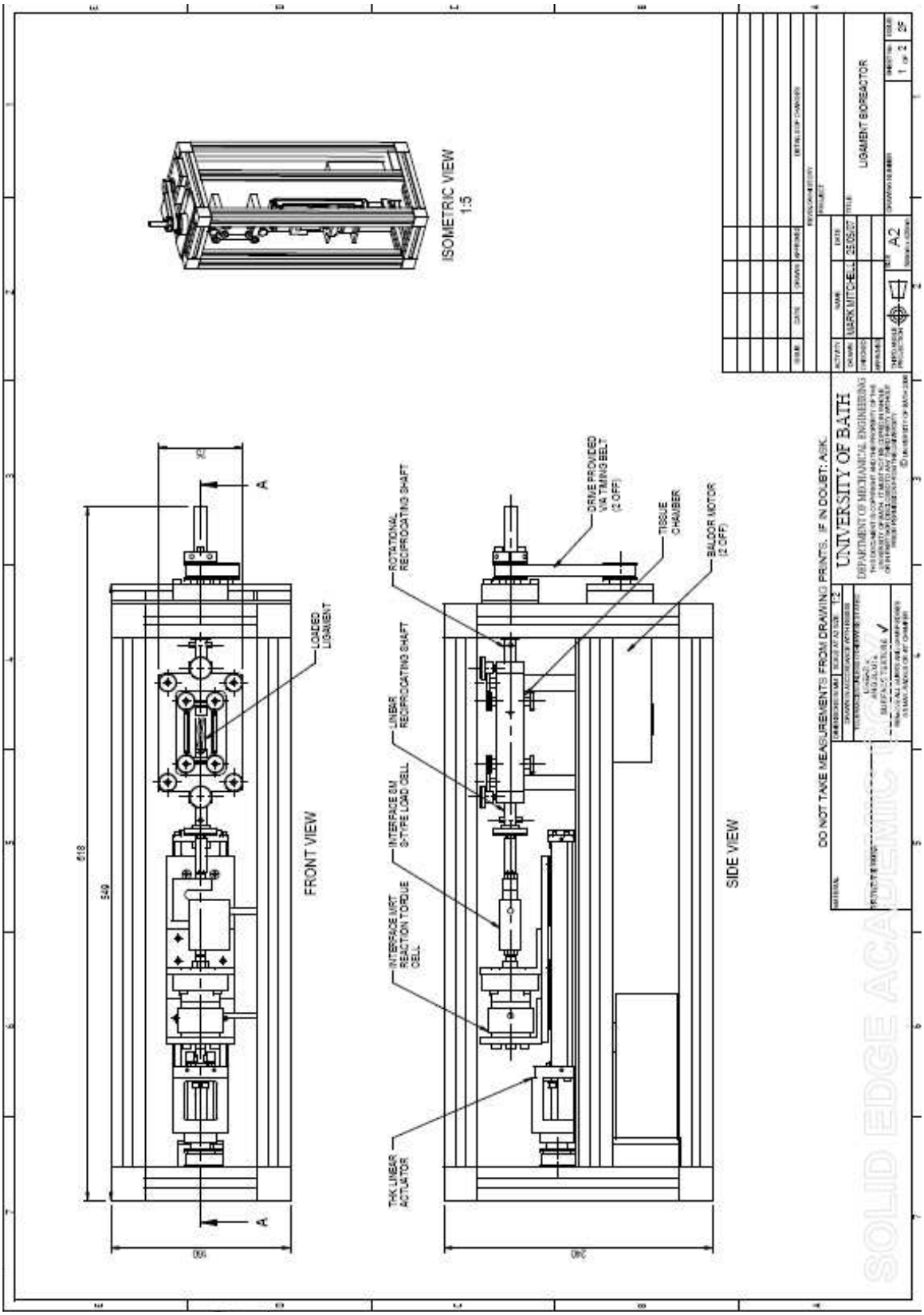

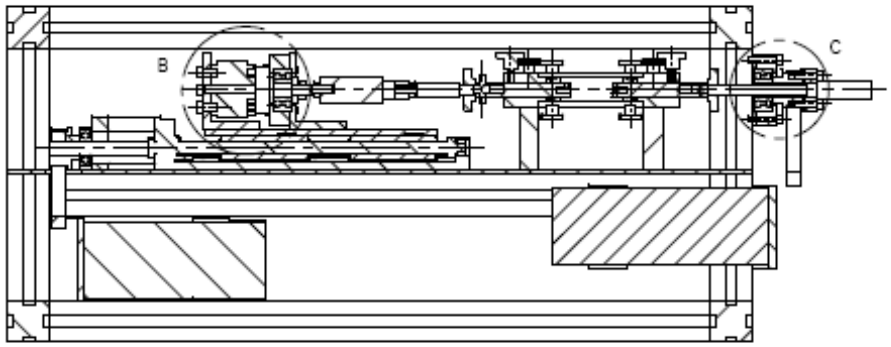

SECTION A-A

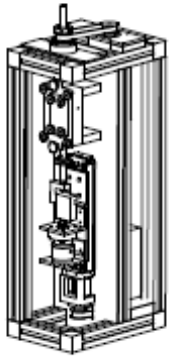

ISOMETRIC VIEW
1:5

FRONT VERTICAL FRAME
REMOVED FOR CLARITY

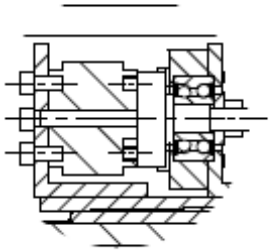

DETAIL B
1:1

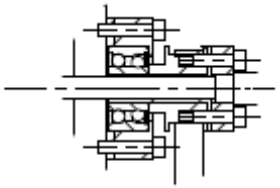

DETAIL C
1:1

DO NOT TAKE MEASUREMENTS FROM DRAWING PRINTS. IF IN DOUBT: ASK.

MATERIAL	DIMENSIONS IN MM	SCALE AT A2 SIZE: 1:2	UNIVERSITY OF BATH	
	DRAWN IN ACCORDANCE WITH BS8888		DEPARTMENT OF MECHANICAL ENGINEERING	
PRODUCT DE PRINCE	TOLERANCES UNLESS OTHERWISE STATED: Linear: ± ANGULAR: ± SURFACE TEXTURE: ✓		THIS DOCUMENT IS COPYRIGHT AND THE PROPERTY OF THE UNIVERSITY OF BATH. IT MUST NOT BE COPIED IN WHOLE OR IN PART NOR DISCLOSED TO ANY THIRD PARTY WITHOUT PRIOR PERMISSION FROM THE UNIVERSITY. © UNIVERSITY OF BATH 2006	
	REMOVE ALL BURRS AND SHARP EDGES 0.5 MAX. RADIUS OR 45° CHAMFER			

ISSUE	DATE	DRAWN	APPROVED	DETAILS OF CHANGES

REVISION HISTORY

PROJECT

ACTIVITY	NAME	DATE
DRAWN	MARK MITCHELL	25/05/07
CHECKED		
APPROVED		

TITLE: LIGAMENT BIOREACTOR

THIRD ANGLE PROJECTION | DATE | A2 Sheet size is 420mm | DRAWING NUMBER | SHEET No. 2 OF 2 | ISSUE 0F

APPENDIX C. CONTROL PROGRAM

The Mint control program which was written to control the bioreactor is shown below.

```
'====================================================================
'
'  Project      : Ligament biorector
'  Filename     : BioreactorControlProg.mnt
'  Date Created : 19/10/07
'  Author       : Mark Mitchell
'  Firmware Rev : 5403
'
'  Description  : Control program for ligament bioreactor
'                 Axis 0 = rotational axis
'                 Axis 1 = linear axis
'
'  Hardware     : BSM50N-133AF
'                 BSM50N-233AF
'                 MicroFlex
'                 Microflex
'                 NextMove ESB
'
'  Revision History:
'
'====================================================================


'Rename the load cell and torque cell inputs
Define TorqueCell = ADC(1)
Define LoadCell = ADC(0)

Dim fLoadCellGain As Float = 0.200624 '(%V/N)
Dim fTorqueCellGain As Float = 48.975173 '(%V/Nm)


'====================================================================
'Comms element definitions
'====================================================================

Define cmMode = COMMS(6)

'COMMS elements for capture task
Define cmCaptureFlag = COMMS(7)
Define cmCaptureTimeStep = COMMS(8)
Define cmCaptureCycles = COMMS(9)
Define cmDoCapture = COMMS(10)
Define cmtmCaptureStartTime = COMMS(11)
Define cmtmDataCaptureInterval = COMMS(12) 'in mins

'COMMS 15 - 19 available for setCalibration subroutine
Define cmLoadOffset = COMMS(15)
Define cmTorqueOffset = COMMS(16)
Const tmCapDuration = 10*1000 'capture duration of 10s
Const _nCaptureArraySize = (10*1000/4)+1
Dim fCaptureLoad(_nCaptureArraySize) As Float
Dim fCaptureTorque(_nCaptureArraySize) As Float

Dim fAverageLoad As Float = 0
Dim fAverageTorque As Float = 0
```

```
'COMMS 20 - 29 available for setHome subroutine
Define cmCalibBlockDone = COMMS(20)
Define cmMinDistReady = COMMS(21)
Define cmCalibBlockSize = COMMS(22)
Define cmMinDist = COMMS(23)
Define cmMinDistFlag = COMMS(24)

'COMMS 30 - 39 available for setStartPos subroutine
Define cmPreLoad = COMMS(30) 'In N
Define cmFibreAlignDone = COMMS(31)
Define cmMinAngle = COMMS(32) 'Must be in revolutions
Define cmInitialLength = COMMS(33)
Define cmInitialLengthFlag = COMMS(34)
Define cmFrictionVoltage = COMMS(35)

'----------------------------------------------------------------
'COMMS 40 - 49 available for common cycle variables for
'doPosCycle and doLoadCycle subroutine
'----------------------------------------------------------------
Define cmRampUpCycles = COMMS(40)
Define cmRampDownCycles = COMMS(41)
Define cmtmLoadingDuration = COMMS(42)
Define cmtmStationaryHome = COMMS(43)
Define cmtmStationaryExt = COMMS (44)
Define cmShaftLockDone = COMMS (45)
Define cmCycleDone = COMMS(46)
'----------------------------------------------------------------
'cmFreq is the freq of one complete cycle excluding stationary
'times at extreme locations
'----------------------------------------------------------------
Define cmFreq = COMMS(50)

'COMMS 50 - 59 available for doPosCycle subroutine
Define cmStroke = COMMS(51)
Define cmMaxAngle = COMMS(52) 'Must be in revolutions

'COMMS 60 - 79 available for doLoadCycle subroutine
Define cmMaxLoad = COMMS(61)
Define cmMinLoad = COMMS(62)
Define cmMaxTorque = COMMS(63)
Define cmMinTorque = COMMS(64)

  Dim fDemandGainLinear As Float = 1
  Dim fDemandOffsetLinear As Float = 0

  Dim fFeedbackGainRotate As Float = 1
  Dim fFeedbackGainLinear As Float = 1
  Dim fFeedbackOffsetRotate As Float = 0
  Dim fFeedbackOffsetLinear As Float = 0

Dim fLinearCamArray(720 + 1) As Float = 720
Dim fKTPropRotate As Float = 1
Dim fKTPropLinear As Float = 0.01
Dim fKTDerivRotate As Float = 0
Dim fKTDerivLinear As Float = 0
Dim fKTIntRotate As Float = 0
Dim fKTIntLinear As Float = 0

'COMMS 80 - 89 available for doStiffnessTest subroutines
Define cmMaxLinearTorque = COMMS(80)
```

```
Define cmMaxRotationalTorque = COMMS(81)

'COMMS 90 - 99 available for doJog and doSlideTopMove subroutines
Define cmJogStep = COMMS(90)
Define cmJogFlag = COMMS(91)
Define cmLinearPos = COMMS(92)
Define cmSlideTopMoveFlag = COMMS(93)

Auto         'Runs program on power up of controller
RESETALL     'Clears errors and enables drives



'Ensure the mode is initially set to zero
cmMode = 0

'====================================================================
'Setup load and torque cell
'====================================================================

'Turn on the load and torque cell inputs
ADCMODE(0) = 0
ADCMODE(1) = 0

'Setup time constant to filter signal at specified ms.
ADCTIMECONSTANT(0) = 3
ADCTIMECONSTANT(1) = 3
'Apply appropriate gain and offset to calibrate signal.
ADCGAIN(0) = 100 '(1/3.8)
ADCGAIN(1) = 100 '1
'ADCOFFSET(0) = 0 '2.02
'ADCOFFSET(1) = 0

'Maximum values for analogue inputs 0 & 1 are set and
'axes 0 & 1 are set to monitor both inputs.  If the inputs
'exceed their max values then both axes will crash stop and
'the drives will be disabled.


ADCMAX(0) = 90
ADCMAX(1) = 90
ADCMONITOR(0) = 3
ADCMONITOR(1) = 3

DACLIMITMAX(1) = 50


'====================================================================


Loop    'loop forever

  'check if the GUI has sent a "stop" command (say cmMode = 99)
  'if so exit the main loop
  If Int(cmMode) = 99 Then
    Exit Loop
  End If

  '====================================================================
  'Select which mode of operation is to be used
  '====================================================================
```

```
  Select Case cmMode
    Case 1
      setBalanceLoad
    Case 2
      setHome
    Case 3
      setStartPos
    Case 4
      doPosCycle
    Case 5
      doLoadCycle
    Case 6
      doLinearStiffnessTest
    Case 7
      doRotationStiffnessTest
    Case 8
      doMoveUp
    Case 9
      doJog
    Case 10
      doMoveSlideToTop
    End Select

  Wait(200)   'wait 200 mSecs
End Loop

'Prior to terminating you might want to do some tidying up

End   'of main program

'====================================================================
'Subroutine for zeroing of load and torque cell
'====================================================================
Sub setBalanceLoad()

  'Reset the mode to zero so it doesn't repeat the subroutine
  'when finished
  cmMode = 0
  cmCaptureFlag = 0
  '-------------------------------------------------------------
  'Code to zero the load and torque values by providing
  'an offset
  '-------------------------------------------------------------
  'Const tmCapDuration = 10*1000 'capture duration of 10s
  'Const _nCaptureArraySize = (10*1000/4)+1
  'Dim fCaptureLoad(_nCaptureArraySize) As Float
  'Dim fCaptureTorque(_nCaptureArraySize) As Float

  'Initialise all the values to zero
'  fCaptureLoad = {0;}
 ' fCaptureTorque = {0;}
  fAverageLoad = 0
  fAverageTorque = 0


  ADCOFFSET(0) = 0
  ADCOFFSET(1) = 0

  DRIVEENABLE(0) = 1
  DRIVEENABLE(1) = 1
```

```
  CAPTUREMODE(0) = _cpANALOG_INPUT
  CAPTUREMODEPARAMETER(0) = 0
  CAPTUREMODE(1) = _cpANALOG_INPUT
  CAPTUREMODEPARAMETER(1) = 1

  CAPTUREDURATION = tmCapDuration

  CAPTURE = _capDURATION

  'Pause until the capture has finished before uploading data
  Pause (CAPTURE = 0)
  cmCaptureFlag = 2

 Pause (cmCaptureFlag = 0)

  ADCOFFSET(0) = -cmLoadOffset
  ADCOFFSET(1) = -cmTorqueOffset

'Code to do capture after offset to allow a before and after graph
  CAPTURE = _capDURATION

  'Wait until the capture has finished before uploading data
  Pause (CAPTURE = 0)

  cmCaptureFlag = 2

End Sub


'=================================================================
'Subroutine to set the home position on the linear axis (1)
'=================================================================
Sub setHome()

  'Reset the comms elements to zero
  cmMode = 0
  cmCalibBlockDone = 0
  cmMinDistReady = 0
  cmMinDistFlag = 0

  DRIVEENABLE(1) = 1

  Beep:Beep

  'Size of the calibration blocks between chamber rods
  'Const fCalibBlock As Float = 22.25
  Dim fMaxDAC As Float = 12

  'Sets the max torque as a percentage of total torque
  DACLIMITMAX(1) = (fMaxDAC+1)

  'Disable following error to prevent error before torque limit is
reached
  FOLERRORMODE(1) = 0

  '---------------------------------------------------------------
  'Sets the speed and moves the motor up.
  'The motor will stop when torque exceeds DACLIMITMAX.
  '---------------------------------------------------------------
  JOG(1) = -0.5
```

```
  'Cancel the move when the torque (DAC) reaches the torque limit
(DACLIMITMAX)
  Loop
    If Abs(DAC(1)) >= fMaxDAC Then
      CANCEL(1)
      Exit
    End If
  End Loop


  '-----------------------------------------------------------------
  'Pause to let the system settle and set the current position to
  'equal the known size of the calibration blocks
  '-----------------------------------------------------------------
  Wait = 200
  POS(1) = cmCalibBlockSize

  'Beep to alert the user
  Beep:Beep

  Print "Position = ", POS(1)
  Print "Ready to remove calibration block?"
  Print "Set cmCalibBlockDone (COMMS 20) = 1 to continue"

  'Pause until the user is ready to remove the calibration blocks
  Pause(Int(cmCalibBlockDone) = 1)

  'Lower the chamber rod to allow the calibration blocks to be removed
  MOVER(1) = 2
  GO(1)

  'Beep to alert the user
  Beep:Beep

  '-----------------------------------------------------------------
  'Pause until the user is ready to set the minimum distance for
  'the chamber at the end stop for the linear slide
  '-----------------------------------------------------------------
  Print "Remove calibration block"; "About to move slide to top"
  Print "Set cmMinDistReady (comms 21) = 1 when ready to continue"
  Pause(Int(cmMinDistReady) = 1)

  '-----------------------------------------------------------------
  'Sets the speed and moves the motor up.
  'The motor will stop when torque exceeds DACLIMITMAX.
  '-----------------------------------------------------------------
  JOG(1) = -0.5

  'Cancel the move when the torque (DAC) reaches the torque limit
(DACLIMITMAX)
  Loop
    If Abs(DAC(1)) >= fMaxDAC Then
      CANCEL(1)
      Exit
    End If
  End Loop

  '-----------------------------------------------------------------
  'Pause to let the system settle and set fMinDist for the chamber
  'as the current position
  '-----------------------------------------------------------------
```

```
  Wait = 200
  cmMinDist = POS(1)

  'Beep to alert the user
  Beep:Beep

  Print "Record>> Minumum Distance of this chamber = ", COMMS(23)

  cmMinDistFlag = 1


  'Re-enable follower error
  FOLERRORMODE(1) = 1

  'Reset max torque
  DACLIMITMAX(1) = 15

  'Disable axis 1
  DRIVEENABLE(1) = 0

End Sub


'====================================================================
'Subroutine to set the start position for the linear
'and rotational axes
'====================================================================
Sub setStartPos()

  'Reset the mode to zero so it doesn't repeat the subroutine
  'when finished
  cmMode = 0
  cmInitialLengthFlag = 0
  cmFibreAlignDone = 0

  Dim fPreLoadVoltage = (cmPreLoad * fLoadCellGain) +
cmFrictionVoltage

  '--------------------------------------------------------------
  'Disable axis 0 and 1 to allow manual alignment of scaffold
  'fibres in the vertical direction
  '--------------------------------------------------------------
  DRIVEENABLE(0) = 0
  DRIVEENABLE(1) = 0

  'Disable follower error on rotational axis
  FOLERRORMODE(0) = 0

  Print "Rotationally align fibres now"
  Print "Set cmFibreAlignDone (comms 31) = 1 to continue"

  'Pause until the user confirms they have aligned the fibres
  Pause (Int(cmFibreAlignDone) = 1)

  'Enable following error on rotational axis
  FOLERRORMODE(0) = 1

  'Set the 0deg rotational position
  POS(0) = 0

  'Clear any follower errors and enable drive 0
```

```
  CANCEL(0)
  DRIVEENABLE(0) = 1

  'Move to the minimum rotational angle for the cycle
  /*
  MOVEA Is IN user units - revolutions I think -
  cmMinAngle therefore needs To be expressed IN revolutions also,
  If it Is Input As an actual angle
  */
  MOVEA(0) = cmMinAngle
  SPEED(0) = 0.25
  GO(0)

  'Clear any follower errors and enable drive 1
  CANCEL(1)
  DRIVEENABLE(1) = 1

  'Set up the speeds to apply the preloads
  Dim fPreLoadSpeed As Float = 0.5
  Dim fPreLoadBackoff As Float = 10

  Print "Sample will now be preloaded..."

  '-----------------------------------------------------------------
  'Pre-load the scaffold
  'Advance the motor at a speed fPreLoadSpeed until it reaches the
  'preload, and then reverse the motor at a speed fPreLoadSpeed
  'divided by fPreLoadBackoff
  '-----------------------------------------------------------------

  If LoadCell < fPreLoadVoltage Then
    JOG(1) = fPreLoadSpeed                'move the motor at constant
speed
    Wait(100)                             'wait 100ms to ignore static
friction
    Pause(LoadCell >= fPreLoadVoltage)    'wait until maximum
condition is met
    CANCEL(1)                             'crash stop the move and
clear errors

    If LoadCell <> fPreLoadVoltage Then   'if LoadCell exactly
equalled cmPreLoad
                                          'do nothing otherwise
backoff
      JOG(1) = -fPreLoadSpeed / fPreLoadBackoff
                                          'reverse and change the jog
speed
      Pause(LoadCell <= fPreLoadVoltage)  'wait until the minimum
condition is met
      CANCEL(1)                           'crash stop the move
    End If
  Else If LoadCell > fPreLoadVoltage Then
    JOG(1) = -fPreLoadSpeed               'move the motor at constant
speed
    Pause(LoadCell <= fPreLoadVoltage)    'wait until maximum
condition is met
    CANCEL(1)                             'crash stop the move and
clear errors

    If LoadCell <> fPreLoadVoltage Then  'if LoadCell exactly equalled
cmPreLoad
```

```
                                          'do nothing otherwise backoff
      JOG(1) = fPreLoadSpeed / fPreLoadBackoff
                                           'reverse and change the jog
speed
      Pause(LoadCell >= fPreLoadVoltage)  'wait until the minimum
condition is met
      CANCEL(1)                           'crash stop the move
    End If
  End If

  'Store the initial length of the scaffold

  /*
  declare globally As you suggested.
  Also it Is bad coding style To declare variables other than
  at the top OF the subroutine - it's not wrong though
  */
  cmInitialLength = POS(1)

  cmInitialLengthFlag = 1

  Print "Record>> Initial Length of this sample = ", COMMS(33)

  'Beep to alert the user
  Beep:Beep

End Sub


'====================================================================
'Subroutine to operate the bioreactor in position control
'====================================================================
Sub doPosCycle()

  'DO NOT set cmMode = 0 here as it will affect the capture task
  cmCycleDone = 0
  cmShaftLockDone = 0

  DRIVEENABLE(0) = 1
  DRIVEENABLE(1) = 1

  'Move to initial length position
  MOVEA(1) = cmInitialLength
  SPEED(1) = 0.5
  MOVEA(0) = cmMinAngle
  SPEED(0) = 0.25
  GO(0,1)
  Pause(IDLE(0) And IDLE(1))


'Number of data points required per cycle
Const nDataPoints As Integer = 360 * 2

'The basic master distance per data point to be used
Const nBasicMasterDist As Integer = 10

'--------------------------------------------------------------
'Speed for virtual axes 2 & 3 is calculated as the basic master
'dist per position data point * the number of data points in the
'cycle * the frequency of the wave
'--------------------------------------------------------------
```

```
Dim fMasterAxisSpeed As Float = nBasicMasterDist * nDataPoints *
cmFreq


'initialises first value of linear positional array as number of data
points
Dim fLinearCamArray(nDataPoints + 1) As Float = nDataPoints

'initialises first value of rotational positional array as number of
data points
Dim fRotateCamArray(nDataPoints + 1) As Float = nDataPoints

'Fills the master distance array with the basic master distance
Dim fCamMasterDistArray(nDataPoints) As Float = {nBasicMasterDist;}

'---------------------------------------------------------------
'Set the middle and end points in the Master distance array
'as the stationary home and extreme times. The master distances
'are calculated as the master axis speed * the stationary times.
'---------------------------------------------------------------
If cmtmStationaryExt <> 0 Then
fCamMasterDistArray(nDataPoints / 2) = fMasterAxisSpeed *
cmtmStationaryExt
End If

If cmtmStationaryHome <> 0 Then
fCamMasterDistArray(nDataPoints) = fMasterAxisSpeed *
cmtmStationaryHome
End If

'---------------------------------------------------------------
'Fill in the linear positional array data for a cos wave.
'Include a phase shift and amplitude shift
'---------------------------------------------------------------
 Dim i As Integer

  For i = 1 To nDataPoints
    fLinearCamArray(i + 1) = cmStroke * (1 + Cos(180 +
i*360/nDataPoints)) * 0.5
  Next i

  MASTERSOURCE(1) = _msPOS    'source of master signal is position
  MASTERCHANNEL(1) = 2        'Master axis is virtual axis 2

  '---------------------------------------------------------------
  'Cam uses slave positional data from fLinearCamArray and master
  'distance data from fCamMasterDistArray
  '---------------------------------------------------------------
  CAMTABLE(1, fLinearCamArray, fCamMasterDistArray)
  DRIVEENABLE(1) = 1
  DRIVEENABLE(2) = 1

  '---------------------------------------------------------------
  'Fill in the rotational positional array data for a cos wave.
  'Include a phase shift and amplitude shift
  '---------------------------------------------------------------
  Dim j As Integer

  For j = 1 To nDataPoints
    fRotateCamArray(j + 1) = cmMinAngle + ((cmMaxAngle - cmMinAngle) *
_
```

```
    0.5 * (1 + Cos(180 + j*360/nDataPoints)))
  Next j

  MASTERSOURCE(0) = _msPOS    'source of master signal is position
  MASTERCHANNEL(0) = 3        'Master axis is virtual axis 2

  '-----------------------------------------------------------------
  'Cam uses slave positional data from fRotateCamArray and master
  'distance data from fCamMasterDistArray
  '-----------------------------------------------------------------
  CAMTABLE(0, fRotateCamArray, fCamMasterDistArray)
  DRIVEENABLE(0) = 1
  DRIVEENABLE(3) = 1

  'Jog master axes 2 & 3 at the Master Axis Speed
  JOG(2) = fMasterAxisSpeed
  JOG(3) = fMasterAxisSpeed

  Time = 0   'Initialise the time to zero milliseconds


  'Provide torque limits to protect the motors and rig
  DACLIMITMAX(0) = 30
  DACLIMITMAX(1) = 50

  'Run the data capture task
  If cmDoCapture = 1 Then
    Run DataCapture
  End If


  '-----------------------------------------------------------------
  'Loop to linearly increase the amplitude of the cam profile up to
  'the full stroke.  Ramps up both the linear and rotational profiles.
  '-----------------------------------------------------------------
  If cmRampUpCycles <> 0 Then

   Dim k As Integer

   For k = 1 To Int(cmRampUpCycles)
     CAMAMPLITUDE(0) = ((2 * k) - 1) / (2 * cmRampUpCycles)
     CAMAMPLITUDE(1) = ((2 * k) - 1) / (2 * cmRampUpCycles)

     CAM(0) = _cmABSOLUTE
     CAM(1) = _cmABSOLUTE

     GO(0,1)


       Pause(IDLE(0) And IDLE(1))

    ' Pause((CAMINDEX(0) = nDataPoints) And (CAMINDEX(1) =
nDataPoints))

   Next k

  End If


  '-----------------------------------------------------------------
  'Run the main loading session
```

```
  '-----------------------------------------------------------------

  'The positional data is absolute and the cam should run continuously
  CAM(1) = _cmABSOLUTE + _cmCONTINUOUS

  'The positional data is absolute and the cam should run continuously
  CAM(0) = _cmABSOLUTE + _cmCONTINUOUS

  GO(1,0)    'Run the linear and rotational cam profile

  '-----------------------------------------------------------------
  'Pause until timer on controller has reached the end of the
  'loading session minus the time required for the ramp-down cycles.
  'Return the scaffold to its initial position.
  '-----------------------------------------------------------------

  'convert mins to ms and subtracts the time required for the ramp-
down cycles
  Pause (Time >= Int(((cmtmLoadingDuration * 60) _
  - (cmRampDownCycles/cmFreq)) * 1000))

  'Pause until the linear axis finishes the current cycle and then
cancel the cam.
  'Cannot wait until both axes finish their current cycle as they may
have gotten slighty
  'out of sync and therefore will wiat until they come back in sync.
  Pause (CAMINDEX(1) = nDataPoints)
  CANCEL(0,1)

  '-----------------------------------------------------------------
  'Loop to linearly decrease the amplitude of the cam profile from
  'the full stroke down to zero.  Ramps down both the linear and
  'rotational profiles.
  '-----------------------------------------------------------------

  If cmRampDownCycles <> 0 Then

    For k = 1 To Int(cmRampDownCycles)
      CAMAMPLITUDE(0) = 1 - (((2 * k) - 1) / (2 * cmRampDownCycles))
      CAMAMPLITUDE(1) = 1 - (((2 * k) - 1) / (2 * cmRampDownCycles))

      CAM(0) = _cmABSOLUTE
      CAM(1) = _cmABSOLUTE

      GO(0,1)

      Pause(IDLE(0) And IDLE(1))
      'Pause((CAMINDEX(0) = nDataPoints) And (CAMINDEX(1) =
nDataPoints))

    Next k

  EndIf

  'End the data capture task
  If cmDoCapture = 1 Then
    End DataCapture
  End If
```

```
  'Ensure that the motors are at the initial positions
  MOVEA(1) = cmInitialLength
  MOVEA(0) = cmMinAngle

  GO(0,1)

  '-----------------------------------------------------------------
  'Wait for the move to complete and so prevent a user termination
  'of the move from the following GUI operation
  '-----------------------------------------------------------------
  Pause(IDLE(0) And IDLE(1))
  Beep

  cmCycleDone = 1
  '-----------------------------------------------------------------
  'After the user has locked the chamber rods in position, he clicks
  'on the GUI to put a value 1 in cmShaftLockDone and the drives
  'can be disenabled.
  '-----------------------------------------------------------------
  Print "Loading complete."
  Print "Lock chamber shafts in place "
  Print "and set cmShaftLockDone (comms 45) = 1 to continue"

  Pause (Int(cmShaftLockDone) = 1)
  CANCEL(1,0)
  'DRIVEENABLE(1) = 0
  'DRIVEENABLE(0) = 0

  Print "Chamber can now be removed"

  'Reset the mode to zero so it doesn't repeat the position
  'subroutine when finished
  cmMode = 0



End Sub


'=================================================================
'Subroutine to operate the bioreactor in load control
'=================================================================
Sub doLoadCycle()

  cmMode = 0

'Configure the linear and roational axes to off so they can be
'controlled by the torque controller
DRIVEENABLE(0) = 0
DRIVEENABLE(1) = 0
CONFIG(0) = 0
CONFIG(1) = 0

'Manually enable the drives as they are configured to off
OUTX(0) = 1
OUTX(2) = 1

'Scale the encoders to the axis scaling.  As the axis is turned off
'the position cannot be read so have to read encoder counts.
ENCODERSCALE(0) = 10000
ENCODERSCALE(1) = 5000
```

```
'Dim fInitialLinPos As Float =
ENCODER(1) = 0

'Number of data points required per cycle
Const nDataPoints As Integer = 360 * 2

'The basic master distance per data point to be used
Const nBasicMasterDist As Integer = 10

'-----------------------------------------------------------------
'Speed for virtual axes 2 & 3 is calculated as the basic master
'dist per load data point * the number of data points in the
'cycle * the frequency of the wave
'-----------------------------------------------------------------
Dim fMasterAxisSpeed As Float = nBasicMasterDist * nDataPoints *
cmFreq

'initialises first value of linear load array as number of data points
'Dim fLinearCamArray(nDataPoints + 1) As Float = nDataPoints

'initialises first value of rotational torque array as number of data
points
Dim fRotateCamArray(nDataPoints + 1) As Float = nDataPoints

'Fills the master distance array with the basic master distance
Dim fCamMasterDistArray(nDataPoints) As Float = {nBasicMasterDist;}

'-----------------------------------------------------------------
'Set the middle and end points in the Master distance array
'as the stationary home and extreme times. The master distances
'are calculated as the master axis speed * the stationary times.
'-----------------------------------------------------------------
If cmtmStationaryExt <> 0 Then
fCamMasterDistArray(nDataPoints / 2) = fMasterAxisSpeed *
cmtmStationaryExt
End If

If cmtmStationaryHome <> 0 Then
fCamMasterDistArray(nDataPoints) = fMasterAxisSpeed *
cmtmStationaryHome
End If

'-----------------------------------------------------------------
'Fill in the linear load array data for a cos wave.
'Include a phase shift and amplitude shift
'-----------------------------------------------------------------
 Dim i As Integer

  For i = 1 To nDataPoints
    fLinearCamArray(i + 1) = cmMinLoad + ((cmMaxLoad - cmMinLoad) * _
    0.5 * (1 + Cos(180 + i*360/nDataPoints)))
  Next i

  MASTERSOURCE(4) = _msPOS    'source of master signal is position
  MASTERCHANNEL(4) = 2        'Master axis is virtual axis 2

  '-----------------------------------------------------------------
  'Cam uses slave load data from fLinearCamArray and master
  'distance data from fCamMasterDistArray
  '-----------------------------------------------------------------
```

```
  CAMTABLE(4, fLinearCamArray, fCamMasterDistArray)
  DRIVEENABLE(4) = 1
  DRIVEENABLE(2) = 1

  '-----------------------------------------------------------------
  'Fill in the rotational torque array data for a cos wave.
  'Include a phase shift and amplitude shift
  '-----------------------------------------------------------------
  Dim j As Integer

  For j = 1 To nDataPoints
    fRotateCamArray(j + 1) = cmMinTorque + ((cmMaxTorque -
cmMinTorque) * _
    0.5 * (1 + Cos(180 + j*360/nDataPoints)))
  Next j

  MASTERSOURCE(5) = _msPOS    'source of master signal is position
  MASTERCHANNEL(5) = 3        'Master axis is virtual axis 2

  '-----------------------------------------------------------------
  'Cam uses slave positional data from fRotateCamArray and master
  'distance data from fCamMasterDistArray
  '-----------------------------------------------------------------
  CAMTABLE(5, fRotateCamArray, fCamMasterDistArray)
  DRIVEENABLE(5) = 1
  DRIVEENABLE(3) = 1

  'Jog master axes 2 & 3 at the Master Axis Speed
  JOG(2) = fMasterAxisSpeed
  JOG(3) = fMasterAxisSpeed

  Time = 0   'Initialise the time to zero milliseconds

  'Provide torque limits to protect the motors and rig
  DACLIMITMAX(0) = 30
  DACLIMITMAX(1) = 50

  'Run the torque controller task
  Run TorqueController

  'Run the data capture task
  If cmDoCapture = 1 Then
    Run DataCapture
  End If


  '-----------------------------------------------------------------
  'Loop to linearly increase the amplitude of the cam profile up to
  'the full stroke.  Ramps up both the linear and rotational profiles.
  '-----------------------------------------------------------------
  If cmRampUpCycles <> 0 Then

   Dim k As Integer

   For k = 1 To Int(cmRampUpCycles)
     CAMAMPLITUDE(4) = ((2 * k) - 1) / (2 * cmRampUpCycles)
     CAMAMPLITUDE(5) = ((2 * k) - 1) / (2 * cmRampUpCycles)

     CAM(4) = _cmABSOLUTE + _cmT_ABSOLUTE
     CAM(5) = _cmABSOLUTE + _cmT_ABSOLUTE
```

```
    GO(4,5)

      Pause(IDLE(4) And IDLE(5))

   Next k

  End If


  '-----------------------------------------------------------------
  'Run the main loading session
  '-----------------------------------------------------------------

  'The positional data is absolute and the cam should run continuously
  CAM(4) = _cmABSOLUTE + _cmT_ABSOLUTE + _cmCONTINUOUS

  'The positional data is absolute and the cam should run continuously
  CAM(5) = _cmABSOLUTE + _cmT_ABSOLUTE + _cmCONTINUOUS

  GO(4,5)    'Run the linear and rotational cam profile


  '-----------------------------------------------------------------
  'Pause until timer on controller has reached the end of the
  'loading session minus the time required for the ramp-down cycles.
  'Return the scaffold to its initial position.
  '-----------------------------------------------------------------

  'convert mins to ms and subtracts the time required for the ramp-
down cycles
  Pause (Time >= Int(((cmtmLoadingDuration * 60) _
  - (cmRampDownCycles/cmFreq)) * 1000))

  'Pause until the program finishes the current cycle and then cancel
the cam
  Pause(CAMINDEX(4) = nDataPoints)
  CANCEL(4,5)

  '-----------------------------------------------------------------
  'Loop to linearly decrease the amplitude of the cam profile from
  'the full stroke down to zero.  Ramps down both the linear and
  'rotational profiles.
  '-----------------------------------------------------------------

  If cmRampDownCycles <> 0 Then

    For k = 1 To Int(cmRampDownCycles)
      CAMAMPLITUDE(4) = 1 - (((2 * k) - 1) / (2 * cmRampDownCycles))
      CAMAMPLITUDE(5) = 1 - (((2 * k) - 1) / (2 * cmRampDownCycles))

      CAM(4) = _cmABSOLUTE + _cmT_ABSOLUTE
      CAM(5) = _cmABSOLUTE + _cmT_ABSOLUTE

      GO(4,5)


      Pause(IDLE(4) And IDLE(5))

    Next k

  EndIf
```

```
  'End the torque controller task
  End TorqueController

  'End the data capture task
  If cmDoCapture = 1 Then
    End DataCapture
  End If


  CONFIG(0) = _cfSERVO
  CONFIG(1) = _cfSERVO

  'Ensure that the motors are at the initial positions
  'MOVEA(1) = fInitialLength
  'MOVEA(0) = cmMinAngle

  'GO(0,1)

  '-----------------------------------------------------------------
  'Wait for the move to complete and so prevent a user termination
  'of the move from the following GUI operation
  '-----------------------------------------------------------------
  Pause(IDLE(0) And IDLE(1))
  Beep

  '-----------------------------------------------------------------
  'After the user has locked the chamber rods in position, he clicks
  'on the GUI to put a value 1 in cmShaftLockDone and the drives
  'can be disenabled.
  '-----------------------------------------------------------------
  'Pause (Int(cmShaftLockDone) = 1)
  CANCEL(1,0)
  DRIVEENABLE(1) = 0
  DRIVEENABLE(0) = 0

  'Reset the mode to zero so it doesn't repeat the load
  'subroutine when finished
  cmMode = 0


End Sub

'=================================================================
'Subroutine for evaluating the linear stiffness of the rig
'=================================================================

Sub doLinearStiffnessTest()
  'reset the mode
  cmMode = 0

  KDERIV(0)=2.5

  'Zero position of axes so deflection can be read
  POS(1) = 0
  POS(0) = 0

  'Enable axis 1 and set a limit for the maximum torque
  DRIVEENABLE(0) = 1
  DRIVEENABLE(1) = 1
  Const nTorquePoints = 10
```

```
  DACLIMITMAX(1) = 20

  'List parameters we want to capture
  CAPTUREMODE(0) = _cpANALOG_INPUT
  CAPTUREMODEPARAMETER(0) = 0
  CAPTUREMODE(1) = _cpANALOG_INPUT
  CAPTUREMODEPARAMETER(1) = 1
  CAPTUREMODE(2) = _cpMEASURED_POSITION
  CAPTUREMODEPARAMETER(2) = 0
  CAPTUREMODE(3) = _cpMEASURED_POSITION
  CAPTUREMODEPARAMETER(3) = 1
  CAPTUREMODE(4) = _cpDAC_DEMAND
  CAPTUREMODEPARAMETER(4) = 1
  CAPTUREMODE(5) = 0

  'Capture data for 2 seconds
  CAPTUREDURATION = 2000

  'Initialise flag to zero
  cmCaptureFlag = 0

  'Set initial torque to zero
  TORQUE(1) = 0

  'Wait to allow system to settle
  Wait (2000)

  'Capture data and pause until capture is complete
  CAPTURE = _capDURATION
  Pause (CAPTURE = 0)
  Beep

  cmCaptureFlag = 2

  'Print "Torque =", TORQUE(1);"Save data and set cmCaptureFlag = 1"

  'Pause until user sets the flag
  'Pause (cmCaptureFlag = 1)

  Dim i As Integer
  'Loop for increasing the torque and capturing the data
  For i = 1 To nTorquePoints

    'cmCaptureFlag = 0

    TORQUE(1) = cmMaxLinearTorque * i / nTorquePoints

    'Wait to allow system to settle
    Wait (2000)

    CAPTURE = _capDURATION
    Pause (CAPTURE = 0)
    Beep

    cmCaptureFlag = 2

    'Print "Torque =", TORQUE(1);"Save data and set cmCaptureFlag = 1
to continue"
    'Print "Set cmCaptureFlag = 2 to exit"

    'Pause (cmCaptureFlag <> 0)
```

```
    'If cmCaptureFlag = 2 Then Exit For

  Next i

  Print "Loading Complete"

  DRIVEENABLE(0) = 0
  DRIVEENABLE(1) = 0

End Sub

'====================================================================
'Subroutine for evaluating the rotational stiffness of the rig
'====================================================================

Sub doRotationStiffnessTest()
  'reset the mode
  cmMode = 0

  KDERIV(0)=2.5

  'Zero the positions at the start of the cycle
  POS(0) = 0
  POS(1) = 0
  'Enable axis 0&1 and set a limit for the maximum torque
  DRIVEENABLE(0) = 1
  DRIVEENABLE(1) = 1
  Const nTorquePoints = 10
  DACLIMITMAX(0) = 75

  'Zero position of linear axis so deflection can be read
  'POS(0) = 0

  'List parameters we want to capture
  CAPTUREMODE(0) = _cpANALOG_INPUT
  CAPTUREMODEPARAMETER(0) = 0
  CAPTUREMODE(1) = _cpANALOG_INPUT
  CAPTUREMODEPARAMETER(1) = 1
  CAPTUREMODE(2) = _cpMEASURED_POSITION
  CAPTUREMODEPARAMETER(2) = 0
  CAPTUREMODE(3) = _cpMEASURED_POSITION
  CAPTUREMODEPARAMETER(3) = 1
  CAPTUREMODE(4) = _cpDAC_DEMAND
  CAPTUREMODEPARAMETER(4) = 1
  CAPTUREMODE(5) = 0

  'Capture data for 2 seconds
  CAPTUREDURATION = 2000

  'Initialise flag to zero
  cmCaptureFlag = 0

  'Set initial torque to zero
  TORQUE(0) = 0

  'Wait to allow system to settle
  Wait (2000)

  'Capture data and pause until capture is complete
  CAPTURE = _capDURATION
  Pause (CAPTURE = 0)
```

```
  Beep

  cmCaptureFlag = 2

  'Print "Torque =", TORQUE(0);"Save data and set cmCaptureFlag = 1"

  'Pause until user sets the flag
  'Pause (cmCaptureFlag = 1)

  Dim i As Integer
  'Loop for increasing the torque and capturing the data
  For i = 1 To nTorquePoints

    'cmCaptureFlag = 0

    TORQUE(0) = cmMaxRotationalTorque * i / nTorquePoints

    'Wait to allow system to settle
    Wait (2000)

    CAPTURE = _capDURATION
    Pause (CAPTURE = 0)
    Beep

    cmCaptureFlag = 2

    'Print "Torque =", TORQUE(0);"Save data and set cmCaptureFlag = 1
to continue"
    'Print "Set cmCaptureFlag = 2 to exit"

    'Pause (cmCaptureFlag <> 0)
    'If cmCaptureFlag = 2 Then Exit For

  Next i

  MOVEA(1)=0

  Print "Loading Complete"

  DRIVEENABLE(0) = 0
  DRIVEENABLE(1) = 0

End Sub

Sub doMoveUp()

  'reset the mode
  cmMode = 0


  'Enable axis 0&1 and set a limit for the maximum torque
  DRIVEENABLE(0) = 1
  DRIVEENABLE(1) = 1
  DACLIMITMAX(0) = 75
  DACLIMITMAX(1) = 75

  Const nSamplePoints = 10
  Const nMaxDist = 10
  'Zero position of linear axis so deflection can be read
  'POS(0) = 0
```

```
  'List parameters we want to capture
  CAPTUREMODE(0) = _cpANALOG_INPUT
  CAPTUREMODEPARAMETER(0) = 0
  CAPTUREMODE(1) = _cpANALOG_INPUT
  CAPTUREMODEPARAMETER(1) = 1
  CAPTUREMODE(2) = _cpMEASURED_POSITION
  CAPTUREMODEPARAMETER(2) = 0
  CAPTUREMODE(3) = _cpMEASURED_POSITION
  CAPTUREMODEPARAMETER(3) = 1
  CAPTUREMODE(4) = _cpDAC_DEMAND
  CAPTUREMODEPARAMETER(4) = 0
  CAPTUREMODE(5) = 0

  'Capture data for 2 seconds
  CAPTUREDURATION = 100000

  'Initialise flag to zero
  cmCaptureFlag = 0

  'Wait to allow system to settle
  'Wait (2000)

  'Capture data and pause until capture is complete
  CAPTURE = _capDURATION
  Pause (CAPTURE = 0)
  Beep

  cmCaptureFlag = 2
   /*
  Dim i As Integer
  'Loop for increasing the torque and capturing the data
  For i = 1 To nSamplePoints

    'MOVEA(1) = nMaxDist * i / nSamplePoints
    'GO(1)

    'Wait to allow system to settle
    Wait (1000)

    CAPTURE = _capDURATION
    Pause (CAPTURE = 0)
    Beep

    cmCaptureFlag = 2

  Next i

  'MOVEA(1) = 0

  'Print "Move Complete"
*/
  DRIVEENABLE(0) = 0
  DRIVEENABLE(1) = 0

End Sub

Sub doJog()

  cmMode = 0
  cmJogFlag = 0
  cmLinearPos = POS(1)
```

```
  MOVER(1) = cmJogStep
  GO(1)
  Pause(IDLE(1))
  cmLinearPos = POS(1)

  cmJogFlag = 1

End Sub
Sub doMoveSlideToTop()

  cmMode = 0
  cmSlideTopMoveFlag = 0

  'Beep to alert the user
  Beep:Beep

  DRIVEENABLE(1) = 1

  Dim fMaxDAC As Float = 12

  'Sets the max torque as a percentage of total torque
  DACLIMITMAX(1) = (fMaxDAC+1)

  'Disable following error to prevent error before torque limit is
reached
  FOLERRORMODE(1) = 0

  '-----------------------------------------------------------------
  'Sets the speed and moves the motor up.
  'The motor will stop when torque exceeds DACLIMITMAX.
  '-----------------------------------------------------------------
  JOG(1) = -0.5

  'Cancel the move when the torque (DAC) reaches the torque limit
(DACLIMITMAX)
  Loop
    If Abs(DAC(1)) >= fMaxDAC Then
      CANCEL(1)
      Exit
    End If
  End Loop

  'Wait to allow system to settle and then set the position
  Wait = 200
  POS(1) = cmMinDist

  cmSlideTopMoveFlag = 1

  'Re-enable follower error
  FOLERRORMODE(1) = 1

  'Reset max torque
  DACLIMITMAX(1) = 15

  'Move the slide down 1 mm
  MOVER(1) = 1
  GO(1)

  'Beep to alert the user
  Beep:Beep
```

```
End Sub

Task TorqueController

  Dim fTorqueDemandRotate As Float = 0
  Dim fTorqueDemandLinear As Float = 0
  Dim fTorqueOutputRotate As Float = 0
  Dim fTorqueOutputLinear As Float = 0
  Dim fTorqueErrorRotate As Float = 0
  Dim fTorqueErrorLinear As Float = 0
  'Dim fFeedbackGainRotate As Float = 1
  'Dim fFeedbackGainLinear As Float = 1
  'Dim fFeedbackOffsetRotate As Float = 0
  'Dim fFeedbackOffsetLinear As Float = 10
  Dim fFeedbackRotate As Float = 0
  Dim fFeedbackLinear As Float = 0

  'Dim fDemandGainLinear As Float = 1
  'Dim fDemandOffsetLinear As Float = 0

  'Torque loop gains
 ' Dim fKTPropRotate As Float = 1
 ' Dim fKTPropLinear As Float = 0.01
 ' Dim fKTDerivRotate As Float = 0
 ' Dim fKTDerivLinear As Float = 0
 ' Dim fKTIntRotate As Float = 0
 ' Dim fKTIntLinear As Float = 0

  Dim fTorqueErrorLastRotate As Float
  Dim fTorqueErrorLastLinear As Float
  Dim fDerivativeRotate As Float
  Dim fDerivativeLinear As Float
  Dim fIntegratorRotate As Float
  Dim fIntegratorLinear As Float
  DAC(0) = 0

  Dim t0 As Time
  Dim lTime As Integer
  Dim nServoTime As Integer = 3

  Loop
    'Wait for servo loop timer to expire (loops every 3ms)
    Pause t0 > lTime + nServoTime
    lTime = t0

    'read feedback
    'Voltage from load & torque cells can be scaled to motor torque
demand
    'with the below gain and offset terms
    'fFeedback = DAC(0) + ((Rnd()-0.5) * 0.01) ' Simulation for
offline test
    'fFeedbackRotate = TorqueCell * fFeedbackGainRotate +
fFeedbackOffsetRotate
    fFeedbackLinear = LoadCell * fFeedbackGainLinear +
fFeedbackOffsetLinear
    'COMMS(1) = fFeedbackRotate 'For sampling purposes

    'Calculate torque error
    'fTorqueErrorRotate = fTorqueDemandRotate - fFeedbackRotate
    fTorqueErrorLinear = fTorqueDemandLinear - fFeedbackLinear
```

```
    'Read demanded torque from torque profiler
    'fTorqueDemandRotate = POSDEMAND(5)
    fTorqueDemandLinear = (POSDEMAND(4) * fDemandGainLinear) + _
       fDemandOffsetLinear


    'Calculate derivative of error
    'fDerivativeRotate = fTorqueErrorRotate - fTorqueErrorLastRotate
    fDerivativeLinear = fTorqueErrorLinear - fTorqueErrorLastLinear

    'fTorqueErrorLastRotate = fTorqueErrorRotate
    fTorqueErrorLastLinear = fTorqueErrorLinear

    'Calculate new integrator value
    'fIntegratorRotate = fIntegratorRotate + fTorqueErrorRotate
    fIntegratorLinear = fIntegratorLinear + fTorqueErrorLinear

    'Range check integrator value
    'If fIntegratorRotate>2000 Then fIntegratorRotate = 2000
    'If fIntegratorRotate<-2000 Then fIntegratorRotate = -2000

    If fIntegratorLinear>2000 Then fIntegratorLinear = 2000
    If fIntegratorLinear<-2000 Then fIntegratorLinear = -2000

    'Calculate new torque output value
    'fTorqueOutputRotate = fTorqueDemandRotate + _
    '     (fKTPropRotate * fTorqueErrorRotate) + _
    '     (fKTIntRotate * fIntegratorRotate) + _
    '     (fKTDerivRotate * fDerivativeRotate)

    'fTorqueOutputLinear = fTorqueDemandLinear + _
    '     (fKTPropLinear * fTorqueErrorLinear) + _
    '     (fKTIntLinear * fIntegratorLinear) + _
    '     (fKTDerivLinear * fDerivativeLinear)
     fTorqueOutputLinear = (fKTPropLinear * fTorqueErrorLinear) + _
                           (fKTIntLinear * fIntegratorLinear) + _
                           (fKTDerivLinear * fDerivativeLinear)


    'Range check torque output
    'If fTorqueOutputRotate>100 Then fTorqueOutputRotate = 100
    'If fTorqueOutputRotate<-100 Then fTorqueOutputRotate = -100

    If fTorqueOutputLinear>7 Then fTorqueOutputLinear = 7
    If fTorqueOutputLinear<-7 Then fTorqueOutputLinear = -7


    'Set analogue putput with calculated torque output
    'DAC(0) = fTorqueOutputRotate
    DAC(1) = fTorqueOutputLinear

    'If ENCODER(1)>10 Then Exit : ABORT
    'If ENCODER(1)<-10 Then Exit : ABORT


  End Loop

End Task
Task DataCapture
```

```
  /*
  'Define the data arrays and their size
  Const _nCaptureArraySize = 2000
  Dim fCaptureTorque(_nCaptureArraySize) As Float
  Dim fCaptureLoad(_nCaptureArraySize) As Float
  Dim fCapturePositionRot(_nCaptureArraySize) As Float
  Dim fCapturePositionLin(_nCaptureArraySize) As Float
  */

  'Calculate capture duration for specified number of cycles
  Dim tmCapDuration As Integer = (Int(cmCaptureCycles * ((1 / cmFreq)
+ cmtmStationaryHome + cmtmStationaryExt) * 1000))

  'Time to wait between each capture session
  Dim tmCapInterval As Integer = Int(cmtmDataCaptureInterval * 1000)

  'Initialise capture flag to zero
  cmCaptureFlag = 0

  If cmMode = 4 Then
    'Capture load, torque and positional data
    CAPTUREMODE(0) = _cpANALOG_INPUT
    CAPTUREMODEPARAMETER(0) = 0
    CAPTUREMODE(1) = _cpANALOG_INPUT
    CAPTUREMODEPARAMETER(1) = 1
    CAPTUREMODE(2) = _cpMEASURED_POSITION
    CAPTUREMODEPARAMETER(2) = 0
    CAPTUREMODE(3) = _cpMEASURED_POSITION
    CAPTUREMODEPARAMETER(3) = 1
    CAPTUREMODE(4) = 0
    CAPTUREMODE(5) = 0
  End If

  If cmMode = 5 Then
    'Capture load, torque and positional data
    CAPTUREMODE(0) = _cpANALOG_INPUT
    CAPTUREMODEPARAMETER(0) = 0
    CAPTUREMODE(1) = _cpANALOG_INPUT
    CAPTUREMODEPARAMETER(1) = 1
    CAPTUREMODE(2) = _cpENCODER
    CAPTUREMODEPARAMETER(2) = 0
    CAPTUREMODE(3) = _cpENCODER
    CAPTUREMODEPARAMETER(3) = 1
    CAPTUREMODE(4) = 0
    CAPTUREMODE(5) = 0
  End If


  'Capture data for 5 cycles at maximum resolution
  CAPTUREDURATION = tmCapDuration

  Loop

  /*
  'Capture data every 20 servo loops(i.e. 20ms) = 50Hz
  CAPTUREINTERVAL = 20
  CAPTURE = _capSINGLE
  */

  CAPTURE = _capDURATION
```

```
  'Flag that the capure has begun
  cmCaptureFlag = 1

  'Record the start time of the capture
  cmtmCaptureStartTime = Time

  'Pause until the capture has finished before uploading data
  Pause (CAPTURE = 0)

  'Calculate the time step for the captured data in ms
  cmCaptureTimeStep = CAPTUREINTERVAL * LOOPTIME / 1000

  'Flag that the capture has been completed
  cmCaptureFlag = 2

  'Upload the captured data for channel zero into a Mint array
  'CAPTURECHANNELUPLOAD(0, fCaptureTorque, _nCaptureArraySize)
  'CAPTURECHANNELUPLOAD(1, fCaptureLoad, _nCaptureArraySize)
  'CAPTURECHANNELUPLOAD(2, fCapturePositionRot, _nCaptureArraySize)
  'CAPTURECHANNELUPLOAD(3, fCapturePositionLin, _nCaptureArraySize)

  'Print fCapturePositionRot(1)

  Wait (tmCapInterval)



  /*
  'Save captured data to file
  MintController1.GetCapturedData "c:\capture.csv", False, False, True

  'Two methods to upload captured data to the host memory
  short GetCaptureNumPoints()

  void DoCaptureChannelUpload(short nChannel, VARIANT* pvData, short
nCount)
  */

  End Loop

End Task

Event STOP
  /*
  Wire emergency STOP button into DIN4. The motion will be crash
stopped
  And this Event will be called.  Could send notification through
COMMS
  To labview To let it know/display emergency STOP has been pressed.
  Clear COMMS when emergency STOP HAD become deactivated.
  */

  Pause(!STOPSWITCH(0))

End Event

Startup

  '--------------------------------
  ' Begin WorkBench Generated Startup Code
  '--------------------------------
```

```
' Generated Friday, December 07, 2007
' for NextMove ESB Build 5403 USB CANopen

Define ALL = 0, 1, 2, 3, 4, 5, 6, 7
Define DINBANKS = 0
Define DOUTBANKS = 0
Define ADCS = 0, 1
Define DACS = 0, 1, 2, 3
Define ENCODERS = 0, 1, 2
Define AUXENCODERS = 0

' Ensure ABORT works as required by resetting ABORTMODE
' NB it is set correctly later in the startup block
ABORTMODE([ALL]) = _emCRASH_STOP_DISABLE;
' Abort any motion currently in progress
ABORT : Wait = 100
' Clear all errors
CANCELALL
Pause IDLE([ALL])
' Clear all axis configurations
CONFIG([ALL]) = _cfOFF;

' Define loop times
LOOPTIME = 1000
PROFILETIME = 2000

' Digital input configuration
INPUTMODE([DINBANKS]) = 0 ' 0x0
INPUTACTIVELEVEL([DINBANKS]) = 01111111111111111111 ' 0xfffff
INPUTPOSTRIGGER([DINBANKS]) = 0 ' 0x0
INPUTNEGTRIGGER([DINBANKS]) = 0 ' 0x0

' Analog input configuration
ADCMODE([ADCS]) = 0, 0

' Digital output configuration
GLOBALERROROUTPUT = -1
OUTPUTACTIVELEVEL([DOUTBANKS]) = 011111111111 ' 0x7ff

' Analog output configuration
DACMODE([DACS]) = 16, 16, 0, 0

' Encoder configuration
ENCODERPRESCALE([ENCODERS]) = 1.00, 1.00, 1.00
ENCODERSCALE([ENCODERS]) = 1.00, 1.00, 1.00
ENCODERWRAP([ENCODERS]) = 0.00, 0.00, 0.00
ENCODERMODE([ENCODERS]) = 1, 1, 0

' Aux Encoder configuration
AUXENCODERPRESCALE([AUXENCODERS]) = 16.00
AUXENCODERSCALE([AUXENCODERS]) = 1.00
AUXENCODERWRAP([AUXENCODERS]) = 0.00
AUXENCODERMODE([AUXENCODERS]) = 4

 ' --------------------------------
' Axis 0 configuration
' --------------------------------
AXISCHANNEL(0) = 0
CONFIG(0) = _cfSERVO
```

```
' Axis 0 scaling
SCALEFACTOR(0) = 10000.00

' Axis 0 limits
SOFTLIMITMODE(0) = _emIGNORE
LIMITMODE(0) = _emCRASH_STOP_DISABLE
LIMITFORWARDINPUT(0) = -1
LIMITREVERSEINPUT(0) = -1
FOLERRORMODE(0) = _emCRASH_STOP_DISABLE
FOLERRORFATAL(0) = 0.10

' Axis 0 error modes
ERRORINPUT(0) = -1
ERRORINPUTMODE(0) = _emCRASH_STOP_DISABLE
ABORTMODE(0) = _emCRASH_STOP_DISABLE
ADCERRORMODE(0) = _emCRASH_STOP_DISABLE

' Axis 0 digital input events
STOPINPUT(0) = 4
STOPINPUTMODE(0) = _siCANCEL

' Axis 0 digital outputs
DRIVEENABLEOUTPUT(0) = 0

' Axis 0 gain terms
KPROP(0) = 1.00
KINT(0) = 0.02
KINTLIMIT(0) = 20.00
KINTMODE(0) = _itSMART
KDERIV(0) = 5.00
KVEL(0) = 0.00
KVELFF(0) = 0.00
KACCEL(0) = 0.00

' Axis 0 profile parameters
PROFILEMODE(0) = _pmTRAPEZOIDAL
SPEED(0) = 10.00
ACCEL(0) = 300.00
DECEL(0) = 300.00
ERRORDECEL(0) = 30.00
ACCELJERK(0) = 300.00
DECELJERK(0) = 300.00
MOVEBUFFERSIZE(0) = 2

' Axis 0 homing parameters
HOMEINPUT(0) = -1
HOMESPEED(0) = 10.00
HOMEBACKOFF(0) = 3.00

' Axis 0 idle conditions
IDLEPOS(0) = 0.10
IDLEVEL(0) = 5000.00
IDLETIME(0) = 0
IDLEMODE(0) = 0

' --------------------------------
' Axis 1 configuration
' --------------------------------
AXISCHANNEL(1) = 1
CONFIG(1) = _cfSERVO
```

```
' Axis 1 scaling
SCALEFACTOR(1) = 5000.00

' Axis 1 limits
SOFTLIMITMODE(1) = _emIGNORE
LIMITMODE(1) = _emCRASH_STOP_DISABLE
LIMITFORWARDINPUT(1) = -1
LIMITREVERSEINPUT(1) = -1
FOLERRORMODE(1) = _emCRASH_STOP_DISABLE
FOLERRORFATAL(1) = 0.5

' Axis 1 error modes
ERRORINPUT(1) = -1
ERRORINPUTMODE(1) = _emCRASH_STOP_DISABLE
ABORTMODE(1) = _emCRASH_STOP_DISABLE
ADCERRORMODE(1) = _emCRASH_STOP_DISABLE

' Axis 1 digital input events
STOPINPUT(1) = 4
STOPINPUTMODE(1) = _siCANCEL

' Axis 1 digital outputs
DRIVEENABLEOUTPUT(1) = 2

' Axis 1 gain terms
KPROP(1) = 1.50
KINT(1) = 0.08
KINTLIMIT(1) = 20.00
KINTMODE(1) = _itSMART
KDERIV(1) = 7.00
KVEL(1) = 0.00
KVELFF(1) = 0.00
KACCEL(1) = 0.00

' Axis 1 profile parameters
PROFILEMODE(1) = _pmTRAPEZOIDAL
SPEED(1) = 20.00
ACCEL(1) = 200.00
DECEL(1) = 200.00
ERRORDECEL(1) = 60.00
ACCELJERK(1) = 600.00
DECELJERK(1) = 600.00
MOVEBUFFERSIZE(1) = 2

' Axis 1 homing parameters
HOMEINPUT(1) = -1
HOMESPEED(1) = 0.20
HOMEBACKOFF(1) = 10.00

' Axis 1 idle conditions
IDLEPOS(1) = 0.20
IDLEVEL(1) = 5000.00
IDLETIME(1) = 0
IDLEMODE(1) = 0

' --------------------------------
' Axis 2 configuration
' --------------------------------
AXISCHANNEL(2) = 2
CONFIG(2) = _cfVIRTUAL
```

```
' Axis 2 scaling
SCALEFACTOR(2) = 1.00

' Axis 2 limits
SOFTLIMITMODE(2) = _emIGNORE
LIMITMODE(2) = _emCRASH_STOP_DISABLE
LIMITFORWARDINPUT(2) = -1
LIMITREVERSEINPUT(2) = -1
FOLERRORMODE(2) = _emCRASH_STOP_DISABLE
FOLERRORFATAL(2) = 1000.00

' Axis 2 error modes
ERRORINPUT(2) = -1
ERRORINPUTMODE(2) = _emCRASH_STOP_DISABLE
ABORTMODE(2) = _emCRASH_STOP_DISABLE
ADCERRORMODE(2) = _emCRASH_STOP_DISABLE

' Axis 2 digital input events
STOPINPUT(2) = -1
STOPINPUTMODE(2) = _emIGNORE

' Axis 2 digital outputs
DRIVEENABLEOUTPUT(2) = -1

' Axis 2 gain terms
KPROP(2) = 0.00
KINT(2) = 0.00
KINTLIMIT(2) = 100.00
KINTMODE(2) = _itALWAYS
KDERIV(2) = 0.00
KVEL(2) = 0.00
KVELFF(2) = 0.00
KACCEL(2) = 0.00

' Axis 2 profile parameters
PROFILEMODE(2) = _pmTRAPEZOIDAL
SPEED(2) = 40000.00
ACCEL(2) = 300000.00
DECEL(2) = 300000.00
ERRORDECEL(2) = 300000.00
ACCELJERK(2) = 3000000.00
DECELJERK(2) = 3000000.00
MOVEBUFFERSIZE(2) = 2

' Axis 2 homing parameters
HOMEINPUT(2) = -1
HOMESPEED(2) = 1000.00
HOMEBACKOFF(2) = 10.00

' Axis 2 idle conditions
IDLEPOS(2) = 1000.00
IDLEVEL(2) = 5000.00
IDLETIME(2) = 0
IDLEMODE(2) = 0

' --------------------------------
' Axis 3 configuration
' --------------------------------
AXISCHANNEL(3) = 3
CONFIG(3) = _cfVIRTUAL
```

```
' Axis 3 scaling
SCALEFACTOR(3) = 1.00

' Axis 3 limits
SOFTLIMITMODE(3) = _emIGNORE
LIMITMODE(3) = _emCRASH_STOP_DISABLE
LIMITFORWARDINPUT(3) = -1
LIMITREVERSEINPUT(3) = -1
FOLERRORMODE(3) = _emCRASH_STOP_DISABLE
FOLERRORFATAL(3) = 1000.00

' Axis 3 error modes
ERRORINPUT(3) = -1
ERRORINPUTMODE(3) = _emCRASH_STOP_DISABLE
ABORTMODE(3) = _emCRASH_STOP_DISABLE
ADCERRORMODE(3) = _emCRASH_STOP_DISABLE

' Axis 3 digital input events
STOPINPUT(3) = -1
STOPINPUTMODE(3) = _emIGNORE

' Axis 3 digital outputs
DRIVEENABLEOUTPUT(3) = -1

' Axis 3 gain terms
KPROP(3) = 0.00
KINT(3) = 0.00
KINTLIMIT(3) = 100.00
KINTMODE(3) = _itALWAYS
KDERIV(3) = 0.00
KVEL(3) = 0.00
KVELFF(3) = 0.00
KACCEL(3) = 0.00

' Axis 3 profile parameters
PROFILEMODE(3) = _pmTRAPEZOIDAL
SPEED(3) = 40000.00
ACCEL(3) = 300000.00
DECEL(3) = 300000.00
ERRORDECEL(3) = 300000.00
ACCELJERK(3) = 3000000.00
DECELJERK(3) = 3000000.00
MOVEBUFFERSIZE(3) = 2

' Axis 3 homing parameters
HOMEINPUT(3) = -1
HOMESPEED(3) = 1000.00
HOMEBACKOFF(3) = 10.00

' Axis 3 idle conditions
IDLEPOS(3) = 1000.00
IDLEVEL(3) = 5000.00
IDLETIME(3) = 0
IDLEMODE(3) = 0

' --------------------------------
' Axis 4 configuration
' --------------------------------
AXISCHANNEL(4) = 0
CONFIG(4) = _cfVIRTUAL
```

```
' Axis 4 scaling
SCALEFACTOR(4) = 1.00

' Axis 4 limits
SOFTLIMITMODE(4) = _emIGNORE
LIMITMODE(4) = _emCRASH_STOP_DISABLE
LIMITFORWARDINPUT(4) = -1
LIMITREVERSEINPUT(4) = -1
FOLERRORMODE(4) = _emCRASH_STOP_DISABLE
FOLERRORFATAL(4) = 1000.00

' Axis 4 error modes
ERRORINPUT(4) = -1
ERRORINPUTMODE(4) = _emCRASH_STOP_DISABLE
ABORTMODE(4) = _emCRASH_STOP_DISABLE
ADCERRORMODE(4) = _emCRASH_STOP_DISABLE

' Axis 4 digital input events
STOPINPUT(4) = -1
STOPINPUTMODE(4) = _emIGNORE

' Axis 4 digital outputs
DRIVEENABLEOUTPUT(4) = -1

' Axis 4 gain terms
KPROP(4) = 0.00
KINT(4) = 0.00
KINTLIMIT(4) = 100.00
KINTMODE(4) = _itALWAYS
KDERIV(4) = 0.00
KVEL(4) = 0.00
KVELFF(4) = 0.00
KACCEL(4) = 0.00

' Axis 4 profile parameters
PROFILEMODE(4) = _pmTRAPEZOIDAL
SPEED(4) = 40000.00
ACCEL(4) = 300000.00
DECEL(4) = 300000.00
ERRORDECEL(4) = 300000.00
ACCELJERK(4) = 3000000.00
DECELJERK(4) = 3000000.00
MOVEBUFFERSIZE(4) = 2

' Axis 4 homing parameters
HOMEINPUT(4) = -1
HOMESPEED(4) = 1000.00
HOMEBACKOFF(4) = 10.00

' Axis 4 idle conditions
IDLEPOS(4) = 1000.00
IDLEVEL(4) = 5000.00
IDLETIME(4) = 0
IDLEMODE(4) = 0

' --------------------------------
' Axis 5 configuration
' --------------------------------
AXISCHANNEL(5) = 1
CONFIG(5) = _cfVIRTUAL
```

```
' Axis 5 scaling
SCALEFACTOR(5) = 1.00

' Axis 5 limits
SOFTLIMITMODE(5) = _emIGNORE
LIMITMODE(5) = _emCRASH_STOP_DISABLE
LIMITFORWARDINPUT(5) = -1
LIMITREVERSEINPUT(5) = -1
FOLERRORMODE(5) = _emCRASH_STOP_DISABLE
FOLERRORFATAL(5) = 1000.00

' Axis 5 error modes
ERRORINPUT(5) = -1
ERRORINPUTMODE(5) = _emCRASH_STOP_DISABLE
ABORTMODE(5) = _emCRASH_STOP_DISABLE
ADCERRORMODE(5) = _emCRASH_STOP_DISABLE

' Axis 5 digital input events
STOPINPUT(5) = -1
STOPINPUTMODE(5) = _emIGNORE

' Axis 5 digital outputs
DRIVEENABLEOUTPUT(5) = -1

' Axis 5 gain terms
KPROP(5) = 0.00
KINT(5) = 0.00
KINTLIMIT(5) = 100.00
KINTMODE(5) = _itALWAYS
KDERIV(5) = 0.00
KVEL(5) = 0.00
KVELFF(5) = 0.00
KACCEL(5) = 0.00

' Axis 5 profile parameters
PROFILEMODE(5) = _pmTRAPEZOIDAL
SPEED(5) = 40000.00
ACCEL(5) = 300000.00
DECEL(5) = 300000.00
ERRORDECEL(5) = 300000.00
ACCELJERK(5) = 3000000.00
DECELJERK(5) = 3000000.00
MOVEBUFFERSIZE(5) = 2

' Axis 5 homing parameters
HOMEINPUT(5) = -1
HOMESPEED(5) = 1000.00
HOMEBACKOFF(5) = 10.00

' Axis 5 idle conditions
IDLEPOS(5) = 1000.00
IDLEVEL(5) = 5000.00
IDLETIME(5) = 0
IDLEMODE(5) = 0

' Terminal configuration
TERMINALMODE(_TERM1) = 01
TERMINALMODE(_TERM2) = 01

'--------------------------------
' End WorkBench Generated Startup Code
```

```
  '---------------------------------

  ' Add user startup code here...

End Startup
```

APPENDIX D. STATISTICAL ANALYSIS

A number of repeated experiments were performed throughout this project and it was necessary to fit a straight line to the data from each of the repetitions using the least-squares fit method and then to combine the repetitions to get a weighted average fit. The method used is outlined below and was based on the work by Taylor (1997).

Least-squares fit to a straight line

The best fit line, $y = mx + c$, for data points $(x_1, y_1),\ldots,(x_N, y_N)$ has coefficients:

$$m = \frac{N\left(\sum x_i y_i\right) - \left(\sum x_i\right)\left(\sum y_i\right)}{\Delta}$$

$$c = \frac{\left(\sum x_i^2\right)\left(\sum y_i\right) - \left(\sum x_i\right)\left(\sum x_i y_i\right)}{\Delta}$$

where

$$\Delta = N\left(\sum x_i^2\right) - \left(\sum x_i\right)^2$$

Uncertainties in the coefficients m and c were calculated as:

$$\sigma_m = \sigma_y \sqrt{\frac{N}{\Delta}}$$

$$\sigma_c = \sigma_y \sqrt{\frac{\sum x^2}{\Delta}}$$

where

$$\sigma_y = \sqrt{\frac{1}{N-2}\sum_{i=1}^{N}\left(y_i - c - mx_i\right)^2}$$

Weighted average of the straight line coefficients

The best fits for each repetition were combined and the weighted average straight line coefficients, m_{wav} and c_{wav}, were calculated as:

$$m_{wav} = \frac{\sum w_{m,i} m_i}{\sum w_{m,i}} \quad , \quad c_{wav} = \frac{\sum w_{c,i} c_i}{\sum w_{c,i}}$$

where

$$w_{m,i} = \frac{1}{\sigma_{m,i}^2} \quad , \quad w_{c,i} = \frac{1}{\sigma_{c,i}^2}$$

The uncertainties in the weighted average coefficients m_{wav} and c_{wav} were calculated as:

$$\sigma_{m,wav} = \frac{1}{\sqrt{\sum w_{m,i}}} \quad , \quad \sigma_{c,wav} = \frac{1}{\sqrt{\sum w_{c,i}}}$$

MatLab algorithm

An algorithm was written in MatLab based these equations and is shown below:

```
%%
%Function to calculate the weighted average of the gradient and
%intercept for repeated experiments (for line y = mx + c).  X and Y
%are arranged such that each repetition is in a separate column.
%Mark Mitchell
%23/02/09
%%
function [m_wav, SD_m_wav, c_wav, SD_c_wav] = weighted_gradient (X,
Y)

%Loop through each repetition
for i = 1:size(X,2)

    N = length(X(:,i));
    sum_x2 = sum(X(:,i).^2);
    sum_x = sum(X(:,i));
    sum_y = sum(Y(:,i));
    sum_xy = sum(X(:,i).*Y(:,i));
    delta = (N * sum_x2) - sum_x^2;

    %Calculate the coefficients using the least-squares method
    m = ((N * sum_xy) - (sum_x * sum_y))/delta;
    c = ((sum_x2 * sum_y) - (sum_x * sum_xy))/delta;

    %Calculate the standard deviation of the coefficients
    SD_y = ((1/(N-2)) * sum((Y(:,i) - c - (X(:,i) * m)).^2))^0.5;
    SD_c = SD_y * ((sum_x2/delta)^0.5);
    SD_m = SD_y * ((N/delta)^0.5);
```

```
    %Write the coefficients and SDs of each repetition to an array
    M(i) = m;
    C(i) = c;
    SD_C(i) = SD_c;
    SD_M(i) = SD_m;

end

%Calculate the weighted average gradient, m, and its SD
wm = 1./(SD_M.^2);
sum_wm = sum(wm);
sum_wmm = sum(wm.*M);

m_wav = sum_wmm/sum_wm;
SD_m_wav = 1/(sum_wm^0.5);

%Calculate the weighted average intercept, c, and its SD
wc = 1./(SD_C.^2);
sum_wc = sum(wc);
sum_wcc = sum(wc.*C);

c_wav = sum_wcc/sum_wc;
SD_c_wav = 1/(sum_wc^0.5);
```

APPENDIX E. COMPLETE SET OF RESULTS FROM BIOLOGICAL VALIDATION EXPERIMENT

E.1 Linear friction data

The linear axis friction within each chamber was evaluated and is displayed in Figure E-1 to Figure E-4 below.

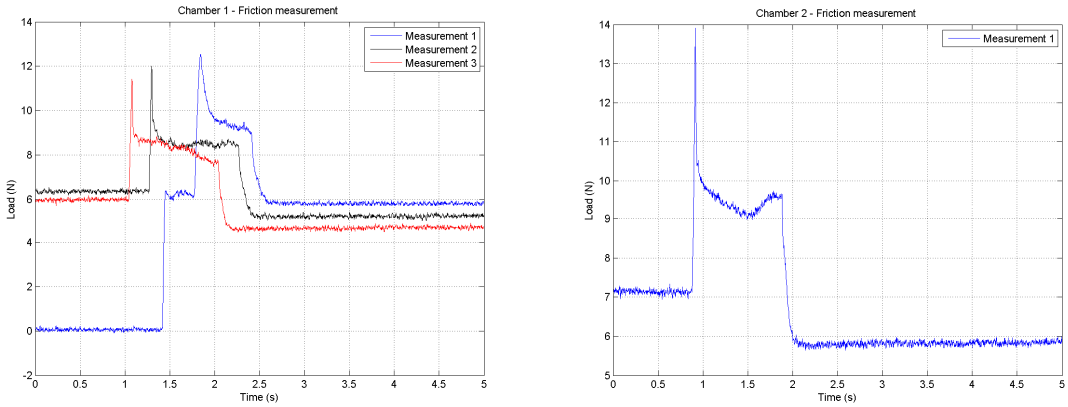

Figure E-1 Evaluation of linear friction for chambers 1 and 2

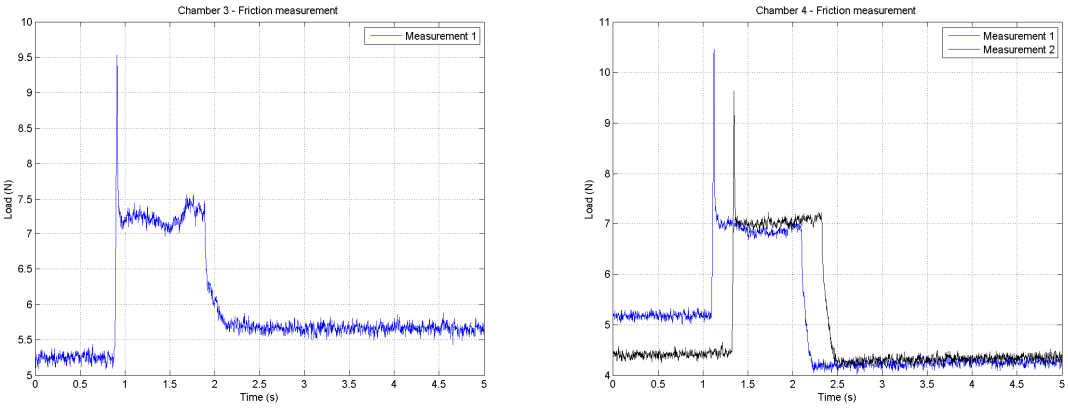

Figure E-2 Evaluation of linear friction for chambers 3 and 4

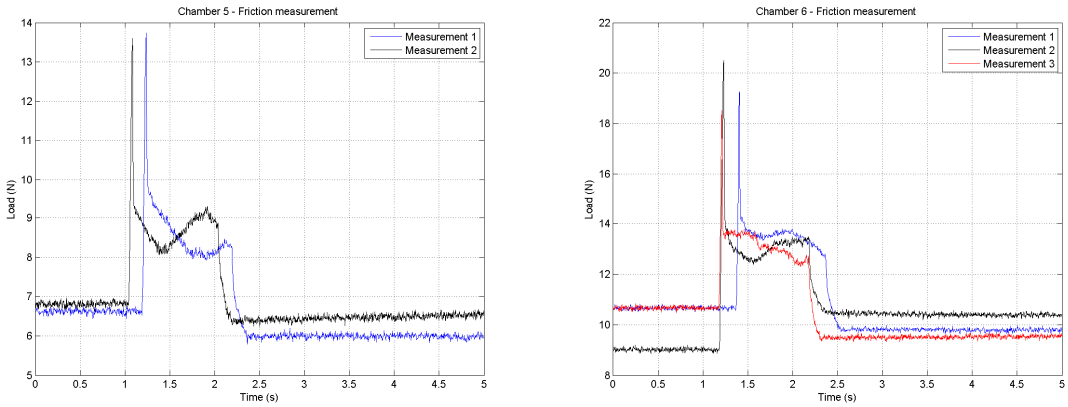

Figure E-3 Evaluation of linear friction for chambers 5 and 6

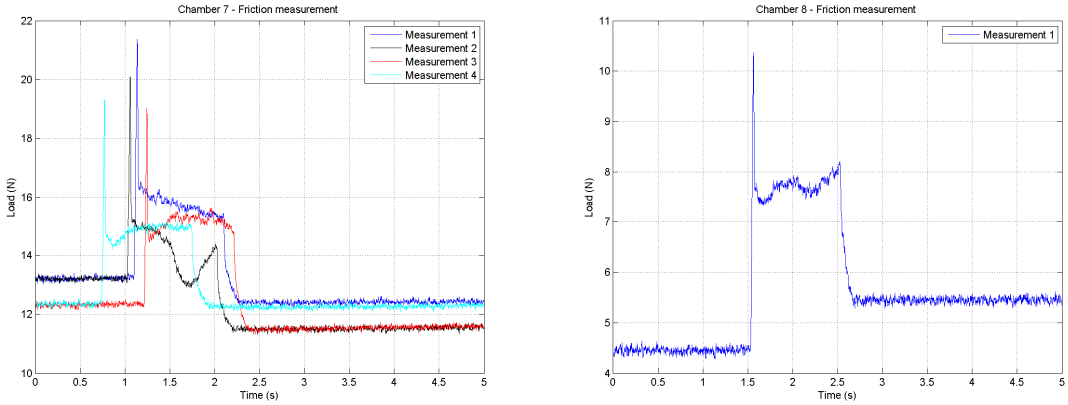

Figure E-4 Evaluation of linear friction for chambers 7 and 8

E.2 Preload data

A preload of 5N was applied to the tissue and the load profiles for each chamber are shown in Figure E-5 to Figure E-8 below.

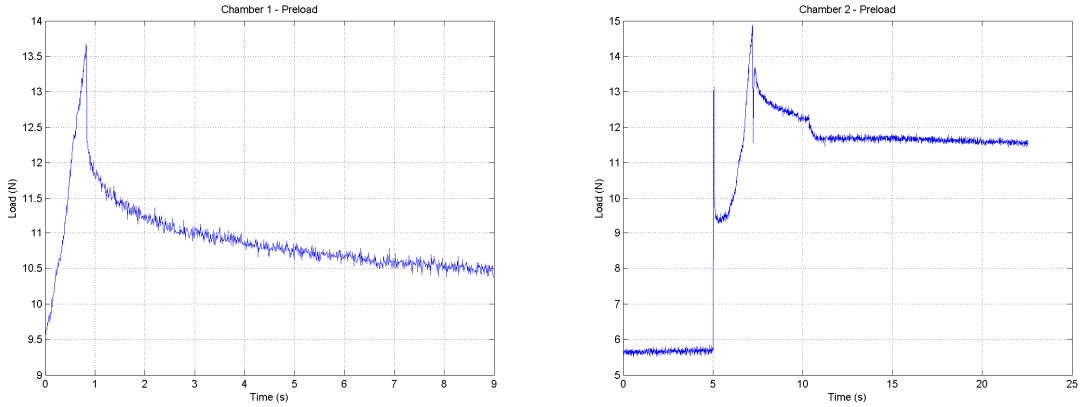

Figure E-5 Preload data for chambers 1 and 2

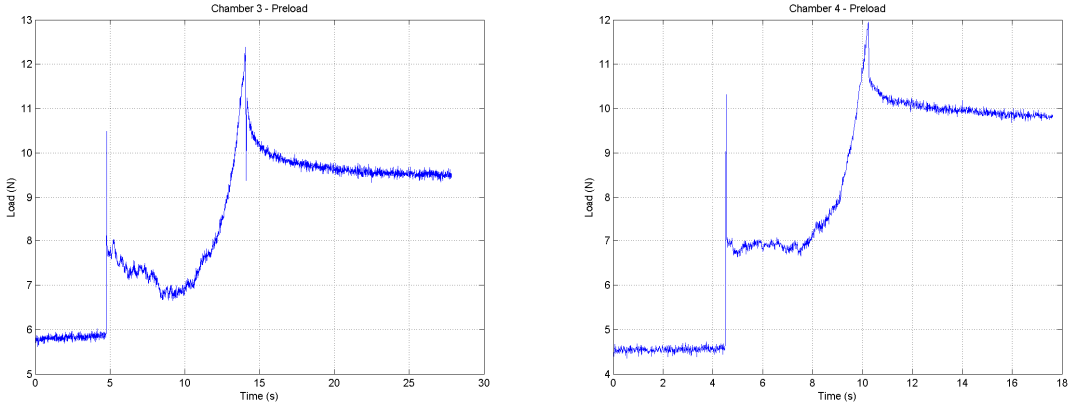

Figure E-6 Preload data for chambers 3 and 4

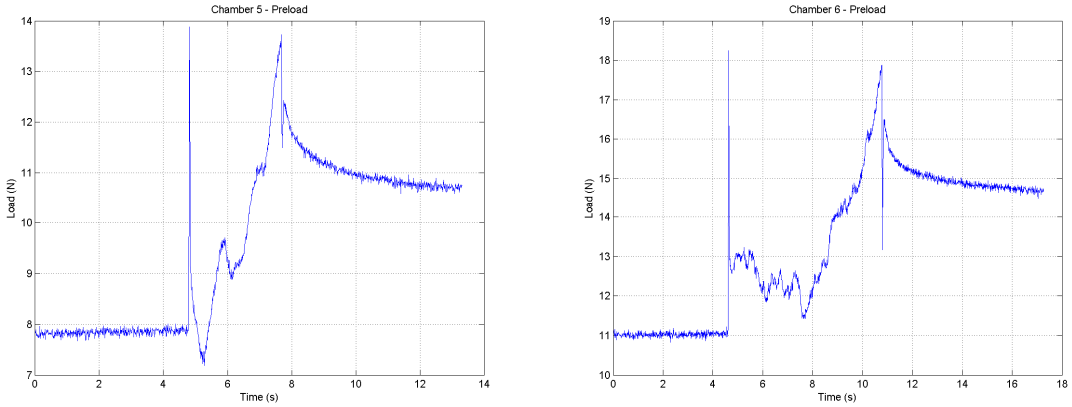

Figure E-7 Preload data for chambers 5 and 6

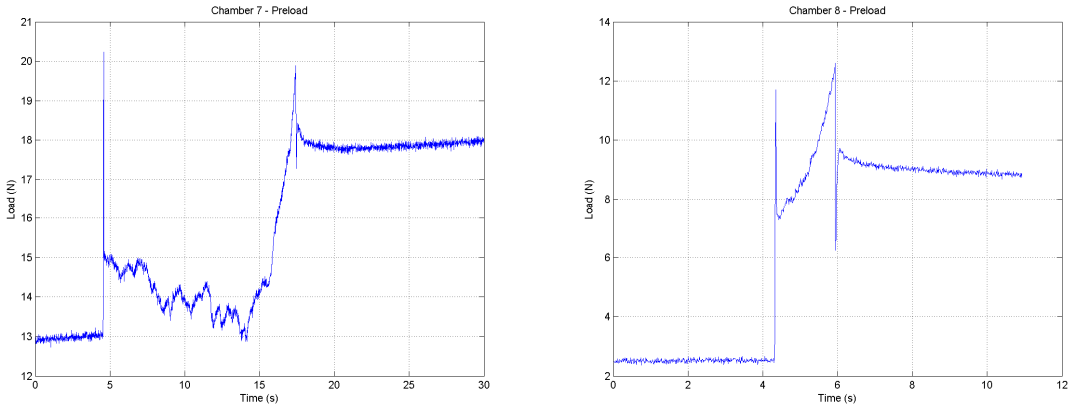

Figure E-8 Preload data for chambers 7 and 8

E.3 Displacement data

The displacement imposed on the four mechanically loaded chambers is shown in Figure E-9 to Figure E-12 to illustrate the repeatability of the displacement profile.

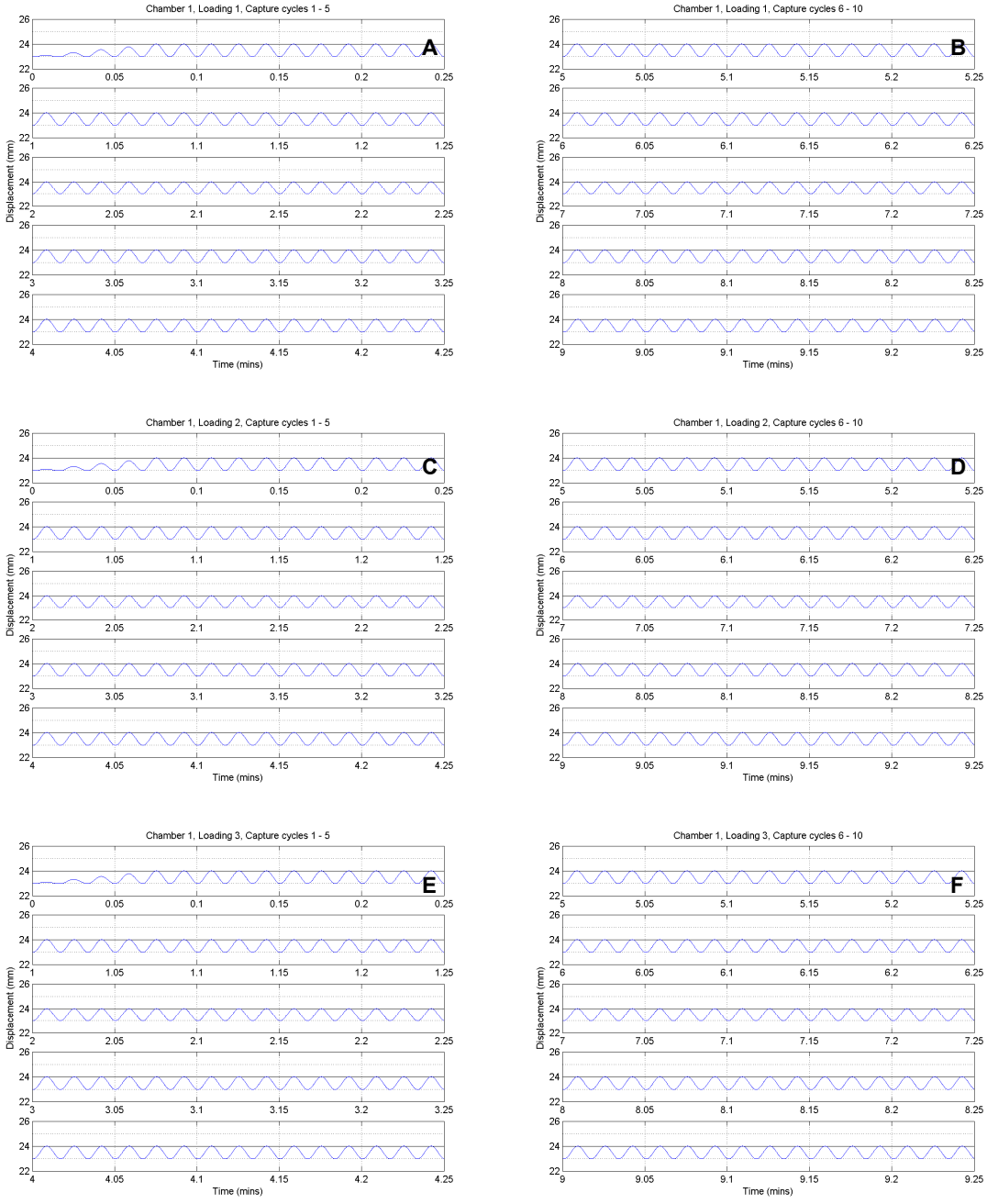

Figure E-9 Displacement plots for all loading sessions of chamber 1 (A-J)

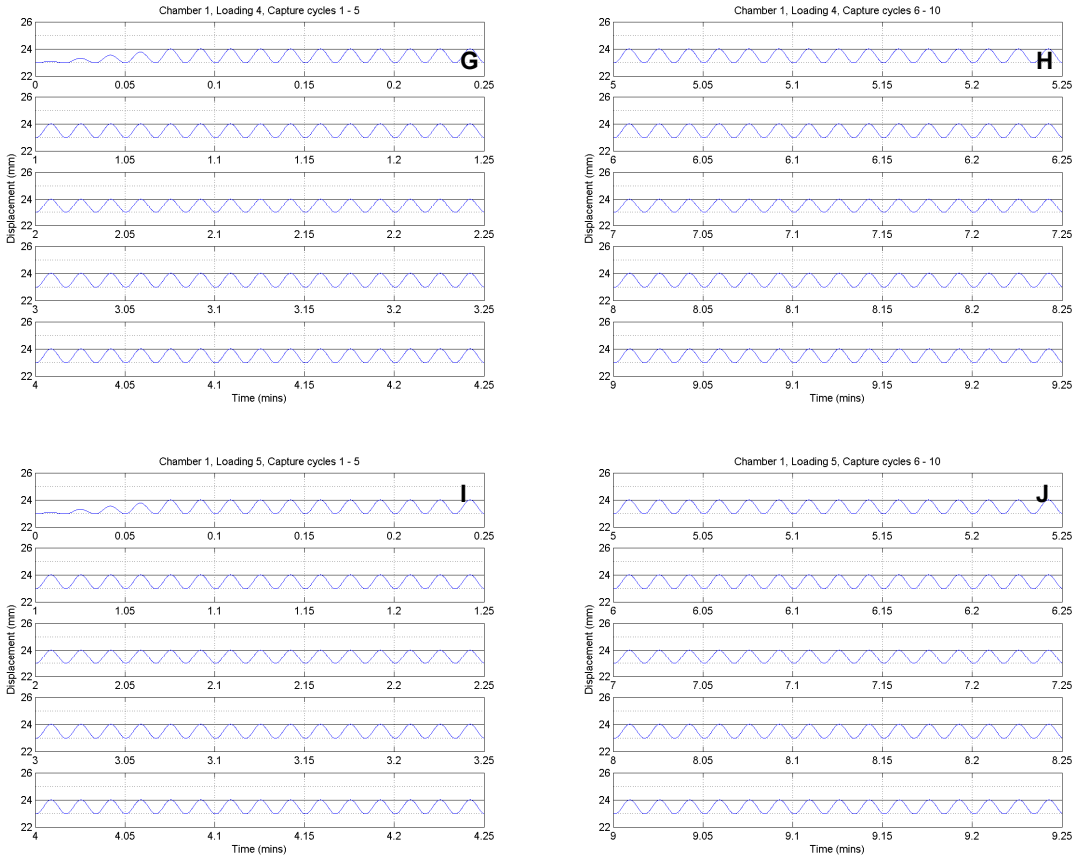

Figure E-9 cont. Displacement plots for all loading sessions of chamber 1 (A-J)

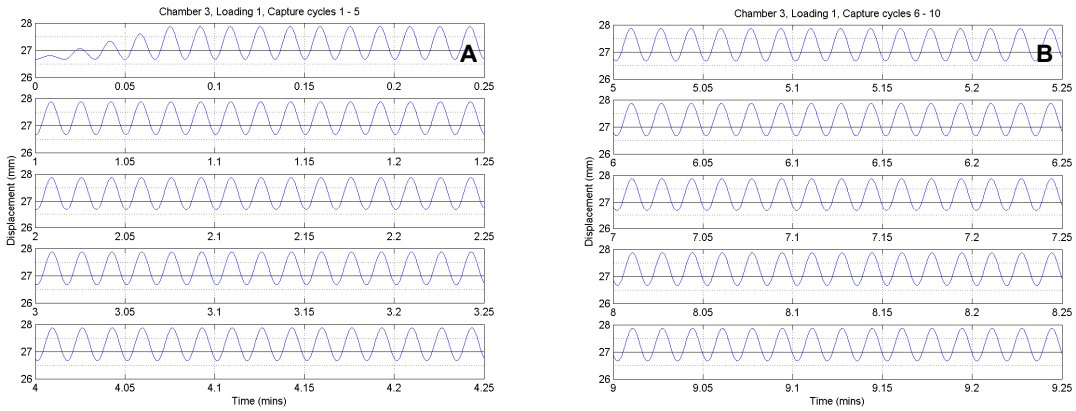

Figure E-10 Displacement plots for all loading sessions of chamber 3 (A-J)

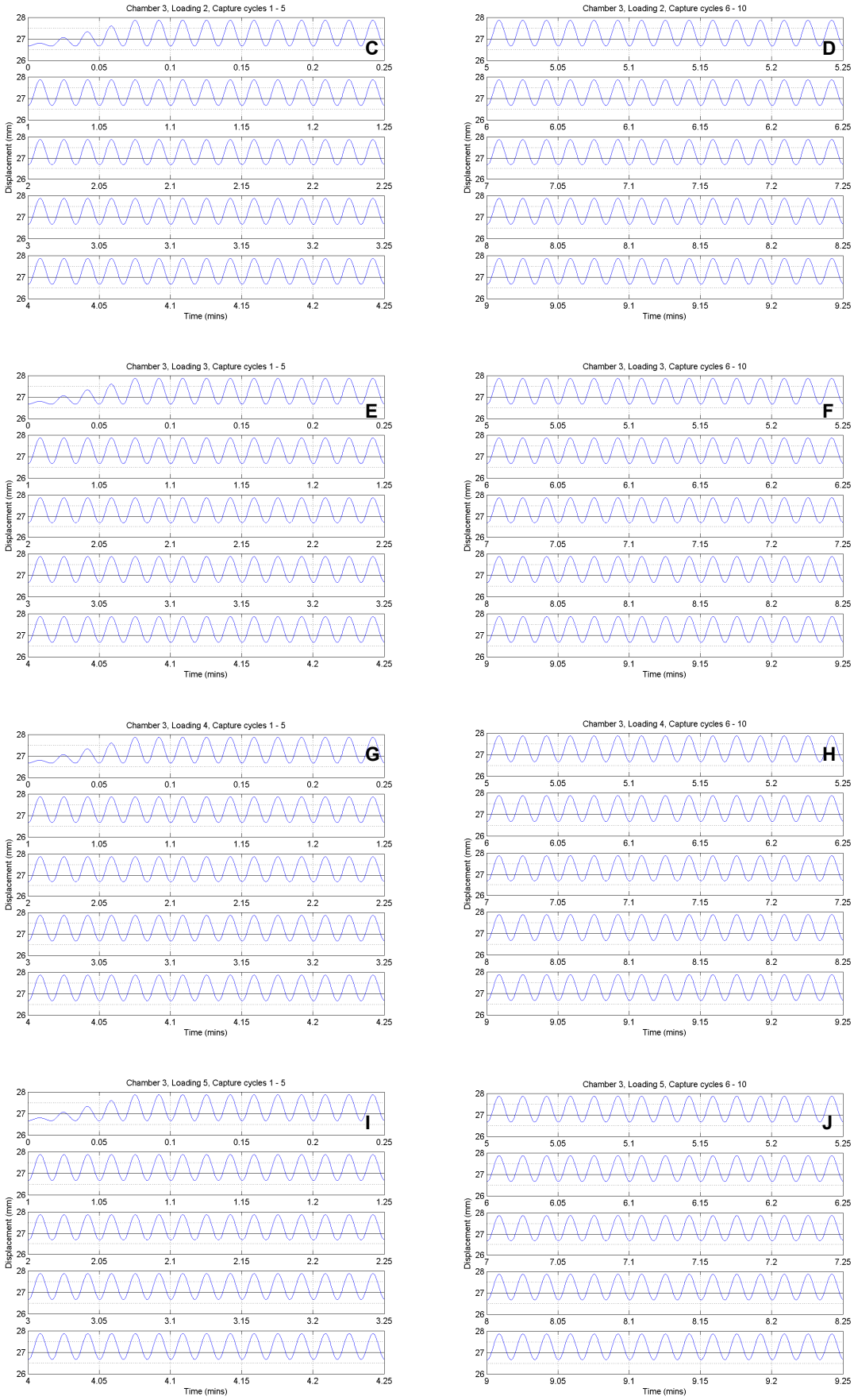

Figure E-10 cont. Displacement plots for all loading sessions of chamber 3 (A-J)

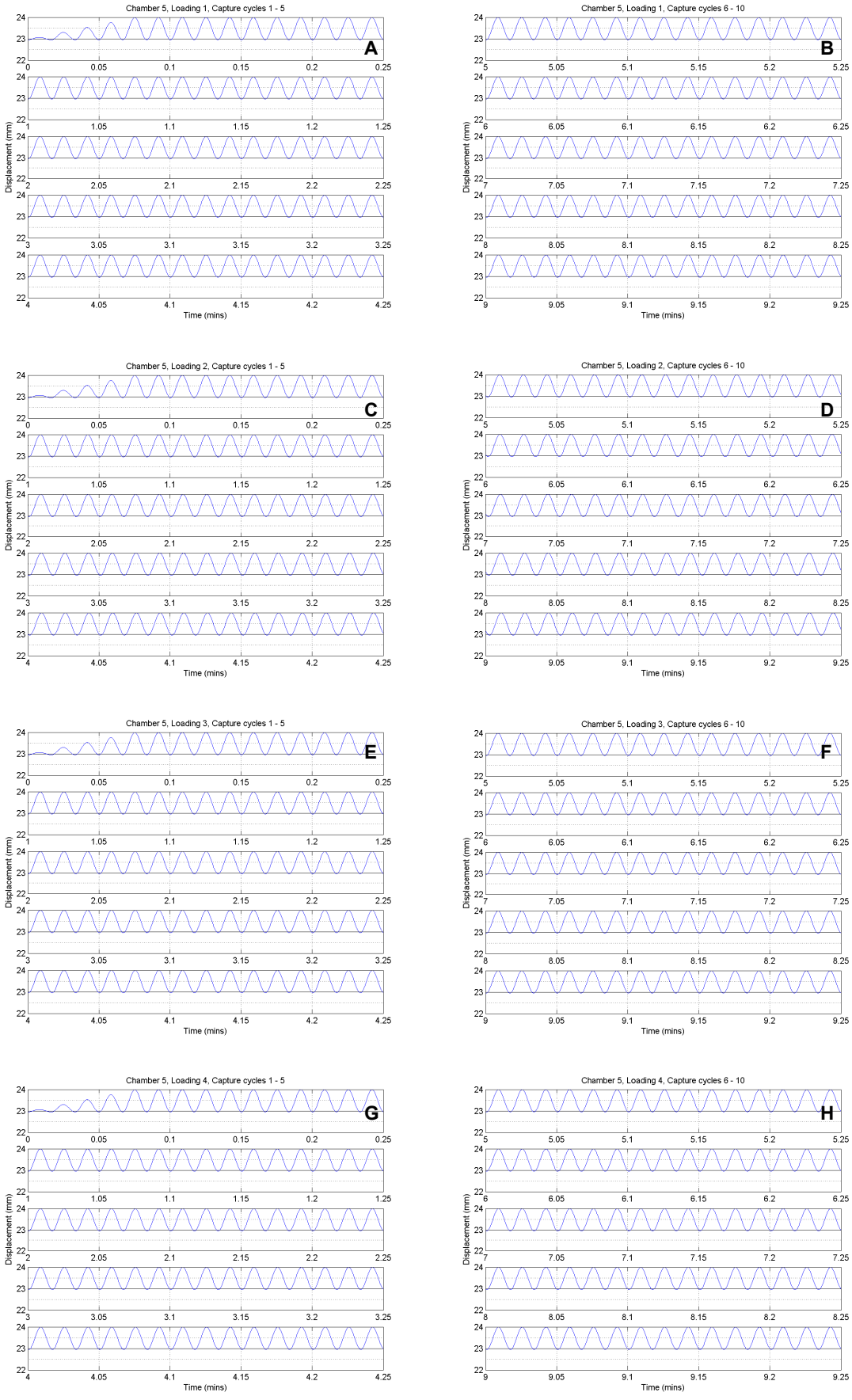

Figure E-11 Displacement plots for all loading sessions of chamber 5 (A-J)

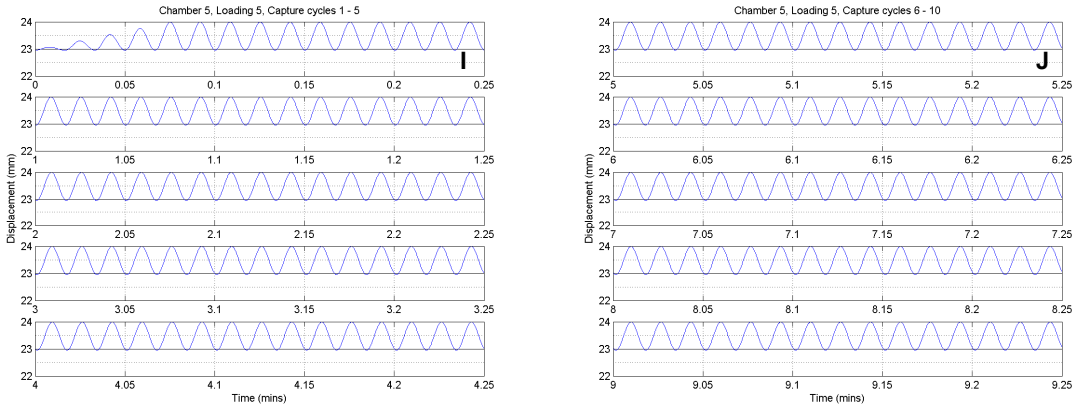

Figure E-11 cont. Displacement plots for all loading sessions of chamber 3 (A-J)

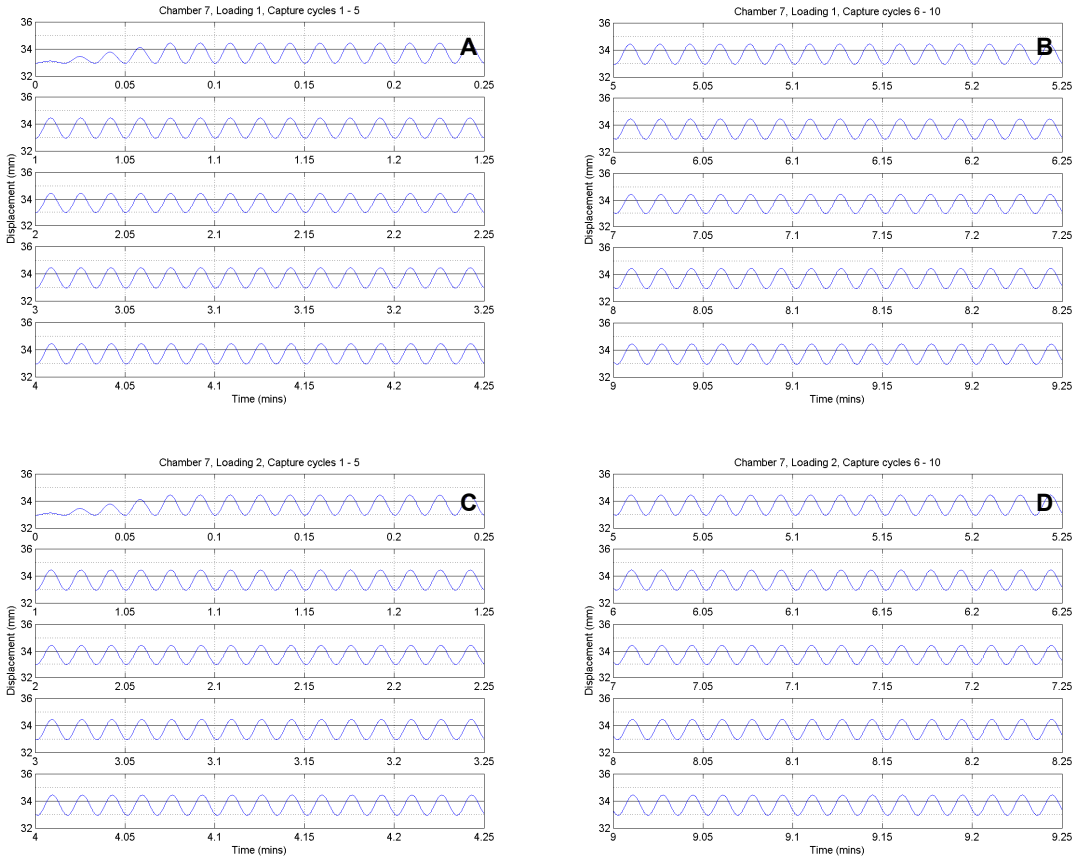

Figure E-12 Displacement plots for all loading sessions of chamber 7 (A-J)

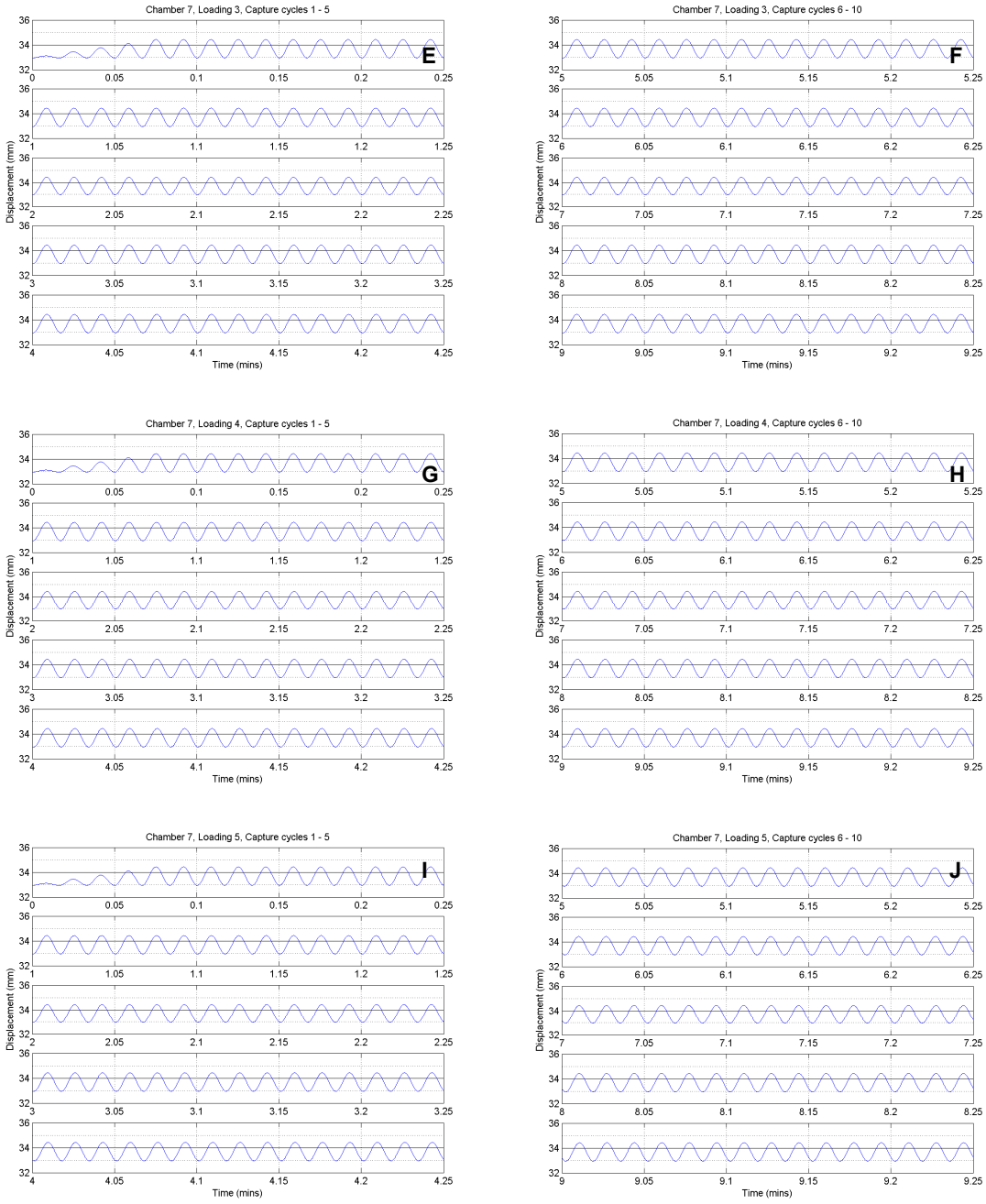

Figure E-12 cont. Figure E-12 Displacement plots for all loading sessions of chamber 7 (A-J)

E.4 Load data

The load experienced by the tissue due to the imposed displacement profile was recorded and is displayed in Figure E-13 to Figure E-16 below.

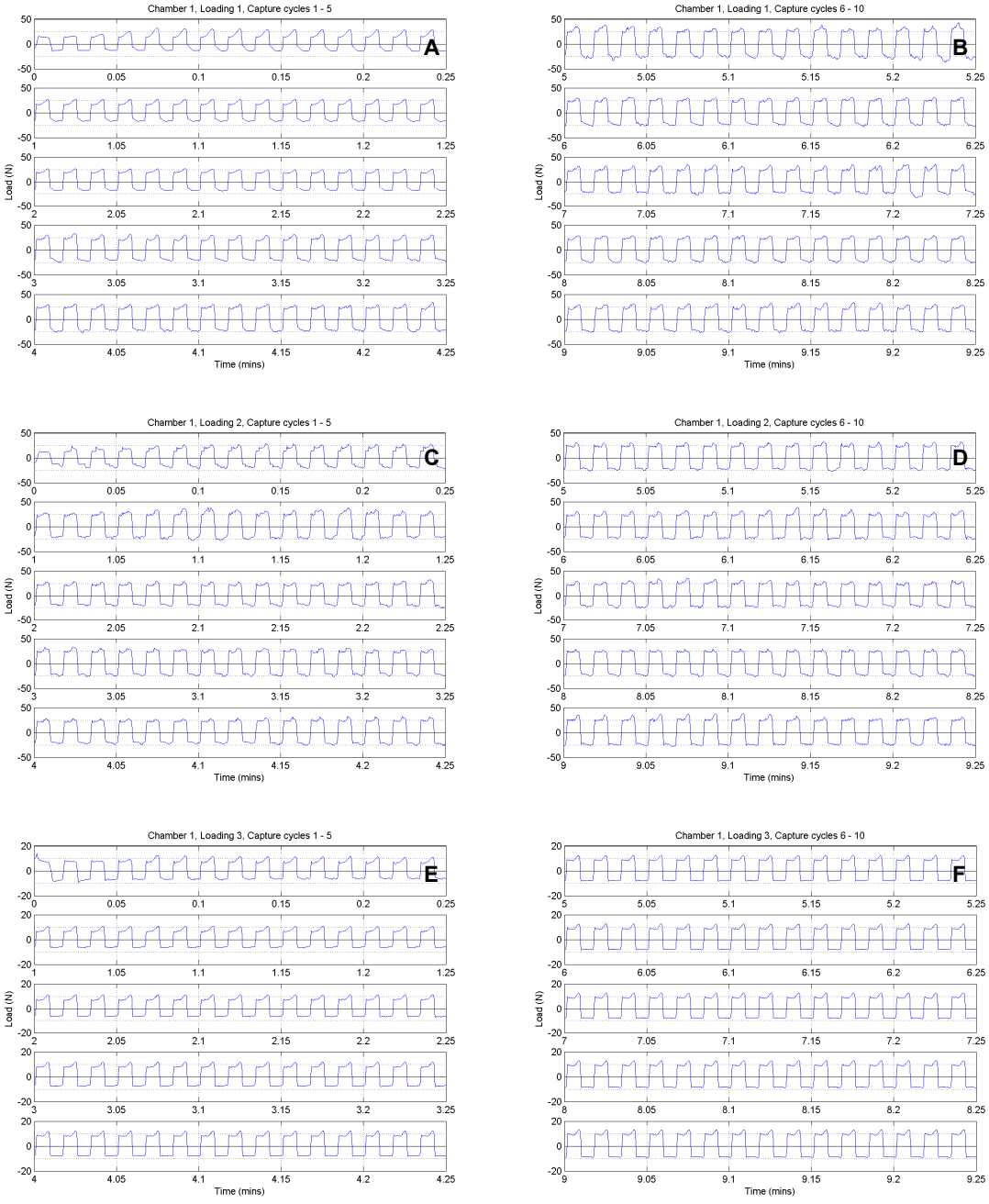

Figure E-13 Load variation for all loading sessions of chamber 1 (A-J)

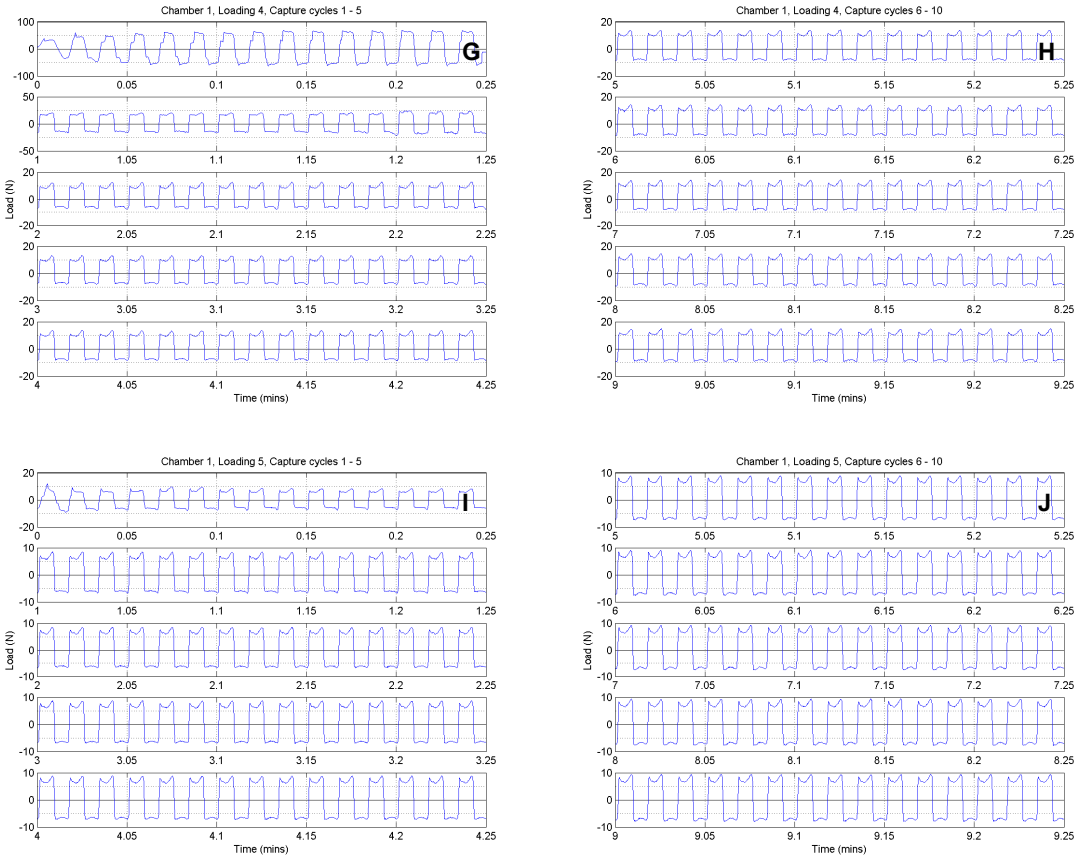

Figure E-13 cont. Figure E-13 Load variation for all loading sessions of chamber 1 (A-J)

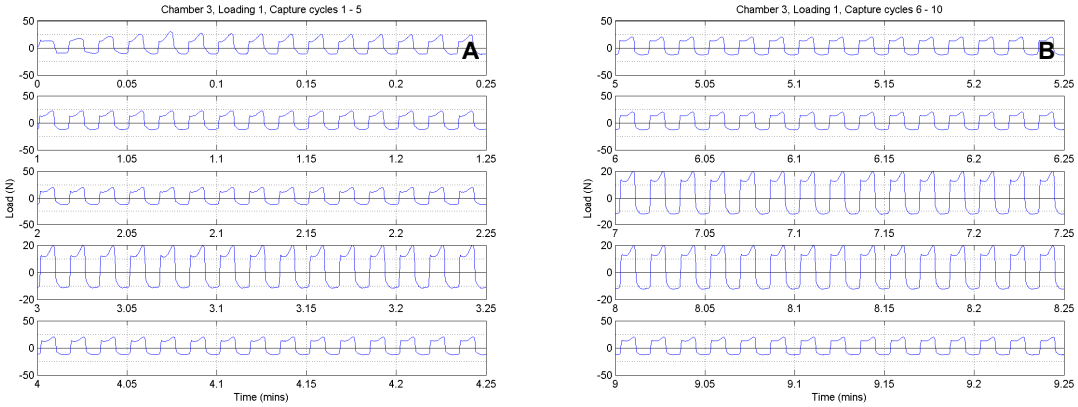

Figure E-14 Load variation for all loading sessions of chamber 3 (A-J)

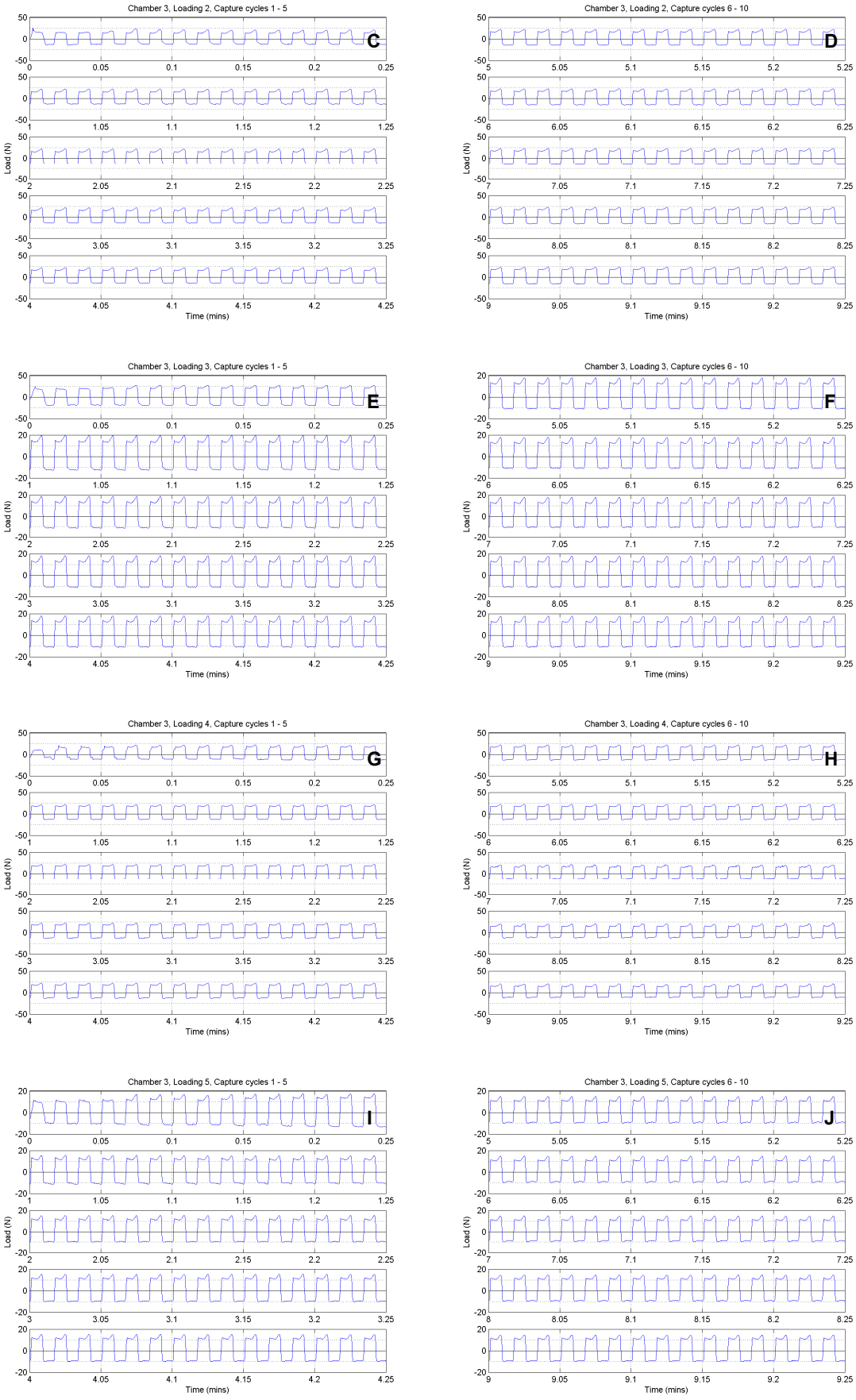

Figure E-14 cont. Figure E-14 Load variation for all loading sessions of chamber 3 (A-J)

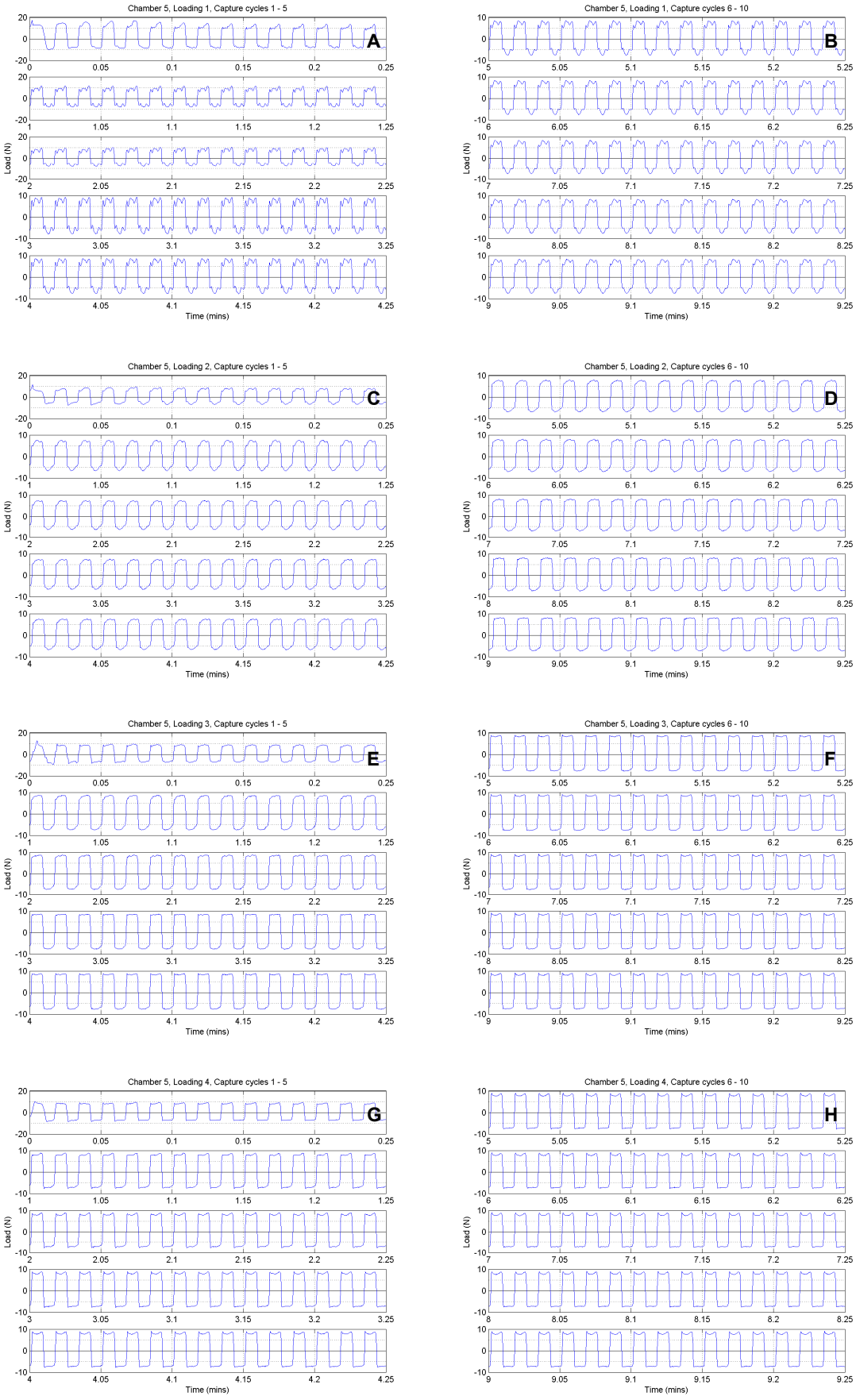

Figure E-15 Load variation for all loading sessions of chamber 5 (A-J)

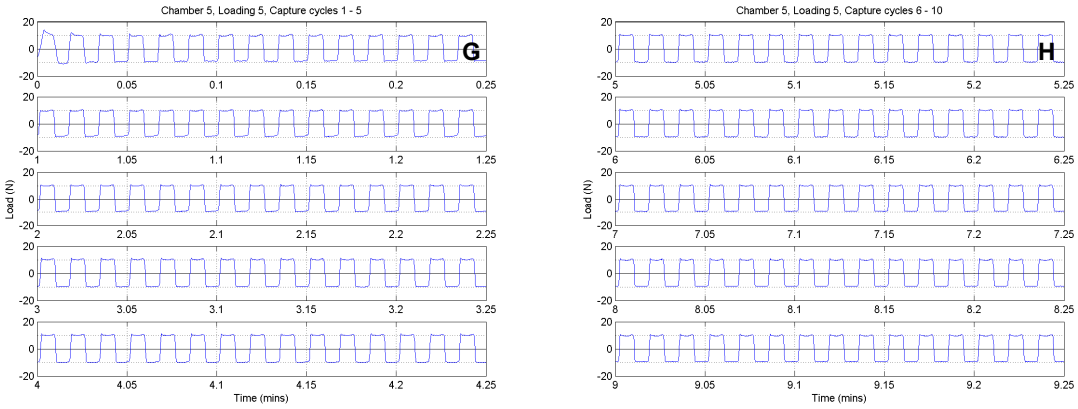

Figure E-15 cont. Figure E-15 Load variation for all loading sessions of chamber 5 (A-J)

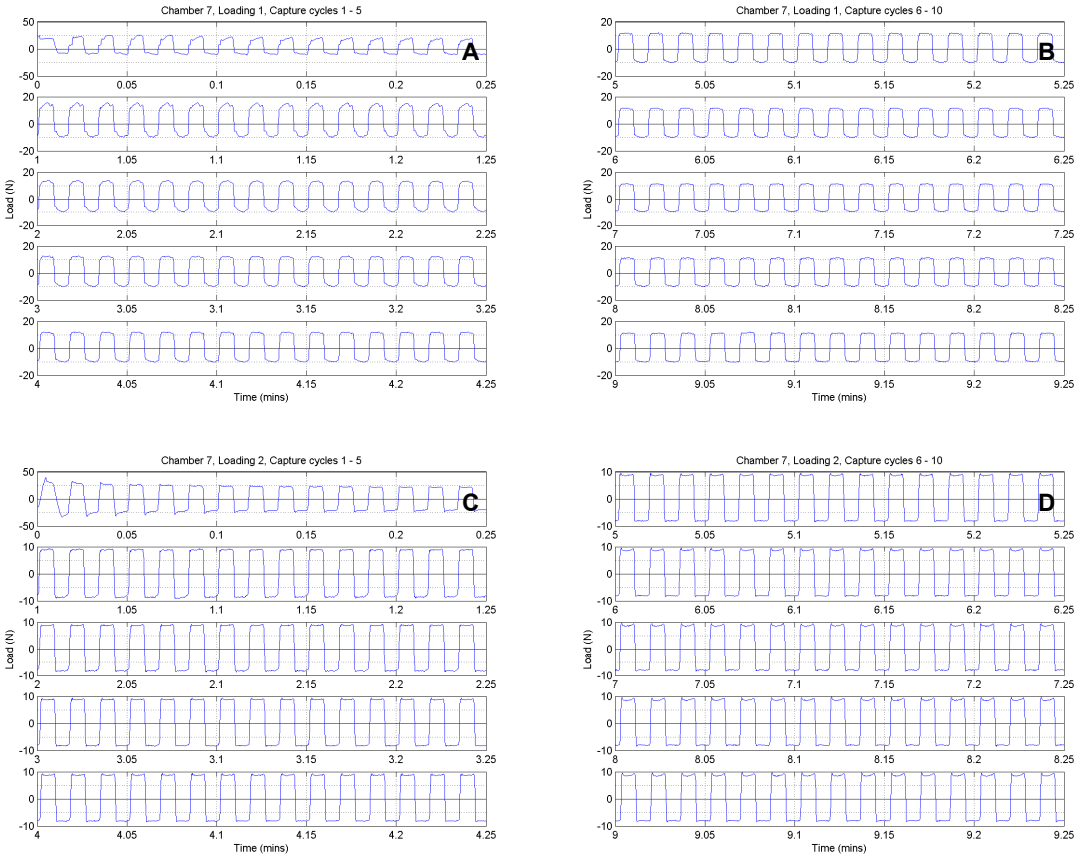

Figure E-16 Load variation for all loading sessions of chamber 7 (A-J)

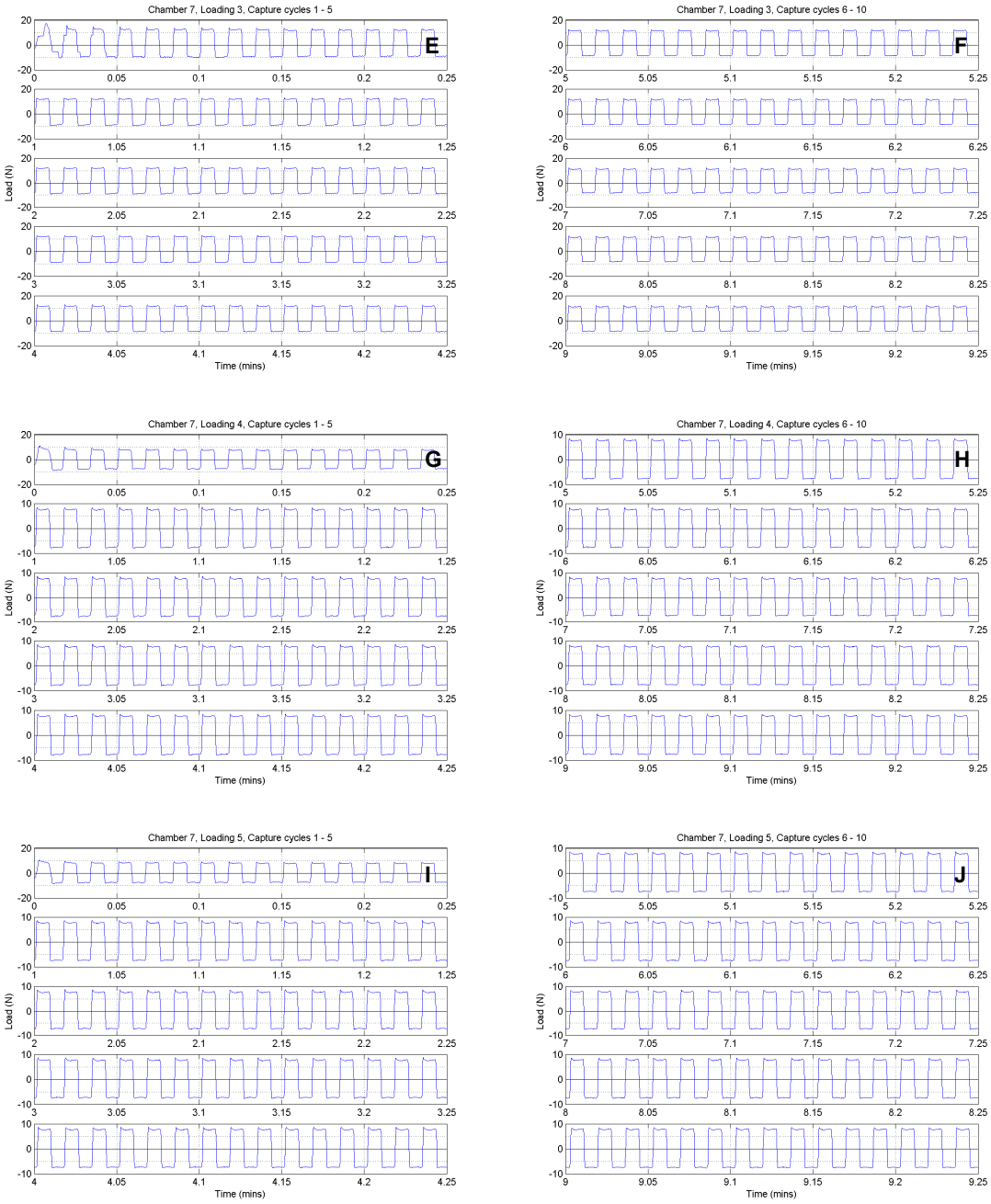

Figure E-16 cont. Figure E-16 Load variation for all loading sessions of chamber 7 (A-J)

E.5 Load-displacement data

The load was plotted against displacement for all the mechanically loaded chambers and the results are shown in Figure E-17 to Figure E-20 below.

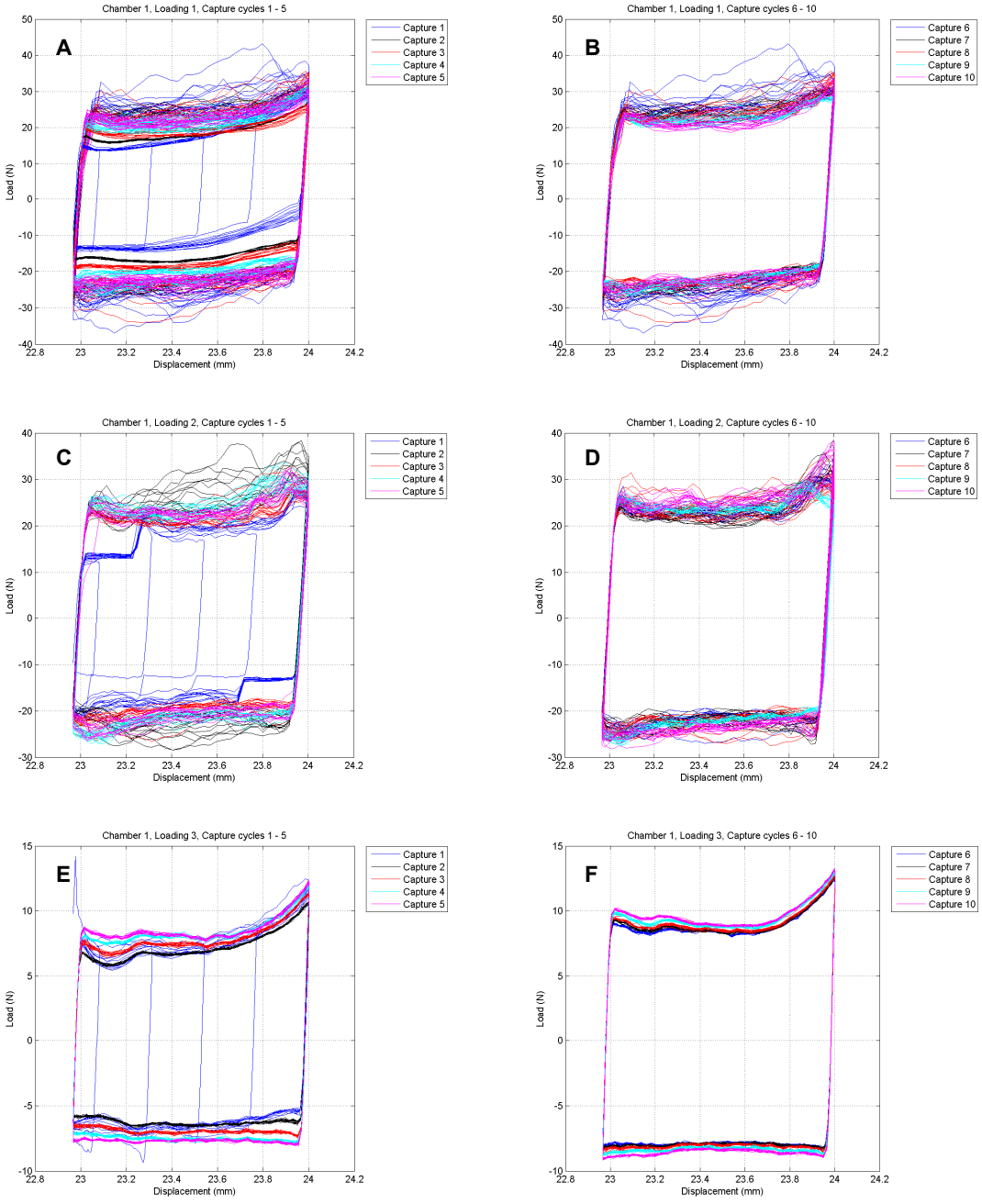

Figure E-17 Load against displacement for all loading sessions of chamber 1 (A-J)

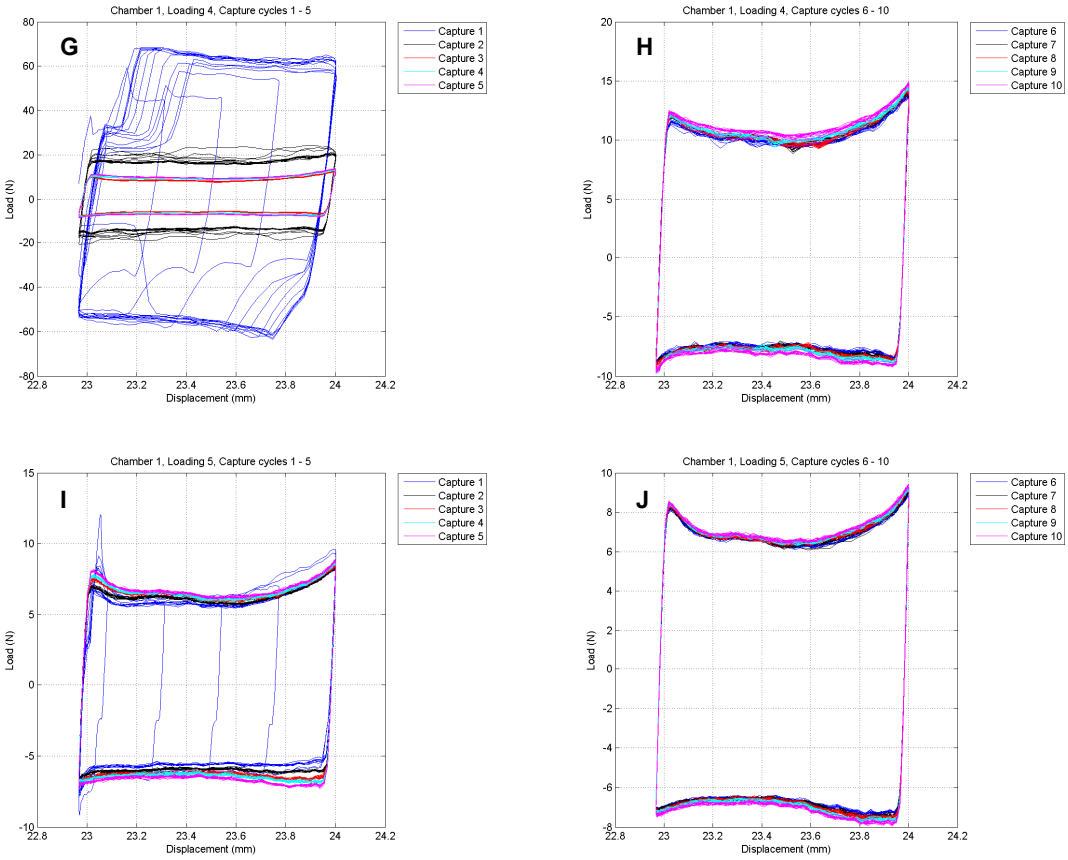

Figure E-17 cont. Load against displacement for all loading sessions of chamber 1 (A-J)

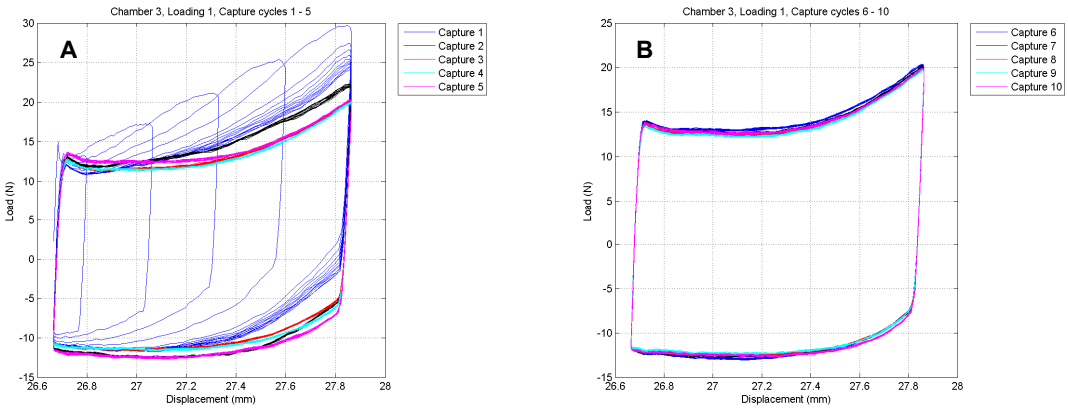

Figure E-18 Load against displacement for all loading sessions of chamber 3 (A-J)

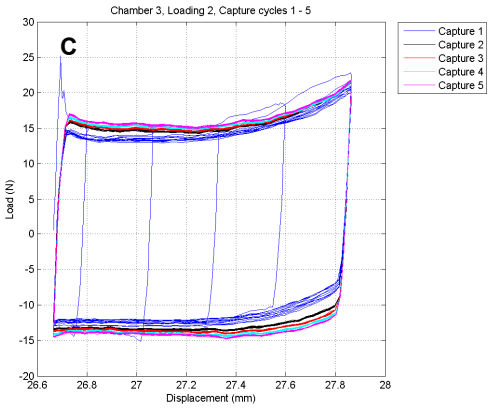
Chamber 3, Loading 2, Capture cycles 1 - 5
C
Capture 1
Capture 2
Capture 3
Capture 4
Capture 5
Load (N)
Displacement (mm)

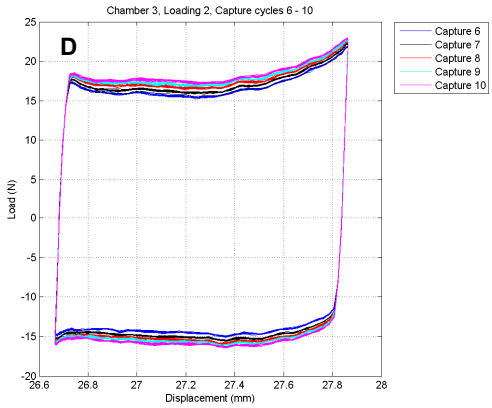
Chamber 3, Loading 2, Capture cycles 6 - 10
D
Capture 6
Capture 7
Capture 8
Capture 9
Capture 10
Load (N)
Displacement (mm)

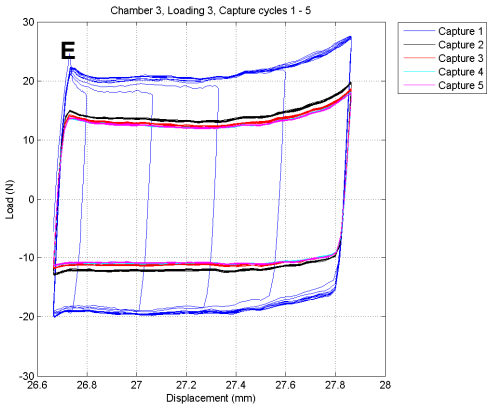
Chamber 3, Loading 3, Capture cycles 1 - 5
E
Capture 1
Capture 2
Capture 3
Capture 4
Capture 5
Load (N)
Displacement (mm)

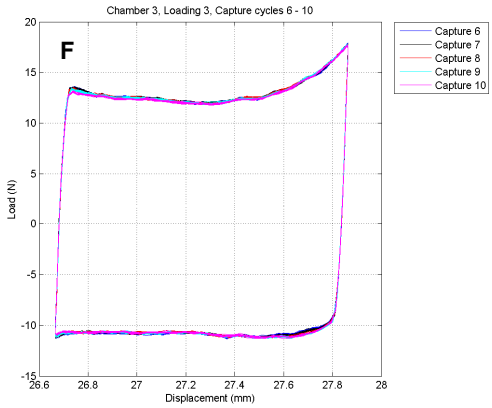
Chamber 3, Loading 3, Capture cycles 6 - 10
F
Capture 6
Capture 7
Capture 8
Capture 9
Capture 10
Load (N)
Displacement (mm)

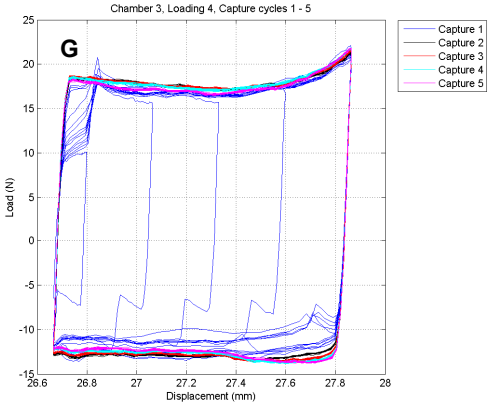
Chamber 3, Loading 4, Capture cycles 1 - 5
G
Capture 1
Capture 2
Capture 3
Capture 4
Capture 5
Load (N)
Displacement (mm)

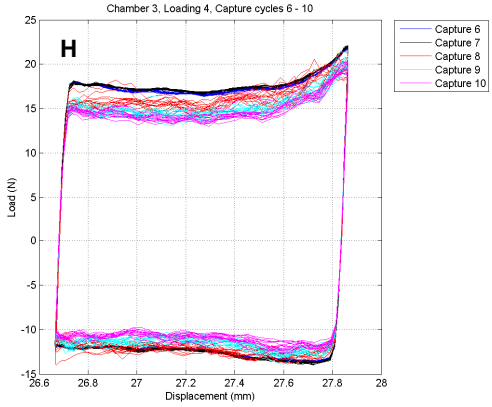
Chamber 3, Loading 4, Capture cycles 6 - 10
H
Capture 6
Capture 7
Capture 8
Capture 9
Capture 10
Load (N)
Displacement (mm)

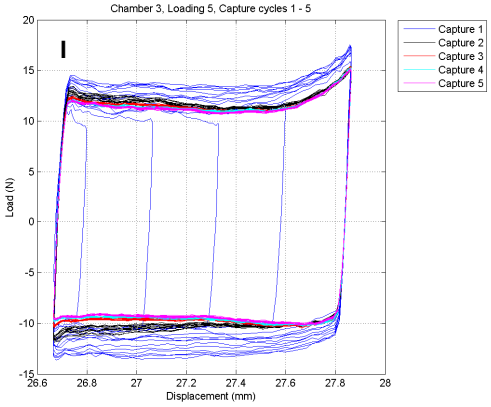
Chamber 3, Loading 5, Capture cycles 1 - 5
I
Capture 1
Capture 2
Capture 3
Capture 4
Capture 5
Load (N)
Displacement (mm)

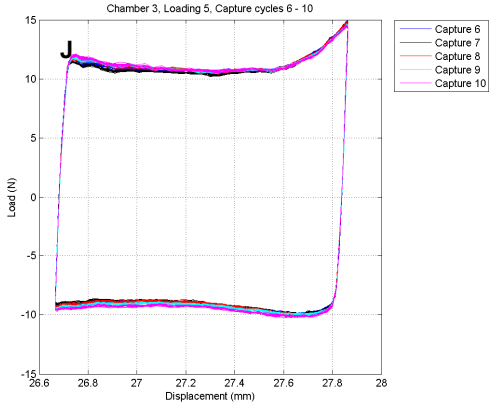
Chamber 3, Loading 5, Capture cycles 6 - 10
J
Capture 6
Capture 7
Capture 8
Capture 9
Capture 10
Load (N)
Displacement (mm)

Figure E-18 cont. Figure E-18 Load against displacement for all loading sessions of chamber 3 (A-J)

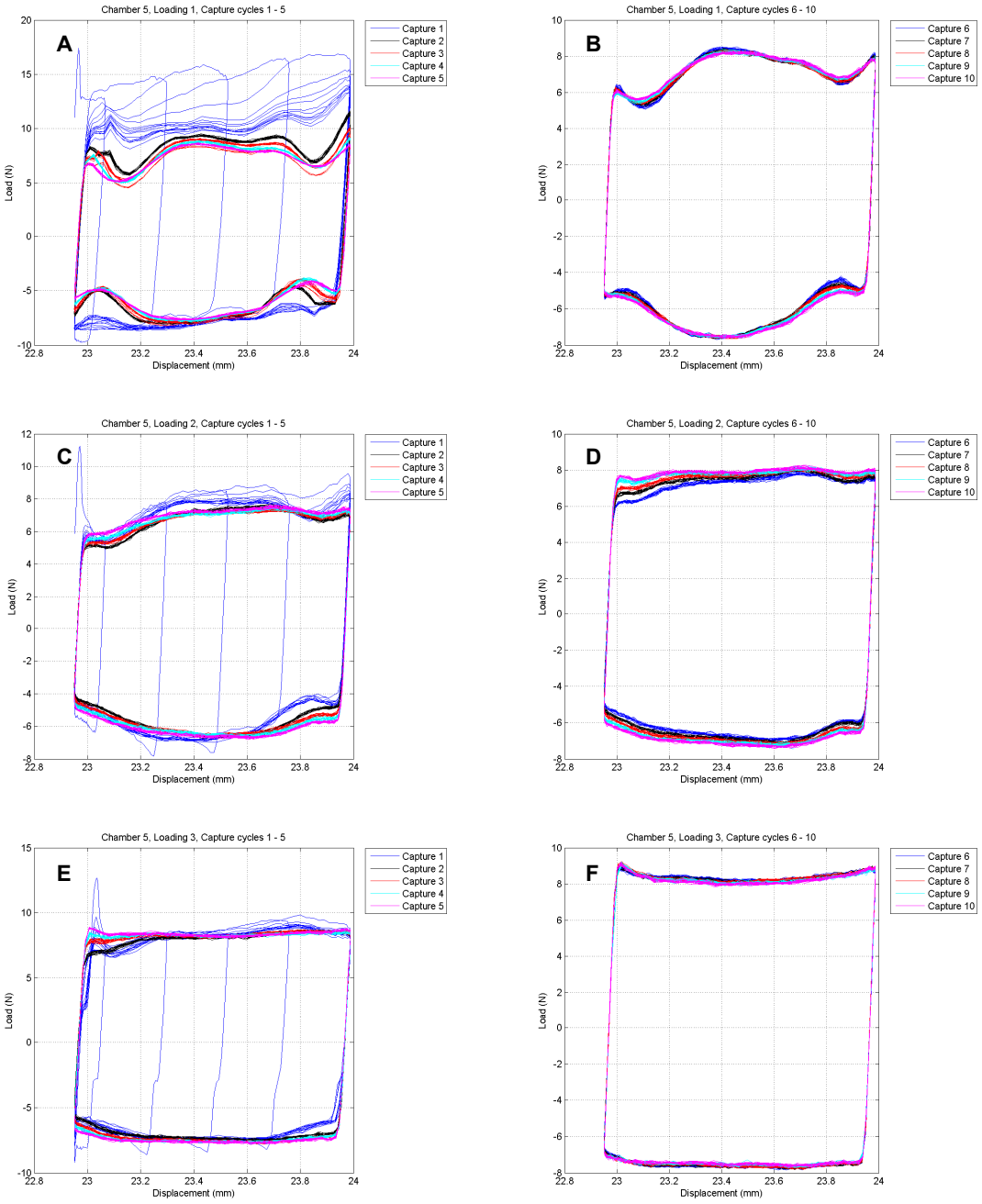

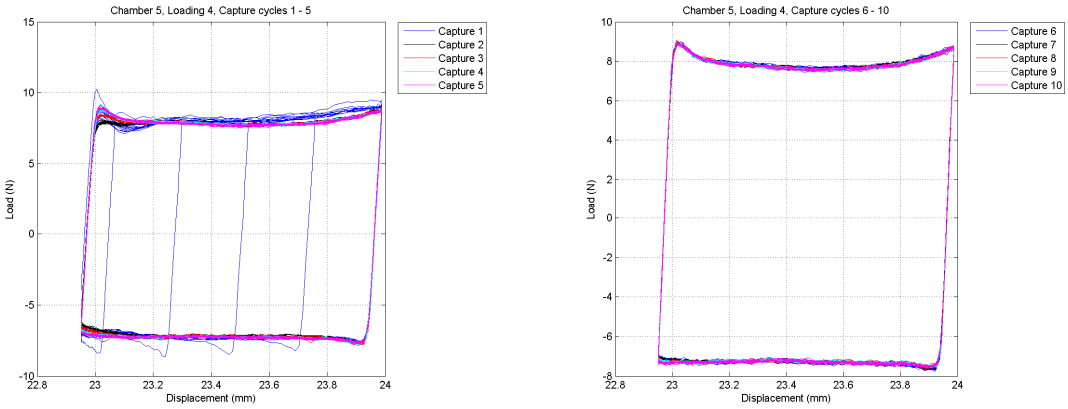

Figure E-19 Load against displacement for all loading sessions of chamber 5 (A-J)

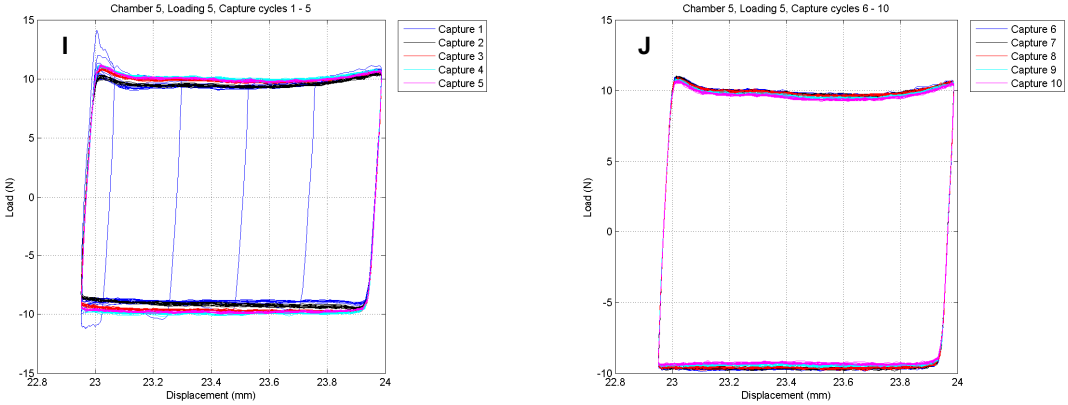

Figure E-19 cont. Figure E-19 Load against displacement for all loading sessions of chamber 5 (A-J)

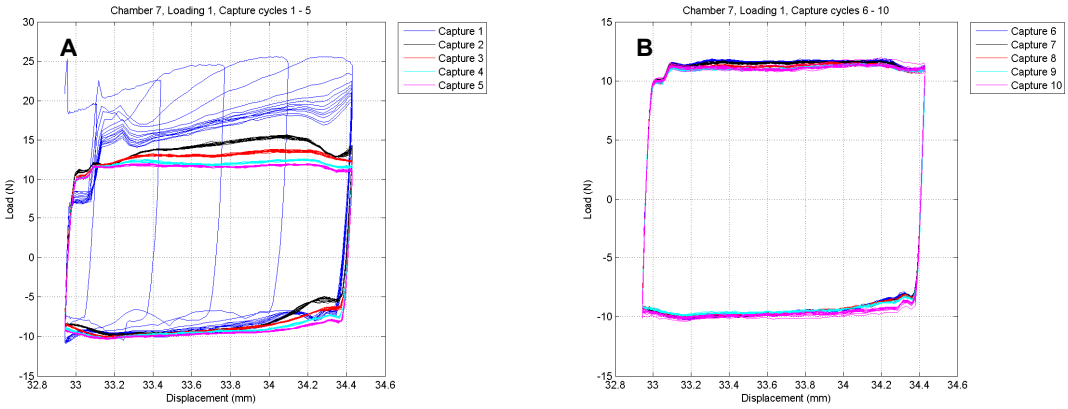

C **D**

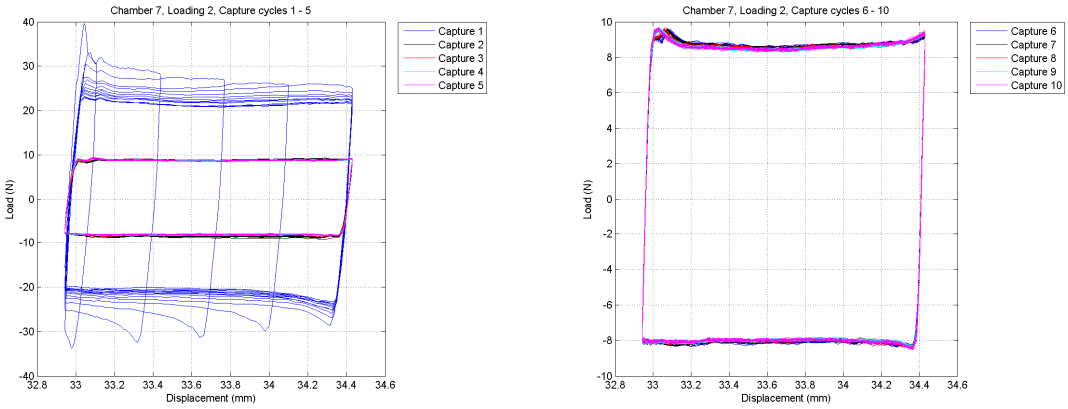

Figure E-20 Load against displacement for all loading sessions of chamber 7 (A-J)

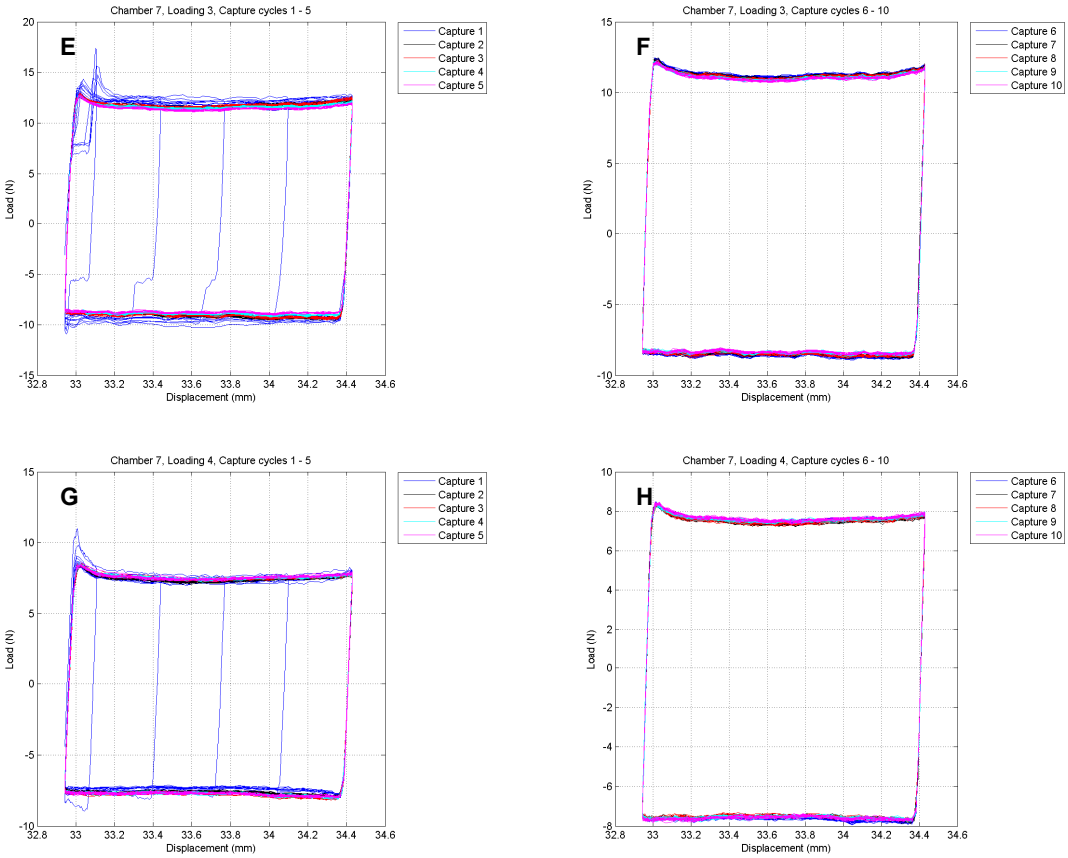

I J

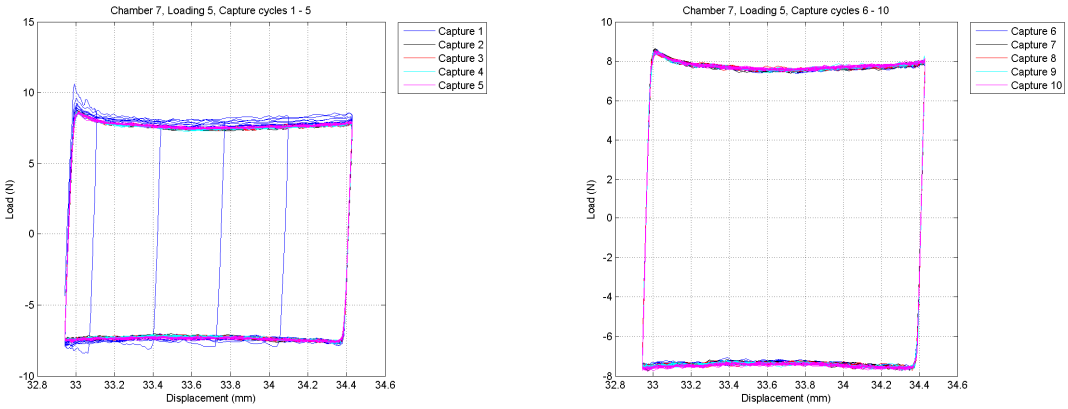

Figure E-20 cont. Figure E-20 Load against displacement for all loading sessions of chamber 7 (A-J)

E.6 Applied load data

An algorithm calculated the applied loads during each loading cycle of the mechanically stimulated chambers and these are displayed in Figure E-21 to Figure E-24. Only loading cycles which produced a valid applied load have been shown (see Section 11.1.5 for details of what constitutes a valid result).

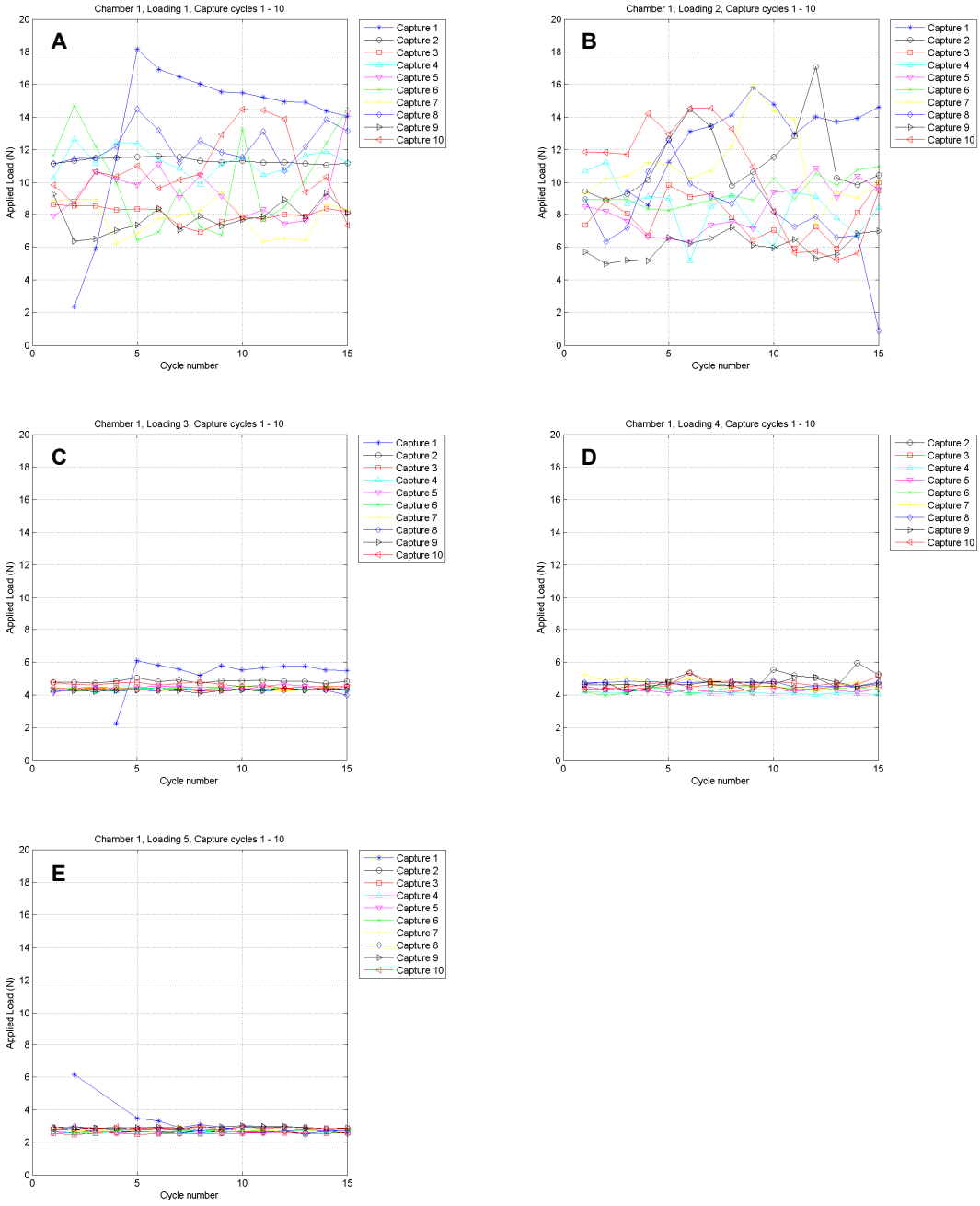

Figure E-21 Applied load for all loading sessions of chamber 1 (A-E)

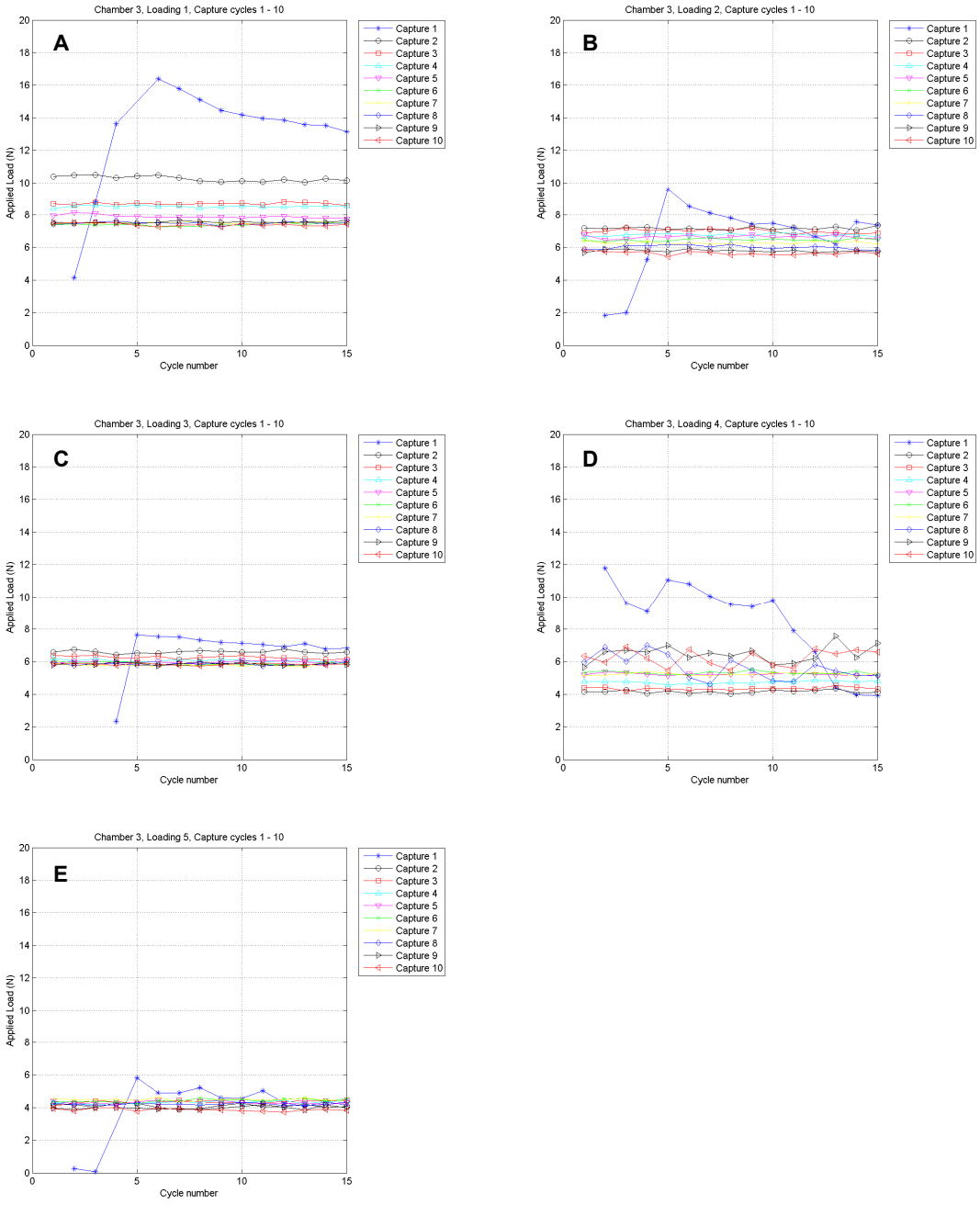

Figure E-22 Applied load for all loading sessions of chamber 3 (A-E)

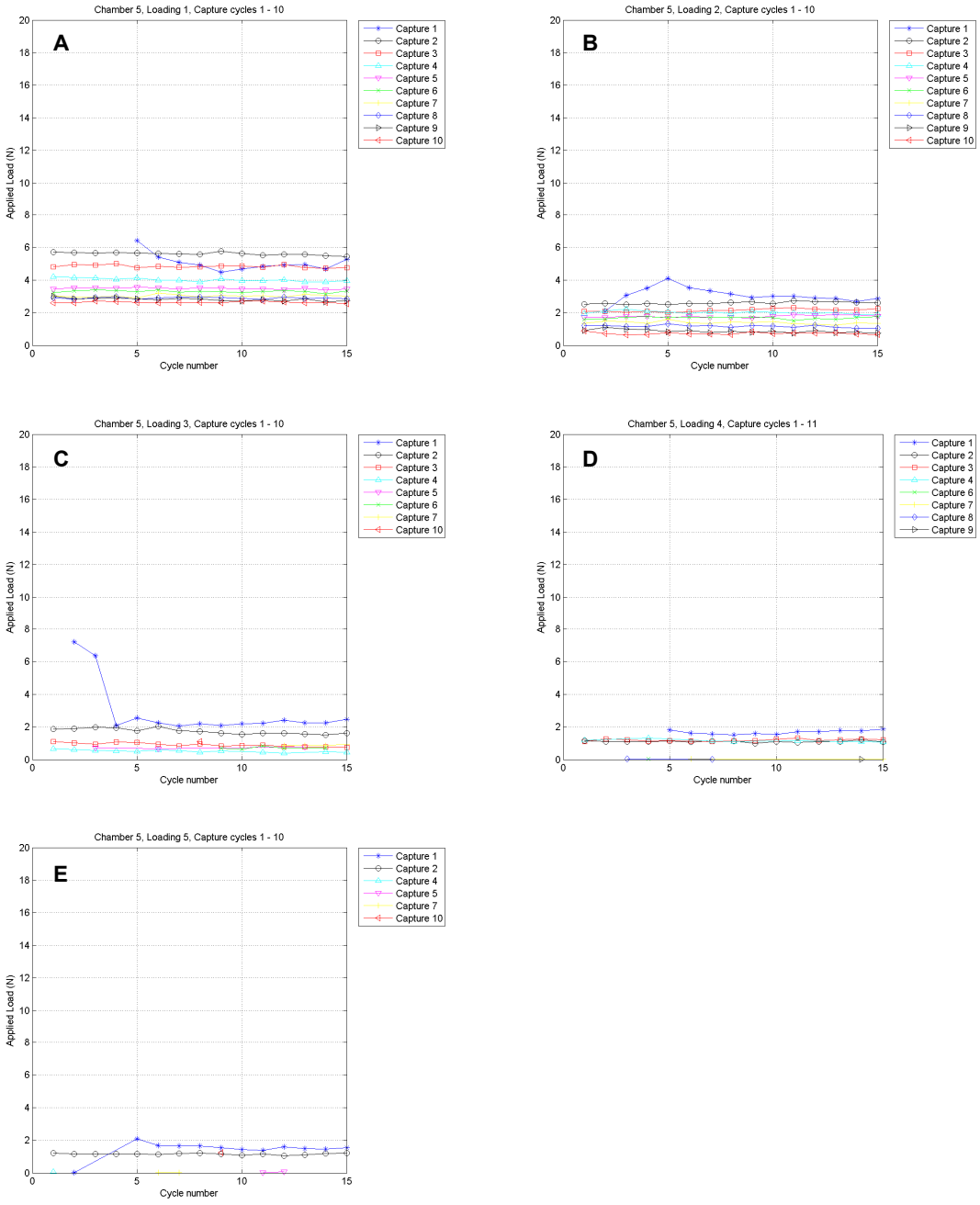

Figure E-23 Applied load for all loading sessions of chamber 5 (A-E)

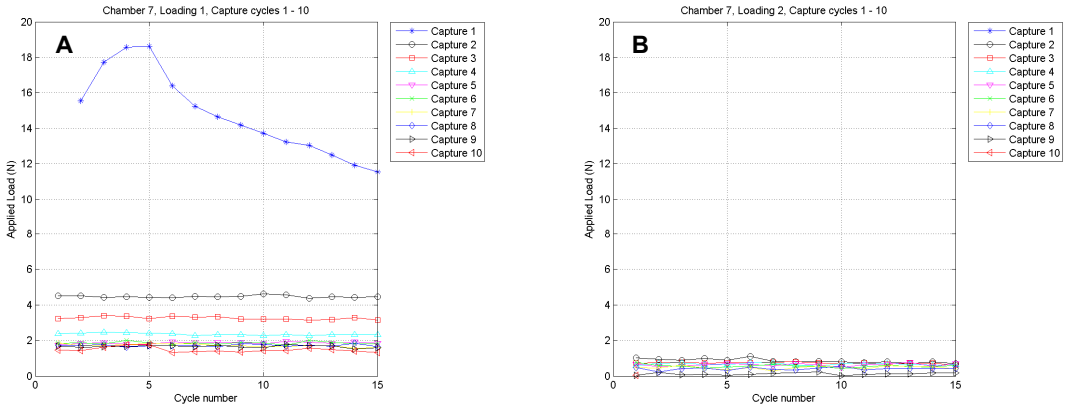

Figure E-24 Applied load for all loading sessions of chamber 7 (A-B)

E.7 Stiffness data

An algorithm calculated the stiffness of the tissue during each loading cycle of the mechanically stimulated chambers and these are displayed in Figure E-25 to Figure E-28. Only loading cycles which produced valid stiffnesses have been shown (see Section 11.1.5 for details of what constitutes a valid result).

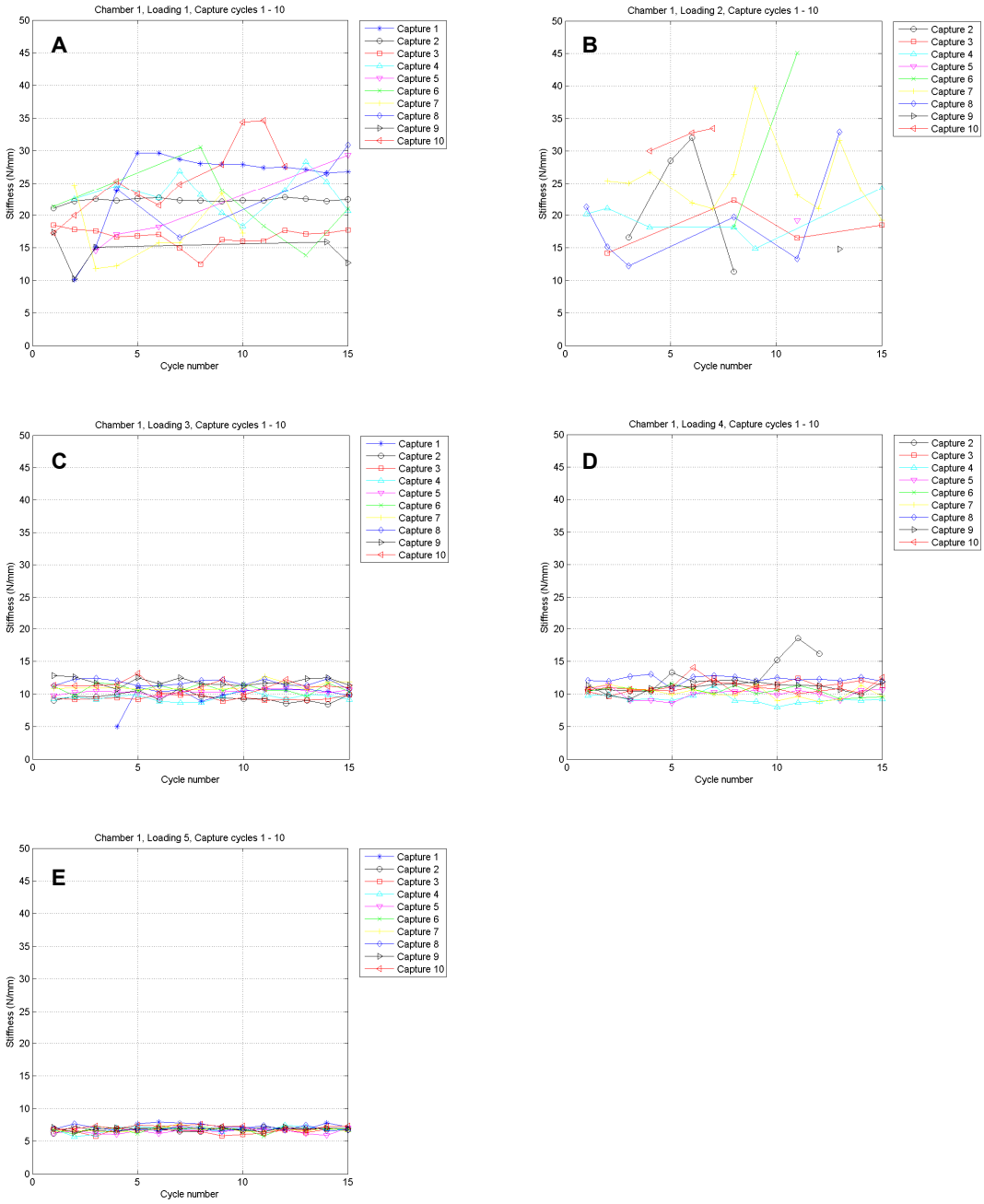

Figure E-25 Stiffness for all loading sessions of chamber 1 (A-E)

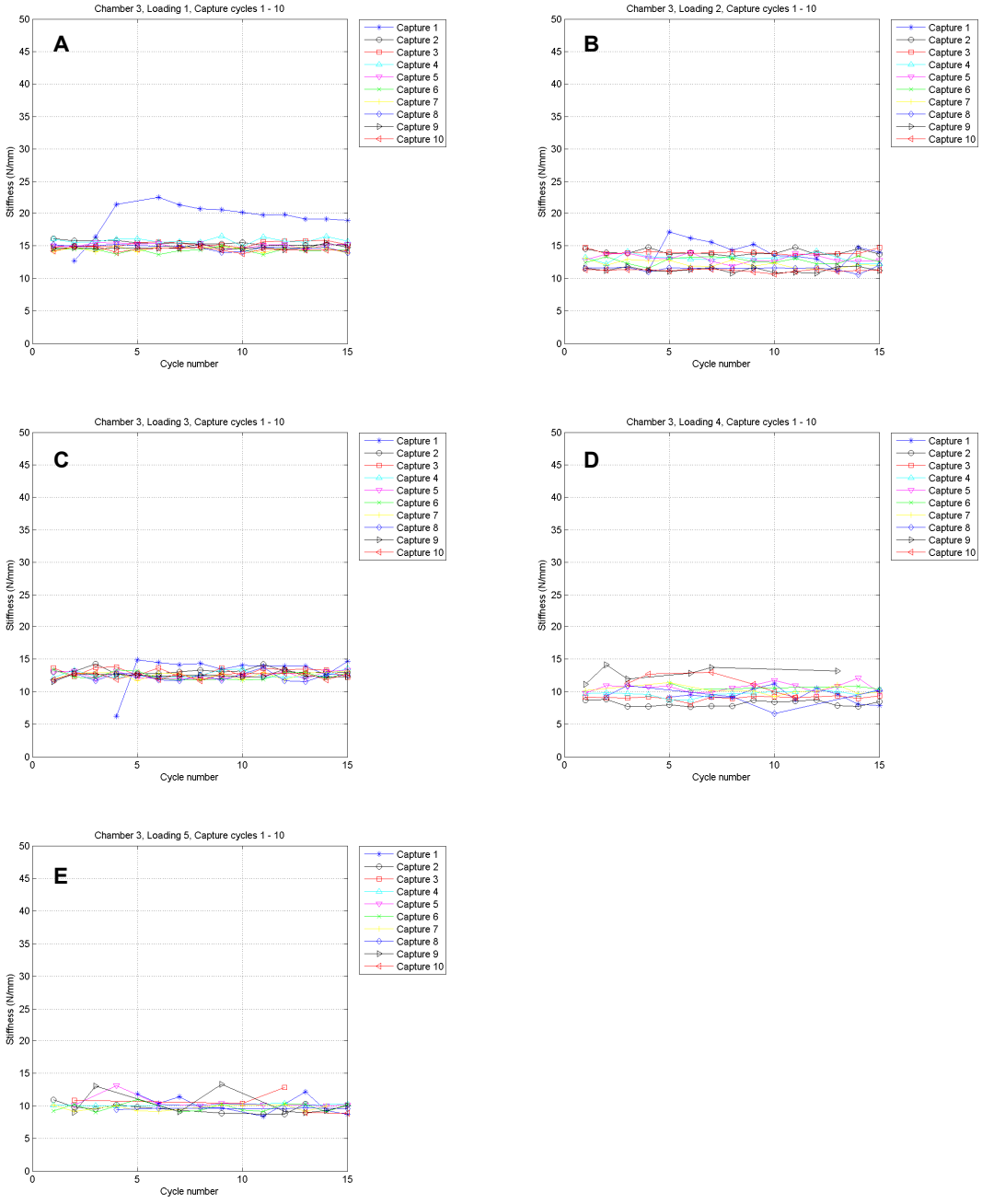

Figure E-26 Stiffness for all loading sessions of chamber 3 (A-E)

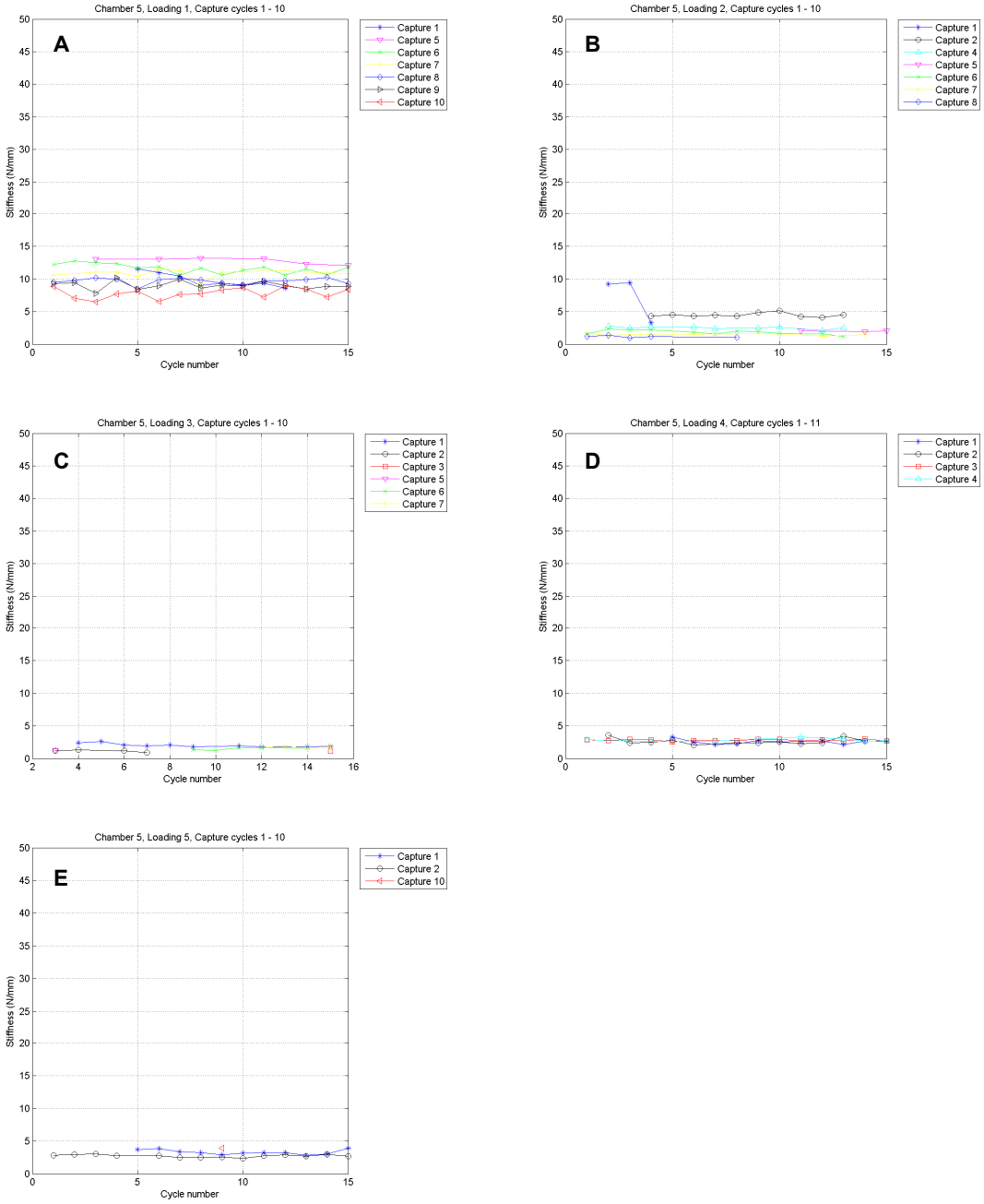

Figure E-27 Stiffness for all loading sessions of chamber 5 (A-E)

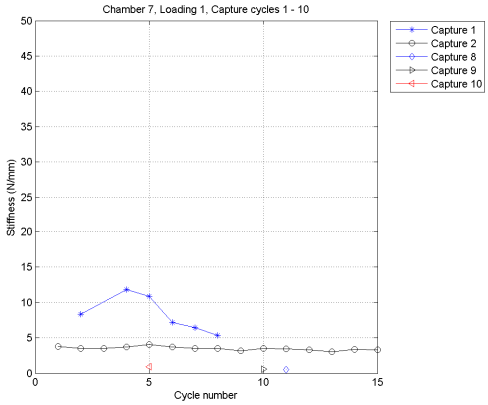

Figure E-28 Stiffness for loading session one of chamber 7

E.8 Histology images

Histological images were produced with the cell nuclei labelled with DAPI stain. The images were from the central portion of two sections from the middle of the tissue and are shown in Figure E-29 to Figure E-40. Baseline tissue which represents the native tissue at the start of the experiment and the tissue from the eight biological chambers were all sectioned.

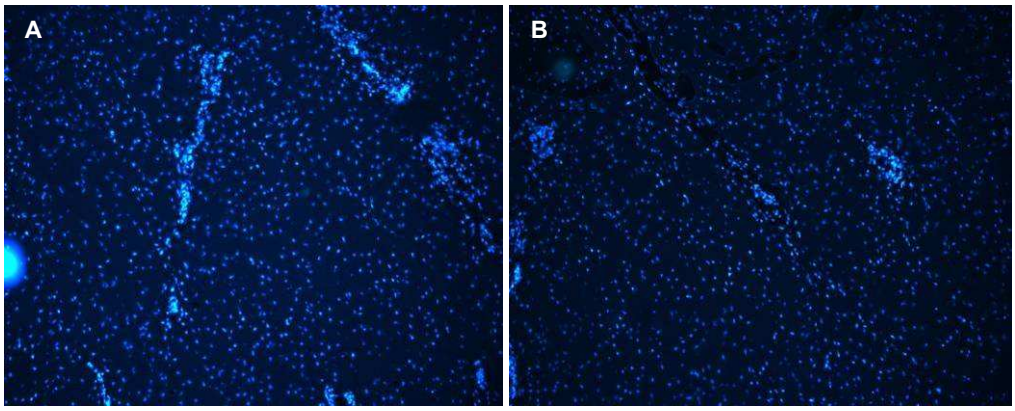

Figure E-29 Histology of two sections from the middle of baseline 1 tissue (A & B)

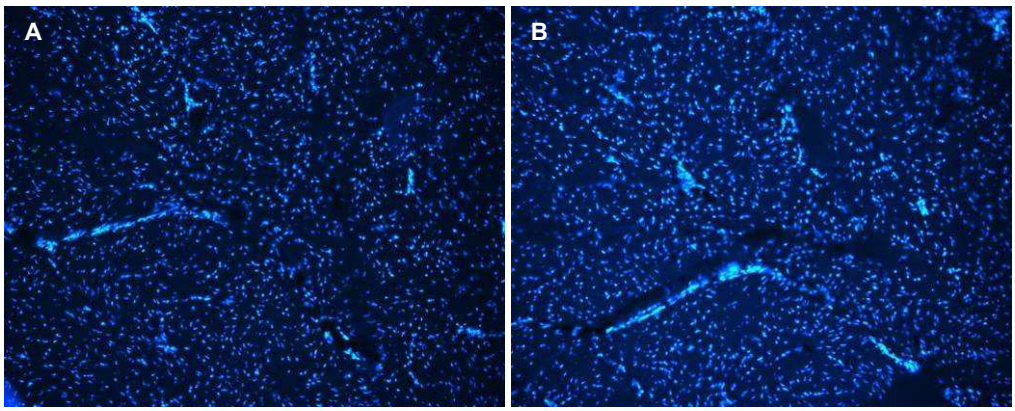

Figure E-30 Histology of two sections from the middle of baseline 2 tissue (A & B)

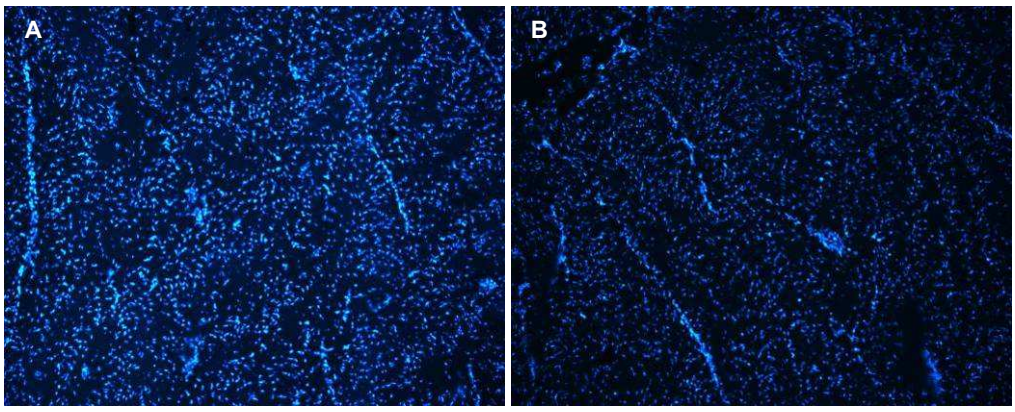

Figure E-31 Histology of two sections from the middle of baseline 3 tissue (A & B)

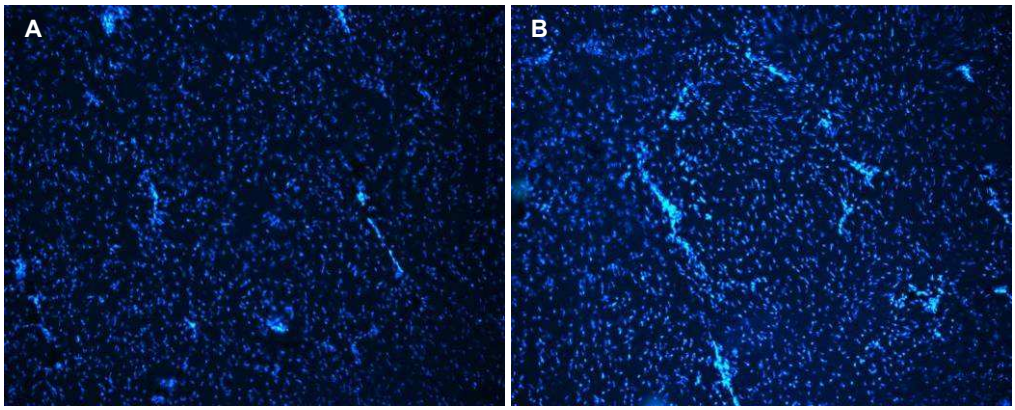

Figure E-32 Histology of two sections from the middle of baseline 4 tissue (A & B)

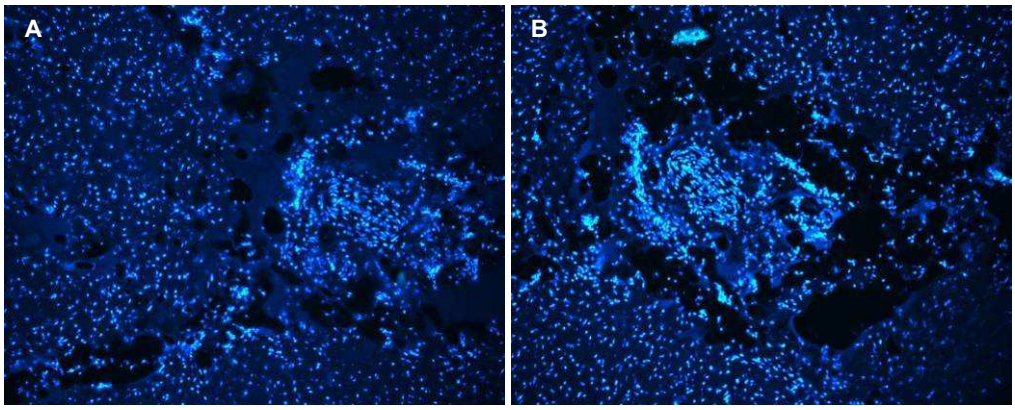

Figure E-33 Histology of two sections from the middle of the tissue from chamber 1 (A & B)

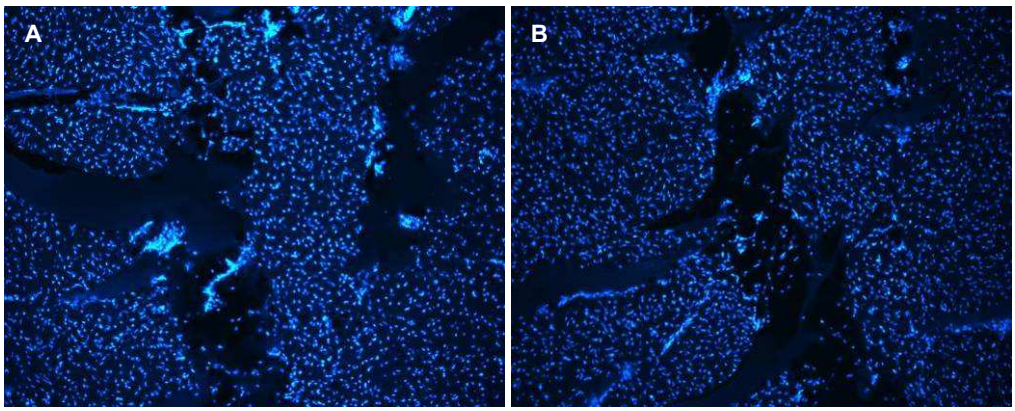

Figure E-34 Histology of two sections from the middle of the tissue from chamber 2 (A & B)

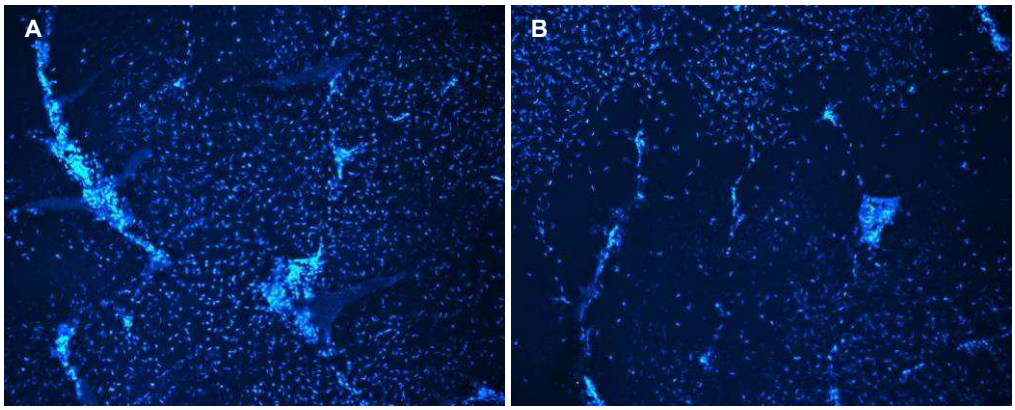

Figure E-35 Histology of two sections from the middle of the tissue from chamber 3 (A & B)

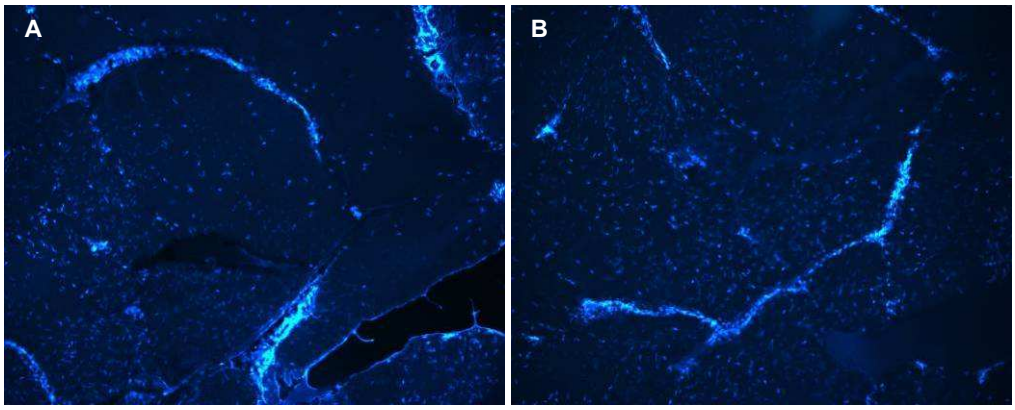

Figure E-36 Histology of two sections from the middle of the tissue from chamber 4 (A & B)

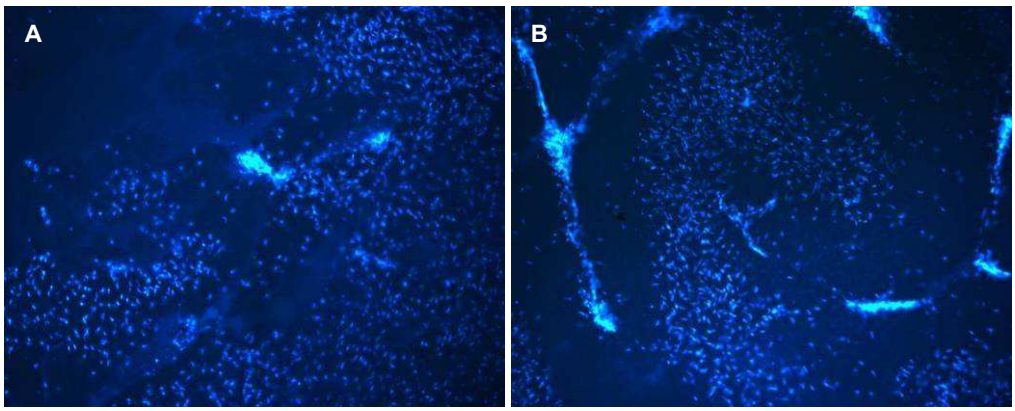

Figure E-37 Histology of two sections from the middle of the tissue from chamber 5 (A & B)

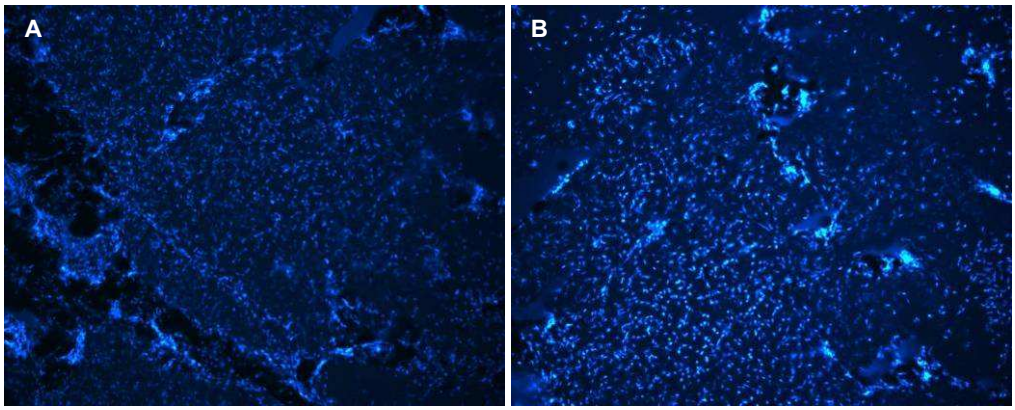

Figure E-38 Histology of two sections from the middle of the tissue from chamber 6 (A & B)

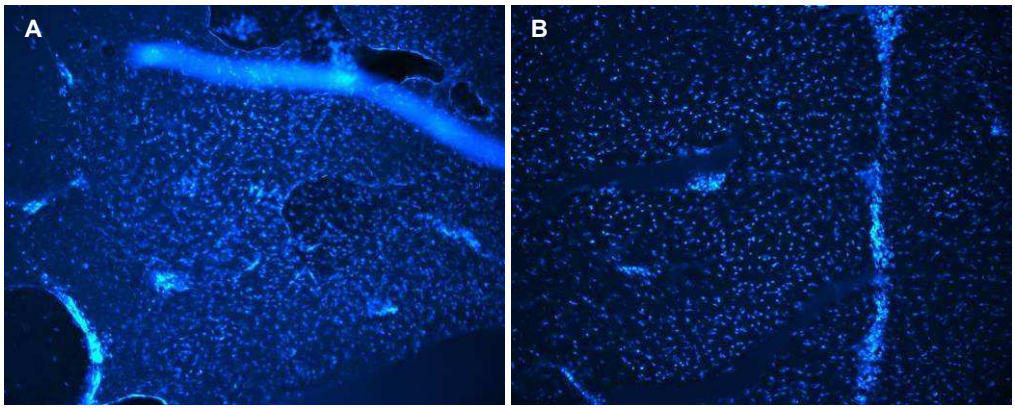

Figure E-39 Histology of two sections from the middle of the tissue from chamber 7 (A & B)

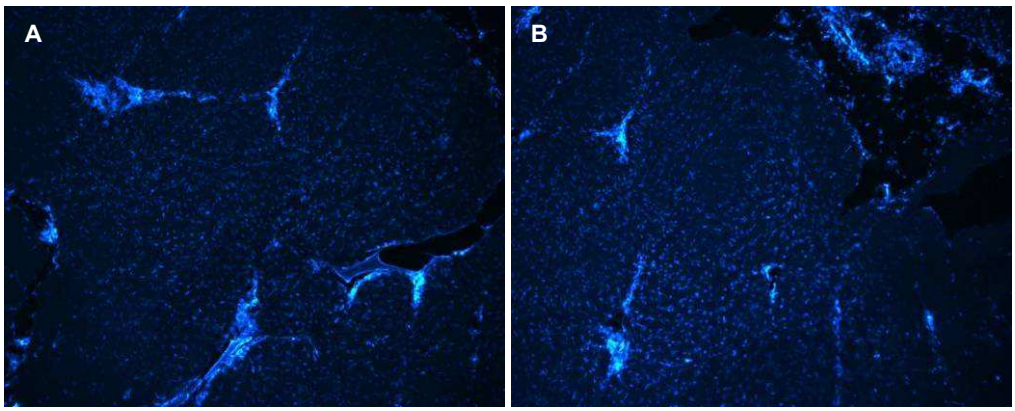

Figure E-40 Histology of two sections from the middle of the tissue from chamber 8 (A & B)